UNIVERSITY OF CALIFORNIA

Irvine

Nonlinear Time-Dependent Seismic Response of Unanchored Liquid Storage Tanks

DISSERTATION

submitted in partial satisfaction of the

requirements for the degree of

DOCTOR OF PHILOSOPHY

in Civil Engineering

by

Ali Abdel-Wahab El-Zeiny

Dissertation Committee:

Professor Medhat A. Haroun, Chair

Professor Jose Pires

Professor Roberto Villaverde

1995

The dissertation of Ali Abdel-Wahab El-Zeiny

is approved, and is acceptable in quality and

form for publication on microfilm:

Roberto Tumarkin

José A. Piqueras

Medhat Haroun

Committee Chair

University of California, Irvine

1995

Dedication

This dissertation is dedicated to my parents,

Abdel-Wahab and Zainub,

and my wife, Manal,

and my children, Mohamed and Ahmed.

Their constant love and caring are every reason for where I am and what I am. My gratitude and my love to them are beyond words.

Contents

List of Figures

List of Tables

Table of Symbols

A_i	Tributary area of a liquid free surface node projected in the horizontal plane.
$\mathbf{B}$ or $\mathbf{B}_o$	Linear strain-displacement matrix.
$\mathbf{B}_l$	Nonlinear strain-displacement matrix.
$\mathbf{C}_s$	Solid domain damping matrix.
$\mathbf{C}_{fs}$	Liquid-solid interaction matrix.
$\mathbf{C}_{sf}$	Solid-liquid interaction matrix.
$\mathbf{C}_{\phi h}$	Liquid-free surface interaction matrix.
$\mathbf{E}$	Constitutive matrix.
$\mathbf{F}_{ext}$	External force/discharge vector.
$\mathbf{F}_{int}$	Internal force/discharge vector.
$\mathbf{F}_I$ and $\mathbf{F}_E$	Interface and external body forces, respectively.
F_n and F_t	Normal and tangential contact forces, respectively.
g	Acceleration of gravity.
$\mathbf{G}$	Ground motion vector.
$\mathbf{h}$	Vector of liquid free surface heights.
H	Tank height.
$\mathbf{J}$	Element Jacobian matrix.
$\mathbf{K}_s$, $\mathbf{K}_f$ and $\mathbf{K}_h$	Solid, liquid and free surface element stiffness matrices, respectively.
$\mathbf{K}_\lambda$	Contact/constraint matrix.
l_x	Projected width of liquid element.
L_1, L_2 and L_3	Nondimensional area coordinates.
$\mathbf{n}$	Unit vector normal to the element face.
N_i	Shape function at node i.
$\mathbf{M}_f^j$	Liquid element face mass matrix.
$\mathbf{M}_s$	Structural mass matrix.
P	Liquid total pressure.
$\mathbf{P}$	Contact penetration vector.
$\mathbf{q}$	Lamina transformation matrix.
$\mathbf{r}$	Nodal position vector.

R	Radius of a cylindrical tank or base width of a rectangular tank.
$\mathbf{R}_d$ and $\mathbf{R}_k$	Residual vectors of the dynamic and kinematic conditions, respectively.
$\mathbf{R}_f$	Residual vector of liquid domain nodes.
T_a	Tributary surface area of a solid domain node.
$\mathbf{u}$, $\dot{\mathbf{u}}$ and $\ddot{\mathbf{u}}$	Nodal displacement, velocity and acceleration vectors, respectively.
$\mathbf{u}'$	Transformed displacement vector.
$\mathbf{v}_3$	Fiber direction.
v_n and $\dot{u}_n$	Liquid and solid normal velocity at a solid-liquid interface, respectively.
$\mathbf{V}$	Velocity of a fluid particle.
$\mathbf{V}_r$	Velocity of a fluid particle relative the fluid mesh.
$\mathbf{x}_i^t$ and $\mathbf{x}_i^b$	Top and bottom nodal coordinate vectors, respectively.
x', y' and z'	Transformed lamina coordinate system.
Γ_f	Liquid domain boundary.
Γ_s	Free surface boundary.
Γ_w	Liquid flexible boundary.
$\boldsymbol{\theta}$	Nodal rotational vector.
$\boldsymbol{\lambda}$	Lagrange multipliers vector.
ν_x and μ	Free surface damping parameters.
Π	Energy functional.
Ω_s and Ω_f	Solid and liquid domains, respectively.
ϕ and Φ	Velocity potential function and vector, respectively.
$\bigtriangledown^2$	Laplacian differential operator.
$\bigtriangledown$	Gradient differential operator.
ξ, η and ζ	Element local non-dimensional coordinates.
ρ_s and ρ_f	Solid and liquid mass densities, respectively.
$\boldsymbol{\sigma}$ and $\boldsymbol{\epsilon}$	Stress and strain vectors, respectively.

Acknowledgements

I would like to express my deep gratitude to Professor Medhat Haroun, my advisor, for his guidance, encouragement and gracious support throughout the course of my graduate study, for his expertise in the field of earthquake engineering, which motivated me to work on this subject, and for his faith in me during the most difficult stages of the research; for all of this I am very thankful. Also, I am very grateful to my committee members, Professor Jose Pires and Professor Roberto Villaverde, for their reading of my work.

I would like to express my gratitude for the financial support provided in the form of fellowships by the Division of Graduate Studies and Research at UCI, in the form of teaching assistantships by the Department of Civil Engineering, and in the form of research assistantships by the National Science Foundation and the National Center of Earthquake Engineering Research.

Finally, special acknowledgement is also due to my wife Manal for her love, support, and untiring encouragement. No words can express my appreciation and gratitude to her.

Curriculum Vitae

1984-1989	B.Sc. in Civil Engineering, Cairo University, Egypt.
1989-1990	Structural Engineer, Arab Consultant Engineers, Cairo, Egypt.
1990-1991	Research Engineer, General Organization for Housing, Building and Planning Research, Cairo, Egypt.
1990-1991	First Part of M.Sc. in Civil Engineering, Cairo University, Egypt.
1991-1995	Instructor, and Graduate Research/Teaching Assistant, University of California, Irvine.
1991-1992	M.S. in Civil Engineering, University of California, Irvine.
1992-1994	Core Courses in Information and Computer Science, University of California, Irvine.
Winter 1995	Dissertation Fellowship, University of California, Irvine.
1992-1995	Ph.D. in Civil Engineering, University of California, Irvine. Dissertation:

Publications

Haroun, M.A., and El-Zeiny, A., *Simulation of Dynamic Behavior of Unanchored Tanks*, Proceedings of the 13th International Conference on Structural Mechanics in Reactor Technology (SMIRT-13), Porto Alegre, Brazil, August 1995.

Haroun, M.A., and El-Zeiny, A., *Nonlinear Transient Response of Unanchored Liquid Storage Tanks*, Proceedings of the International Pressure Vessels and Piping Conference, ASME, Hawaii, July 1995, pp. 35-41.

Haroun, M.A., and El-Zeiny, A., *Dynamic Interaction of an Uplifted Beam with the Supporting Soil*, Proceedings of the Third International Conference on Recent Advances in Geotechnical Earthquake Engineering and Soil Dynamics, St. Louis, April 1995, pp. 409-412.

Haroun, M.A., El-Zeiny, A., and Bhatia, H., *Seismic Design Guidelines for Liquefied Natural Gas Tanks*, Vol. 272, Pressure Vessels and Piping Conference, ASME, June 1994, pp. 43-50.

Haroun, M.A., El-Zeiny, A., and Bhatia, H., *Seismic Qualification of Tanks for Storage of Liquefied Natural Gas*, Egyquake Proceedings, December 1993, pp. 665-674.

Haroun, M.A., and El-Zeiny, A., *Seismic Design Considerations for Uplifted Tanks*, Proceeding of the Structures Congress, Structural Engineering in Natural Hazards Mitigation, Vol. 1, April 1993, pp. 139-144.

Abstract of the Dissertation

Nonlinear Time-Dependent Seismic Response of Unanchored Liquid Storage Tanks

by

Ali Abdel-Wahab El-Zeiny

Doctor of Philosophy in Civil Engineering

University of California, Irvine, 1995

Professor Medhat A. Haroun, Chair

The present study investigates the effects of liquid hydrodynamic pressures exerted on thin-walled liquid storage tanks during earthquake motions. Several complexities are involved in the analysis of such tanks depending on their boundary conditions. In the case of unanchored liquid storage tanks, complexities arise due to successive contact and separation between base plates and foundations, large amplitude deformations of base plates, pre- and post-buckling behavior of shells, material yielding, soil-tank interaction, and large-amplitude free surface sloshing.

The main objective of this research is to develop a two/three dimensional computer model capable of performing simulation of the complex dynamic behavior of various types of liquid storage tanks subjected to a strong seismic base excitation.

The model takes into consideration both large amplitude liquid sloshing and nonlinear liquid-structure interaction using the finite element method. The program also has the following features:

- An up-to-date finite element technology for the analysis of solids and curved shells using the degeneration concept, and considering material plasticity and geometric nonlinearity. The program is expandable to accommodate any desired new plastic model.

- Modeling of potential flow problems using an efficient Eulerian finite element.

- Modeling of free surface sloshing that utilizes the nonlinear wave theory formulation. The updated Lagrangian description of the liquid domain boundaries is utilized to keep track of the free surface position at any time.

- A variational principle that forms the basis for the numerical discretization of nonlinear fully coupled liquid-structure interaction problems with free surface sloshing. Since a Lagrangian description of the solid motion is utilized, the program uses an updated Eulerian-Lagrangian description of the liquid-solid interface in order to enforce compatibility between solid and liquid elements. The resulting nonlinear Euler-Lagrange equations are solved using an efficient time integration technique that has been specially developed to solve the liquid-structure interaction problems.

- General contact analysis that accommodates a wide range of contact problems including liquid-structure interaction problems. A Lagrange multiplier technique was employed to enforce both displacement compatability and force transmissibility constraints along unknown contact surfaces. The program efficiently handles the special case of contact of unanchored liquid storage tanks.

Chapter 1

Historical Background

1.1 Introduction

Liquid storage tanks are important components of lifeline and industrial facilities. They are critical elements in municipal water supply and fire fighting systems, and in many industrial facilities for storage of water, oil, chemicals and liquefied natural gas. Behavior of large tanks during seismic events has implications far beyond the mere economic value of the tanks and their contents. If, for instance, a water tank collapses, as occurred during the 1933 Long Beach and the 1971 San Fernando earthquakes, loss of public water supply can have serious consequences. Similarly, failure of tanks storing combustible materials, as occurred during the 1964 Niigata, Japan and the 1964 Alaska earthquakes, can lead to extensive uncontrolled fires. Many researchers have investigated the dynamic behavior of liquid storage tanks both theoretically and experimentally. Investigations have been conducted to seek possible improvements in the design of such tanks to resist earthquakes. Intensive research on the subject started in the late 1940s in fields of aerospace technology. The emphasis of those studies was on the influence of the vibrational characteristics of liquid containers on the flight control system of space vehicles (e.g. [2]).

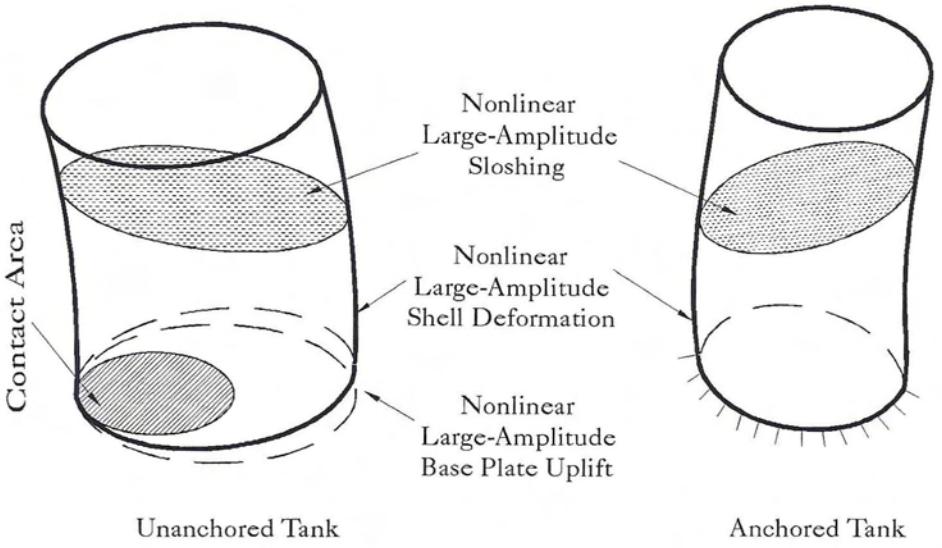

Figure 1.1: Classification of Tanks According to Support Condition

Liquid storage tanks can be found in many configurations: elevated, ground-based, and underground. Steel ground-based tanks consist essentially of a steel wall that resists outward liquid pressure, a thin flat bottom plate that prevents liquid from leaking out, and a thin roof plate that protects contents from the atmosphere. It is common to classify such tanks in two categories depending on support conditions: anchored and unanchored tanks, as illustrated in Figure (1.1). Anchored tanks must be connected to large foundations to prevent the uplift in the event of earthquake occurrence. However, improperly detailed anchors may damage the shell under seismic loading resulting in a ripped tank bottom. Hence, it is common, particularly for large size tanks, to support the shell on a ring wall foundation without anchor bolts and to support the bottom plate on a compacted soil though, sometimes, ring walls are omitted. Based on the orientation of the axis of symmetry, anchored tanks are either horizontal or vertical. Circular vertical tanks made of carbon steel are more numerous than any other type because they are efficient in resisting liquid hydrostatic pressure mostly by membrane stresses, simple in design, and easy in construction.

1.2 Relevant Areas of Study

Problems associated with the seismic behavior of liquid storage tanks involve the analysis of three systems: the tank, the soil and the liquid, as well as the interaction between them along their boundaries. The up-to-date technology in the nonlinear finite element analysis of plates and shells is utilized to model the tank wall and base plate. The Eulerian finite element method is used to model the liquid inside the liquid domain while the Lagrangian-Eulerian finite element method is used to model the liquid boundaries. Interaction between the tank and the liquid is due to the liquid hydrodynamic pressure that transfers a significant amount of energy to the tank. In addition, the motion of the tank shell is the main source of the liquid energy. Since this energy transfer occurs simultaneously throughout the liquid boundary, it becomes essential in the analysis of such systems to consider the liquid-structure interaction effect.

Analysis of the seismic behavior of unanchored tanks also includes the effect of large amplitude base uplifting. It has been observed in past earthquakes that the bottom plate can be lifted by as much as one foot or more, and therefore, its behavior affects the response of the overall system in a dominant way. The uplifting problem is a special type of the nonlinear contact problem between two bodies. Thus, the evolution of contact analysis as well as Large deflection and rotation analysis of plates and shells are strongly related to the area of the seismic behavior of unanchored tanks. It also involves the seismic behavior of the soil and the dynamic soil-structure interaction.

In summary, the previous work related to the seismic analysis of on ground liquid storage tanks may be characterized mainly by the method of the analysis and

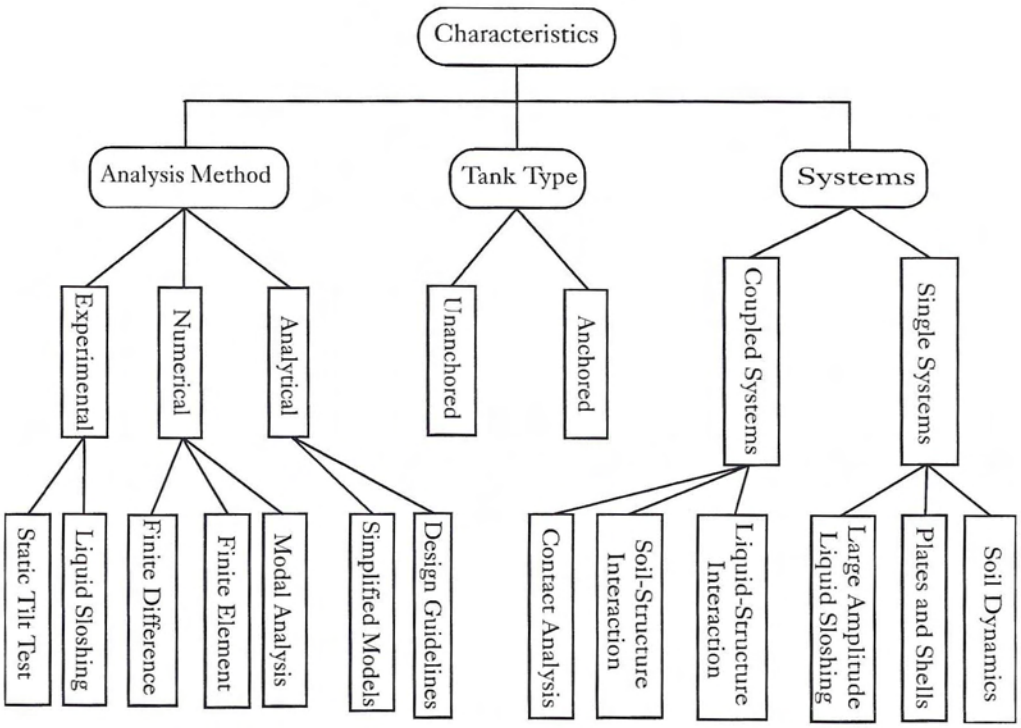

Figure 1.2: Main Characteristics of the Analysis of On-Ground Liquid Storage Tanks

the investigated problem, as shown in Figure (1.2). The method of investigation of such problems is either experimental, analytical or numerical. As computers have evolved, numerical methods became the most effective method to analyze complex problems. Many researchers have been employing the finite element method to investigate contact problems, soil plasticity and large amplitude liquid sloshing as well as both fluid-structure and soil-structure interactions.

1.3 Past Studies of Anchored Tank

Although the response of anchored tanks is totally different from that of unanchored tanks, the development of numerous analyses for the dynamic behavior of the

former under horizontal and vertical excitations has greatly affected the understanding of the seismic response of unanchored tanks. Early developments of the seismic response of liquid storage tanks considered the tank to be rigid, and focused attention on the dynamic response of the contained liquid, such as the work performed by Jacobsen [129], Graham and Rodriguez [71], and Housner [112]. Later, the 1964 Alaska earthquake caused large scale damages to tanks of modern design [79] and profoundly influenced research into vibrational characteristics of flexible tanks. Different solution techniques and simplified models were employed to obtain the seismic response of flexible anchored liquid storage tanks.

1.3.1 Numerical Technique Investigations

Evolution of digital computers and associated numerical techniques have significantly enhanced solution capabilities of complex problems. The first use of a digital computer in analyzing anchored liquid storage tanks was completed by Edwards [51]. He employed the finite element method and a refined shell theory to predict seismic stresses and displacements in a vertical cylindrical tank having a height to diameter ratio smaller than one. This investigation treated the coupled interaction between the elastic wall of the tank and the contained liquid. The tank cross section was assumed to be restrained against cross section distortions. Shaaban and Nash [248] undertook a similar research concerned with the earthquake response of cylindrical elastic tanks using the finite element method. Shortly after, Balendra and Nash [14] offered a generalization of the analysis by including an elastic dome on the tank. Fenves [61] used a mixed displacement-fluid pressure formulation for the fluid, and a standard displacement finite element formulation for the structure.

A different approach to the analysis of flexible containers was developed by Veletsos [284]. He presented a simple procedure for evaluating hydrodynamic forces induced in flexible liquid filled tanks. The tank was assumed to behave as a single degree of freedom system, to vibrate in a prescribed mode and to remain circular during vibrations. Hydrodynamic pressure distribution, base shears and overturning moments corresponding to several assumed modes of vibration were presented. Later, Veletsos and Yang ([282], [283]) estimated maximum base overturning moment induced by a horizontal earthquake motion by modifying Housner's model to consider the first cantilever mode of the tank. They presented simplified formulas to obtain the fundamental natural frequencies of liquid filled shells by the Rayleigh-Ritz energy method. Another approach was attempted by Natsiavas [200]. He expanded the structural displacements in appropriate series forms which involve both rigid body and flexible components. The latter components were expressed as linear combinations of terms, each of which is a product of a function with assumed spatial dependence and an unknown time-dependent function. These time functions were then determined from solving the equations of the fluid-structure system, which were set up by employing Hamilton's principle.

In 1980 and 81, Haroun and Housner [106] used a boundary integral theory to drive the fluid added mass matrix, rather than using the displacement based fluid finite elements. The former approach substantially reduced the number of unknowns in the problem. They conducted a comprehensive study ([97], [98], [100], [101], [102], [103], [104], [106]) which led to the development of a reliable method for analyzing the dynamic behavior of deformable cylindrical tanks. A mechanical model [104], which takes into account the deformability of the tank wall, was derived and parameters of the model were displayed in charts to facilitate the computational work. The model

may be applied to predict the maximum seismic response by means of a response spectrum. It received wide spread application because the previous models were either too complicated to be used in the design or too simple to give accurate results. Later, Haroun included more complicating effects in his analyses, such as the effect of out of roundness on the dynamic response of flexible tanks, the effect of initial hoop stress on the $\cos n\theta$-type modes and the soil-structure-fluid interaction ([83], [87], [88], [92], [105], [188], [189]).

The boundary integral technique was also employed by Williams and Moubayed ([289], [290]) to investigate the response of liquid storage tanks. They utilized a fluid Green's function to reduce the fluid domain to a line integral of the velocity potential on the surface of the structure. They calculated the hydrodynamic pressure distribution on a rigid submerged cylindrical tank subjected to a horizontal or vertical harmonic ground excitation. In a following work [288], they expressed both the structural and fluid axisymmetric motions in terms of appropriate Green's functions that lead to a pair of coupled line integral equations for the fluid velocity potential and its normal derivative on the walls of the tank. They studied the influence of the frequency of the ground excitation and the various geometric and material parameters on the hydrodynamic pressure distribution and the associated dynamic response of liquid storage tanks when subjected to high frequency vertical ground motions.

The finite element method combined with the boundary element method was used by several investigators, such as Grilli [72], Huang [114] and Kondo [142], to investigate the problem. Hwang ([119], [120]) employed the boundary element method to determine the hydrodynamic pressures associated with small amplitude excitations and negligible surface wave effects in the liquid domain. He obtained frequency-dependent terms related with the natural modes of vibration of the elastic tank and

incorporated them into a finite element formulation of an elastic tank in frequency domain. Generalized displacements were computed by synthesizing the complex frequency response using the Fast Fourier Transform procedure.

The vibrations of a thin-walled cylindrical shell filled with an ideal liquid were investigated by Goncalves [70]. He used modal expansions for the displacements of the shell and expanded the velocity potential function in terms of harmonic functions which satisfy the Laplace equation. The Galerkin method was used to reduce the problem to a system of coupled algebraic nonlinear equations for the modal amplitudes. All of these studies showed that seismic effects in a flexible tank may be substantially greater than those in a similarly excited rigid tank.

1.3.2 Geometrically Nonlinear Effects

In order to simplify the problem, former investigations ignored some nonlinear factors that may affect the response of anchored liquid storage tanks. Several researchers tried to refine the analysis by including the effects of these factors in the analysis. Sakai and Isoe ([234], [235]) investigated the nonlinearity due to partial sliding of the anchored tank base plate on its foundation. Huang [113] performed geometrically nonlinear analysis of tanks to investigate the large deflection effect. He stated that the beneficial effects of large deflections were most pronounced in plates having restraint against in-plane displacements. This restraint can be provided by adjoining plates in tank structures. Haroun and Mourad ([86], [88], [186], [187], [188], [189]) used experimental modal analysis techniques to assess the effects of out-of-roundness imperfections on the structure response. They also examined the buckling of the actual tanks. Costley et al ([41], [42]) presented a method to determine the

critical buckling load of tanks using experimental modal analysis techniques. Rinne [231] developed a criterion for buckling of the shell due to lateral forces and defined a shell buckling resistance coefficient.

Uras et al [273] studied the influence of geometrical imperfections on the dynamic stability of liquid filled shells under horizontal ground excitations. He introduced a general imperfection pattern in the circumferential direction to analyze the geometrical stiffness term. Imperfection effects on buckling of liquid-filled shells were also discussed in ([4], [35], [266]).

Zhou et al [299] presented a method for analyzing the elephant-foot buckle failure of ground-supported broad cylindrical tanks under horizontal excitations. Peek ([217], [218]) reviewed buckling criteria and showed that the plastic collapse criteria developed by axisymmetric analyses were also approximately applicable when the loading was not axisymmetric. Chiba [33] presented a theoretical analysis for the dynamic stability of a cylindrical shell partially filled with a liquid, under periodic shearing forces. He used a dynamic version of the Donnell equations and the velocity potential theory to determine the instability boundaries. Other issues related to buckling of liquid storage tanks were also presented in ([133], [158], [159], [170], [181], [190]).

1.3.3 Effect of Rocking and Vertical Excitations

Investigations of the effect of a rocking motion on the seismic response of liquid storage tanks started in 1980 by Ishida [128]. Later, in 1985, Haroun and Ellaithy [96] presented an analytical mechanical model for flexible cylindrical tanks undergoing both a lateral translation and a rigid base rocking motion. Using a classical

hydrodynamic pressure approach and assuming an approximate deflected shape for the tank walls, explicit expressions for parameters of the model were obtained. In addition, they investigated the effect of large deflections on the dynamic response of flexible tanks. Veletsos et al [279] analyzed the dynamic response of upright circular cylindrical tanks to a rocking base motion of an arbitrary temporal variation. He generalized the mechanical model for laterally excited tanks to include the effects of base rocking of both rigid and flexible tanks.

The response of liquid storage tanks to vertical excitations has not drawn much attention as most studies were concerned with the response due to lateral excitations. Bleich [25] studied the forced axial response of tanks by idealizing the tank shell as a system of rings stacked on top of one another, but he ignored the axial deformations and bending rigidity of the tank wall. Marchaj [176] conducted a simplified study that focused attention on the importance of the vertical acceleration in the design of tanks. Kumar [145] carried out a critical study of axisymmetric seismic behavior of tanks in which the radial motion of partly filled tanks was considered but effects of axial deformations were neglected. He reported that for near full tanks, such approximation has negligible effects on the accuracy of results, but for near empty tanks, axial deformations may influence the response especially for tall tanks. Veletsos and Kumar [281] presented a design procedure for evaluating the effects of vertical shaking on tanks.

In 1985, Haroun and Tayel [95] reported on a comprehensive study of effects of the vertical component of a ground excitation. They evaluated the natural frequencies using both numerical and analytical techniques. In their study, they considered both fixed and partly fixed tanks. They calculated tank response under simultaneous

action of both vertical and lateral excitations in order to assess the relative importance of the vertical component of a ground acceleration, which has been shown to be important. Rammerstorfer et al [230] developed an iterative procedure using the added mass concept to obtain the dynamic pressure resulting from a horizontal excitation. They showed that the formula for rigidly based tanks can be used to add the dynamic pressure caused by the vertical excitation. They reported that the stiffness dependent radiational damping causes the maximum dynamic pressure due to the vertical earthquake component to depend essentially on the stiffness of the soil. They discussed three different possibilities for superposing the dynamic pressures due to the horizontal and the vertical earthquake components on the static pressure, and the different modes of wall instabilities.

1.3.4 Experimental Investigations

In addition to analytical studies, several experimental investigations have been conducted in recent years. These include ambient and forced vibration tests on full-scale water storage tanks [106], laboratory tests on small plastic tank models subjected to harmonic and transient excitations at their base ([249], [250]), tests with simulated earthquake ground motions of several aluminum tank models ([36], [204]), tests on constructed welded steel tanks which believed to be the largest of its kind in the world [130], and of a full-scale wine storage tank of type damaged during the 1980 earthquake in Livermore, California [203].

Several other experimental studies have also been reported. Ishada and Mieda [125] carried out a static tilt test of a model tank and a stress analysis by the finite element method in order to investigate the stress distribution in the bottom plate

of an anchored cylindrical tank under the seismic loading. Manos [169] studied the behavior of a metallic cylindrical tank subjected to a horizontal earthquake loading by examining the response to horizontal Inertial loads introduced to the structure through a static tilt test. He also evaluated the performance of anchored wine tanks during the San Juan earthquake [167]. Minowa [183] conducted a shaking table test of a cylindrical tank with a spring-mass system.

Response of liquid storage tanks to impact loading was also investigated. Ruiz et al [233] combined numerical, analytical and experimental techniques to find the strength of thin-wall cylindrical shells under blast loading. Birk and Chidley [24] conducted experimental study concerned with the pressures that can be generated on the ends of cylindrical tanks by the contained liquids when the tank is suddenly accelerated along the longitudinal axis of the tank. These experimental studies have provided improved insight into the dynamic behavior of anchored tanks, and have helped to clarify the limitations of the present methods of analysis.

1.3.5 Free Vibration Studies

Since a knowledge of the free vibration characteristics of the structure is essential to obtain its dynamic response, free vibration analyses were performed on tanks and liquid-filled shells by many investigators. Tedesco et al [268] summarized the results of a comprehensive, computer based, numerical investigation of lateral free vibrations of cylindrical liquid storage tanks. Gupta et al ([74], [75], [76]) used variational principles to obtain a functional describing coupled oscillations between a linear elastic body and a liquid of small wave heights. They introduced a complementary Rayleigh's

quotient to obtain the natural frequencies of circular cylindrical tanks partially filled with liquid and oscillating in an axisymmetric manner.

Tani et al [265] analyzed the linear free vibration of partially liquid-filled shells of revolution using the finite element method. They used thick isoparammetric shell elements for the axisymmetric shell and isoparammetric quadrilateral elements and line elements for the liquid interior and exterior surfaces, respectively. They reported that the static liquid pressure has a significant effect on the natural frequency of LNG tanks. Singhal and Williams [258] discussed the free vibrations of thick circular cylindrical shells and rings using the energy method. They carried out experimental investigations on several models in order to assess the validity of the analysis and reported that comparison with experimental values showed very close agreement.

1.4 Investigations on Other Types of Tanks

The research on other types of tanks has also provided improved insight into the dynamic behavior of anchored tanks. Several investigations for other types of tanks have helped to clarify the complex behavior of fluid vibrations in flexible containers.

Liquefied natural gas (LNG) tanks are very common type of anchored tanks. They are, usually, composed of two tanks: inner tank and outer tank. The inner tank is directly in contact with the liquefied natural gas and cold gas vapor. Several researchers have investigated the coupled gas-liquid-structure systems in order to understand the seismic behavior of these tanks. Thompson [269] investigated the response of double-walled cylindrical storage tanks. Joos et al [134] developed an analysis that applies to such systems in which a hydrodynamic transient response

of the gas creates pressure forces dependent on the flexibility of the liquid boundary surfaces. Identical experiments were conducted on two geometrically identical cylindrical tanks, one of which was rigid while the other was flexible.

Asai et al [9] instrumentally observed earthquake responses of an on-ground LNG storage tank having a pile group foundation. The objectives of the study were to examine whether behavior patterns other than those considered during the design exist and to ascertain safety margins in the current aseismic design. They remarked that the buckling vibration due to the liquid-tank shell interaction was observed but has small influences, the ground deformation effect predominates in the bending moment on the piles, and scaled up observed moments on the piles were half those of estimated in the design. Haroun and El-Zeiny [81] provided an aseismic design guidelines for LNG tanks. Haroun's mechanical analog was used to evaluate the seismic demand on the LNG tanks and compare it to the seismic capacity of the tank to evaluate its safety.

Other configurations of anchored tanks were also investigated. Pavlovic et al [216] conducted a comprehensive parametric study for the problem of thin spherical containers filled to capacity with liquid. The investigation placed particular emphasis on the effect of the bending disturbances arising at the support location.

Solutions to tanks supported on towers were also attempted. Haroun and Lee [89] presented a finite element analysis of axisymmetric shell towers supporting elevated, liquid-filled vessels. The tank tower was modeled using a curved high order ring element while the liquid was accounted for by coupling the liquid added mass matrix to the consistent mass matrix of the shell. They used a mechanical model which takes into account both the flexibility of the tank wall and the global rocking

motion of the vessel. In further works, Haroun analyzed tanks supported on x-braced frames ([93], [94]). Buckling of elevated tanks has also been investigated by Allen et al [5].

In addition to elevated tanks, large-sized, multi-walled coaxial cylindrical tanks have been studied in recent years. Since various kinds of oil can be stored in these tanks, it is common to find such tanks in oil industrial facilities. Yoshida [295] described theoretical studies of coupled vibrations of the contained liquid and the shell plate of such tanks in response to lateral earthquake excitation by the finite element method. He analyzed the buckling motion which occurs in the relatively high frequency region due to flexibility of the shell.

The LMR reactor tanks were also studied. Chang et al [30] presented a method for the seismic analysis of these tanks. Mathematical models of a reactor tank and an LMR plant were given. They described various methods of seismic analysis suitable for the analysis of fluid-structure interaction of LMR plant and their advantages and drawbacks. Emphasis was placed on the efficiency of the numerical algorithm. They presented the computer code FLUSTR-ANL that was developed for the seismic analysis of LMR components.

1.5 Evolution of Seismic Analyses of Unanchored Tanks

Researchers did not realize until 1967 that unanchored tanks need more attention than anchored tanks. Rinne [231] reported that the Prince William Sound,

Alaska, earthquake of 1964 caused more extensive damage to oil storage tanks, most of which were unanchored, than to other structures. This damage highlighted the need for a careful analysis of such tanks. Shell buckling near the bottom of unanchored tanks was a phenomenon experienced during this earthquake. In a few tanks, buckling was followed by a total collapse of the tank. For most tanks, uplift occurred typically around the periphery of the tank bottom plate, which was lifted as much as two inches off the supporting foundation, causing yielding and plastic deformations in the plate.

The Balboa Water Treatment Plant was under construction when the 1971 San Fernando earthquake struck. Housner, Jennings and Brady [132] estimated that ground shaking at the plant's site was in the range of 0.3-0.5 g peak acceleration, and reported that there were many tanks affected and damaged by the earthquake. A large steel wash-water tank with a diameter of 100 ft and a height of 30 ft was approximately 1/2 to 3/4 full. After the earthquake, the tank showed signs of having rocked on its foundation. Some anchor bolts failed in tension, and others failed in bond and were pulled up off their anchorage. The pullout varied from 2-14 inches. The upper part of the shell buckled inward due to high stresses that existed in the tank when it was tilting on its toe. Another tank suffered damage in the form of an axisymmetric outward bulge of its shell close to ground level almost all the way around the circumference. The bulge covered a height of approximately 20 inches with an amplitude of about 8 inches.

In 1982, Niwa and Clough [203] investigated the earthquake response behavior and the buckling mechanism of a tall cylindrical wine storage tank similar to those damaged in the 1980 Livermore earthquake. It was reported that most of damaged tanks were unanchored and completely full of wine. The elephant foot buckling,

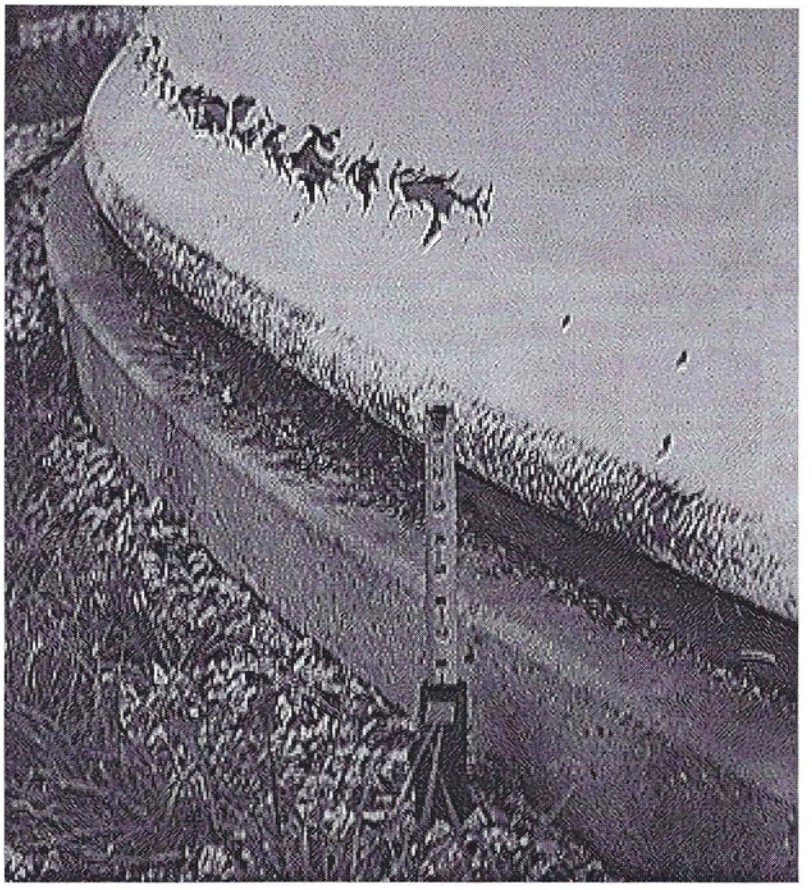

Figure 1.3: Elephant Foot Buckling

Figure (1.3), was the most common damage in broad tanks while tall tanks suffered a diamond shaped buckling spreading around the circumference, Figure (1.4). A 9.5 ft diameter by 20 ft high tank was tested under simulated earthquake accelerations up to $0.95g$, and buckling patterns similar to those that occurred in the earthquake were observed during tests. The critical buckling stress observed during the development of the diamond-shaped buckle pattern was about 60% of the theoretical buckling stress. This value was considerably higher than that adopted in the API 650 and AWWA D100 Standards. Hence, Niwa and Clough concluded that the critical buckling stress assumed in current standards for the steel tank design might lead to rather conservative estimates of the buckling strength of a free base tank subjected to rocking

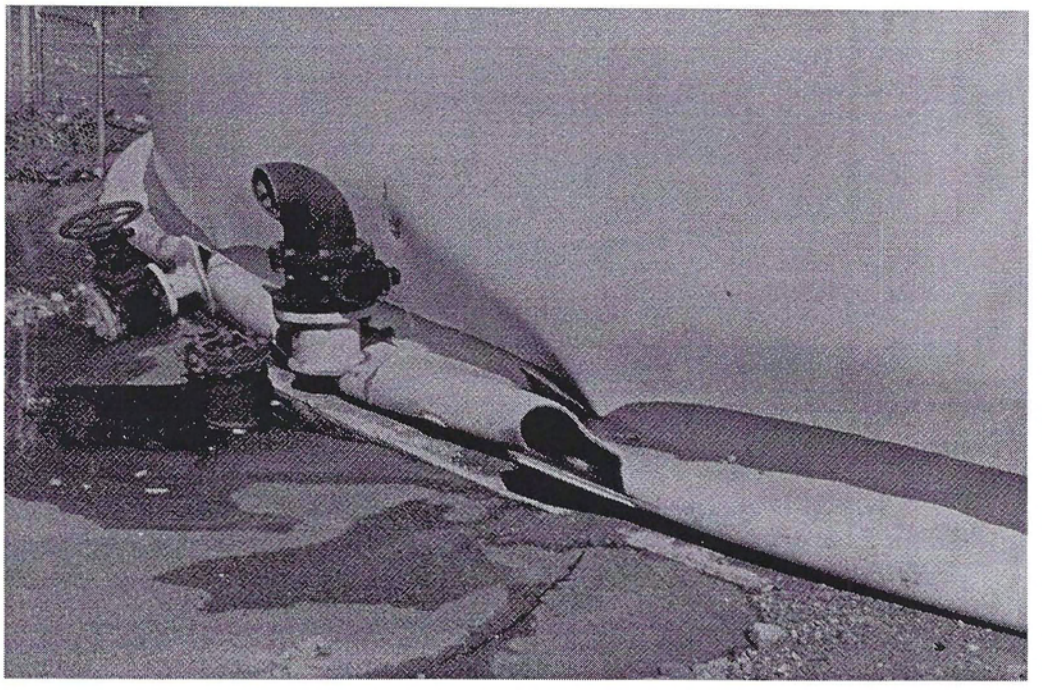

Figure 1.4: Diamond Shape Buckling

motions. The actual loading conditions during the uplift response were far different from those provided in static buckling tests of small cylinders under uniform axial compression, on which the current design buckling stress has been based. It was also reported that the uplifting behavior of the bottom plate showed that ignoring the membrane stress mechanism considerably underestimated the uplifting stiffness of the bottom plate, and they recommended further studies of uplifting kinematics of free base tanks.

Hanson [79] discussed the behavior of liquid storage tanks during the 1964 Alaska earthquake. He reported that although considerable damage to such tanks has occurred during the earthquake by tsunamis, earth settlement and subsoil liquefaction, a significant portion of damage resulted from direct structural action of the tank and its contents generated by the earthquake ground shaking. He showed that earthquake forces can cause an uplift of the tank edge, and this uplift increases the

possibility of the tank damage and subsequent loss of its contents. By using Housner's model, and assuming a 20% g peak ground acceleration and a lightly damped spectral velocity, he concluded that this ground motion was sufficiently intense to cause a typical tank to uplift and to account for the observed damage. For an uplifted tank, he found that true stresses and the precise progress of failure is very hard to analyze, and that any reasonable estimate of the factor of safety against collapse is difficult to make. However, he recommended that liquid storage tanks should be designed and constructed to resist realistic earthquake forces without significant uplift, or provisions should be made to contain the contents of tank after its collapse.

A brief description of the structural and nonstructural damages of unanchored tanks during the 1979 Imperial Valley earthquake was presented by Haroun [99] in 1983. Observed damages were similar to those produced by past major earthquakes. He reported that buckling of the bottom of tank shells due to excessive compressive stresses, damage to fixed roofs due to liquid sloshing and failure of attached pipes due to their inability to allow for the shell movement, had occurred. He also reported that tall tanks have suffered shell damage. In addition, he investigated the validity of current standards and codes by comparing observed damages with predictions obtained by using existing methods of analysis. Based on an approximate analysis of damage, he concluded that current design codes for seismic analysis of unanchored tanks can lead to a conservative design because of the very low allowable buckling stress. Further evaluations and comparisons between design codes and guidelines were performed by Haroun in different publications such as ([82], [85], [91]).

The 1983 Coalinga earthquake subjected many unanchored oil storage cylindrical tanks to an intense ground shaking. Damages occurred to these tanks were studied by Manos and Clough [173]. Observed damages included elephant foot buckling of the

tank wall at the base, joint rupture, top shell buckling, bottom plate rupture, damage to floating roofs and pipe connections, and spilling of oil over the top of many tanks. They estimated peak ground accelerations at various tank sites to range from $0.39g$ to $0.82g$. Based on a correlation of observed damages with the response parameters specified by current codes, Manos and Clough concluded that current U.S. practice underestimates sloshing response of unanchored tanks with floating roofs, and does not adequately address the dynamic uplift mechanism and buckling behavior.

All aforementioned studies showed the need for rigorous analysis of unanchored tanks. Improved methods of analysis need to properly account for the effects of large-amplitude of base uplifting, large-amplitude liquid sloshing, liquid-structure interaction, pre- and post-buckling behavior of the shell, material plasticity and soil-structure interaction. Thus, the problem associated with the seismic behavior of unanchored tanks was cited by the National Research Council [194] as the most challenging problem in fluid-structure systems.

1.5.1 Experimental Investigations

Most of pioneering studies performed to investigate the seismic behavior of unanchored liquid storage tanks were experimental in nature because of the complexities associated with the analytical solution of the problem. The majority of these experiments were performed on small scale models. A pioneer work in this field was performed by Clough and his coworkers during a large experimental program with model tanks on the EERC shaking table. A broad tank, 12 ft in diameter by 6 ft in height, was investigated by D. Clough [36] and a few years later by Manos ([168], [171]). In addition, Manos and Clough ([174], [175]) presented the dynamic response

results of an unanchored broad aluminum tank model of a similar size due to one horizontal component of the 1940 El Centro earthquake record applied with $0.5g$ peak acceleration. The tank base was free to uplift from either a rigid or a flexible base surface. The tank response was dominated by the uplift mechanism which varied nonlinearly with the intensity and frequency of input motions. For a rigid foundation, the coupling of uplift mechanism with out-of-round distortions resulted in high compressive axial membrane stresses developed over a narrow contact zone. For a more flexible foundation, lower compressive stresses, distributed more widely along the base of the tank wall, were observed. Also, for a less rigid foundation, large uplift accompanied by high levels of compressive hoop stresses on the uplifted part of the tank wall, and correspondingly large bending and membrane stresses in the bottom plate, were reported. They concluded that a realistic uplift mechanism prediction, out-of-round distortional response, foundation flexibility and a more realistic failure criterion should be incorporated in design procedures. They also recommended further experimental work to establish allowable values of buckling stresses suitable for use in the seismic design of such tanks. In a following work [173], they examined two cases of the behavior of tank models when subjected to lateral loads. In the first case, these loads were introduced by a static-tilt test. In the second case, the dynamic characteristics of the same model were examined by subjecting it to a variety of horizontal base motions.

In 1979, Clough et al [37] summarized results of an experimental study on tank models that started in 1975. Objectives of the study were to measure the actual behavior of two aluminum cylindrical tank models when subjected to realistic base motions, and to compare this behavior with predictions based on standard design procedures. They reported that due to the tank wall flexibility, impulsive hydrodynamic

pressure component was amplified beyond the value expected in a rigid tank, and flexibility associated with the uplift mechanism drastically altered the entire tank behavior. Significant out-of-round displacements were observed in both tanks and were believed to be related to initial imperfections of the tank's geometry. It was noted that for the same input acceleration amplitude, shell displacement and stress amplitudes were much higher in unanchored tanks than those in anchored tanks. They also reported that for unanchored tanks, there was a poor correlation between predicted and observed results, and the unexpected behavior observed in these tests with respect to uplifting kinematics demonstrated the need for additional analytical studies of seismic response of unanchored tanks.

In addition to tests on broad tanks, tall tanks were also tested. In 1979, Clough and Niwa [38] reported the results of a static tilt test of a cylindrical liquid storage tank. The tilt test was carried out on the same aluminum tall tank model (7-3/4 ft by 15 ft) used earlier in previous shaking table tests performed by Niwa [204]. Results of typical design calculations were compared with the observed behavior, and it was noted that the unanchored tank tilted more and developed much greater axial stresses than were indicated by typical design procedures. Compressive stresses were concentrated over a much narrower contact zone than was expected, leading to an amplified peak stress. In a following work, Niwa and Clough [203] investigated the buckling of these tanks under earthquake loadings.

Small scale models were also tested experimentally. Ishida et al [127] performed a vibration test and a static tilt test on a small stainless steel tank model. In 1984, Shih and Babcock ([249], [250]) reported on an experimental project which was carried out to provide a better understanding of damages produced by the 1979 Imperial Valley earthquake to oil storage tanks. They studied the buckling behavior of a small

unanchored tank model constructed of Mylar A sheet with a floating roof. The tank model was subjected to a single axis horizontal base excitation, and harmonic as well as simulated earthquake base motion. They found that buckling of the model was in reasonable agreement with field observations, and that floating roof had no effect on the buckling behavior. Following a comparison with API 650 design provisions, it was found that buckling predictions and tip over calculations of the code were conservative by over a factor of two. They also showed a marked difference between the response of anchored and unanchored tanks.

Tests on full scale models have also been attempted. It started in 1987 when Sakai et al [239] presented a static tilt test with a full scale tank model in order to investigate the uplift behavior of large size cylindrical liquid storage tanks. They made a comparison with theory and reported that experimental results did not agree with their theoretical analysis around the bottom of the tank. They concluded that the stress distribution around the shell-base corner and the contact condition between the bottom plate and the foundation should be considered carefully because of the complicated uplift behavior. In a following work, they carried out a static tilt tests ([236], [237], [238]) in order to investigate complicated uplifting phenomena in details. They have used such a big model as were not employed in the past studies. They reported that their model satisfied almost perfectly the similitude law to a large-scaled prototype tank, and consequently should grasp very well the fundamental behavior of actual tank's uplift.

In 1983, Cambra ([27], [28]) investigated the earthquake response behavior of an unanchored broad tank model, also 12 ft in diameter by 6 ft in height. The study included axial symmetric lift tests, static tilt tests and dynamic shaking table tests using both a rigid mortar as well as flexible rubber foundations. It was concluded

that seismic response of tanks was significantly affected by the variation of foundation flexibility, and there was a strong correlation between the tank shell eccentricities created by fabrication imperfections and/or shell deformations and out-of-round response. An empirical tie element model representing the uplift behavior of the tank base plate was also described in order to improve design procedures for unanchored tanks. Wozniak and Mitchell's model [292] was modified by analyzing two elastic beams: one in the uplift region and the other in the contact region. Both beams were subjected to a transverse distributed load which produces longitudinal membrane forces. In contact region, the beam was assumed to be supported on a Winkler foundation. This was considered an improvement since it took into account both the membrane force and the bending moment at the beginning of the uplift region whereas, on a rigid foundation, there were no moments assumed at junction of uplift and contact regions. The membrane force was calculated by considering the strip beam as an extensible string with no longitudinal displacements allowed at its ends, and by assuming that the total load on the strip is carried only by membrane force. This membrane force was later introduced as a given longitudinal force in the linear equation of an elastic beam which is incompatible with the general equilibrium as the total load is already carried through the bending of the beam. In reality, part of the load carried by membrane effects of the plate and the remainder by bending effects. Only the elastic behavior of the plate was considered in contradiction to the valid assumption of the existence of plastic hinges. However, based on this model, it was found that both the wall uplift and the separation of the tank bottom plate occurred at values larger than what design codes anticipate for credible earthquake magnitudes.

Theoretical studies were also performed to support the static tilt test. Lau ([147], [148], [149]) adopted a general method for predicting the static tilt performance of a cylindrical liquid storage tank that is free to uplift. The base plate, subjected to both membrane tension and plate bending, was divided into contact and uplifted regions. Deformations of the bottom plate were evaluated by a Ritz-type method using iterations to determine the boundary of the contact region and full continuity was maintained with the tank wall. The cylindrical tank shell was analyzed by using Flugge thin shell theory and its stiffness was cast in a form comparable with that of the base plate for direct stiffness summation. The stiffening effects of the top rim wind girder and the bottom toe ring were also included. Friction exerted along the bottom edge of the shell still in contact with the platform was modeled by lateral support springs of a stiffness that was fine tuned to model frictional forces. Using this analytical approach, the responses of a broad and a tall model tank to various angles of tilt were evaluated and the results were compared with measured data. The differences in uplift behavior between the broad and tall tank models were discussed. Finally, the sensitivity of the uplift behavior to various parameters characterizing the tank system were studied.

1.5.2 Simplified Models

Based on simplified theoretical investigations, many researchers have attempted to develop simplified models for unanchored tanks. Most of these investigations have focused attention on the behavior of the bottom plate which is a governing factor for the behavior of unanchored tanks. It started in 1977 when Clough [36] proposed a simplified model for uplifting of unanchored tanks, but he ignored the load carrying

capacity of the tank bottom plate. It was assumed that the bottom plate remains in contact with foundation on a circular area of a radius slightly less than the radius of the tank, and that the edge of shell rests on an arc of the tank's perimeter of an unknown central angle. A geometrical relation was found between the central angle and the radii of the contact area before and after uplift. Total overturning moment which causes the plate to uplift consists of two components: the moment exerted on the tank wall by the liquid and the additional moment on the tank bottom. The values of these moments were found from Housner's analysis of tanks with rigid walls [272]. The two unknowns of the problem (the maximum compressive stress in the tank shell and the central angle of the contact area) were found by solving two nonlinear algebraic equations which govern both global vertical force equilibrium and global moment equilibrium. One disadvantage of this model is that it does not take into account the flexibility of either the tank wall or the bottom plate. Furthermore, it neglects the variation of dynamic pressure on the bottom plate and uses a constant value equal to the static pressure. In 1978, Wozniak and Mitchell [292] suggested a more realistic model for uplifting by including the flexural stiffness of the bottom plate, and this analysis was introduced in the AWWA D100 [6] and the API 650 Standards [7]. It was assumed that the contact area of the bottom plate with the foundation is a segment of an unknown central angle. Flexibility of the tank wall was not considered but the elastic behavior of the bottom plate was taken into account. The base plate was represented by a strip of a unit width in the circumferential direction because the relevant uplift region is assumed to be an annular ring of a width much smaller than the radius of the tank. The strip acts as a beam resting on a rigid foundation subjected to a liquid pressure and lifted up by a vertical force at its free end. The maximum value of the force that can be carried by the beam is calculated by invoking two plastic hinges: one at its free end and one at an intermediate point

in the uplifted portion of the beam. Because the wall thickness is usually larger than the thickness of the bottom plate, the assumption of a plastic hinge at the edge of the bottom plate is justified. Assuming no restraining effects from the shell and no membrane stress in bottom the plate, relations between the thickness of the plate, the plastic stress, applied distributed loads and the uplifted length can be found explicitly. If the tank experiences uplift, two forces resist such deformation, namely, the weight of the roof and the shell, and the weight of liquid that will be lifted up. By writing the equations of equilibrium of vertical forces and moments, the maximum compressive stress and the central angle can be found as in previous model. In 1986, Leon and Kausel [151] proposed some modifications to Wozniak and Mitchell's model. They concluded that this model, which forms the basis of provisions of API 650 Standard, can lead to a significant underestimation of maximum compressive stresses in the shell under the condition of moderate shell uplift, and overestimation of the contribution of fluid weight in resisting lift-off.

Moore and Wong [184] modified parameters defining the maximum width of the uplifted strip of the tank base and the associated compressive stresses in tank walls from those specified in the API 650 Standard which gives conservative values. They collected an extensive set of damage data from the 1964 Alaska, the 1971 San Fernando, the 1978 Miyagi-Ken-Oki and the 1980 Livermore earthquakes as well as past experimental results and reported that the correlation between predicted seismic resistance using the modified API code model and the observed damage was good, and that unanchored tanks with an aspect ratio of H/D between 0.6 and 1.4 were more prone to damage than were broader or more slender tanks with the same depth of contents. In the same year, 1984, Sakai, Ogawa and Isoe [240] discussed the elastic behavior of a cylindrical liquid storage tank under horizontal, vertical and rocking

motions. The shell was assumed ideally cylindrical, and nonlinear effects of the bottom plate uplift were neglected. They conducted experiments on model tanks to verify their analysis, and presented simplified procedures for analyzing fluid response to each type of motion. In 1986, Manos [172] proposed an empirical design approach regarding the tank-wall earthquake stability for unanchored cylindrical liquid storage tanks. Based on experimental evidences, he assumed an empirical compressive axial membrane stress distribution with a maximum value equal to 75% of theoretical buckling stress of a uniformly compressed perfect cylinder. By equating the tank resisting overturning moment calculated from assumed stress distribution with the earthquake induced overturning moment obtained from modified Housner's model considering impulsive response only, he found a limit impulsive acceleration coefficient that uplifting tanks could withstand. However, the complex dynamic uplift behavior of the bottom plate and its stiffness were ignored. In addition, this approach was only a design approximation and was not based on any rigorous analytical model. Manos concluded that existing approaches were unreliable in predicting damages, and that they underestimated the actual limit impulsive acceleration that tanks might withstand, and recommended that a realistic analytical treatment of nonlinear dynamic response mechanism of uplifting tanks should be developed.

In 1988, Natsiavas and Babcock [199] presented an analytical model for the response of an unanchored tank subjected to horizontal base excitation by using Hamilton's principle. Base plate uplift was modeled as a rotational nonlinear spring whose characteristics were obtained from previous static tilt tests. It was assumed that the tank rests on a flexible ground but with a rigid foundation, and equivalent springs were used for formulation of ground flexibility. They concluded that it can be significantly unconservative to calculate loads for an unanchored tank by assuming

the tank to be anchored. In another work, Natsiavas [198] showed that base uplift causes a dramatic reduction in the deflective beam-type stiffness of a tank which in turn reduces the tank response frequency and changes developed hydrodynamic loads significantly. He also provided an explanation for some great qualitative and quantitative differences in the behavior of a tank, resulting from its base fixity condition alone. He also showed comparisons between numerical results from his analysis with experimental data. In a following work [197], he presented another analytical model for the problem. He solved the hydrodynamic problem in closed form for the most general motion of the structure. Then, he applied Hamilton's principle to derive the equations of motion of the system. The uplifting behavior was modeled by an appropriate rotational spring placed between the foundation and the bottom of the tank. Effects due to ground flexibility, shell flexibility and liquid sloshing were also included. Using this model, results were obtained and compared with experimental data. Buckling of scale model tanks during experiments was also investigated. Furthermore, in 1989, he presented a couple of simplified models [196] determining the hydrodynamic loads during the seismic response of tall unanchored liquid storage tanks. In both models, the general procedure starts by solving the fluid response problem in closed form to eliminate all the unknowns associated with the hydrodynamic problem but the sloshing ones. In the first model, the geometrical discretization was performed by applying Hamilton's principle. In the second model, the system, parameters were identified by requiring the same base loads when the real system and the model were subjected to the same base motion.

In 1988, Peek [220] simplified a method of analysis for static lateral loads based on the assumption that the restraining action of the base plate can be modeled with

equivalent nonlinear springs. The displacements was decomposed using Fourier analysis. The solutions were compared with those from experiments and current U.S. design analysis methods. In a following work, Peek et al [217] described a simplified approach for determining the extent of the elephant foot buckling for ground supported unanchored liquid storage tanks subjected to seismic overturning moments. He reported that the ultimate seismic overturning moment that can be withstood by a tank is higher than the overturning moment at which the elephant foot buckling first occurs. In 1989, Fischer [64] considered analytically the frictional contact behavior of extensible and flexible strips on rigid grounds and loaded by a transversal pressure. He also investigated the uplift behavior of the strip. In 1994, Malhotra and Veletsos ([165], [166]) simplified the unanchored tank-liquid system to one degree of freedom system with rotational spring representing the rocking resistance of the base plate. The relationship between the base moment and the spring rotation was established by considering uniformly loaded, semi-infinite, prismatic beams that are connected at their ends to the cylindrical tank wall. However, the flexibility of the tank itself was ignored.

1.5.3 Numerical Analyses

The numerical techniques, specially the finite element method, are powerful tools to analyze the problem of unanchored tanks because of their flexibility and ability to model all the complications involved with the analysis of such tanks. Many researchers have employed these techniques to analyze the problem. Auli, Fischer and Rammerstorfer [11] presented an analysis for uplifting of unanchored tanks in 1985. They used the finite element technique to solve an axisymmetric uplift problem

whereas the bottom plate experiences a uniform uplift all around circumference. As an approximation, they considered the tank as a cylindrical shell resting on nonlinear springs without a bottom plate. Hence, the number of degrees of freedom and the number of elements were reduced, and no contact elements were needed to model the bottom plate. The stiffness of the uplifted bottom plate was represented by equivalent Winkler springs distributed on the lower edge of the shell wall. In order to determine the nonlinear characteristics of these springs, the bottom plate was modeled as a strip resting on a rigid foundation, and loaded by uniformly distributed as well as uplift forces. In addition to these forces, two springs representing bending and extensional stiffness of the tank wall were introduced at the free end, assuming that the fluid pressure acted only on the bottom plate and not on the tank shell. Based on resulting relationship between the uplifting force and the uplifting displacement, the vertical restraining action due to the weight of the fluid resting on the uplifted portion of the base plate was obtained and applied around the circumference of the shell. In Wozniak and Mitchell's model [292], this vertical resistance force was equal to the maximum hold down force, and was applied around the entire circumference except in the contact region leading to an overestimation of the resistance of the bottom plate, whereas in Auli's model this force was a deflection dependent force varied around the circumference.

Using a general purpose finite element computer code, Barton and Parker [16] investigated the seismic response of the liquid-filled cylindrical storage tanks. A time history analysis of a three-dimensional finite element model of an unanchored tank and its contents with a specified gap conditions between the tank base and the supporting floor to allow lift-off of the base was performed. Neither material nor geometric nonlinearities were considered in the analysis and the tank was assumed

to be subjected to only one direction of horizontal excitation. Furthermore, the fluid hydrodynamic problem was eliminated by lumping assumed percentage of the fluid mass to the tank wall and base plate. Results of the investigation indicated that stresses in the tank and resultant loads on the floor of an unanchored tank were much greater than those for a rigidly restrained tank and showed the importance of carefully considering the restraint conditions when performing seismic design calculations on storage tanks.

In 1986, a simplified method of analysis of unanchored tanks under static lateral loads was developed by Peek [222]. He used a similar analytical concept to that developed earlier by Auli et al. The interaction between the shell and the bottom plate was modeled by placing axial springs all around the lower edge of the shell. Axisymmetric solution of the bottom plate subjected to a uniform amount of uplift all around the circumference was used in order to obtain a force-deflection relationship for equivalent Winkler springs which represent the restraining action of the base plate. Knowing the relationship between the hold-down force and the uplift displacement, and using axisymmetric shell elements, the analysis of cylindrical shell was performed based on linear shell theory. It was also assumed that both the base plate and the shell remain elastic, and foundation is rigid. In a following work, Peek [219] used the finite difference energy method in conjunction with a Fourier series representation of the circumferential variation of displacements and obtained a numerical solution of two dimensional contact problem of a base plate under static lateral loads. Nonlinearities due to contact finite displacements and yield of the steel were included in the analysis. The equations for the shell were linearized to uncouple the equations for the Fourier displacement coefficients in the cylindrical shell and to enable the degrees of freedom for the shell to be eliminated by means of static the condensation at a little

computational cost. He compared the analytical results to experimental results and reported that they were in good agreement in some cases and not so good in others. He discussed a number of effects that could give rise to such differences and stated that in most cases they represent experimental conditions that were not known or modeled in the analysis. The analysis results were also compared to those from a simplified analysis in which the hold down action of the base plate was modeled by means of nonlinear Winkler springs. Peek concluded that large membrane stresses developed in the bottom plate carry most of the load on the uplifted region. In addition, Peek and Jennings [221] suggested that in order to increase the capacity of an unanchored tank to withstand lateral loads due to tilting, tank wall could be pre-uplifted all around the circumference by means of a ring filler. Depending on the frequencies of earthquake, lateral loads generated by ground motion for a preuplifted tank could be higher or lower than those for a tank without preuplift. However, they recommended that further investigations are needed to study the effectiveness of the method and to investigate the behavior of the base plate of a pre-uplifted tank before and after the earthquake.

In 1988, Haroun and Badawi [12] modeled the base plate in both its strip and circular configurations and investigated its nonlinear behavior under equivalent static uplifting forces using an approximate energy-based approach. This analysis differs from other available analyses in that the plate is modeled as a circular plate with an uplifted, crescent-shaped region rather than being modeled as a strip. The behavior of the plate under both small and large deflection assumptions, and the effects of stretching of its midplane were studied. The reliability of the crescent-shaped model was confirmed through a comparison with the analysis of an axisymmetric circular

model. The governing set of nonlinear equations was derived for the system by minimizing its potential energy with respect to the generalized coordinates. Upon solving these equations, the bending moments and stresses were evaluated throughout the plate by making use of the generalized coordinates. Results of these models clearly showed that for moderate values of the ground acceleration, the membrane actions developed in the plate increased its load-carrying capacity, yielding a much lower value for uplift displacements. They noted that the analysis under axisymmetric conditions yielded results comparable to those of the asymmetric case, but the former analysis is much simpler; it showed that the assumed deflection shape of the plate is an important factor only under small deflection assumptions since the solution is governed by the bending actions. Under large deflections, the membrane actions dominate and loads are carried mainly by inplane forces. A concurrent work, also was performed by Haroun and Bains [13], sought the same characteristics of the base plate by a nonlinear finite element shell program to study the static behavior of uplifted unanchored tanks. The program was extended to analyze the base plate and to assess the accuracy of the developed simplified energy-based models. A mesh generation scheme was used for the plate and an iterative scheme was adopted to find the location of the periphery of contact area. This area was found to be more as an ellipse rather than a circle but the corresponding changes in the maximum uplift length and the maximum uplift displacement were found to be negligible. It was shown that uplift is greatly reduced if the outer edge of the plate is restrained against rotation. Although the two approaches are different, they conform in results and conclusions.

In 1990, Yi and Natsiavas [294] presented a finite element model for the seismic response of liquid-filled tanks. They discretized the shell structure using cylindrical finite elements and applied Hamilton's principle in the structural domain to obtain

the equations of motion for the coupled fluid-structure system. The above analytical procedure eliminated the fluid hydrodynamic problem by employing the closed form solution for the hydrodynamic response problem, resulting in a compact system of equations of motion. Primary attention was paid to the formulation of the nonlinear base uplift problem. Effects due to the shell and ground flexibility also were included.

1.6 Simplified Design Guidelines

In addition to the conventional design standards and codes; The New Zealand recommendations [195], AWWA D100 [6] and API 650 Standards [7], the seismic design of cylindrical tanks was discussed by many investigators. URS Consultants [274] provided seismic verification of nuclear plant liquid storage tanks. Scharf et al [243] proposed rules for the design of unanchored liquid storage tanks. They described the present code as insufficient for the earthquake resistance design. Adams [3] developed a set of design rules that permit assessments to large liquid storage tanks. These rules have proposed to form an Appendix to the new British Standard BS7777. Kelly et al [138] examined conceptual methods and design issues of installing seismic isolators beneath liquid storage tanks. The performance of isolated tanks was then assessed with the use of two case studies. Tedesco [267] summarized the results of a comprehensive analytical investigation concerning the seismic analysis of ground supported circular cylindrical liquid storage tanks subject to a horizontal component of an earthquake ground motion. A procedure to evaluate the dynamic seismic response of a wide range of cylindrical liquid storage tanks was developed and incorporated into a BASIC computer program.

Shimizu ([252], [253], [254]) presented methods for seismic design of liquid storage tanks which account for the soil effect. In a following work [251], he presented a review of seismic studies and design of cylindrical liquid storage tanks. Sone and Suzuki [259] presented a calculation method from the viewpoint of the aseismic design convenience for liquid storage tanks and various piping systems established in industrial facilities such as petrochemical plant complexes. Utilizing the results obtained in the previous studies, he prepared a numerical diagram for various system parameters. Hashimoto et al [80] evaluated the seismic capacity of tanks against the potential failure modes of such tanks. Melerski [179] developed a simple method to analyze axisymmetric cylindrical liquid storage tanks. He further implemented the analysis into a computer program [178]. Veletsos [280] developed guidelines for designing of liquid storage tanks. Liu et al [155] presented a development and survey of some of the available analysis methods at that time.

1.7 Contribution of Research on Fluid Dynamics

1.7.1 Free Surface Sloshing Analysis

Sloshing is a free surface flow problem in a tank which is subjected to forced oscillation. Clarification of the sloshing phenomena is very important in the design of the tank. The violent sloshing creates localized high impact loads on the tank roof and walls which may damage the tank. Early simulations of the liquid sloshing problem have mostly been performed with waves of small steepness. The sloshing height was assumed to be too small so that the nonlinear boundary conditions may be neglected. Jacobsen [129] determined hydrodynamic pressures on a cylindrical

tank. Graham and Rodriguez [71] gave a very thorough analysis of the impulsive and convective pressures in a rectangular container.

The most commonly applied idealization for estimating liquid response in seismically excited rigid, rectangular and cylindrical tanks was formulated by Housner [112] in 1957. He divided hydrodynamic pressures of contained liquid into two components: the impulsive pressure caused by the portion of the liquid accelerating with the tank and the convective pressure caused by the portion of the liquid sloshing in the tank. The convective component was modeled as a single degree of freedom oscillator. The study presented values for equivalent masses and their locations which duplicate forces and moments exerted by a liquid on a tank. Properties of the mechanical model can be computed from the geometry of the tank and the characteristics of the contained liquid. Housner's model ([111], [112]) is widely used to predict the maximum seismic response of tanks by means of a response spectrum characterizing the design earthquake ([272], [292]).

In 1989, Mclver [177] considered the two-dimensional sloshing of a fluid in a horizontal circular cylindrical container and the three-dimensional sloshing of a fluid in a spherical container. He used the linearized theory of water waves to determine the frequencies of free oscillations under gravity of an arbitrary amount of fluid in such tanks. Special coordinate systems were used and the problems were formulated in terms of integral equations which were solved numerically for the eigen values. Tables of the sloshing frequencies were presented for a range of fill-depths of the containers.

It was not until late that researchers started to investigate the nonlinear fluid sloshing problem. Numerical methods presented previously for the sloshing analysis can be roughly classified into three methods: the finite difference method, the

boundary element method and the finite element method. In 1963, Hutton [118] and Kamatsu [136] obtained nonlinear frequency response curves of a liquid by using perturbation techniques. They also studied the stability of the surface sloshing. In 1980, Nakayama and Washizu ([191], [192]) modeled the nonlinear sloshing by finite element and boundary element methods and carried out numerical simulations of a two-dimensional liquid under horizontal and pitching periodic ground motions. In 1986, Ramaswamy [229] modeled the nonlinear sloshing of sinusoidally-excited liquids with viscous damping. In a following work [228], he used a Lagrangian-Eulerian finite element method to model the free surface fluid flow.

In 1987, Yamada [293] discussed the effect of nonlinear boundary conditions at the liquid surface on the sloshing heights in cylindrical tanks under horizontal and vertical ground motions. Based on a comparison with data obtained by linear analysis, he reported that this effect depends mainly on both the dimensionless sloshing height and the dimensionless liquid depth, as far as a small sloshing height is concerned. He proposed a simple formula for estimating this effect. On the basis of the large sloshing heights recorded during the 1983 Nihonkaichubu earthquake, he estimated the sloshing heights under nonlinear conditions to be about 10-25% larger than those calculated under linear conditions. Taking this into account, he stated that the response spectra of relatively long-period ground motions deduced from the recorded sloshing heights are nearly equal to the two-dimensional response spectra calculated from strong-motion seismograms. In the same year, Ibrahim [122] has conducted experimental investigations concerning the liquid sloshing in an excited tank. In 1988, Lepelletier [152] developed a nonlinear model to describe the fluid motion in a tank. He studied the liquid response behavior near resonance and the transient behavior

of liquid in the sense of modal superposition when the liquid is subjected to steady-state periodic basin excitations. It was observed that shallow water waves predicted by linear theory becomes inadequate near resonance and that the wave shape is very sensitive to the frequency of excitation near resonance.

The fluid-structure interaction problem with the free surface sloshing was also investigated. Liu ([154], [156], [157]) presented a variational principle for fluid-structure interaction problems with sloshing that accounts for both seismic and body forces. He showed that various fluid-structure interaction formulations may be obtained from the developed functional. Bauer et al [19] analyzed the nonlinear hydroelastic vibrations of two cases of an infinitely long rectangular container of finite width and filled to a certain height with a compressible and non-viscous liquid. The first case was that in which the free surface was covered by a flexible membrane, exhibiting a nonlinear stress-strain relation and large oscillation amplitudes. This system exhibited a hard vibration. In the second case the hydroelastic vibrations of a liquid with a free surface, performing large amplitudes, and a nonlinear flexible membrane bottom has been treated. The influence of various system parameters on the coupled natural frequencies was investigated. The liquid exhibited a softening vibration characteristic, while the membrane shows a hardening effect, which with the increase of membrane prestrain could change to a soft vibration.

In 1989, Barron and Chng [15] studied fluid sloshing problems in circular containers by both theoretical and experimental methods. A circular cylindrical container with various levels of fluid attached to a low frequency suspension was analyzed by means of the method of asymptotic expansion. Experimental studies in the form of resonance and transient vibration tests have been conducted on a test rig. A theoretical analysis was applied to a mathematical model of the test rig. The equations of

motion were simulated by a digital simulation method, for both linear and nonlinear conditions. Results showed parametric resonance effects of the fluid wave height and a horizontal fluid force wave forms. Kobayashi et al [140] conducted experimental and analytical study to determine the liquid natural frequencies and the resultant slosh forces in horizontal cylindrical tanks. They presented a study of the liquid sloshing response for small and large wave heights. In the former case, they presented an effective calculation method of the longitudinal slosh response by substituting an equivalent rectangular tank for a horizontal cylindrical tank. In the latter case, impulsive sloshing forces were observed for longitudinal excitation when the slosh liquid hit the top of the tank. They reported that the measured slosh forces including the impulsive forces were larger than the calculated ones.

Nash et al [193] treated large amplitude surface waves by expanding liquid elevations above mean free surface and velocity potentials in terms of a power series involving a dimensionless parameter which is a function of the peak amplitude of the tank excitation as well as the tank radius. Minowa [182] performed a similar study and concluded that the deformation of side walls produced the heaving type sloshing mode. He tried some nonlinear and linear sloshing analyses to reach a better understanding of the high sloshing waves. Popov et al [225] presented a numerical solution of the nonlinear liquid motion in a horizontal cylindrical container with circular cross section. They discretized and solved the 2-D governing differential equations in an Eulerian mesh. Li et al [153] obtained the critical stability conditions for large amplitude water wave oscillations.

In 1991, Krasnopol'skaya et al [143] studied the possible modes of vibration of the free surface of a liquid in a rigid container. They presented results of a study on interaction of regular and chaotic vibrations of the free surface of a liquid inside

a rigid cylindrical shell, excited by an electric motor. In 1992, Kurihara et al [144] investigated experimentally the sloshing impact on a roofed tank. They proposed a formula to predict the impact pressures caused on the roofed liquid tanks due to sloshing. Hwang et al [121] employed the panel method, which was based on the boundary integral technique, to investigate the three dimensional sloshing problem. In 1993, Veletsos [276] investigated the sloshing action of layered liquids in rigid cylindrical and long rectangular tanks. The analysis was formulated for systems with N superimposed layers of different thickness and densities. In the same year, Isaacson [124] studied the earthquake-induced sloshing in rigid circular tanks.

In addition to these investigations, shaking table tests were conducted by Okamoto et al ([207], [208], [209]) to simulate the two-dimensional liquid sloshing behavior. They also performed numerical simulations for the sinusoidally-excited liquids by employing the Lagrangian-Eulerian finite element method. They considered the large amplitude 2-D sloshing wave in a multi-sloped wall tank with roof. In this investigation, the developed analysis accommodates double-valued free surface function.

Prediction of the transient response of liquid subjected to seismic-type ground excitation has not been attempted until recently due to the complex nature of the physical and numerical behavior of liquid under prolonged transient and steady state base shaking. Haroun and Chen ([32], [90]) addressed the sloshing phenomenon in seismically-excited rectangular liquid storage tanks. They employed a semi-analytical method to study the effect of large amplitude sloshing on two-dimensional tanks under arbitrary horizontal excitations. The nonlinearity of both the kinematic and the dynamic conditions was considered. Because the location of the free surface is unknown, a numerical scheme was developed to transform a two dimensional uniform rectangular grid into boundary conforming curvilinear grid with prescribed arbitrary

boundaries. A set of governing nonlinear equations was obtained and solved in the uniform rectangular mesh by employing a finite difference scheme. Three-dimensional large amplitude sloshing in rectangular tanks has also been attempted. Su ([261], [262]) has performed numerical simulation of the three-dimensional large amplitude liquid sloshing in rectangular containers subjected to vertical excitation.

1.7.2 Fluid-Structure Interaction

The dynamic interaction between an elastic structure and a fluid has been the subject of intensive investigations in recent years, e.g. ([45], [57], [67], [73], [161], [163], [232], [255]). Since analytical solutions procedures are available only for very simple problems, numerical approaches, which can be formulated in the time or frequency domain, had to be employed, e.g. ([54], [131], [150], [210], [241], [242]). Vonestorff et al [285] investigated the coupled fluid-structure systems subjected to dynamic loads using the finite element and boundary element methods. Feng et al [58] analyzed the nonlinear three dimensional fluid-structure interaction by using the finite element method for the structure and the finite-infinite element method for the fluid. The infinite element was also used by Olson [211] to present a procedure to analyze fluid-structure interaction.

Since the variational principles are employed to derive numerical solutions, many researchers have attempted to derive variational principles for different classes of the fluid-structure interaction problems. Pinsky and Abboud [224] proposed two mixed variational principles for transient and harmonic analyses of non-conservative coupled exterior fluid-structure interaction systems. Kock and Olson [141] presented a finite element formulation directly derived from a variational indicator based on Hamilton's

principle. Liu [157] presented a general variational principle for fluid-structure interaction problems with sloshing. Abboud [1] proposed a mixed variational principle for transient and harmonic analysis of nonconservative coupled structure-exterior fluid systems. The formulation provided a basis for finite element approximation which is applicable to the analysis of radiation from shell structures with viscoelastic compliant coatings. In addition to the variational principles, energy methods have been employed to investigate the problem. Zeng et al [298] developed an energy-based symmetric coupled finite element and boundary integral method which is valid for all frequencies.

The size of the coupled fluid-structure interaction problem is generally large. Many researchers have attempted to reduce the problem size in different ways. Seybert [247] employed Ritz Vectors and Eigenvectors along with a combination of finite element and boundary element methods to reduce the problem size. Haroun [106] employed a boundary integral technique to evaluate the added mass matrix to the tank shell due to the fluid. Rajasankar et al [227] presented the results of investigations conducted to evaluate the added mass to represent the fluid effect in 3-D problems.

Out of all the work done in the area of developing a finite element method for fluid-structure interaction problems, two approaches predominate. In the first approach, the displacement based method, the displacements are the nodal variables in both the fluid and the structure. Belytschko and Kennedy ([20], [21], [22]), Bathe and Hahn [18], Nitikitpaiboon and Bathe [202] and Chopra et al [34] described the method in detail. This approach is not well suited for problems with large fluid displacements. Another difficulty with this method is that special care must be taken to prevent zero-energy rotational modes from arising. In the second approach, the

potential-based method, displacements remain the nodal variables in the structure, while velocity potentials or pressures are the unknowns in the fluid. Zienkiewicz and Newton [301], Morand and Ohayon [185], Everstine et al ([55], [56]), Olson and Bathe ([212], [213]) and others ([77], [206], [300]) demonstrated techniques for formulating finite elements using potential-based methods. In all these works, only a linearized version of the problem has been considered.

Several finite element studies have considered the gravity and free surface effects along with the fluid structure interaction. Wilson and Khalvati [291] incorporated the gravity and the free surface effects in a displacement-based method with rotational constraints. They demonstrated results for both a static and a dynamic floating body problem. Their method necessitates the use of a reduced integration scheme to prevent element locking. Aslam [10] incorporated the linearized dynamic free surface condition into a velocity potential-based finite element fluid formulation, but did not consider the fluid-structure interaction problem. Ohayon [205] included gravity terms in a displacement-based finite element method for fluid-structure modal analysis.

The search for variational principles resembling Hamilton's principle for fluid mechanics problems has concerned many researchers including Seliger and Whitham [245], Miles [180], Serrin [246] and Luke [162]. While Seliger and Whitham have pointed out that the Lagrangian density for the fluid variational principle is the pressure, they did not consider the implication of a variable boundary. Luke has incorporated a variable boundary in his variational principle in order to generate the governing equations for the special case of gravity waves in an incompressible fluid. The role of the Bernoulli constant as a Lagrange multiplier constraining global conservation of mass was not noted by any of the aforementioned researchers. Kock and Olson [141] were the first to use Bernoulli constant in there formulation to conserve

the total mass. Ikegawa and Washizu [123] introduced a variational principle, utilizing the stream function, in order to model incompressible flow with a free surface under gravity using the finite element method but did not extend their method to the general compressible fluid-structure problem. More recently, Ecer and his coworkers ([50], [286], [49]) suggested variational approaches for use in modelling incompressible, viscous fluid flows but have not extended their approach to include fluid-structure interaction. Liu and Uras [157] using a variational principle which is not based on Hamilton's principle, developed a mixed variational formulation and demonstrated that several of the fluid-structure interaction formulations already in use can be obtained from it.

Birk et al [24] investigated the influence of fluid-containing appendages on the dynamic response of multi-degree-of-freedom system subjected to stochastis environmental loads. They expressed the modal properties of the system comprising of a fluid-containing appendage attached to a multi-degree-of-freedom system in terms of the individual dynamic properties of the primary and the secondary systems. They obtained the peak response value at any level on the structure by following the evolutionary distribution of the extreme values and reported that an important feature of the combined system was that the response of the primary system was suppressed when one of the sloshing modes of the secondary fluid appendage is tuned to the fundamental mode of the primary system. They used a building with a water tank situated at any floor and excited by an earthquake to illustrate the methodology.

1.8 Soil-Tank Interaction

The problem of soil-tank-fluid interaction was addressed by many investigators. Haroun and Abdel Hafiz [92] considered soil-tank interaction effects and showed that it substantially reduced the amplified tank response. Haroun and Abou-Izzeddine ([83], [84]) performed parametric study on the dynamic soil-tank interaction under horizontal seismic excitations. Hori [109] presented the effects of soil on the dynamic response of liquid-tank systems. Fisher et al [65] presented a dynamic response analysis of vertically excited liquid storage tanks including both the liquid-tank and the liquid-soil interaction. The system considered was a thin-walled elastic cylindrical shell entirely filled with an incompressible and inviscid fluid, resting on a flexible foundation over an elastic halfspace with frequency dependent stiffness and damping parameters.

Zaman et al [296] developed an analytical formulation to examine the flexural behavior of rectangular foundations resting on elastic half space and supporting cylindrical tanks. The formulation was based on the principle of minimum potential energy and was applicable to problems having geometric and loading symmetry with respect to the x and y axes. The deflected shape of the foundation was approximated by a polynomial in terms of the even powers of x and y, and the contact stress distribution was assumed to be a function of the foundation deflection. The wall-foundation interaction was included by modifying the wall deflection function and satisfying the compatibility conditions applicable to the junction between the foundation and the tank wall.

Shimizu [254] presented a study which investigated the seismic design of cylindrical liquid storage tanks with a rigid foundation slab resting on elastic soil subjected

to sway and rocking motions. This study concerned with the derivation of a vibration for a cylindrical tank as a super-structure. In a following work [253], he presented a study that concerns the seismic design of a cylindrical liquid storage tank with rigid foundation resting on elastic soil subjected to earthquake ground motions. He showed a procedure of a whole vibration model of the tank-foundation-soil system and proposed a conventional seismic design procedure for the tank. Furthermore, Shimizu [252] presented a seismic design method of cylindrical liquid storage tanks resting on elastic soils that are subjected to horizontal ground motions. He derived equations of motion of a lumped-mass model for describing the coupled motion of the tank-liquid-foundation system.

Zaman and Mahmood [297] examined the response of a cylindrical storage tank foundation system using the finite element technique which considered the interaction between the tank wall foundation and supporting soil medium. Emphasis was given to modeling of nonlinear deformation characteristics of the interface between the foundation and the soil medium using a joint element. He presented parametric studies to assess the effects of depth of foundation embedment, interface roughness, soil nonhomogeneity, nonlinearity, and relative rigidities of the tank wall-foundation and soil systems.

Seeber et al [244] presented three dimensional analysis of the dynamic behavior of liquid filled elastic cylindrical tanks based on flexible grounds, undergoing horizontal and vertical earthquake excitation. The interaction of the ideal fluid with the elastic shell and with the flexible ground yielded a problem of linear potential theory which was solved together with the equations of motion of the shell and of the ground. With the unknown nodal shapes of vibration developed in Fourier and

in Fourier Bessel series, the partial differential equations were transformed into coupled generalized equations of vibration by a weighted residual approach. The results showed the strong influence of the flexible ground characterized by a remarkable shifting of natural frequencies, by the existence of additional natural frequencies and by high damping ratios.

Veletsos et al [278] made a study of the effects of soil-structure interaction on the response of liquid containing upright circular cylindrical tanks subjected to a horizontal component of ground shaking. He generalized the mechanical model for laterally excited rigid tanks supported on a nondeformable medium to permit consideration of the effects of tank and ground flexibilities, and base rocking. Responses were evaluated for harmonic and seismic excitations over a range of tank proportions and soil stiffnesses, and the results were presented in a form convenient for use in practical applications.

Hangai and Ohmori [78] investigated a soil-structure interaction problem which dealt with the nonlinear contact vibration of a rigid as well as a flexible bar rested on uniformly distributed Winkler type springs and considered uplift of a portion of the bar. Bars were subjected to both vertical dead load and time varying moment around the center of gravity to model the external excitation from the superstructure. The finite difference method was used in order to discretize the equilibrium equations of motion, derived under small deflection theory, and the Runge-Kutta method was applied to the numerical analysis. Hangai and Ohmori concluded that, for a flexible structure, soil reaction took complicated modes along the time history and vertical displacement components of the center of gravity played an important role in the nonlinear soil-structure interaction problem considering uplift.

Ishida et al ([126], [127]) presented a dynamic mechanical model of a four degree of freedom mass-spring system for the rocking response analysis of unanchored tanks by considering the partial uplift of the bottom plate as a rotational spring of bilinear type. The finite element method was used to analyze the deflection of the bottom plate by replacing it with an elastic-plastic beam model. Also, they proposed a calculation method for the bottom plate uplift based on the small deflection theory and assuming a rigid foundation. They performed a shaking table experiment and a static tilt test on a stainless steel model tank, provided with a rubber mat in order to simulate the actual soil foundation effect, and test results were compared with those obtained from the four degrees of freedom system.

D'Orazio [47] simulated the uplift behavior with model tests and measured both the amount of uplift and the radial displacements. He gave an interpretation of the measurements, and illustrated a method for estimating radial displacements based primarily on deformations at the foundation level. Both flexible and rigid foundations were considered. Radial displacements of uplifted and anchored tanks were compared. He concluded that the foundation deformation and uplifting control the radial displacements.

The settlement of soil due to the large pressure exerted from liquid storage tanks was also investigated. Ma et al [164] presented analysis of such a system. The analysis includes the effect of sloshing of liquid in the tank and the associated hydrodynamic pressure, and the effect of coupling between liquid, tank and soil foundation. The effect of tank settlement on its response was also presented in ([23], [46], [48], [59], [60], [110], [260], [263], [264]). In addition, analysis and design of the tank foundation was discussed ([201], [275], [287]).

1.9 Contact Analysis

The evolution of the contact analysis is strongly related to the analysis of unanchored liquid storage tanks. The successive contact and separation between tank base plate and underlying foundation is a special case of the contact problem between two bodies. However, the developed algorithm handles the contact problem in its general form which make it necessary to present a brief review of contact mechanics history.

Modern contact mechanics begins in 1882 with the publication of the work by Hertz [107]. Analytical solutions to the problem were presented before the appearance of digital computers. These solutions employed the theory of elasticity and were limited to simple linear cases of contact. Moreover, since for most problems the exact contact surfaces are not known a prior, their application is further restricted. Gladwell [68] tackled the problem with the aid of Papkovich-Neuber form of the equilibrium equations. Signorini [257] formulated the general problem of a linear elastic body in frictionless contact with a rigid foundation. Shtaerman [256] showed various solutions using the methods of integral transforms and complex potentials in theory of elasticity. These methods allowed for a more general analytical treatment of certain, still very restricted, classes of contact problems. Fichera [63] presented a formal mathematical treatment of the Signorini problem within the framework of boundary value problems governed by unilateral constraints. In a following work [62], he presented a more complete and general solution of the problem.

The numerical techniques are powerful tools to analyze the contact problem because of their flexibility and ability to model all complications involved with the analysis of such problems. The finite element method was introduced for the problems of structural analysis by Turner [271], Clough, [39], and simultaneously by Argyris [8].

Later the method was extended to structural mechanics, among many other fields, by numerous researchers. Numerical contact algorithms have been proposed in the early 70s to handle the complex nature of the physical and numerical behavior of contact problems. Conry and Seireg [40] treated contact problems as quadratic programming problems. Subsequently, Chan and Tuba [29], Kalker [135] and Panagiotopoulos [214] among others explored the same line of thought. At the same time, the work of Hughes [117], based on a Lagrange Multiplier method, significantly contributed to the development of robust finite element algorithms applicable to large scale computations. Glowinski and coworkers [69] offered a comprehensive exposition of various optimization techniques and their application to the solution of problems characterized by unilateral boundary conditions. Courant [43] used the penalty approximations to solve the contact problem. Luenberger [160] reviewed solutions to the contact problem in his book. Hestenes [108] used augmented Lagrangian methods to solve the problem. Powell [226] improved this method by combining the classical penalty treatment with that of Lagrange multipliers to attaining more satisfactory performance than either one of the above methods when employed separately. A detailed presentation of both theoretical and some numerical aspects of contact problems is contained in [139].

Recently, several contact algorithms have been proposed [215] and incorporated into commercially available Finite Element softwares. Bathe and Chaudhary ([17], [31]) presented a solution methods for the analysis of contact between two or more contact bodies. In there work, they implicitly enforced the contact constraints using an augmented Lagrange multiplier technique which seriously affects the quadratic convergence of the Newton-Rapson method. Eterovic et al [53] proposed a solution technique to enforce these constraints explicitly by means of a gap function. He presented a solution technique that admits the use of a line search procedure to enlarge

the region of convergence. He reported that this approach has significantly improved the convergence of the analysis, however, it yields unsymmetrical stiffness matrix. Pian et al [223] derived a modified complementary energy principle by introducing the continuity at the contact surface as the condition of constraint and the reactions at contact surface as additional field variables. He outlined an iterative procedure using a stress hybrid element for incorporation in numerical analyses.

Chapter 2

Nonlinear Dynamic Analysis of Plates and Shells

In this chapter, a nonlinear finite element formulation is presented for the three and two dimensional analysis of shells which accounts for large deformation and rotation effects, and accommodates material nonlinearities. The formulation applies to the practically important cases of shells of revolution, tubes, rings, beams, frames, arches, plates and doubly curved shells. Transverse shear deformations and geometric nonlinearities are accounted for. The approach is deduced and adapted from several other works in the area, [13], [115] and [116].

2.1 Degenerated Isoparametric Shell Element

The analysis of thin-walled structures requires a reduction from three to two dimensions. This may be carried out before or together with discretization using either a plate or shell theory, or directly the three dimensional field equations. Despite the fact that in both cases the continuum is degenerated to a surface structure, the

term "degeneration" is used only for the latter approach. The simplicity in accommodating arbitrarily large deformation and rotation problems is a favorite advantage to degenerated curved shell elements.

2.1.1 Basic Assumptions

The shell theory used is based on a degeneration of 3-D elasticity using the following three assumptions

1. Normals to the shell middle surface before deformation remain straight, but not necessarily normal to the middle surface after deformation.
2. The normal stress, in the thickness direction, is zero.
3. The shell thickness remains constant during the deformation

Assumption (1) is equivalent to taking into account the effect of transverse shear deformation and it has been widely used in recent years both in the context of linear and nonlinear analysis of shells. On the other hand, assumption (2) is the typical plane stress condition, traditionally used in plate and shell theory. This condition, namely plane stress hypothesis, is then used to reduce the three-dimensional constitutive relations to surface ones. Finally, assumption (3) implies that the thickness of the shell, measured along the fiber direction, at each point does not change in different deformed configurations of the shell, which implies zero strain along the fiber direction. This last assumption, namely fiber inextensibility condition, is essential for an adequate kinematic description of the large rotations of the fiber directions.

2.1.2 Three Dimensional Element Mechanics

Coordinate Systems

Four different coordinate systems have been used in the development of the curved degenerated shell element. These coordinate systems are defined as follows

1. The global Cartesian coordinate system which is used as a fixed reference frame for the shell motion, deformation and geometry. The unit vectors $\mathbf{i}$, $\mathbf{j}$ and $\mathbf{k}$ are in the directions of X, Y and Z, respectively.

2. The nodal vectors system denoted by $\mathbf{v}_{1i}$, $\mathbf{v}_{2i}$ and $\mathbf{v}_{3i}$ for node i with its origin at the midsurface. This system is used as a reference frame for the rotations. The nodal vector $\mathbf{v}_{3i}$ represent the fiber direction which determines the direction on which the fiber inextensibility condition is enforced, and is given by

$$\mathbf{v}_{3i} = \frac{\mathbf{x}_i^t - \mathbf{x}_i^b}{\|\mathbf{x}_i^t - \mathbf{x}_i^b\|} \tag{2.1}$$

   where $\mathbf{x}_i^t$ and $\mathbf{x}_i^b$ are the coordinates of node i on the top and bottom shell surfaces, respectively. The other two nodal vectors are picked up such that if $\mathbf{v}_{3i}$ is close to $\mathbf{k}$, then $\mathbf{v}_{1i}$ and $\mathbf{v}_{2i}$ are close to $\mathbf{i}$ and $\mathbf{j}$, respectively. Figure (2.1) shows the algorithm used to satisfy this condition.

3. Natural coordinate system ξ, η and ζ in which ξ and η lie in the middle plane, whereas the linear coordinate ζ spans the thickness direction.

4. The lamina system denoted by $\mathbf{x}'$, $\mathbf{y}'$ and $\mathbf{z}'$ is defined at each integration point to describe the directions in which the stresses and strains are obtained. The constitutive relations are written and reduced with respect to this coordinate

system. The direction $\mathbf{z}'$ is the direction in which the zero normal stress condition, $\sigma_{z'} = 0$, is satisfied. As shown in Figure (2.2), the vector $\mathbf{z}'$ is constructed to be perpendicular to the midsurface at the integration point, while $\mathbf{x}'$ and $\mathbf{y}'$ vectors are constructed to be as close as possible from the unit tangent vectors to the ξ and η coordinates, $\mathbf{e}_\xi$ and $\mathbf{e}_\eta$, respectively. This is achieved as follows

$$\mathbf{e}_\xi = \frac{\partial \mathbf{x}}{\partial \xi} / \| \frac{\partial \mathbf{x}}{\partial \xi} \| \tag{2.2}$$

$$\mathbf{e}_\eta = \frac{\partial \mathbf{x}}{\partial \eta} / \| \frac{\partial \mathbf{x}}{\partial \eta} \| \tag{2.3}$$

$$\mathbf{z}' = \frac{\mathbf{e}_\xi \times \mathbf{e}_\eta}{\|\mathbf{e}_\xi \times \mathbf{e}_\eta\|} \tag{2.4}$$

$$\mathbf{e}_\alpha = \frac{\frac{1}{2}[\mathbf{e}_\xi + \mathbf{e}_\eta]}{\|\frac{1}{2}[\mathbf{e}_\xi + \mathbf{e}_\eta]\|} \tag{2.5}$$

$$\mathbf{e}_\beta = \frac{\mathbf{z}' \times \mathbf{e}_\alpha}{\|\mathbf{z}' \times \mathbf{e}_\alpha\|} \tag{2.6}$$

$$\mathbf{x}' = \frac{\mathbf{e}_\alpha - \mathbf{e}_\beta}{\sqrt{2}} \tag{2.7}$$

$$\mathbf{y}' = \frac{\mathbf{e}_\alpha + \mathbf{e}_\beta}{\sqrt{2}} \tag{2.8}$$

It is worth noting that $\mathbf{v}_{3i}$ can be obtained as the effective normal vector to the isoparametric shell surface at each node. Alternatively, it could be a given thickness direction, not necessarily orthogonal to the shell middle surface, specified for each node. This latter definition, adopted in this work, is useful for avoiding geometry discontinuities in folded shell situations.

For the purpose of transformation between various coordinate systems, the following two transformation matrices $[q]$ and $[s]$ are constructed from the lamina and nodal vectors, respectively. The matrix $[q]$ transforms from the global system to the lamina system and given as

$$\mathbf{q} = [\mathbf{x}' \ \ \mathbf{y}' \ \ \mathbf{z}']^T \tag{2.9}$$

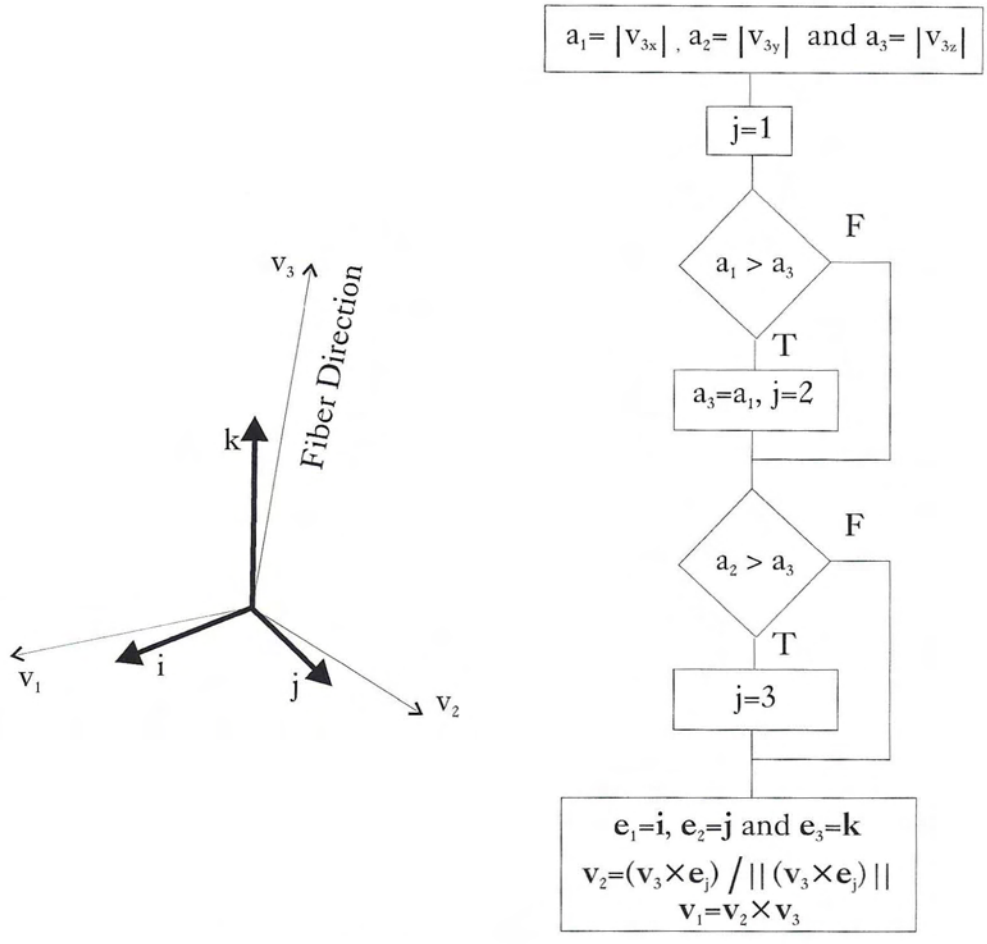

Figure 2.1: Nodal Coordinate System

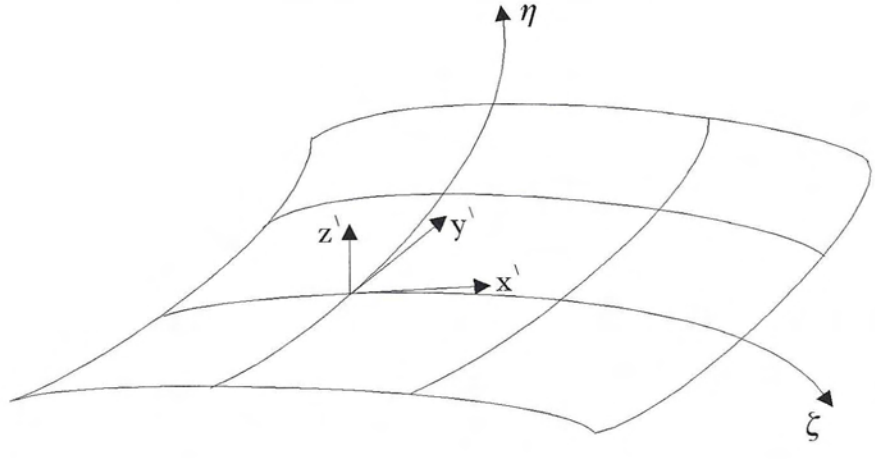

Figure 2.2: Lamina Coordinate System

while the matrix $[s]$ transforms from the nodal system to the global system and given as

$$\mathbf{s} = [\mathbf{v}_{1i} \;\; \mathbf{v}_{2i} \;\; \mathbf{v}_{3i}] \tag{2.10}$$

Figure (2.3) shows the relationship between the various coordinate systems.

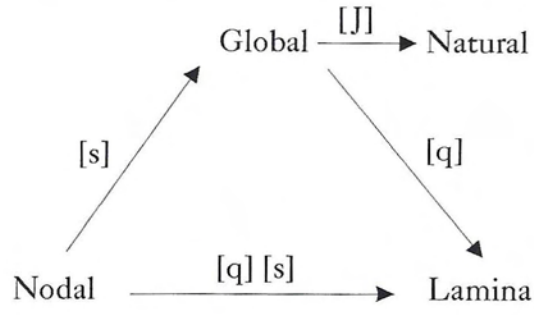

Figure 2.3: The Relationship Between the Coordinate Systems

Geometric Description

The geometry of a typical three dimensional shell element is defined using the Cartesian coordinates of the top and bottom surfaces corresponding to each node, thus

$$\begin{Bmatrix} x \\ y \\ z \end{Bmatrix} = \sum_{i=1}^{n} N_i(\xi,\eta) \left[\frac{1+\zeta}{2} \begin{Bmatrix} x_i^t \\ y_i^t \\ z_i^t \end{Bmatrix} + \frac{1-\zeta}{2} \begin{Bmatrix} x_i^b \\ y_i^b \\ z_i^b \end{Bmatrix} \right] \tag{2.11}$$

$$= \sum_{i=1}^{n} N_i(\xi,\eta) \begin{Bmatrix} x_i \\ y_i \\ z_i \end{Bmatrix}_{\zeta} \tag{2.12}$$

or consizly as

$$\mathbf{x} = \sum_{i=1}^{n} N_i(\xi,\eta)\mathbf{x}_{i\zeta} \tag{2.13}$$

where the index i refer to the i'th node and n is the number of nodes per element. In order to construct the Jacobean matrix, the natural coordinate derivatives are obtained as

$$\frac{\partial \mathbf{x}}{\partial \xi} = \sum_{i=1}^{n} \frac{\partial N_i(\xi,\eta)}{\partial \xi} \mathbf{x}_{i\zeta} \tag{2.14}$$

$$\frac{\partial \mathbf{x}}{\partial \eta} = \sum_{i=1}^{n} \frac{\partial N_i(\xi,\eta)}{\partial \eta} \mathbf{x}_{i\zeta} \tag{2.15}$$

$$\frac{\partial \mathbf{x}}{\partial \zeta} = \frac{1}{2} \sum_{i=1}^{n} N_i(\xi,\eta) \left[\mathbf{x}_i^t - \mathbf{x}_i^b\right] \tag{2.16}$$

The Jacobean matrix required to transform derivatives between the global and natural coordinate systems is then given by

$$\mathbf{J} = [\frac{\partial \mathbf{x}}{\partial \xi} \ \frac{\partial \mathbf{x}}{\partial \eta} \ \frac{\partial \mathbf{x}}{\partial \zeta}]^T \tag{2.17}$$

Kinematic Description

The kinematics of the shell element are defined by invoking the isoparametric hypothesis that the same expressions are used for kinematics as for geometry with displacement variables in place of coordinate variables. This assumption leads to

$$\left\{ \begin{array}{c} u \\ v \\ w \end{array} \right\} = \sum_{i=1}^{n} N_i(\xi,\eta) \left[\left\{ \begin{array}{c} \overline{u}_i \\ \overline{v}_i \\ \overline{w}_i \end{array} \right\} + \frac{\zeta t_i}{2} \mathbf{R}_i \boldsymbol{\theta}_i \right] \tag{2.18}$$

or concisely

$$\mathbf{u} = \sum_{i=1}^{n} N_i(\xi,\eta) \left[\overline{\mathbf{u}}_i + \frac{\zeta t_i}{2} \mathbf{R}_i \boldsymbol{\theta}_i \right] \tag{2.19}$$

where $\overline{u}_i$, $\overline{v}_i$ and $\overline{w}_i$ are the middle surface displacements at node i in the X, Y and Z directions, respectively, and t_i is the shell thickness at node i computed as

$$t_i = \|\mathbf{x}_i^t - \mathbf{x}_i^b\| \tag{2.20}$$

At this point, there are two possible choices for the rotation vector $\boldsymbol{\theta}$: either the rotations around the global axis or the rotations around the vectors $\mathbf{v}_{1i}$ and $\mathbf{v}_{2i}$ are used. Thus,

$$\mathbf{R}_i\boldsymbol{\theta}_i = \begin{bmatrix} 0 & v_{3z} & -v_{3y} \\ -v_{3z} & 0 & v_{3x} \\ v_{3y} & -v_{3x} & 0 \end{bmatrix}_i \begin{Bmatrix} \theta_x \\ \theta_y \\ \theta_z \end{Bmatrix}_i \tag{2.21}$$

or

$$\mathbf{R}_i\boldsymbol{\theta}_i = \begin{bmatrix} -\mathbf{v}_{2i} & \mathbf{v}_{1i} \end{bmatrix} \begin{Bmatrix} \theta_1 \\ \theta_2 \end{Bmatrix}_i \tag{2.22}$$

The global rotations are required when other elements that uses global rotations are used with the degenerated shell element. In such a case, special attention has to be paid to the drilling degree of freedom to avoid singular stiffness matrix.

Strain-Displacement Matrix

In application to shells, special attention needs to be given to transverse shear and membrane components to prevent the mesh locking phenomena. A particularly effective treatment may be performed by employing the reduced selective integration concept. In the present formulation, the strain-displacement matrix is formulated such that each component is separated from the others. This is achieved through the following definition of $\mathbf{B}$

$$\mathbf{B} = [\mathbf{B}_1\ \mathbf{B}_2\ \cdots\ \mathbf{B}_n] \tag{2.23}$$

where n is the number of nodes per element. The strain-displacement transformation may be written as

$$\boldsymbol{\epsilon} = \left\{ \begin{array}{c} \epsilon_{x'} \\ \epsilon_{y'} \\ \gamma_{x'y'} \\ \gamma_{z'y'} \\ \gamma_{z'x'} \end{array} \right\} = \left\{ \begin{array}{c} \frac{\partial u'}{\partial x'} \\ \frac{\partial v'}{\partial y'} \\ \frac{\partial v'}{\partial x'} + \frac{\partial u'}{\partial y'} \\ \frac{\partial v'}{\partial z'} + \frac{\partial w'}{\partial y'} \\ \frac{\partial u'}{\partial z'} + \frac{\partial w'}{\partial x'} \end{array} \right\} = \sum_{i=1}^{n} \mathbf{B}_i \left\{ \begin{array}{c} \overline{\mathbf{u}}_i \\ \boldsymbol{\theta}_i \end{array} \right\} \tag{2.24}$$

where $\boldsymbol{\epsilon}$ is the strain vector with its components in the lamina coordinate system. The main reason behind this choice for the strain vector components is to facilitate the separation between various strain components. Therefore, the $\mathbf{B}_i$ matrix is written in the form

$$\boldsymbol{B}_i = \left[\begin{array}{cc} \boldsymbol{B}^u_{MN} & \boldsymbol{B}^\theta_{MB} \\ \boldsymbol{B}^u_{MS} & \boldsymbol{B}^\theta_{BS} \\ \boldsymbol{B}^u_{TS} & \boldsymbol{B}^\theta_{TS} \end{array} \right] \tag{2.25}$$

in which the subscripts MN, MB, MS, BS and TS denote membrane normal, membrane bending, membrane shear, bending shear and transverse shear components, respectively. In order to find these components the displacement vector given by Equation (2.19) is transformed to the lamina coordinate system. Thus,

$$\mathbf{u}' = \sum_{i=1}^{n} N_i(\xi, \eta) \left[\mathbf{q}\overline{\mathbf{u}}_i + \frac{\zeta t_i}{2} \mathbf{q}\mathbf{R}_\mathbf{i}\boldsymbol{\theta}_i \right] \tag{2.26}$$

taking the derivative of $\mathbf{u}'$ with respect to x', y' and z' gives

$$\frac{\partial \mathbf{u}'}{\partial x'} = \sum_{i=1}^{n} \left[\frac{\partial N_i}{\partial x'} \mathbf{q}\overline{\mathbf{u}}_i + \frac{t_i}{2} \frac{\partial (\zeta N_i)}{\partial x'} \mathbf{q}\mathbf{R}_\mathbf{i}\boldsymbol{\theta}_i \right] \tag{2.27}$$

$$\frac{\partial \mathbf{u}'}{\partial y'} = \sum_{i=1}^{n} \left[\frac{\partial N_i}{\partial y'} \mathbf{q}\overline{\mathbf{u}}_i + \frac{t_i}{2} \frac{\partial (\zeta N_i)}{\partial y'} \mathbf{q}\mathbf{R}_\mathbf{i}\boldsymbol{\theta}_i \right] \tag{2.28}$$

$$\frac{\partial \mathbf{u}'}{\partial z'} = \sum_{i=1}^{n} \left[\frac{\partial N_i}{\partial z'} \mathbf{q}\overline{\mathbf{u}}_i + \frac{t_i}{2} \frac{\partial (\zeta N_i)}{\partial z'} \mathbf{q}\mathbf{R}_\mathbf{i}\boldsymbol{\theta}_i \right] \tag{2.29}$$

Thus, the components of the strain-displacement matrix are given as

$$\mathbf{B}^u_{MN} = \begin{bmatrix} \frac{\partial N_i}{\partial x'} & 0 & 0 \\ 0 & \frac{\partial N_i}{\partial y'} & 0 \end{bmatrix} \mathbf{q} \tag{2.30}$$

$$\mathbf{B}^u_{MS} = \begin{bmatrix} \frac{\partial N_i}{\partial y'} & \frac{\partial N_i}{\partial x'} & 0 \end{bmatrix} \mathbf{q} \tag{2.31}$$

$$\mathbf{B}^u_{TS} = \begin{bmatrix} 0 & \frac{\partial N_i}{\partial z'} & \frac{\partial N_i}{\partial y'} \\ \frac{\partial N_i}{\partial z'} & 0 & \frac{\partial N_i}{\partial x'} \end{bmatrix} \mathbf{q} \tag{2.32}$$

$$\mathbf{B}^\theta_{BN} = \frac{t_i}{2} \begin{bmatrix} \frac{\partial(\zeta N_i)}{\partial x'} & 0 & 0 \\ 0 & \frac{\partial(\zeta N_i)}{\partial y'} & 0 \end{bmatrix} \mathbf{q}\mathbf{R}_i \tag{2.33}$$

$$\mathbf{B}^\theta_{BS} = \frac{t_i}{2} \begin{bmatrix} \frac{\partial(\zeta N_i)}{\partial y'} & \frac{\partial(\zeta N_i)}{\partial x'} & 0 \end{bmatrix} \mathbf{q}\mathbf{R}_i \tag{2.34}$$

$$\mathbf{B}^\theta_{TS} = \frac{t_i}{2} \begin{bmatrix} 0 & \frac{\partial(\zeta N_i)}{\partial z'} & \frac{\partial(\zeta N_i)}{\partial y'} \\ \frac{\partial(\zeta N_i)}{\partial z'} & 0 & \frac{\partial(\zeta N_i)}{\partial x'} \end{bmatrix} \mathbf{q}\mathbf{R}_i \tag{2.35}$$

where the derivatives of the shape functions with respect to the lamina coordinate system are given by

$$\begin{Bmatrix} \frac{\partial N_i}{\partial x'} \\ \frac{\partial N_i}{\partial y'} \\ \frac{\partial N_i}{\partial z'} \end{Bmatrix} = \mathbf{q}\ \mathbf{J}^{-1} \begin{Bmatrix} \frac{\partial N_i}{\partial \xi} \\ \frac{\partial N_i}{\partial \eta} \\ 0 \end{Bmatrix} \tag{2.36}$$

Mass Matrix

The consistant mass matrix for curved shells is computed by performing a volume integration over the element domain, as follows

$$\mathbf{M} = \int_\Omega \rho\ \mathbf{A}^T\mathbf{A}\ d\Omega \tag{2.37}$$

$$\mathbf{A} = [\mathbf{A}_1\ \mathbf{A}_2\ \cdots] \tag{2.38}$$

$$\mathbf{A}_i = [\mathbf{N}_i\ \mathbf{Z}_i] \tag{2.39}$$

$$\mathbf{N}_i = \begin{bmatrix} N_i & 0 & 0 \\ 0 & N_i & 0 \\ 0 & 0 & N_i \end{bmatrix} \tag{2.40}$$

$$\mathbf{Z}_i = \zeta N_i \frac{t_i}{2} \mathbf{R}_i \tag{2.41}$$

where the subscript i denotes the node number.

For degenerated shells, the terms that correspond to the translational degrees of freedom are dominant as compared to the rotational terms. Sometimes, it is desired to diagonalize the resulting matrix to simplify the analysis and to avoid ill-conditioned mass matrix. In this work, Hinton technique is used to diagonalize the mass matrix. This is achieved by setting the entries of the lumped-mass matrix proportional to the diagonal entries of the consistant mass. The constant of proportion, selected to conserve the total element mass, is computed as follows

$$M_t = \int_\Omega \rho d\Omega \tag{2.42}$$

$$M_d = \sum_{i=1}^{m} \int_\Omega \rho N_i^2 d\Omega \tag{2.43}$$

$$\alpha = \frac{M_t}{M_d} \tag{2.44}$$

where M_t is the total element mass, M_d is the sum of translational diagonal entries of the consistent mass matrix and m is the total number of translational degrees of freedom. The rotational diagonal and off-diagonal terms are then set to zero.

Fiber Numerical Integration

In the general nonlinear case, fiber integrals need to be evaluated by a numerical integration technique. Several ways of going about this present themselves, each having advantages in certain circumstances.

If the integrand is a smooth function of ζ, e.g. when the shell consists of one homogeneous elastic layer, then Gaussian quadrature is most efficient. For the case when the reference surface is taken to be in the middle, the one point Gauss rule only senses membrane effects. At least two points are required to manifest the bending behavior. If it is desired to include the outermost fiber points, i.e. $\zeta = \pm 1$, in the evaluation, then the Lobatto rules are most accurate. The two point trapezoidal rule and the three point Simpson's rule are the first two members of the Lobatto family.

In the case when the shell is built up from a series of layers of different materials such that the material properties and stresses are discontinuous function of ζ, then Gaussian rules may be effectively used over each layer. If there are a large number of approximately equal-sized layers, then the midpoint rule on each layer should suffice. On the other hand, if there are a small number of layers or if the layers vary considerably in thickness, then different Gaussian rules should be assigned to individual layers. This is facilitated in this work by allowing the user to choose from different integration rules or input the location and weights of the fiber quadrature rule. Thus, any special set of circumstances may be accommodated.

Reduced Selective Integration

It is well known that certain class of problems produce excessively stiff solutions when the degenerated shell elements are used to solve them. This is attributed to that the degenerated shell elements are not capable to represent pure bending without shear or membrane effects which causes the shear locking and membrane locking phenomena. The shear locking phenomenon is caused by two main reasons

1. Some shape functions lead automatically to shear in pure bending because the transverse shear energy does not diminish as desired if the shell becomes thin
2. Sometimes, the transverse shear stiffness dominates the bending stiffness leading to an ill conditioned stiffness matrix.

Membrane locking is present in most curved elements but is less pronounced for higher order interpolation polynomials. It should be pointed out that facet shell elements which are initially free from membrane locking become curved in large displacement analyses and therefore may show considerable locking during bending deformation.

Several schemes have been proposed in order to avoid locking. The most popular procedures are uniform or selectively reduced integration. This may result in undesired internal mechanism which produces hour-glass modes. Even if these zero energy modes do not exist at the beginning, they may show up in a later deformed stage. Some procedures are available to control these hour-glass modes.

The method used in this work is the so called b-treatment. In this method, the reduced components of the $\mathbf{B}$ matrix are replaced by an equivalent component $\overline{\mathbf{B}}_{ij}$ which is computed from

$$\overline{\mathbf{B}}_{ij}(\xi,\eta) = \sum_{l=1}^{m} \overline{N}_l(\xi,\eta)\mathbf{B}_{ij}(\xi_l,\eta_l) \tag{2.45}$$

where $\overline{N}_l$ are the shape functions obtained by considering nodes at the quadrature points, and ξ_l and η_l are the natural coordinates of the reduced integration points. The strain-displacement matrix is then rewritten as

$$\boldsymbol{B} = \begin{bmatrix} \overline{\boldsymbol{B}}^{u}_{MN} & \boldsymbol{B}^{\theta}_{MB} \\ \overline{\overline{\boldsymbol{B}}}^{u}_{MS} & \boldsymbol{B}^{\theta}_{BS} \\ \overline{\overline{\boldsymbol{B}}}^{u}_{TS} & \overline{\overline{\boldsymbol{B}}}^{\theta}_{TS} \end{bmatrix} \tag{2.46}$$

where different number of bars represents components that are integrated using different reduced integration rules.

2.1.3 Two Dimensional Element Mechanics

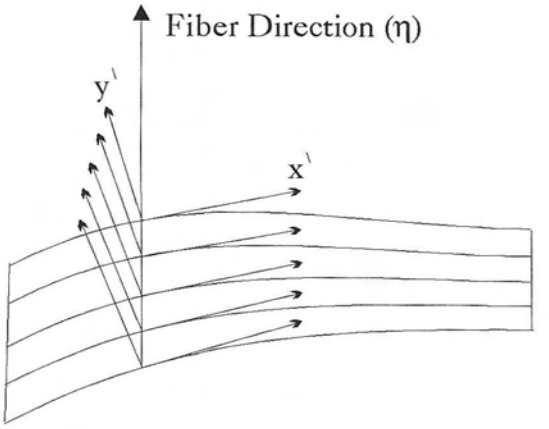

Figure 2.4: Coordinate Systems for Plane Shell Elements

The two dimensional shell element is deduced from the three dimensional shell element presented in the previous section. The formulation is reduced by omitting one coordinate out of each of the coordinate systems used, Figure (2.4), and replacing the three dimensional plasticity problem with a plane one. The lamina coordinate system and its transformation matrix $\mathbf{q}$ are given in this case as

$$\mathbf{x}' = \frac{1}{\sqrt{\left(\frac{\partial x}{\partial \xi}\right)^2 + \left(\frac{\partial y}{\partial \xi}\right)^2}} \left\{ \begin{array}{c} \frac{\partial x}{\partial \xi} \\ \frac{\partial y}{\partial \xi} \end{array} \right\} \tag{2.47}$$

$$\mathbf{y}' = \frac{1}{\sqrt{\left(\frac{\partial x}{\partial \xi}\right)^2 + \left(\frac{\partial y}{\partial \xi}\right)^2}} \left\{ \begin{array}{c} -\frac{\partial y}{\partial \xi} \\ \frac{\partial x}{\partial \xi} \end{array} \right\} \tag{2.48}$$

$$\mathbf{q} = [\mathbf{x}' \; \mathbf{y}']^T \tag{2.49}$$

The fiber direction v_{2i} at node i is given by

$$\mathbf{v}_{2i} = \frac{\mathbf{x}_i^t - \mathbf{x}_i^b}{\|\mathbf{x}_i^t - \mathbf{x}_i^b\|} \tag{2.50}$$

Geometric Description

The geometry of a typical plane shell element is also defined using the Cartesian coordinates of the top and bottom surface corresponding to each node, thus

$$\begin{Bmatrix} x \\ y \end{Bmatrix} = \sum_{i=1}^{n} N_i(\xi) \left[\frac{1+\eta}{2} \begin{Bmatrix} x_i^t \\ y_i^t \end{Bmatrix} + \frac{1-\eta}{2} \begin{Bmatrix} x_i^b \\ y_i^b \end{Bmatrix} \right] \tag{2.51}$$

$$= \sum_{i=1}^{n} N_i(\xi) \begin{Bmatrix} x_i \\ y_i \end{Bmatrix}_\eta \tag{2.52}$$

or consizly as

$$\mathbf{x} = \sum_{i=1}^{n} N_i(\xi) \mathbf{x}_{i\eta} \tag{2.53}$$

where the index i refer to the i'th node. In order to construct the Jacobian matrix, the natural coordinate derivatives are obtained as

$$\frac{\partial \mathbf{x}}{\partial \xi} = \sum_{i=1}^{n} \frac{\partial N_i(\xi)}{\partial \xi} \mathbf{x}_{i\eta} \tag{2.54}$$

$$\frac{\partial \mathbf{x}}{\partial \eta} = \frac{1}{2} \sum_{i=1}^{n} N_i(\xi) \left[\mathbf{x}_i^t - \mathbf{x}_i^b \right] \tag{2.55}$$

The Jacobian matrix required to transfer derivatives between the global and natural coordinate systems is then given by

$$\mathbf{J} = [\frac{\partial \mathbf{x}}{\partial \xi} \quad \frac{\partial \mathbf{x}}{\partial \eta}]^T \tag{2.56}$$

Kinematic Description

The kinematics of the plane shell element are defined also by invoking the isoparametric hypothesis which leads to

$$\left\{ \begin{array}{c} u \\ v \end{array} \right\} = \sum_{i=1}^{n} N_i(\xi) \left[\left\{ \begin{array}{c} \overline{u}_i \\ \overline{v}_i \end{array} \right\} + \frac{t_i \eta}{2} \mathbf{R}_i \theta_i \right] \tag{2.57}$$

or concisely

$$\mathbf{u} = \sum_{i=1}^{n} N_i(\xi) \left[\overline{\mathbf{u}}_i + \frac{t_i \eta}{2} \mathbf{R}_i \theta_i \right] \tag{2.58}$$

where $\overline{u}_i$ and $\overline{v}_i$ are the middle surface displacements in the X and Y directions at node i, respectively, and $\mathbf{R}_i$ is the rotation arm vector at node i given by

$$\mathbf{R}_i = \left\{ \begin{array}{c} -v_{2y} \\ v_{2x} \end{array} \right\}_i \tag{2.59}$$

Strain-Displacement Matrix

As mentioned in the previous section, the following definition of the strain vector is required to support the selective reduced integration

$$\boldsymbol{\epsilon} = \left\{ \begin{array}{c} \epsilon_{x'} \\ \gamma_{x'y'} \\ \epsilon_{z'} \end{array} \right\} = \left\{ \begin{array}{c} \frac{\partial u'}{\partial x'} \\ \frac{\partial v'}{\partial x'} + \frac{\partial u'}{\partial y'} \\ \frac{u}{x} \end{array} \right\} = \sum_{i=1}^{n} \mathbf{B}_i \left\{ \begin{array}{c} \overline{\mathbf{u}}_i \\ \theta_i \end{array} \right\} \tag{2.60}$$

in which $\epsilon_{z'} = 0$ in case of plane shell. This definition yields the following strain-displacement matrix

$$\mathbf{B}_i = \left[\begin{array}{cc} \mathbf{B}^u_{MN} & B^\theta_{MB} \\ \mathbf{B}^u_{TS} & B^\theta_{TS} \\ \mathbf{B}^u_{H} & B^\theta_{H} \end{array} \right] \tag{2.61}$$

where the subscript H denotes the hoop strain components which are non-zero only in case of axisymmetric shell. In order to find the strain displacement matrix, the displacement vector given by Equation (2.58) is transformed to the lamina coordinate system. Thus,

$$\mathbf{u}' = \sum_{i=1}^{n} N_i(\xi) \left[\mathbf{q}\overline{\mathbf{u}}_i + \frac{t_i \eta}{2} \mathbf{q}\mathbf{R}_\mathbf{i}\theta_i \right] \tag{2.62}$$

Taking the derivative of $\mathbf{u}'$ with respect to x' and y' gives

$$\frac{\partial \mathbf{u}'}{\partial x'} = \sum_{i=1}^{n} \left[\frac{\partial N_i}{\partial x'} \mathbf{q}\overline{\mathbf{u}}_i + \frac{t_i}{2} \frac{\partial (\eta N_i)}{\partial x'} \mathbf{q}\mathbf{R}_\mathbf{i}\theta_i \right] \tag{2.63}$$

$$\frac{\partial \mathbf{u}'}{\partial y'} = \sum_{i=1}^{n} \left[\frac{\partial N_i}{\partial y'} \mathbf{q}\overline{\mathbf{u}}_i + \frac{t_i}{2} \frac{\partial (\eta N_i)}{\partial y'} \mathbf{q}\mathbf{R}_\mathbf{i}\theta_i \right] \tag{2.64}$$

Thus, the components of the strain-displacement matrix are given as

$$\mathbf{B}^u_{MN} = \begin{bmatrix} \frac{\partial N_i}{\partial x'} & 0 \end{bmatrix} \mathbf{q} \tag{2.65}$$

$$\mathbf{B}^u_{TS} = \begin{bmatrix} \frac{\partial N_i}{\partial y'} & \frac{\partial N_i}{\partial x'} \end{bmatrix} \mathbf{q} \tag{2.66}$$

$$\mathbf{B}^u_{H} = \begin{bmatrix} \frac{N_i}{x} & 0 \end{bmatrix} \tag{2.67}$$

$$B^\theta_{BN} = \frac{t_i}{2} \begin{bmatrix} \frac{\partial(\eta N_i)}{\partial x'} & 0 \end{bmatrix} \mathbf{q}\mathbf{R}_i \tag{2.68}$$

$$B^\theta_{TS} = \frac{t_i}{2} \begin{bmatrix} \frac{\partial(\eta N_i)}{\partial y'} & \frac{\partial(\eta N_i)}{\partial x'} \end{bmatrix} \mathbf{q}\mathbf{R}_i \tag{2.69}$$

$$B^\theta_{H} = \begin{bmatrix} \frac{\eta t_i N_i}{2x} & 0 \end{bmatrix} \{R_i\} \tag{2.70}$$

Mass Matrix

The consistant mass matrix for plane and axisymmetric curved shells is computed by performing a volume integration over the element domain, as follows

$$\mathbf{M} = \int_\Omega \rho \, \mathbf{A}^T \mathbf{A} \, d\Omega \tag{2.71}$$

$$\mathbf{A} = [\mathbf{A}_1 \, \mathbf{A}_2 \, \cdots] \tag{2.72}$$

$$\mathbf{A}_i = [\mathbf{N}_i \; \mathbf{Z}_i] \tag{2.73}$$

$$\mathbf{N}_i = \begin{bmatrix} N_i & 0 \\ 0 & N_i \end{bmatrix} \tag{2.74}$$

$$\mathbf{Z}_i = \eta N_i \frac{t_i}{2} \mathbf{R}_i \tag{2.75}$$

where the subscript i denotes the node number.

2.1.4 Geometric Nonlinearity

In the analysis of shells, two types of geometric nonlinearities, namely large deformation and large rotation nonlinearities, may arise. Large deformation nonlinearity is attributed to the membrane stress developed due to the midplane stretching when the shell experience large displacements as compared to its dimensions. Large rotation nonlinearity is caused by large change of element slope during the analysis. This change causes the transformation matrix to change during the analysis. It also causes the relationship between the displacement field and the nodal rotation to be trigonometric, Figure (2.5).

The objective of the analysis is to evaluate the equilibrium positions of the shell, at the discrete time points or load levels Δt, $2\Delta t$, $3\Delta t$, $4\Delta t$, ..., t, $t+\Delta t$. It is assumed that the solution for the kinematic and static variables for all time steps from time zero (initial configuration) to time t, inclusive, have been obtained, and that the solution for time $t + \Delta t$ is required next. Two approaches may be used to handle geometric nonlinearities: Updated Lagrangian description and Total Lagrangian description. The Updated Lagrangian description uses the last known deformed shell geometry at time t as a reference configuration for all variables, whereas the total Lagrangian description uses as a reference configuration the initial undeformed shell geometry.

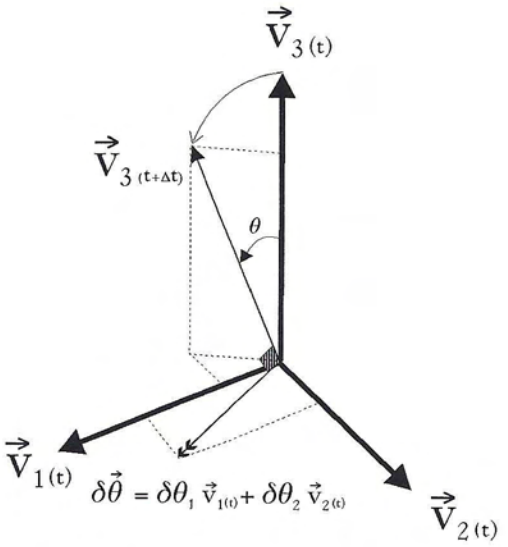

Figure 2.5: Finite Rotation of the Fiber Direction

The first approach is general and suitable for both nonlinearities while the second approach in this section is developed only to handle large deformation effects.

Updated Lagrangian Description

Geometric update is incrementally performed by superimposing the current time step incremental displacement vector to the previous time step geometry. The new geometry is then given as

$$\overline{\mathbf{x}}_{(t+\Delta t)} = \overline{\mathbf{x}}_{(t)} + \delta\overline{\mathbf{u}}_{(t+\Delta t)} \tag{2.76}$$

$$\mathbf{x}^t_{(t+\Delta t)} = \overline{\mathbf{x}}_{(t+\Delta t)} + \frac{t_i}{2}\,\mathbf{R}\,\delta\boldsymbol{\theta}_{(t+\Delta t)} \tag{2.77}$$

$$\mathbf{x}^b_{(t+\Delta t)} = \overline{\mathbf{x}}_{(t+\Delta t)} - \frac{t_i}{2}\,\mathbf{R}\,\delta\boldsymbol{\theta}_{(t+\Delta t)} \tag{2.78}$$

It should be pointed out that Equations (2.77) and (2.78) are first order accurate in enforcing the fiber inextensibility condition. This condition requires that the thickness of the shell measured in the fiber direction to remain the same at all times. If

the change in rotations is relatively large during the time step, an error may occur as shown in Figure (2.6). This error may be reduced either by using second order coordinate update or by using smaller time step. Alternatively, as shown in Figure (2.5), the new fiber direction and updated nodal coordinates at time $t+\Delta t$ may be obtained as

$$\mathbf{v}_{3\ (t+\Delta t)} = \frac{\delta\theta_2}{\delta\theta}\sin\delta\theta\ \mathbf{v}_{1\ (t)} - \frac{\delta\theta_1}{\delta\theta}\sin\delta\theta\ \mathbf{v}_{2\ (t)} + \cos\delta\theta\ \mathbf{v}_{3\ (t)} \tag{2.79}$$

$$\mathbf{x}^t_{(t+\Delta t)} = \overline{\mathbf{x}}_{(t+\Delta t)} + \frac{t_i}{2}\mathbf{v}_{3\ (t+\Delta t)} \tag{2.80}$$

$$\mathbf{x}^b_{(t+\Delta t)} = \overline{\mathbf{x}}_{(t+\Delta t)} - \frac{t_i}{2}\mathbf{v}_{3\ (t+\Delta t)} \tag{2.81}$$

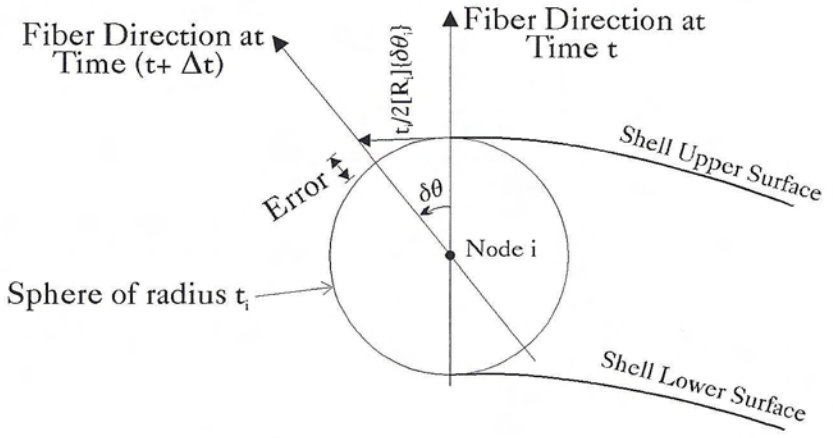

Figure 2.6: Geometric Update Error

Total Lagrangian Description for Three-Dimensional Shells

In some cases, the deformed geometry does not show large change in slope but still indicate relatively large displacements. In such cases, it is desired to include the effect of large displacements into the strain displacement matrix and use the original geometry in the analysis. This is achieved by adding the additional membrane strains caused by the large displacements. Following the work presented in [13], the strain

vector is written as

$$\boldsymbol{\epsilon} = \begin{Bmatrix} \epsilon_{x'} \\ \epsilon_{y'} \\ \gamma_{x'y'} \\ \gamma_{z'y'} \\ \gamma_{z'x'} \end{Bmatrix} = \boldsymbol{\epsilon}_o + \boldsymbol{\epsilon}_l = \begin{Bmatrix} \frac{\partial u'}{\partial x'} \\ \frac{\partial v'}{\partial y'} \\ \frac{\partial v'}{\partial x'} + \frac{\partial u'}{\partial y'} \\ \frac{\partial v'}{\partial z'} + \frac{\partial w'}{\partial y'} \\ \frac{\partial u'}{\partial z'} + \frac{\partial w'}{\partial x'} \end{Bmatrix} + \begin{Bmatrix} \frac{1}{2}\left[\frac{\partial w'}{\partial x'}\right]^2 \\ \frac{1}{2}\left[\frac{\partial w'}{\partial y'}\right]^2 \\ \frac{\partial w'}{\partial x'}\frac{\partial w'}{\partial y'} \\ 0 \\ 0 \end{Bmatrix} \tag{2.82}$$

$$= \sum_{i=1}^{n} (\mathbf{B}_o + \mathbf{B}_l)_i \begin{Bmatrix} \overline{\mathbf{u}}_i \\ \boldsymbol{\theta}_i \end{Bmatrix} \tag{2.83}$$

where $\mathbf{B}_o$ is the linear strain-displacement matrix computed as before and $\mathbf{B}_l$ is the nonlinear strain-displacement matrix. In order to find $\mathbf{B}_l$, the nonlinear strain component is rewritten as

$$\boldsymbol{\epsilon}_l = \frac{1}{2} \begin{bmatrix} \frac{\partial w'}{\partial x'} & 0 \\ 0 & \frac{\partial w'}{\partial y'} \\ \frac{\partial w'}{\partial y'} & \frac{\partial w'}{\partial x'} \\ 0 & 0 \\ 0 & 0 \end{bmatrix} \begin{Bmatrix} \frac{\partial w'}{\partial x'} \\ \frac{\partial w'}{\partial y'} \end{Bmatrix} = \frac{1}{2} [D] \{\epsilon_c\} \tag{2.84}$$

where $\boldsymbol{\epsilon}_c$ is the strain vector that couples the membrane strain to the out of plane displacements. These coupling strains are related to the nodal degrees of freedom by

$$\boldsymbol{\epsilon}_c = \sum_{i=1}^{n} \begin{bmatrix} \mathbf{G}^u & \mathbf{G}^\theta \end{bmatrix}_i \begin{Bmatrix} \mathbf{u}_i \\ \boldsymbol{\theta}_i \end{Bmatrix} \tag{2.85}$$

The matrix $\mathbf{B}_l$ is then given by

$$[B_l]_i = [D]_i \begin{bmatrix} \mathbf{G}^u & \mathbf{G}^\theta \end{bmatrix}_i$$

$$= \mathbf{D}_i \, \mathbf{G}_i \tag{2.86}$$

$$\mathbf{G}^u = \begin{bmatrix} 0 & 0 & \frac{\partial N_i}{\partial x'} \\ 0 & 0 & \frac{\partial N_i}{\partial y'} \end{bmatrix} [q] \tag{2.87}$$

$$\mathbf{G}^{\theta} = \frac{t_i}{2}\begin{bmatrix} 0 & 0 & \frac{\partial(\zeta N_i)}{\partial x'} \\ 0 & 0 & \frac{\partial(\zeta N_i)}{\partial y'} \end{bmatrix}[q]\,[R_i] \tag{2.88}$$

In large deformation analysis, the strain vector is incrementally updated after each time step by

$$\delta\boldsymbol{\epsilon} = \sum_{i=1}^{n}[B_o + B_l]_i \begin{Bmatrix} \delta\mathbf{u}_i \\ \delta\boldsymbol{\theta}_i \end{Bmatrix} \tag{2.89}$$

The stiffness matrix is then given by

$$[K] = \int_{\Omega}\left[[B_o + B_l]^T[E]\,[B_o + B_l] + [G]^T\begin{bmatrix} \sigma_{x'} & \tau_{x'y'} \\ \tau_{x'y'} & \sigma_{y'} \end{bmatrix}[G]\right] d\Omega \tag{2.90}$$

Total Lagrangian Description for Two-Dimensional Shells

In case of plane and axisymmetric shells, the formulation is deduced from the three-dimensional shell formulation. The strain vector is given by

$$\boldsymbol{\epsilon} = \begin{Bmatrix} \epsilon_{x'} \\ \gamma_{x'y'} \\ \epsilon z' \end{Bmatrix} = \boldsymbol{\epsilon}_o + \boldsymbol{\epsilon}_l = \begin{Bmatrix} \frac{\partial u'}{\partial x'} \\ \frac{\partial v'}{\partial x'} + \frac{\partial u'}{\partial y'} \\ \frac{u}{x} \end{Bmatrix} + \begin{Bmatrix} \frac{1}{2}\left[\frac{\partial v'}{\partial x'}\right]^2 \\ 0 \\ 0 \end{Bmatrix} \tag{2.91}$$

$$= \sum_{i=1}^{n}(\mathbf{B}_o + \mathbf{B}_l)_i \begin{Bmatrix} \overline{\mathbf{u}}_i \\ \theta_i \end{Bmatrix} \tag{2.92}$$

where $\epsilon_{z'} = 0$ in case of plane shell. The nonlinear strain component is rewritten as

$$\boldsymbol{\epsilon}_l = \frac{1}{2}\frac{\partial v'}{\partial x'}\begin{Bmatrix} \frac{\partial v'}{\partial x'} \\ 0 \\ 0 \end{Bmatrix} = \frac{1}{2}\epsilon_c\,\{D\} \tag{2.93}$$

The coupling strain is related to the nodal degrees of freedom by

$$\epsilon_c = \sum_{i=1}^{n} \left[\begin{array}{cc} \mathbf{G}^u & G^\theta \end{array} \right]_i \left\{ \begin{array}{c} \mathbf{u}_i \\ \theta_i \end{array} \right\} \tag{2.94}$$

The matrix $\mathbf{B}_l$ is then given by

$$\begin{aligned} [B_l]_i &= \{D\}_i \left[\begin{array}{cc} \mathbf{G}^u & G^\theta \end{array} \right]_i \\ &= \mathbf{D}_i \, \mathbf{G}_i \qquad (2.95) \\ \mathbf{G}^u &= \left[\begin{array}{cc} 0 & \frac{\partial N_i}{\partial x'} \end{array} \right] [q] \qquad (2.96) \\ G^\theta &= \frac{t_i}{2} \left[\begin{array}{cc} 0 & \frac{\partial (\eta N_i)}{\partial x'} \end{array} \right] [q] \{R_i\} \qquad (2.97) \end{aligned}$$

The stiffness matrix is then given by

$$[K] = \int_\Omega \left[[B_o + B_l]^T [E] [B_o + B_l] + \sigma_{x'} [G]^T [G] \right] d\Omega \tag{2.98}$$

2.2 Computer Implementation and Testing

The previous formulation for the shell element was incorporated into DYNAZ, the nonlinear multi-system-analysis finite element code. The developed shell element allows the use of variable nodes to accommodate wide variety of problems and to allow for appropriate mesh refinements. Several cases are then tested and compared with other analytical and numerical solutions to verify the correctness of the formulation.

2.2.1 Two-Dimensional Numerical Examples

Linear and Nonlinear Deflection of a Circular Plate

A circular plate of radius r and thickness t with clamped edges is subjected to a uniform load q that covers the entire plate. The plate material has a Poisson's ratio of 0.3 and a Young's modulus of E. The central deflection parameter, $W = \frac{w}{t}$, is plotted against the load parameter, $Q = \frac{qr^4}{Et^4}$, in Figure (2.7) and found to agree with the analytical solution presented in [270]. The magnitude of the central deflection was significantly reduced when large deflection effects were included.

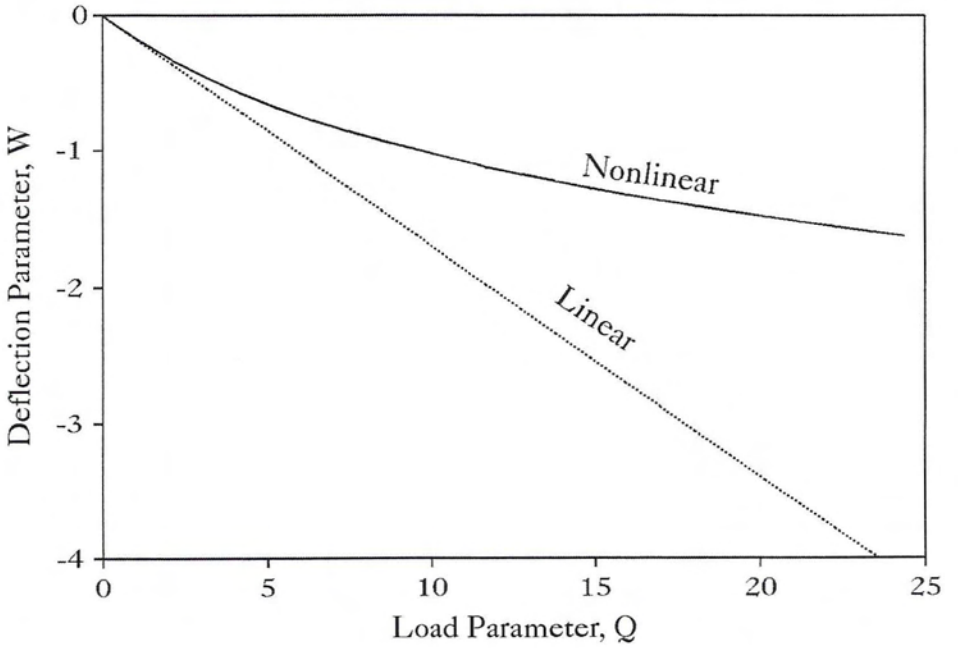

Figure 2.7: Linear and Nonlinear Deflection of a Circular Plate

Linear and Nonlinear Deflection of an Infinitely long Plate

An infinitely long plate of width b and thickness t with clamped edges is subjected to uniform load q that covers the entire plate. The central deflection parameter, $W = \frac{w}{t}$, is plotted against the load parameter, $Q = \frac{12qb^4(1-\nu^2)}{Et^4}$, in Figure (2.8) and found to agree with the analytical solution presented in [270].

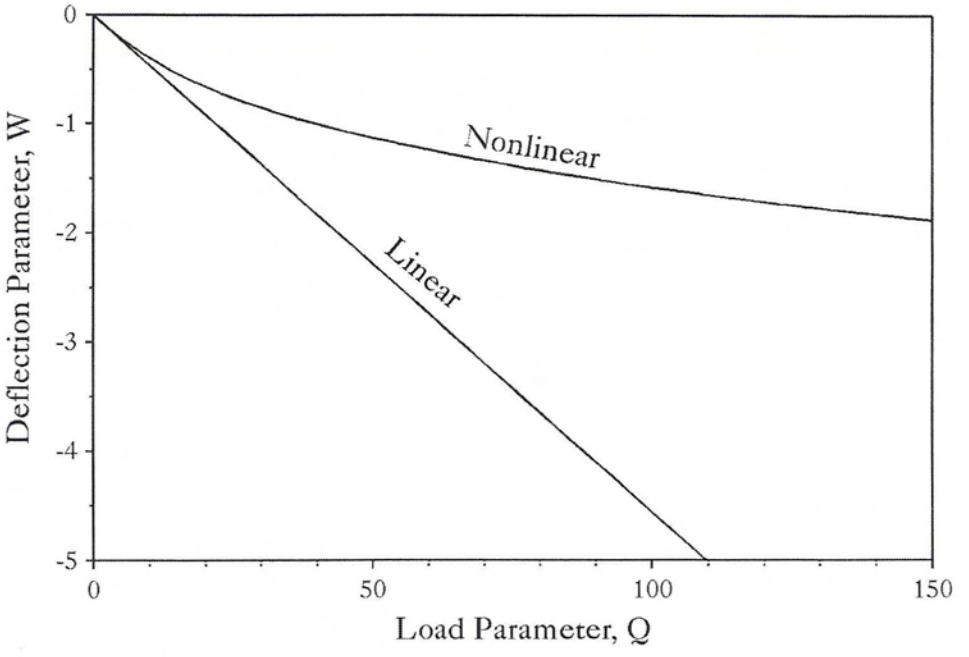

Figure 2.8: Linear and Nonlinear Deflection of an Infinitely Long Plate

Linear and Nonlinear Buckling of a Hinged-Hinged Column

A hinged-hinged column of length L and thickness t is subjected to an axial load p at the end. The lateral central deflection is plotted against the load parameter, $P = \frac{pL^2}{EI}$, in Figure (2.15). The column buckles as expected at a load parameter value $P = \pi^2$.

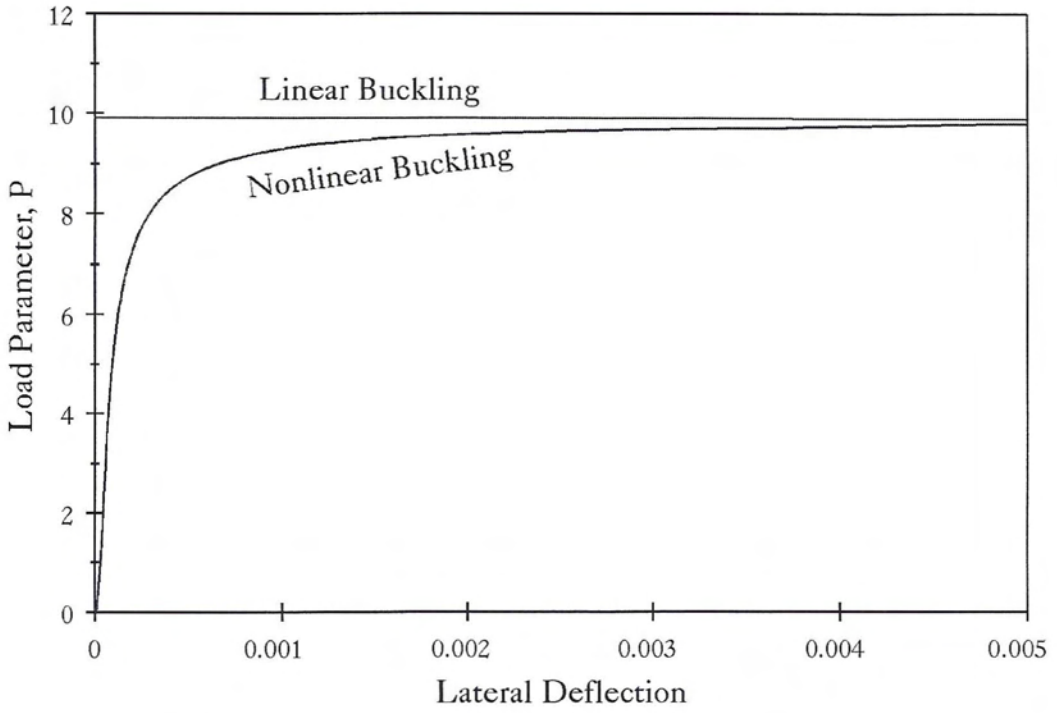

Figure 2.9: Linear and Nonlinear Buckling of a Hinged-Hinged Column

Large Deflection and Rotation Analysis of a Beam Column

A beam column of length L and cross section area A is subjected to a load W, as shown in Figure (2.10). The beam is hinged from the left end, and supported from the other end by a spring of stiffness K_s and a roller. The analytical solution presented in [44] gives the following relation between the load W and the deflection w

$$W = \frac{EA}{L^3}(z^3 w + \frac{3}{2} z w^2 + \frac{1}{2} w^3) \tag{2.99}$$

The beam is modeled with one shell element. Different values of the spring stiffness parameter $k = \frac{K_s L^3}{EAz^2}$ are chosen. Figure (2.11) shows the relation between the load parameter $P = \frac{W}{EA}\frac{L}{z^3}$ and the deflection parameter $D = \frac{w}{z}$ which is found to be identical to the analytical solution. It should be pointed out that if the spring stiffness

parameter is less than or equal to 0.5, then the displacement control should be used in the analysis in lou of the load control to achieve convergence.

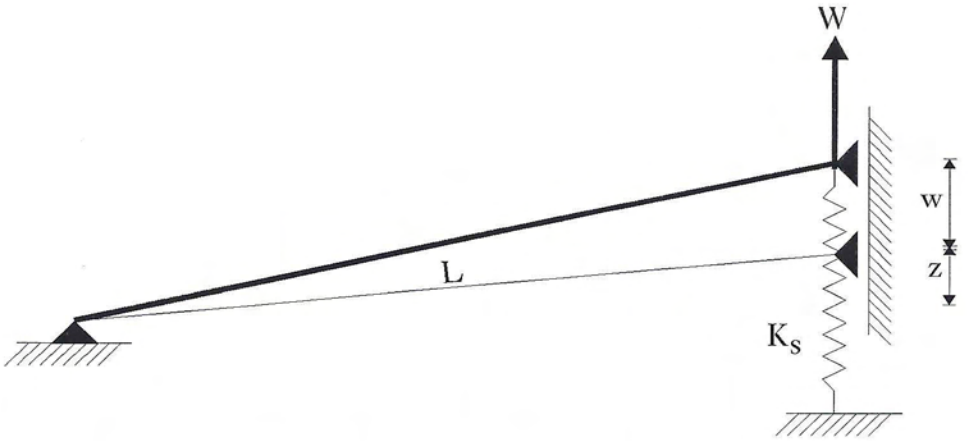

Figure 2.10: Large Deflection and Rotation Analysis of a Beam Column

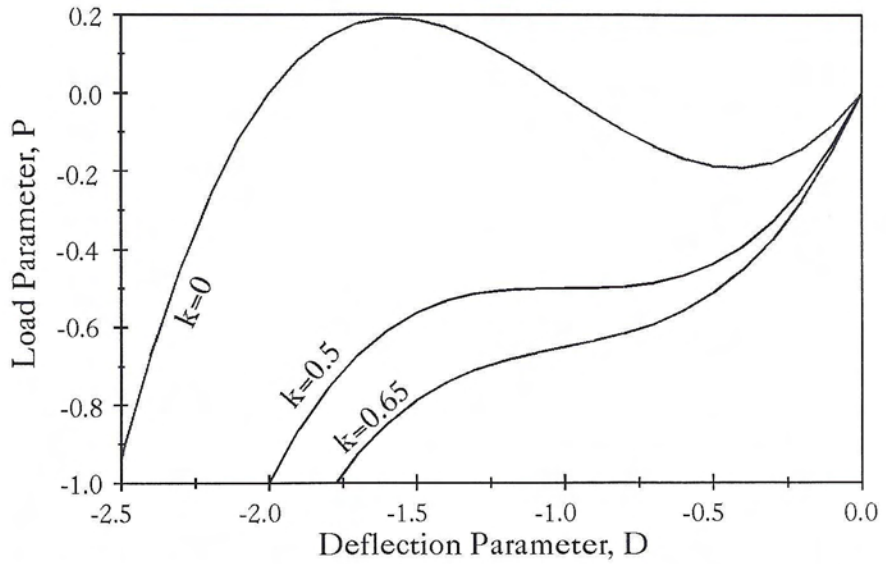

Figure 2.11: Large Deflection and Rotation Analysis of a Beam Column: Force-Deflection Curve

The same problem is also tested in dynamic analysis. The equation of motion is written for constant applied force W which gives

$$M\ddot{w} + \frac{EA}{L^3}(z^3 w + \frac{3}{2}zw^2 + \frac{1}{2}w^3) = W \tag{2.100}$$

where $M = \rho AL/2$. The series solution to the equation of motion gives

$$\begin{aligned} w(t) &= 0.5\frac{W}{M}t^2 - 0.0416667\frac{EAz^2W}{L^3M^2}t^4 + 0.001388889\frac{WzEA(\frac{EA}{L^3}z^3 - 9W)}{M^3L^3}t^4 \\ &- 0.0000248015873\frac{EAW((\frac{EA}{L^3})^2z^6 - 54\frac{EA}{L^3}z^3W + 45W^2)}{M^4L^3}t^8 \\ &+ 0.2755732\times 10^{-6}\frac{E^2A^2z^2W(1431W^2 + (\frac{EA}{L^3})^2z^6 - 243\frac{EA}{L^3}z^3W)}{L^6M^5}t^{10} \\ &+ \cdots O((\frac{t^2}{M})^6) \end{aligned} \tag{2.101}$$

The first term of the solution represent the rigid motion of the beam column with no contribution from its elasticity. This term is found to be dominant when $t/\sqrt{M}$ is relatively small. Figure (2.12) shows a comparison between the response time history of the analytical solution and that obtained from the program DYNAZ.

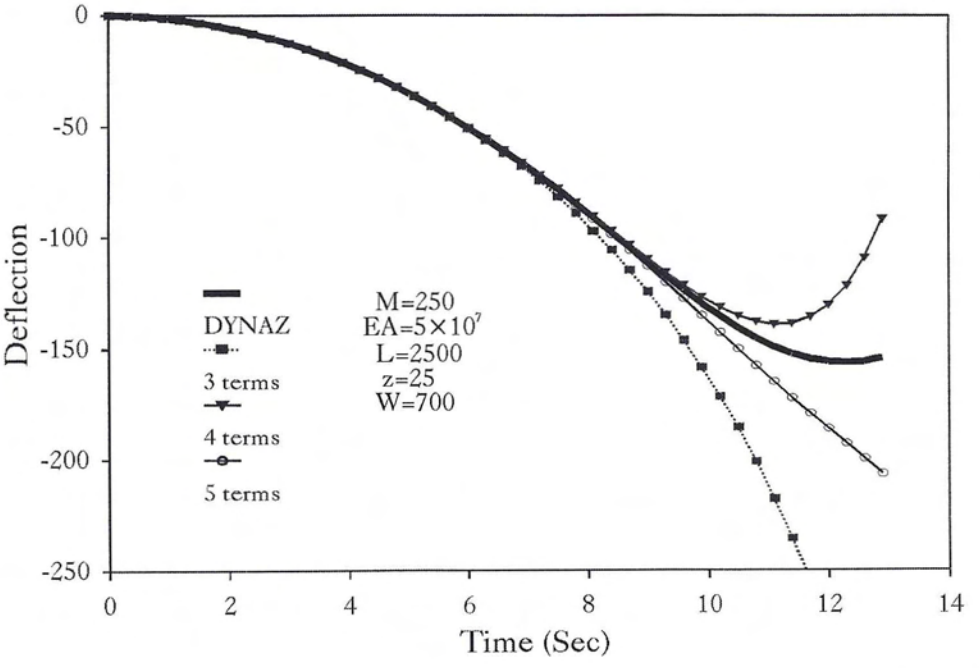

Figure 2.12: Large Deflection and Rotation Analysis of a Beam Column: Response Time History

Linear Vibration of a Beam

A hinged-hinged beam of length 4 m, width 0.15 m and thickness 0.20 m with clamped edges is subjected to a suddenly applied load of 5000 N at the middle of the beam. The beam material has a Young's modulus of 1×10^{12} N/m^2 and mass density of 100 kg/m. Two different models for the beam are tested: 18 two-noded degenerated shell elements model and 4×10 four-noded isoparametric solid elements in which four elements are used across the thickness. The central deflection time history is plotted and compared to the analytical solution in Figure (2.13).

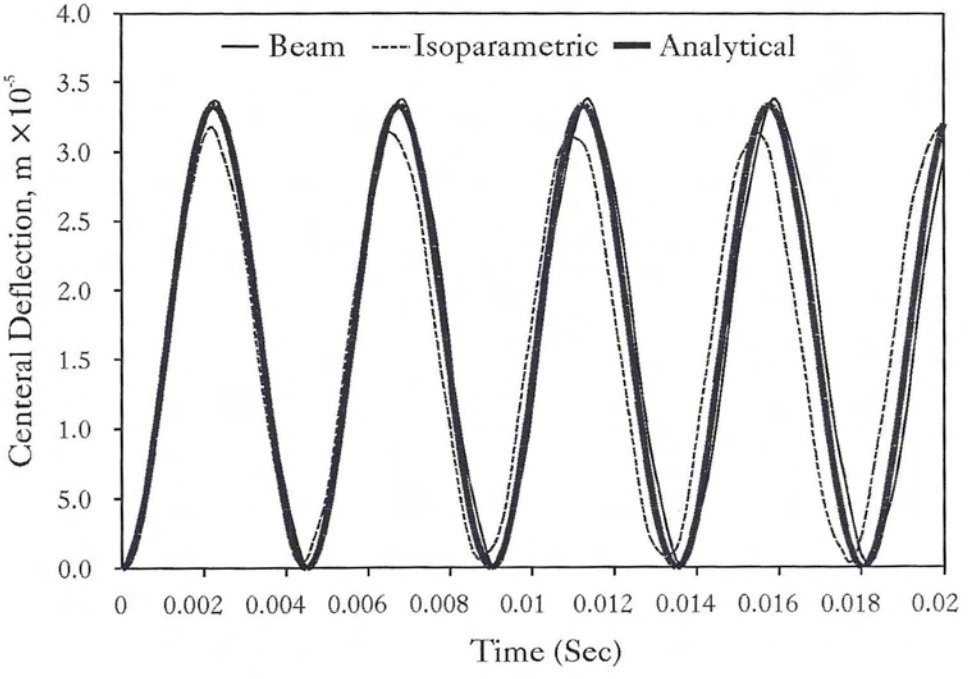

Figure 2.13: Linear Vibration of a Beam

Node	DYNAZ	Ref. [13]
1	$-3.62685788 \times 10^{-3}$	-3.6369×10^{-3}
2	$-3.62685788 \times 10^{-3}$	-3.6369×10^{-3}
3	$-3.62685788 \times 10^{-3}$	-3.6369×10^{-3}
4	$-1.14438860 \times 10^{-3}$	-1.1454×10^{-3}
5	$-1.14438860 \times 10^{-3}$	-1.1454×10^{-3}
9	$-1.14438860 \times 10^{-3}$	-1.1454×10^{-3}

Table 2.1: The Curved Cantilever Problem: Comparison of the Results

2.2.2 Three-Dimensional Numerical Examples

Linear Analysis of a Curved Cantilever

A curved cantilever shell is subjected to vertical loads as shown in Figure (2.14). The nodal deflections are computed and compared to the corresponding values presented in reference [13]. As concluded from Table (2.1), the results produced by DYNAZ agree with those presented in the aforementioned reference.

Linear and Nonlinear Deflection of a Square Plate

A square plate of width b and thickness t with clamped edges is subjected to uniform load q that covers the entire plate. The central deflection parameter, $W = \frac{w}{t}$, is plotted against the load parameter, $Q = \frac{12qb^4(1-\nu^2)}{Et^4}$, in Figure (2.15) and found to agree with the analytical solution presented in [270]. It should be pointed out that the central deflection at the middle of the square plate was less than the corresponding deflection in the middle of the circular or the infinitely long plate. In addition, the

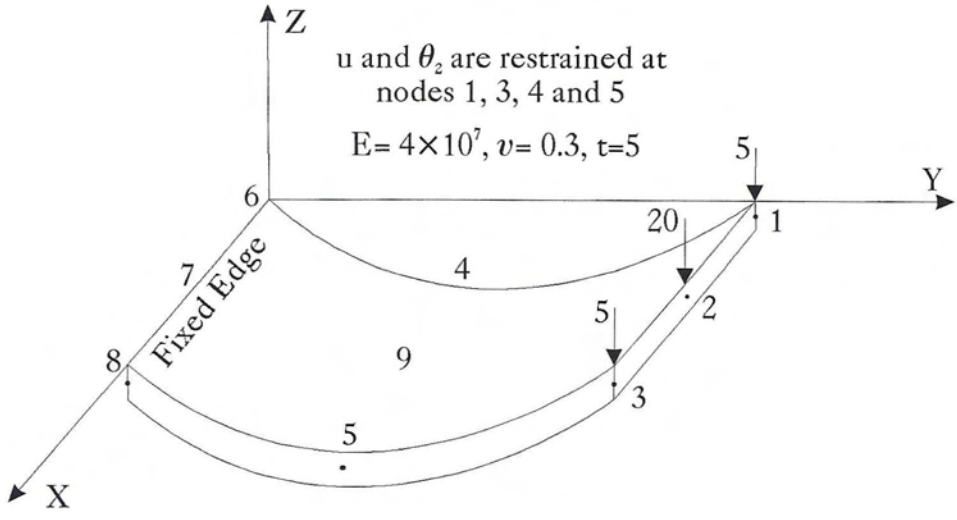

Figure 2.14: Linear Analysis of a Curved Cantilever

magnitude of the central deflection was significantly reduced when large deflection effects were included.

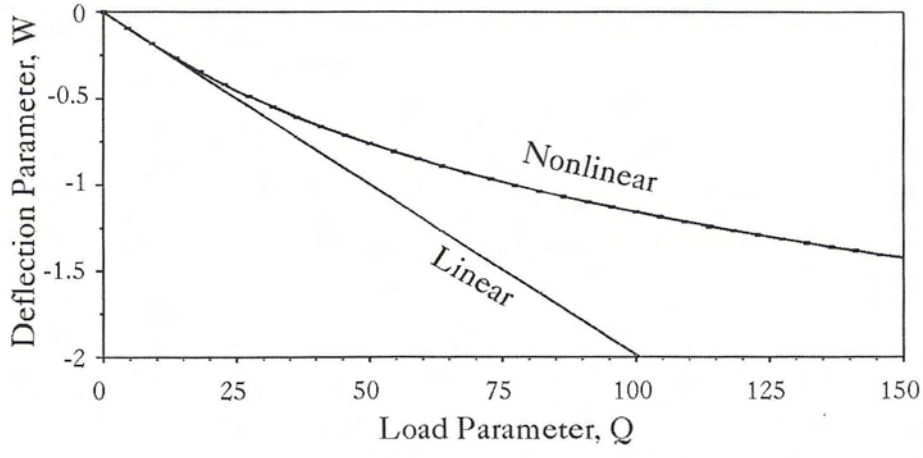

Figure 2.15: Linear and Nonlinear Deflection of an Infinitely Long Plate

Chapter 3

Contact Analysis

Mechanical contact is encountered whenever two or more bodies physically interact along their boundaries. The formulation presented in this chapter deals with the static and dynamic stress analysis of two or more bodies when they come into contact with each other under the action of external loads. The formulation is not restricted to the special case of an unanchored tank resting on the ground, rather it handles the general contact problem in two and three dimensions.

In many engineering problems, externally applied forces are considered independently from their source. This assumption simplifies the analysis significantly and, on many occasions, does not seriously affect the accuracy of the solution. In contact analysis, the contact forces that arise from the inequality constraints over the contact area are unknowns. In addition, the contact area and deformation status of the bodies in contact are also unknowns. These unknowns associated with any contact problem render the resulting problem nonlinear. Hence, analytical solutions are obtained for very few of relatively simple problems. As it almost invariably happens in these cases, complicated practical problems are simulated by numerical methods. The numerical algorithm used in this study is adapted from the work done by Chaudhary and Bathe ([17], [31]).

3.1 Contact Mechanics

In this chapter, the contact problem is formulated under the assumption that at least one of the bodies is deformable. Attention is directed towards the geometric intricacies stemming from the interaction of the bodies, the mathematical description of their relative motions and the complications introduced in the time history solution of actual boundary value problems.

3.1.1 Contact Inequality Constraints

Figure (3.1) shows schematically the problem under consideration. Two generic bodies are shown and denoted as contactor and target. The contactor contains the finite element boundary nodes that comes into contact with the target elements. The target and contactor could be within a single body that folds during deformation in a fashion that invokes contact between parts of its boundaries, see Figure (3.2). The displacement compatibility between the two bodies requires that no material overlap can occur along the region of contact. As a result, contact forces are developed that act along the region of contact upon the target and the contactor. The force transmissibility condition requires that these forces to be equal and opposite. In addition, it requires that normal contact forces can only exert a compressive action, and the tangential contact forces have to satisfy a law of frictional resistance. Coulomb's law of friction is used in the current formulation to regulate the friction forces. It requires that the friction force has to be greater than $\nu_s F_n$ for a slippage to occur. Once slippage has occurred, the friction force is set equal to $\nu_s F_n$, where ν_s and ν_d are the static and dynamic coefficients of friction, respectively. These two conditions

impose inequality constraints on the system that mathematically represent the stress analysis model of the contact bodies. These constraints are given as

$$\text{No penetration condition:} \quad \mathbf{P}_i.\mathbf{n} \geq 0 \tag{3.1}$$

$$\text{No tension condition:} \quad F_n > 0 \tag{3.2}$$

$$\text{Coulomb's law of friction condition:} \quad F_t \leq \nu_s F_n \quad \text{for no slippage} \tag{3.3}$$

$$F_t = \nu_d F_n \quad \text{for slippage} \tag{3.4}$$

where $\mathbf{P}_i$ is the penetration vector of contactor node number i into the target's element, $\mathbf{n}$ is the normal to the target element, F_n is the compressive normal contact force and F_t is the tangential contact force. It should be noted that Equation (3.1) ensures that the contactor nodes can not be within the region of the target body, but the target node can be inside or outside the contactor body as shown in Figure (3.3). This introduces some discretization error which may be reduced by using a finer mesh. In addition, by using Coulomb's law of friction, the elasticity between the particles in contact is neglected and a rigid plastic contact behavior is assumed.

3.1.2 Treatment of Inequality Constraints

To impose the displacement compatibility condition along the contact area, additional Lagrange multiplier degrees of freedom, $\boldsymbol{\lambda}$, are introduced to the system to minimize the potential function π under the contact constraints defined by the function $g(\mathbf{u}, \dot{\mathbf{u}}) = 0$. By adding the contact conditions to the usual variational indicator, the following function is obtained

$$\Pi(\mathbf{u}, \dot{\mathbf{u}}) = \pi(\mathbf{u}, \dot{\mathbf{u}}) + \boldsymbol{\lambda}\, g(\mathbf{u}, \dot{\mathbf{u}}) \tag{3.5}$$

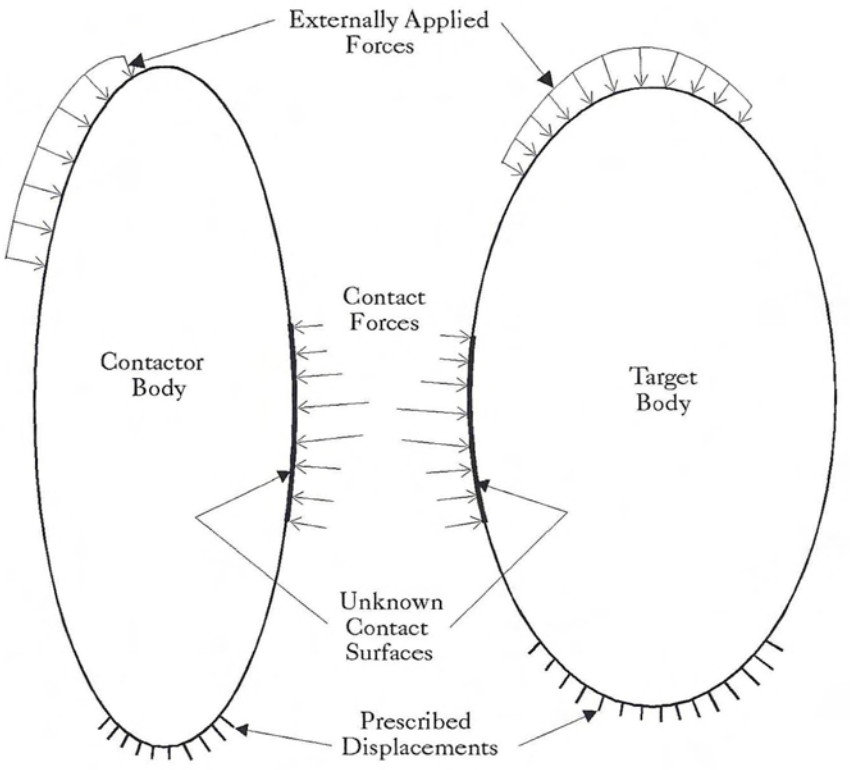

Figure 3.1: Geometry of a General Contact Problem

Figure 3.2: Single Body Contact

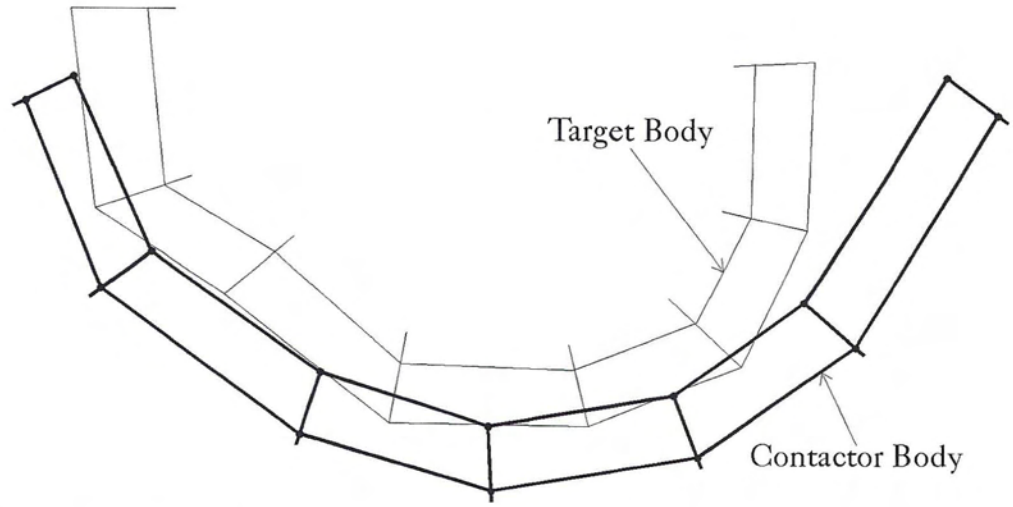

Figure 3.3: Discretization Error in the Modeling of Some Contact Problems

The second term of the equation may be physically interpreted as the potential of the contact forces. The values of the vector $\boldsymbol{\lambda}$ are the contact forces resulting from imposing the contact conditions on the system.

The friction part of the force transmissibility condition is not enforced yet in Equation (3.5). This condition is handled separately after each iteration and the appropriate boundary conditions are set for the next iteration. This approach causes the status of the boundary conditions applied on the system to change after each iteration. As a result, the quadratic convergence of the Newton-Rapson method may be seriously affected.

3.2 Finite Element Formulation

Invoking the stationary of II in Equation (3.5) gives the following system of incremental equations

$$\begin{bmatrix} \mathbf{M}_s & \mathbf{0} \\ \mathbf{0} & \mathbf{0} \end{bmatrix} \begin{Bmatrix} \delta\ddot{\mathbf{u}} \\ \delta\ddot{\boldsymbol{\lambda}} \end{Bmatrix} + \begin{bmatrix} \mathbf{C}_s & \mathbf{0} \\ \mathbf{0} & \mathbf{0} \end{bmatrix} \begin{Bmatrix} \delta\dot{\mathbf{u}} \\ \delta\dot{\boldsymbol{\lambda}} \end{Bmatrix} + \begin{bmatrix} \mathbf{K}_s & \mathbf{K}_\lambda \\ \mathbf{K}_\lambda^T & \mathbf{0} \end{bmatrix} \begin{Bmatrix} \delta\mathbf{u} \\ \delta\boldsymbol{\lambda} \end{Bmatrix} = \begin{Bmatrix} \mathbf{R} \\ \mathbf{0} \end{Bmatrix} + \begin{Bmatrix} \mathbf{F} \\ \mathbf{P} \end{Bmatrix} \tag{3.6}$$

where $\mathbf{K}_\lambda$ is the contact matrix, $\mathbf{F}$ is the contact force vector that results from the implementation of the contact forces transmissibility condition, $\mathbf{R}$ is the conventional residual vector and $\mathbf{P}$ is the penetration vector resulting from the current material overlap.

3.2.1 Condition of Sticking Contact

A contactor node c is assumed to be in sticking contact during iteration i under one of two conditions:

1. The contactor node has penetrated into the target body in iteration $(i-1)$ whereas it was not in contact after iteration $(i-2)$.
2. The friction resistance during contact is sufficient to prevent sliding.

In the first case, the penetration vector $\mathbf{P}$ on the right hand side of Equation (3.6) is set such that $\delta\mathbf{u}$ for the next iteration eliminates the current penetration of the contactor node into the target surface. Such constraints on the displacement vector generate the contact forces. These contact forces is further checked against the law of friction to determine whether state of sticking contact will remain or slippage will take place.

The constraints to be enforced in the case of sticking contact are

$$\mathbf{P} = 0 \tag{3.7}$$

$$F_n > 0 \tag{3.8}$$

$$F_t \leq \nu_s F_n \tag{3.9}$$

These constraints are enforced through the matrix $\mathbf{K}_\lambda$, and the vectors $\mathbf{F}$ and $\mathbf{P}$. The vector $\mathbf{F}$ is required to recover the residual from the contact forces resulting from the applied constraints. This residual has been previously computed from the equilibrium of the entire system. Although the contact forces could be directly computed from the values of $\boldsymbol{\lambda}$, but the equilibrium approach gives better accuracy.

Figure (3.4) shows a contactor node c that is in contact with the target element connected to the three nodes i, j and k. A geometric analysis of the nodal coordinates and deformations is performed to determine the target element associated with each contactor node, the target's attached nodes, coordinates of point c' and the nondimensional triangular coordinates L_1, L_2 and L_3. If node c penetrates inside the target element, then the penetration vector required to correct this error is given by

$$\mathbf{P} = \mathbf{r}_{c'} - \mathbf{r}_c \tag{3.10}$$

where $\mathbf{r}_{c'}$ and $\mathbf{r}_c$ are the position vector of points c' and c in the current iteration, respectively. Sticking point c' to the target element requires that

$$\mathbf{r}_{c'} = L_1\mathbf{r}_i + L_2\mathbf{r}_j + L_3\mathbf{r}_k \tag{3.11}$$

Eliminating the penetration vector $\mathbf{P}$ gives the constraint matrix as

$$[K_\lambda^T] = C_\lambda \begin{bmatrix} -1 & 0 & 0 & L_1 & 0 & 0 & L_2 & 0 & 0 & L_3 & 0 & 0 \\ 0 & -1 & 0 & 0 & L_1 & 0 & 0 & L_2 & 0 & 0 & L_3 & 0 \\ 0 & 0 & -1 & 0 & 0 & L_1 & 0 & 0 & L_2 & 0 & 0 & L_3 \end{bmatrix} \tag{3.12}$$

where C_λ is a scale factor used to scale the constraint matrix and the penetration vector to avoid ill-conditioned coefficient matrix in the left hand side. The matrix

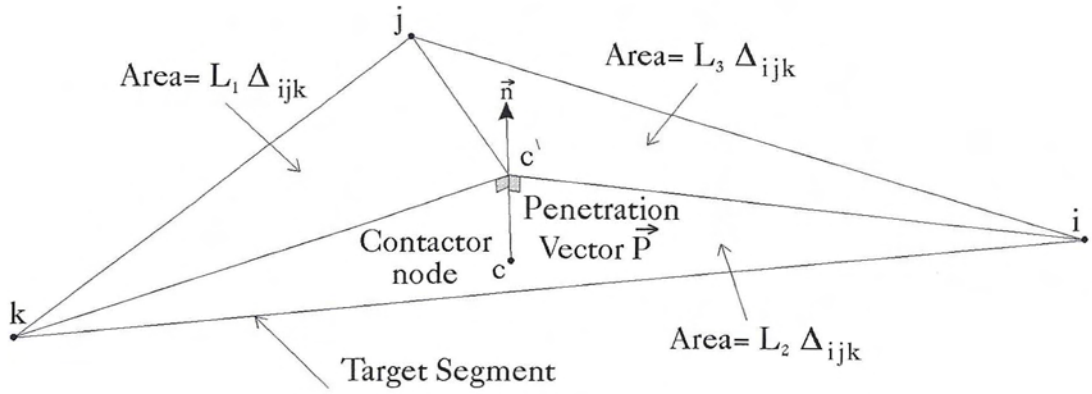

Figure 3.4: Geometry of Sticking Contact Condition

equation given as

$$[K_\lambda^T] \begin{Bmatrix} \mathbf{u}_c \\ \mathbf{u}_i \\ \mathbf{u}_j \\ \mathbf{u}_k \end{Bmatrix} = \{P\} \tag{3.13}$$

is then assembled to the global system to enforce the sticking contact Condition.

3.2.2 Condition of Sliding Contact

A contactor node c is assumed to be in sliding contact if the tangential force exceeds the frictional capacity. The sliding contact condition has to be preceded by either sticking or sliding contact condition. Thus, the penetration vector $\mathbf{P}$ on the right hand side of Equation (3.6) is set to zero. The inequality constraints to be enforced in this case are

$$\delta \mathbf{u}_r.\mathbf{n} = 0 \tag{3.14}$$

$$F_n > 0 \tag{3.15}$$

$$F_t = \nu_d F_n \tag{3.16}$$

where $\delta \mathbf{u}_r$ is the incremental relative displacemnt vector, which is given by

$$\delta \mathbf{u}_r = \delta \mathbf{u}_c - L_1 \delta \mathbf{u}_i - L_2 \delta \mathbf{u}_j - L_3 \delta \mathbf{u}_k \tag{3.17}$$

These constraints are enforced through the matrix $\mathbf{K}_\lambda$, and the vector $\mathbf{F}$. Figure (3.5) shows a contactor node c that is in contact with the target element connected to the three nodes i, j and k. After the geometric analysis of the nodal coordinates and deformations is performed and the target element, the attached nodes and the nondimensional triangular coordinates L_1, L_2 and L_3, are determined, the vector $\mathbf{F}$ is computed from the residual vector resulting from the global equilibrium of node c. The normal and tangential components of the contact force are then given by

$$F_n = \mathbf{F}.\mathbf{n} \tag{3.18}$$

$$F_t = \nu_d F_n \tag{3.19}$$

The tangential component is then applied in a direction opposite to the velocity direction at node c. The constraint matrix $\mathbf{K}_\lambda$ is given by

$$[K_\lambda^T] = C_\lambda \begin{bmatrix} -l & -m & -n & lL_1 & mL_1 & nL_1 & lL_2 & mL_2 & nL_2 & lL_3 & mL_3 & nL_3 \end{bmatrix} \tag{3.20}$$

where l, m and n are the direction cosines of the vector normal to the target surface that contains nodes i, j and k.

3.2.3 Condition of Tension Release

When the normal force F_n is tension, separation between the contactor node and the target element takes place. The displacements of the contactor node and the target element are totally independent. In this case, the Lagrange multiplier degrees of freedom are disabled.

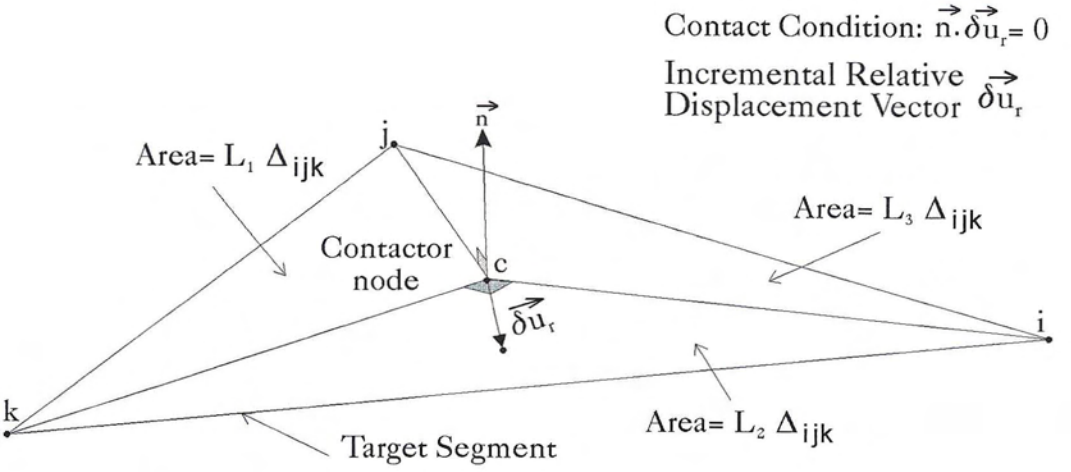

Figure 3.5: Geometry of Sliding Contact Condition

3.3 Contact Algorithms

An implementation of the contact analysis using the Lagrange multiplier technique is incorporated into DYNAZ, the nonlinear multi-system-analysis finite element code. In this section, an outline of the procedures used are presented.

3.3.1 Geometric Analysis

Geometric analysis is performed over the coordinates and displacements of the contactor node and the target surface nodes to determine the following

1. The target element and its corner nodes i, j and k
2. The normal to the target surface that contains nodes i, j and k
3. The coordinates of the contactor node projection on the target element, point c'
4. The nondimensional triangular coordinates L_1, L_2 and L_3 that describe the location of point c' inside the triangle of vertices i, j and k.

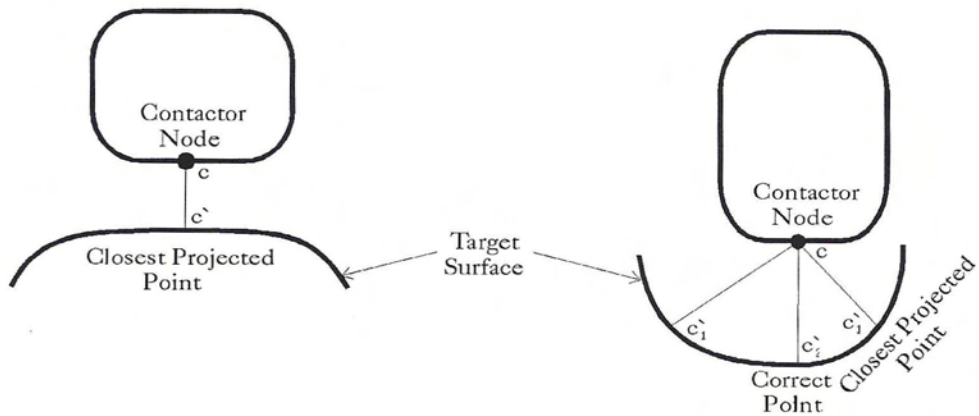

Figure 3.6: Closest Point Projection

In order to find the potential target element, the projection of the contactor node c on each of the potential target elements is found. This projection is achieved in a closed form for a linear surface and by means of an elementary Newton scheme for a quadratic surface. In the latter case, there is an evident non-uniqueness problem due to the lack of convexity of the target surface. It is conceivable that there are three distinct projections to the target surface. To avoid such a problem, the closest point policy is proposed, see Figure (3.6). The algorithm used to perform the aforementioned tasks is summarized as follows

Loop (A) over the potential target elements

Loop (B) over the nodes on the target surface

Get the closest node and the attached elements

End loop (B)

End loop (A)

Loop (C) over the target elements attached to the closest node

Get the normal to the element

Get the contactor projection (point c')

Get L_1, L_2 and L_3 for point c' with respect to nodes i, j and k

If point c' is between points i, j and k then

Return

End if

End loop (C)

No target element is found

Return

3.3.2 Determination of the Contact Condition

In time history analysis , the contact condition changes as loads and ground excitation change. Determination of the contact condition is based on the law of friction, the previous contact condition and the current material overlap. The contact condition decision is made as follows

If the previous iteration condition was tension release then

If there is a penetration then

The new condition is sticking contact

Else

The new condition is tension release

End if

Else

If the force F_n is tension then

The new condition is tension release

Else

Set the new condition to be the same as the previous condition

If the previous condition was sticking contact then

If $F_t > \nu_s F_n$ then the new condition is sliding contact

Else

If $F_t < \nu_d F_n$ then the new condition is sticking contact

End if

End if

If it is the first iteration then

Set the new condition to be sticking contact

End if

End if

3.3.3 Overall Procedure Outline

Contact analysis is performed within each iteration until the equilibrium condition is satisfied. The residual vector that results from the global equilibrium is computed before the contact analysis starts. This vector is used to compute the contact forces resulting from the contact inequality constraints applied on the system. The constraint matrix $\mathbf{K}_\lambda$ is constructed and assembled to the left-hand-side coefficient matrix in each iteration. This would require the entire coefficient matrix to be reformulated and decomposed after each iteration, which is computationally expensive. Alternatively, using Crout factorization technique and isolating the Lagrange multiplier degrees of freedom at the end of the left-hand-side coefficient matrix, makes this action unnecessary. Only the part of the coefficient matrix corresponding to the

Lagrange multiplier degrees of freedom is assembled and decomposed in each iteration without having to reconstruct and decompose the entire coefficient matrix. This technique saves a tremendous amount of computation.

The overall contact analysis procedure is performed, for each node on the contactor surface, as follows:

1. Read the contact forces from the residual vector
2. For the current contactor node c, perform the geometric analysis
3. Make the contact decision to determine the contact condition and compute the constraint matrix $\mathbf{K}_\lambda$
4. Compute the contact force vector $\mathbf{F}$
5. Transfer the contact forces to the target nodes as follows

$$\mathbf{F}_i = L_1\mathbf{F} \tag{3.21}$$

$$\mathbf{F}_j = L_2\mathbf{F} \tag{3.22}$$

$$\mathbf{F}_k = L_3\mathbf{F} \tag{3.23}$$

6. Assemble the constraint matrix and force vectors to the global left-hand-side coefficient matrix and the right-hand-side load vector, respectively.

3.4 Computer Implementation and Testing

The algorithm for solution of contact problems presented in this chapter has been incorporated into DYNAZ. The solution method is applicable to wide range of

static and dynamic problems with material and geometric nonlinearities. Although the Lagrange multiplier values are the incremental contact forces based on the solution of the governing equations of equilibrium, they are not used by the algorithm because such a procedure may introduce serious errors of linearization in nonlinear analyses with contact. Instead, the total contact forces are directly evaluated from equilibrium of the applied external loads, inertia forces, damping forces and the nodal point forces equivalent to the current element stresses. Thus, the sole function of the Lagrange multipliers is to enforce that, in each iteration, the incremental displacements of contactor and target surfaces are compatible with each other in the region of contact.

Integral statements generally form the basis of the finite element approximations to problems in elastodynamics. The simplest, and, hence, most popular approach is to perform separate approximations for the two distinct types of independent variables, associated with the temporal and the spatial dimensions. Typically, domain approximation precedes time integration, so that the latter is applied to a set of ordinary differential equations in time. This decomposition leads to what are known as semi-discrete, or direct, time integration methods. A broader class of integration methods resulting in space-time finite element emanate from a priori coupling of temporal and spatial variables in the discretization. In this work, the Newmark family direct time integration technique is used. It should be pointed out, as was also observed in other references ([31], [215]), that the integration of the dynamic response gives better accuracy if performed by using the time integration parameters, $\beta = 0.5$ and $\gamma = 0.25$, which corresponds to the well-known trapezoidal rule. It is reported that these values of the time integration parameters give a dynamic contact solution that fulfill the total energy conservation and the impulse-momentum relationship.

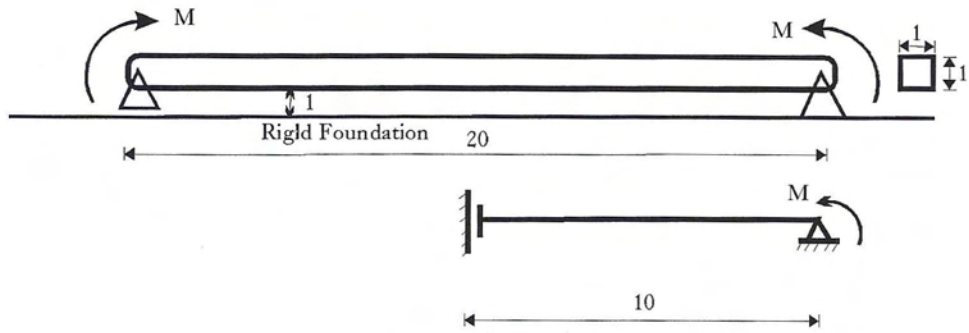

Figure 3.7: Elastic Beam on Rigid Foundation

3.4.1 Two-Dimensional Numerical Examples

Beam on Rigid Foundation

A long simply supported rectangular beam is bent by two equal end-point moments, M As the beam deflects, it approaches, and eventually reaches, a flat rigid surface, see Figure (3.7). The material behavior of the beam is described by linear elastics model of $E = 3.0 \times 10^3$ and $\nu = 0.3$. Solution to this problem may be obtained by means of various linear beam theories. Also, a similar problem has been presented in [215].

The beam was uniformly discretized into 100 degenerated plane stress shell elements and symmetry was observed. A reduced selective integration technique was used to avoid shear locking phenomenon. The finite element solution qualitatively conforms with the other results, as it predicts release from the rigid surface in the middle of the beam with the increase of the applied moments. Figure (3.8) shows the deformation for different values of the applied moment M. The corresponding contact pressure between the beam and the foundation is shown in Figure (3.9). The change of beam length in contact with the foundation is shown in Figure (3.10). The support vertical reaction that represent the integration of the contact pressure over

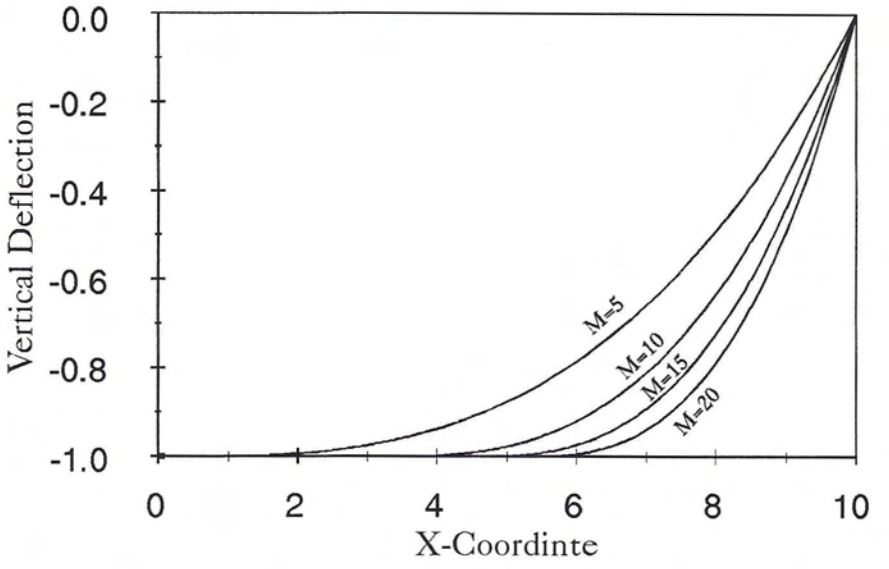

Figure 3.8: Elastic Beam on Rigid Foundation: Deformation

the area is show in Figure (3.11). All results are presented only for the right half of the beam.

Contact of two flexible trusses

Figure (3.12) shows two flexible trusses A and B. Truss A is moving towards truss B which is fixed. The horizontal and vertical displacement are prescribed for nodes 1 and 3 in truss A. The dynamic and static coefficients of friction are assumed to be 0.5 between the two trusses. Analytical solution for the problem can be readily found. The results precisely agrees with the analytical solution. Figures (3.13) and (3.14) show the displacements of nodes 1, 2 and 6. Figure (3.15) shows the contact forces at node 2.

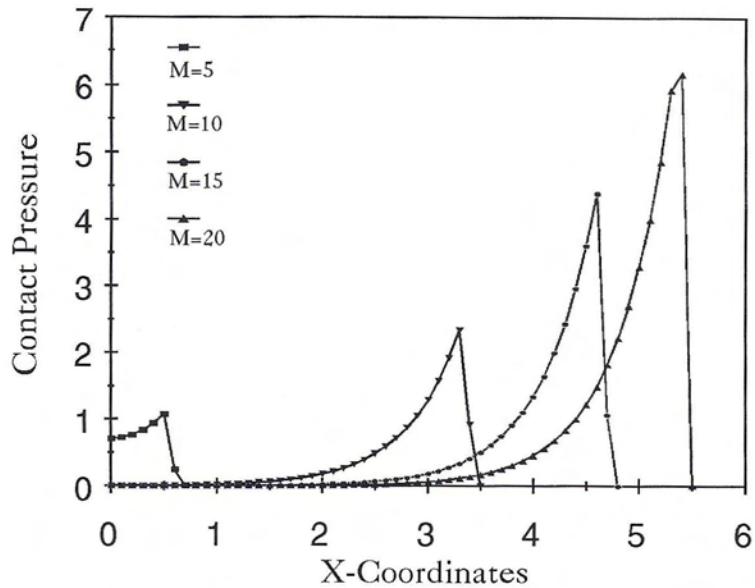

Figure 3.9: Elastic Beam on Rigid Foundation: Contact Pressure

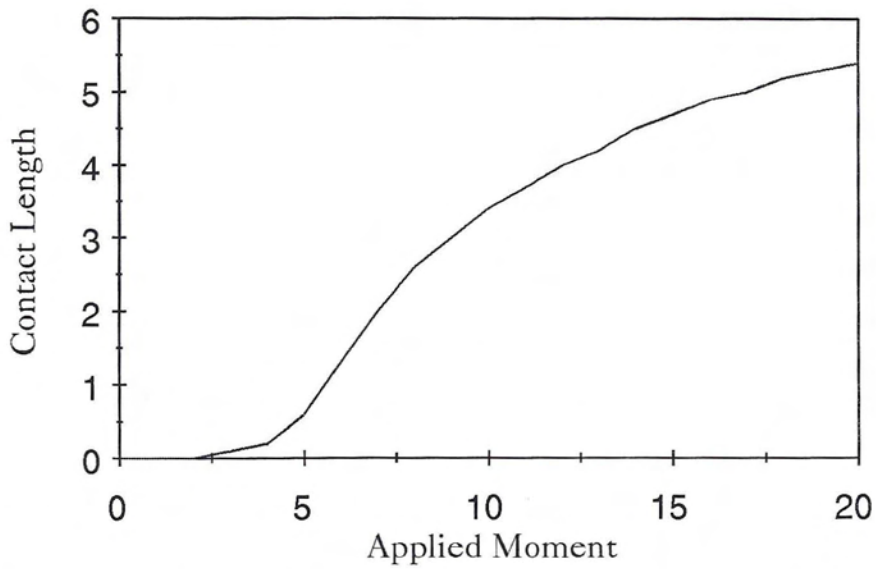

Figure 3.10: Elastic Beam on Rigid Foundation: Contact Length

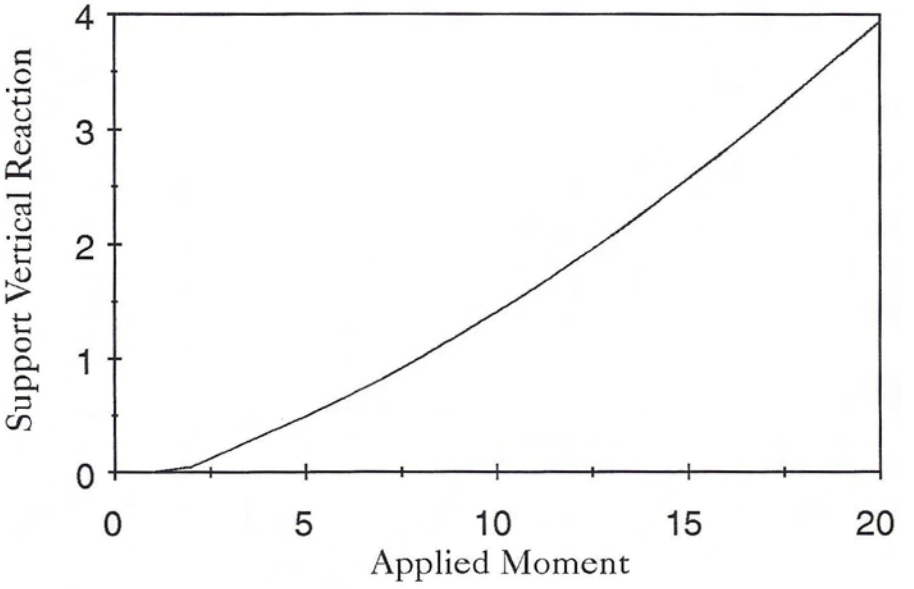

Figure 3.11: Elastic Beam on Rigid Foundation: Support Reaction

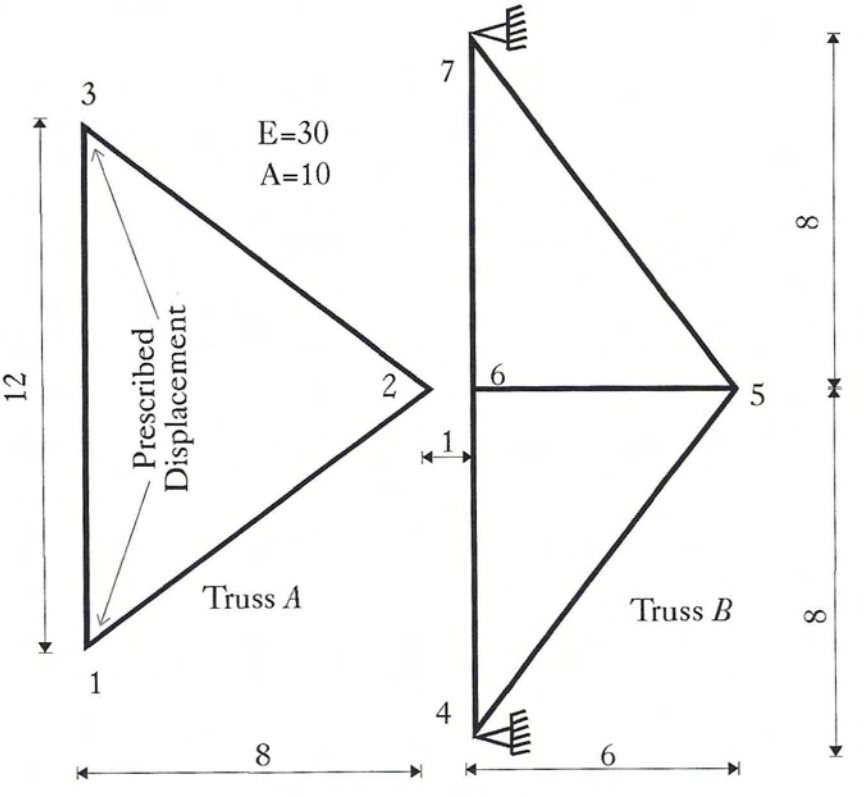

Figure 3.12: Contact of Two Flexible Trusses

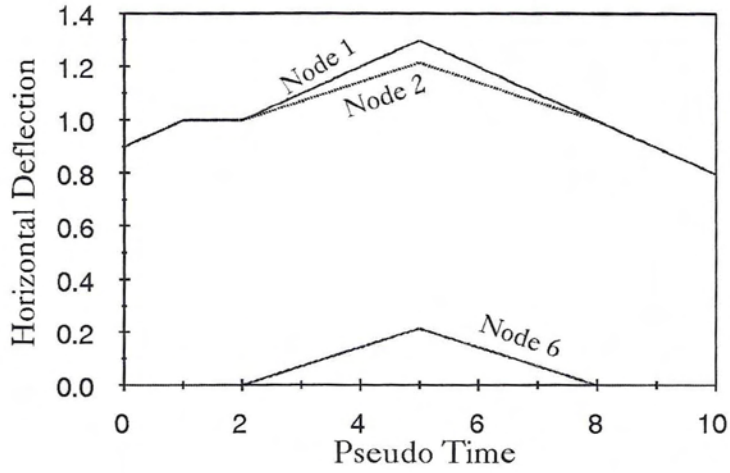

Figure 3.13: Contact of Two Flexible Trusses: Nodal Horizontal Displacement

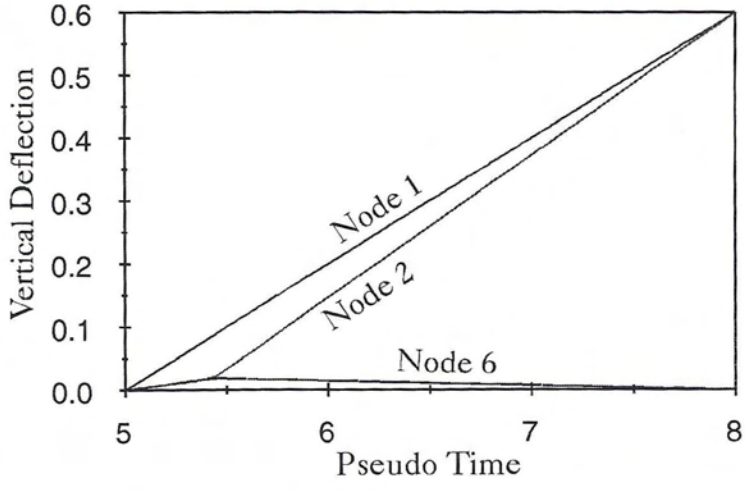

Figure 3.14: Contact of Two Flexible Trusses: Nodal Vertical Displacement

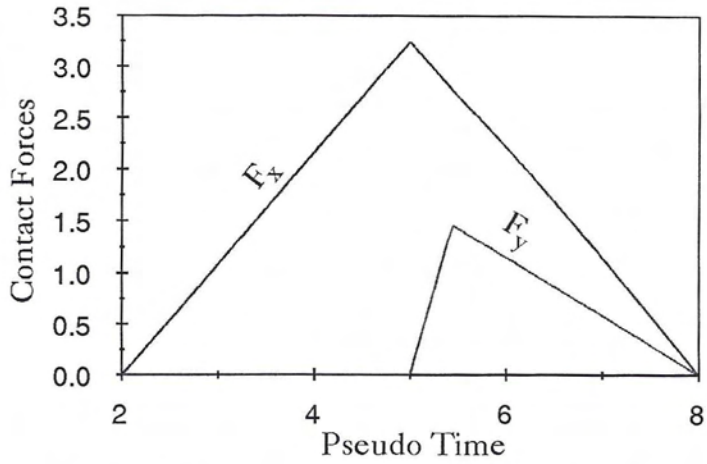

Figure 3.15: Contact of Two Flexible Trusses: Contact Forces at Node 2

3.4.2 Three-Dimensional Numerical Examples

Nonlinear Uplift Behavior of a Circular Plate

A nonlinear behavior has been demonstrated by unanchored liquid storage tanks during earthquakes. Amongst the factors which contribute to such a complex behavior, there are two characteristics associated with base plate uplifting that add to the intricacy of the problem. The first complexity arises because the contact area of base plate with its supporting foundation is continually changing as uplift forces change. Secondly, the transverse deflection of the plate may become large in comparison with the base plate thickness, thereby inducing membrane forces that could not be ignored in the analysis. In this example, a thin circular plate of 1.25 cm thickness and 6 m radius was subjected to a downward hydrostatic pressure of 49.1 KN/m^2 and an uplifting force acting along the periphery of the outer circle which is given by

$$p_u = P_u \frac{1 + \cos\theta}{2} \tag{3.24}$$

where P_u is the amplitude of the uplift force, and θ is an angle measured from the direction of the earthquake excitation. The plate has been discretized as shown in

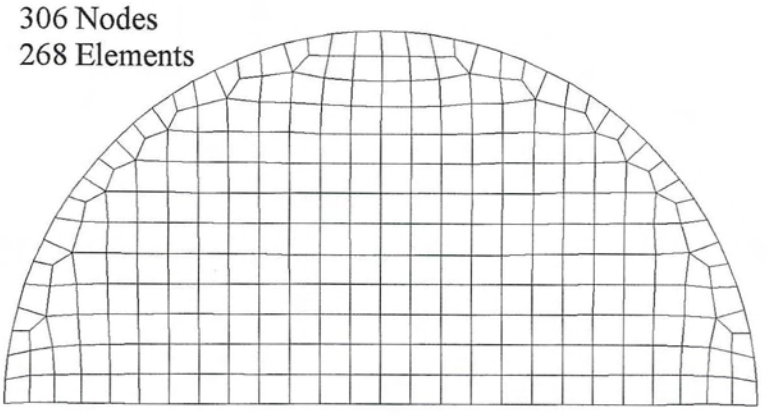

Figure 3.16: The Finite Element Model Used for the Plate

Figure (3.16). The membrane degrees of freedom along the periphery of the outer circle of the plate and the boundaries of the contact area were assumed fixed. Three cases of the rotation degrees of freedom along the periphery of the outer circle of the plate are presented in Figure (3.17): free, fully restrained and partially restrained. Results conform with those presented in [13].

Longitudinal Impact of a Bar on a Rigid Wall

A slender elastic bar moving with a uniform velocity V is considered to impact a rigid half space, see Figure (3.18). The analysis is performed to calculate the generated impact stresses in the bar material.

The bar is chosen to be the contactor body and it is discretized using twenty eight-node 3 D solid elements. The contactor surface consists of one four node segment. The rigid half space is the target body and the target surface is defined by four nodes each having no degrees of freedom. The average impact stress at the bar tip is found to be 1.0 which agrees with both the analytical and numerical solution presented in [31].

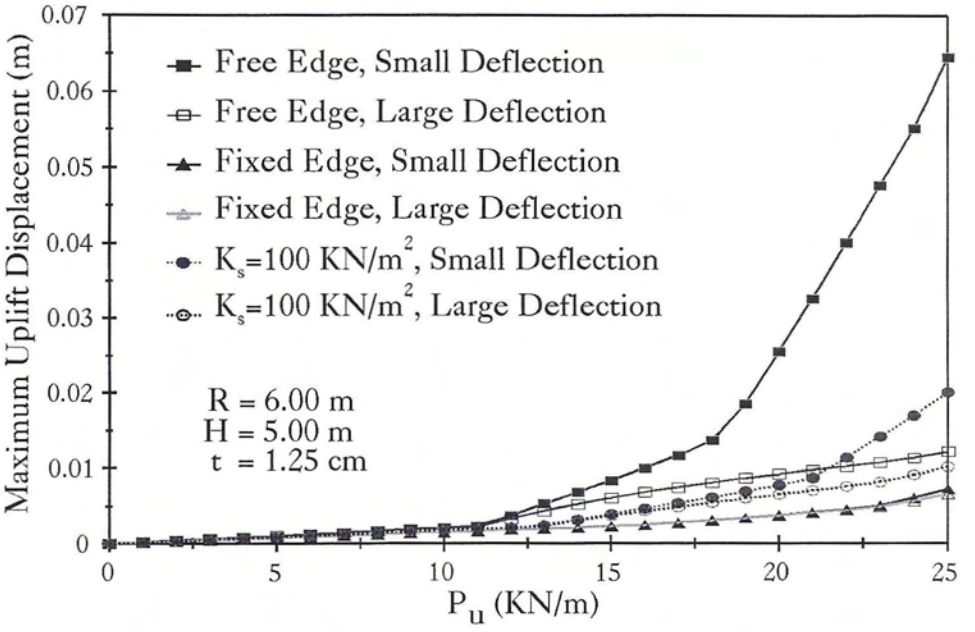

Figure 3.17: Uplift Displacement vs Uplift Force

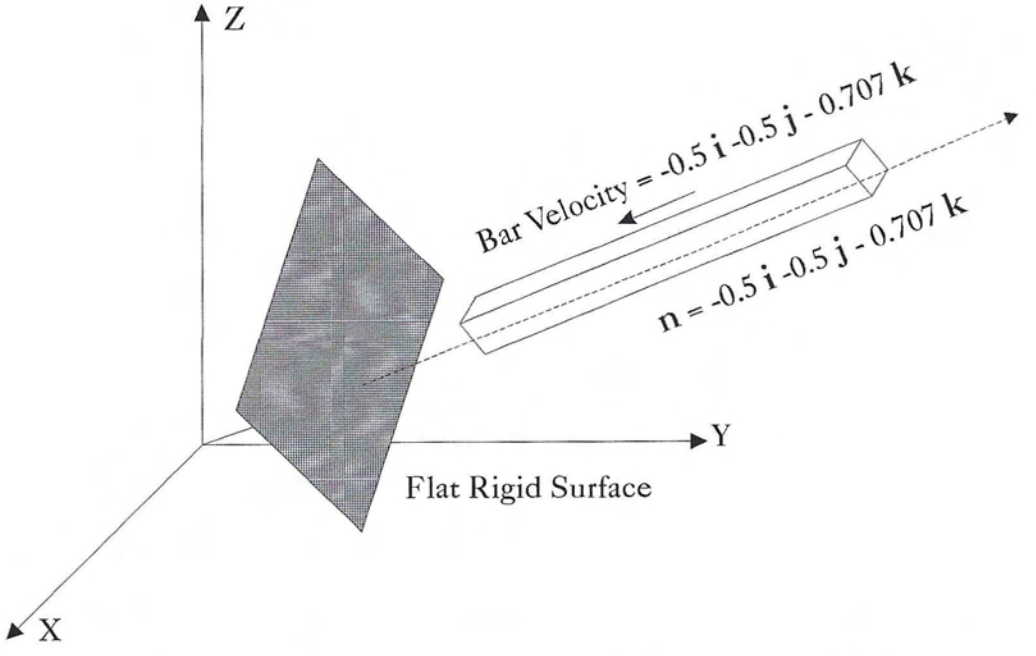

Figure 3.18: Analysis of Longitudinal Impact of a Bar onto a Rigid Surface

Chapter 4

Liquid Domain Formulation

The dynamic response of liquids has significant influence on the response of their containers. Inappropriate approximation of the liquid motion may lead to major errors in estimating the seismic response of the containers. The liquid pressures and the impact forces form the measurable level of the energy transferred to the tank shell. In addition, the motion of the tank wall is the primary source for the liquid energy. Since this energy transfer occurs simultaneously throughout the liquid boundary, it is essential in the finite element analysis of such problems to use a model that effectively deals with the coupling between the liquid and the tank wall.

The equations of motion of a liquid may be formulated by two different approaches, corresponding to the two ways in which the problem of determining the motion of a liquid mass, acted on by given forces and subjected to given boundary conditions, may be viewed. The Eulerian formulation is obtained by considering the object of our investigations to be the knowledge of the velocity, pressure and density at all points of space occupied by the liquid for all instances. On the other hand, the Lagrangian form is obtained by considering the object to be the determination of the history of each particle. Detailed discussions of the two forms may be found in [146]. In the current investigation, a Lagrangian description of the structure's

motion is utilized, which makes it necessary to use a Lagrangian description of the liquid-structure interface in order to enforce compatibility between the structure and liquid elements. The continuity equation in the Eulerian form is utilized inside the liquid domain to mathematically describe the liquid motion inside the tank.

The liquid in this analysis is considered to be inviscid, irrotational and incompressible. Such simplifying assumptions allow displacements, pressures or velocity potentials to be the variables in the liquid domain. The displacement-based liquid elements may be easy to incorporate in finite element programs for structural analysis and simplify the enforcement of the liquid-structure interface constraints. However, such elements require two or three degrees of freedom per node. In addition, this approach is not well suited for problems with large liquid displacements and requires special care to prevent zero-energy rotational modes from arising. Alternatively, using pressures or velocity potentials as the unknown degrees of freedom requires only one degree of freedom per node inside the liquid domain, which significantly reduces the computational cost of the analysis, and adequately represent the physical behavior of the liquid. The latter approach is used in this investigation.

4.1 Variational Principles of the Liquid-Structure Interaction Problem

In general, liquid-structure interaction may be divided into five categories. Each category requires specific formulation and unknowns that may not be suitable for others. As shown in Figure (4.1), category five is characterized by the free surface

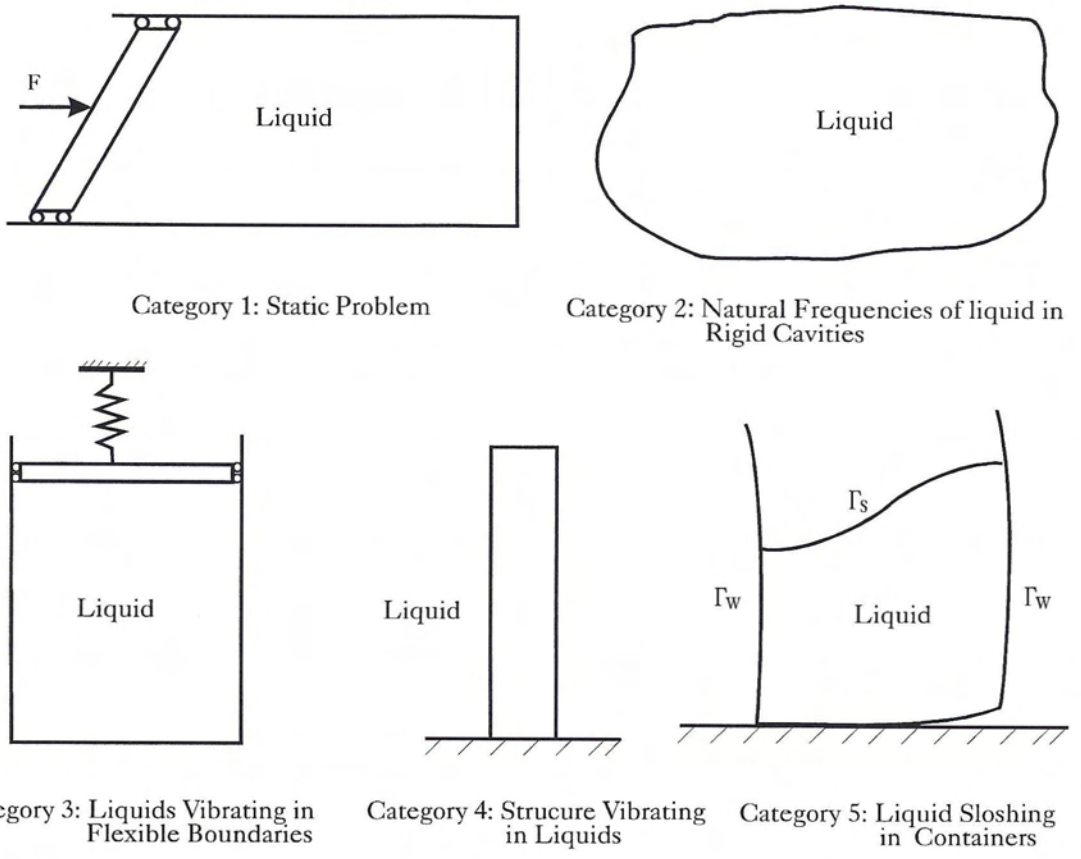

Category 1: Static Problem

Category 2: Natural Frequencies of liquid in Rigid Cavities

Category 3: Liquids Vibrating in Flexible Boundaries

Category 4: Strucure Vibrating in Liquids

Category 5: Liquid Sloshing in Containers

Figure 4.1: Categories of the Liquid-Structure Interaction Problems

existence, which combines the sloshing phenomenon with the liquid-structure interaction. The free surface may also be viewed as a structure boundary for the liquid, but with zero stiffness. Since this structure boundary can not take any force, the liquid pressure has to be eliminated on this boundary in order to fulfill the equilibrium conditions.

The virtual work statement that is used to describe the nonlinear liquid sloshing in either anchored or unanchored tanks (category 5) is developed in this section. Figure (4.2) shows the general geometry of a liquid sloshing in an unanchored tank. It should be pointed out that unanchored tanks are characterized by the successive contact and separation between the tank base plate and its foundation. The nonlinear

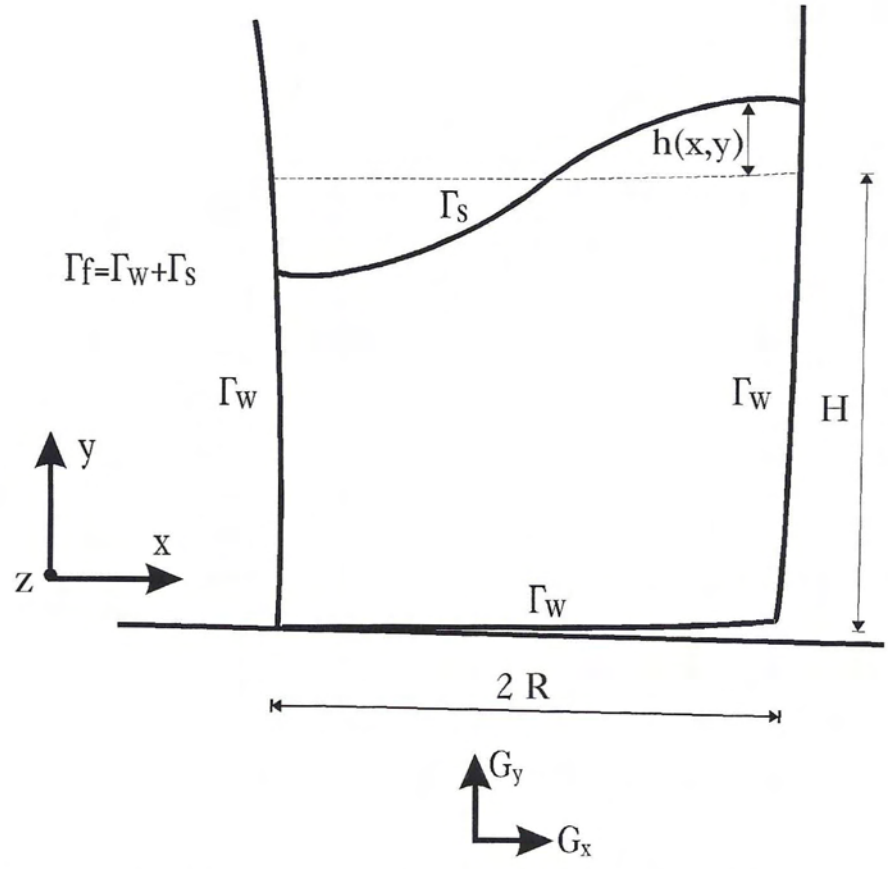

Figure 4.2: Geometry of the Nonlinear Liquid Sloshing in Flexible Tanks

boundary conditions that result from this behavior are enforced separately by means of the contact analysis presented before. Thus, the formulation presented in this section is independent of the tank support condition. This property of the current formulation allows it to be used in the analysis of various liquid storage tanks with different support conditions, such as anchored, unanchored and elevated tanks. Also, the formulation is not restricted to containers with vertical walls but rather allows the modeling of tanks of any shape.

4.1.1 Structural Domain

Following Hamilton's principle, the energy function for the structural domain may be written as

$$\begin{aligned}\Pi_s &= \int_{t_1}^{t_2} \left[\frac{1}{2} \int_{\Omega_s} \boldsymbol{\epsilon}^T \mathbf{E}\, \boldsymbol{\epsilon}\, d\Omega_s - \frac{1}{2} \int_{\Omega_s} \rho_s \dot{\mathbf{u}}^T \dot{\mathbf{u}}\, d\Omega_s \right. \\ &- \left. \int_{\Gamma_w} \mathbf{u}^T \mathbf{f}^I\, d\Gamma_w - \int_{\Omega_s} \mathbf{u}^T \mathbf{f}^E\, d\Omega_s \right] dt \end{aligned} \tag{4.1}$$

where $\mathbf{E}$ is the stress-strain matrix, $\boldsymbol{\epsilon}$ is the strain vector, $\mathbf{u}$ is the displacement vector, Ω_s is the structural domain, Γ_w is the wet surface of the structure, $\mathbf{f}^I$ is the liquid pressure vector, $\mathbf{f}^E$ is the body force vector and ρ_s is the mass density of the structure. Setting variations on Π_s to zero gives the principle of virtual displacements

$$\begin{aligned}\delta\Pi_s = \int_{\Omega_s} \delta\boldsymbol{\epsilon}^T \mathbf{E}\, \boldsymbol{\epsilon}\, d\Omega_s &+ \int_{\Omega_s} \rho_s \delta\mathbf{u}^T \ddot{\mathbf{u}}\, d\Omega_s - \int_{\Gamma_w} \delta\mathbf{u}^T \mathbf{f}^I\, d\Gamma_w \\ &- \int_{\Omega_s} \delta\mathbf{u}^T \mathbf{f}^E\, d\Omega_s = 0 \end{aligned} \tag{4.2}$$

4.1.2 Liquid Domain

Following the work done by Kock and Olson [141], the variational indicator of an incompressible liquid flowing under gravity field is obtained by subtracting the kinetic energy from the potential energy of an infinitesimal element of volume $d\Omega_f$, then integrating over the liquid domain Ω_f, which yields

$$\Pi_f = \int_{t_1}^{t_2} \left[\int_{\Omega_f} \left\{ \rho_f g y - \frac{1}{2} \rho_f \mathbf{V}.\mathbf{V} \right\} d\Omega_f \right] dt \tag{4.3}$$

where ρ_f is the mass density of the liquid, y is the Cartesian coordinate measured in a direction opposite to that of the gravitational acceleration g, and $\mathbf{V}$ is the velocity vector. The continuity condition and the kinematic condition are still need to be

enforced on the liquid domain. The kinematic condition insures that the normal liquid velocity at the liquid boundary matches the rate of normal displacement of the boundary. Using Lagrange multipliers, the two conditions are added to the variational indicator as follows

$$\Pi_f = \int_{t_1}^{t_2} \left[\int_{\Omega_f} \left\{ \rho_f g y - \frac{1}{2} \rho_f \mathbf{V}.\mathbf{V} - \lambda_1 \rho_f \nabla \mathbf{V} \right\} d\Omega_f + \int_{\Gamma_f} \lambda_2 \left\{ v_n - \dot{u}_n \right\} d\Gamma_f \right] dt \quad (4.4)$$

where λ_i refers to the i th Lagrange Multiplier, $\dot{u}_n$ is the time derivative of the normal displacement of the boundary and v_n is the normal velocity at the liquid boundary. Taking variations with respect to $\mathbf{V}$ gives the following Euler-Lagrange equations

$$\delta \mathbf{V} : \quad -\rho_f \mathbf{V} + \rho_f \nabla \lambda_1 = 0 \qquad \text{in } \Omega_f \quad (4.5)$$

$$\delta v_n : \quad \lambda_2 - \rho_f \lambda_1 = 0 \qquad \text{on } \Gamma_f \quad (4.6)$$

Thus,

$$\mathbf{V} = \nabla \lambda_1 \quad (4.7)$$

$$\lambda_2 = \rho_f \lambda_1 \quad (4.8)$$

It is evident from Equation (4.7) that physically λ_1 is the scalar velocity potential. Therefore, Equation (4.4) may be rewritten as

$$\Pi_f = \int_{t_1}^{t_2} \rho_f \left[\int_{\Omega_f} \left\{ g y - \frac{1}{2} \nabla^2 \phi - \phi \nabla^2 \phi \right\} d\Omega_f + \int_{\Gamma_f} \phi \left\{ \frac{\partial \phi}{\partial \mathbf{n}} - \dot{u}_n \right\} d\Gamma_f \right] dt \quad (4.9)$$

After integrating by parts, Equation (4.9) may be rewritten as

$$\Pi_f = \int_{t_1}^{t_2} \rho_f \left[\int_{\Omega_f} \left\{ g y + \frac{1}{2} \nabla^2 \phi + \dot{\phi} \right\} d\Omega_f \right] dt \quad (4.10)$$

or concisely,

$$\Pi_f = \int_{t_1}^{t_2} \left[\int_{\Omega_f} P d\Omega_f \right] dt \quad (4.11)$$

where P is the total pressure which may be also written as

$$P = P_o - \gamma_f \left[\frac{1}{g} \frac{\partial \phi}{\partial t} + \frac{\nabla \phi . \nabla \phi}{2g} + y \right] \quad (4.12)$$

where P_o is the hydrostatic pressure at the point.

4.1.3 Coupled Liquid-Structure System

In order to apply the variational principle to the liquid-structure interaction problem, the liquid and the structure functionals, given by Equations (4.1) and (4.10), are combined together. The two statements are coupled at the liquid-structure interfaces by

$$\ddot{u}_n = \frac{\partial \phi}{\partial \mathbf{n}} \tag{4.13}$$

$$\mathbf{f}^I = P\,\mathbf{n} \tag{4.14}$$

where $\mathbf{n} = (n_x, n_y, n_z)$ is the outward normal unit vector from the liquid towards the structure.

4.2 Finite Element Discretization

The development of the liquid element that is capable of modeling the liquid behavior in flexible liquid storage tanks is achieved throughout several stages. First, the classical isoparametric liquid element, which is also used to model the liquid motion inside the liquid domain, is developed. Then, the element is enhanced with the nonlinear sloshing and liquid-structure interaction in order to model the liquid boundaries.

4.2.1 Isoparametric Liquid Element Formulation

The strong form of the steady state velocity potential flow of incompressible liquid may be stated as follows:

Given $v_n(\mathbf{x}) : \Gamma_f \rightarrow \mathbf{R}$ find $\phi(\mathbf{x}) : \Omega_f \rightarrow \mathbf{R}$ such that

$$\text{Continuity Condition:} \qquad \rho_f \bigtriangledown^2 \phi(\mathbf{x}) = 0, \qquad \forall \ \mathbf{x} \in \Omega_f \tag{4.15}$$

$$\text{Kinematic Condition:} \qquad \frac{\partial \phi}{\partial \mathbf{n}} = v_n, \qquad \forall \ \mathbf{x} \in \Gamma_f \tag{4.16}$$

where v_n is the prescribed normal velocity across the liquid boundaries. This strong form yields the following variational equation

$$\rho_f \int_{\Omega_f} \bigtriangledown(\delta\phi) \bigtriangledown\phi \, d\Omega_f = \rho_f \int_{\Gamma_f} \delta\phi \, v_n \, d\Gamma_f \tag{4.17}$$

Following the classical isoparametric finite element discretization, the following relations are obtained;

$$\mathbf{K}_f = \rho_f \int_{\Omega_f} \mathbf{B}_f^T \mathbf{B}_f \, d\Omega_f \tag{4.18}$$

$$\mathbf{F}_{int} = \rho_f \int_{\Omega_f} \mathbf{B}_f^T \mathbf{V}_f \, d\Omega_f \tag{4.19}$$

$$\mathbf{F}_{ext} = \rho_f \int_{\Gamma_f} \mathbf{N} v_n \, d\Gamma_f \tag{4.20}$$

$$= \rho_f \int_{\Gamma_f} \begin{bmatrix} N_1N_1 & N_1N_2 & \dots \\ N_2N_1 & N_2N_2 & \dots \\ \vdots & \vdots & \ddots \end{bmatrix} d\Gamma_f \begin{Bmatrix} v_{n1} \\ v_{n2} \\ \vdots \end{Bmatrix} \tag{4.21}$$

$$= \mathbf{M}_f^j \mathbf{v}_n \tag{4.22}$$

$$[B_f] = \begin{bmatrix} \frac{\partial N_1}{\partial x} & \frac{\partial N_2}{\partial x} & \dots \\ \frac{\partial N_1}{\partial y} & \frac{\partial N_2}{\partial y} & \dots \\ \vdots & \vdots & \ddots \end{bmatrix} \tag{4.23}$$

$$\{V_f\} = \bigtriangledown\phi = \mathbf{B}_f \Phi \tag{4.24}$$

where $\mathbf{K}_f$ is the liquid stiffness matrix, $\mathbf{F}_{int}$ and $\mathbf{F}_{ext}$ are the liquid internal and external flow vectors, respectively, $\mathbf{V}_f$ is the liquid velocity vector, Φ is the nodal velocity potential vector, j is the liquid element edge number that is subjected to a normal discharge of speed v_n, $\mathbf{M}_f^j$ is the liquid element mass matrix for edge number j and N_i

is the ith isoparametric shape function. Physically, $\mathbf{F}_{ext}$ is the nodal discharge vector entering or leaving the element domain as a result of the normal velocity of the liquid across the liquid domain boundaries. This natural boundary condition ensures the normal velocity compatibility at the liquid boundaries (kinematic condition). The tangential velocity does not contribute to the discharge vector and consequently will have no effect on the continuity equation. $\mathbf{F}_{int}$ is the internal discharge vector resulting from the current gradient of the velocity potential function, ϕ. The continuity equation is satisfied when $\mathbf{F}_{int}$ and $\mathbf{F}_{ext}$ are in equilibrium. The residual discharge is then given by

$$\mathbf{R}_f = \mathbf{F}_{ext} - \mathbf{F}_{int} \tag{4.25}$$

This residual is mainly caused by the free surface motion and the consequent remeshing of the liquid domain. This yields to an iterative modified Newton-Rapson scheme in the form

$$[K_f]\{\delta\phi\}_i = \{R_f\}_i \tag{4.26}$$

The vector $\delta\Phi_i$ is then used to correct the velocity potential vector after the ith iteration.

4.2.2 Nonlinear Liquid Sloshing in Rigid Tanks

liquid sloshing is defined to be the free surface gravity waves caused by an excitation to a liquid domain. Figure (4.3) shows the geometry of the problem of liquid sloshing in a rigid tank. In the special case of rigid tank, the translational motion of the liquid boundaries are directly proportional to the ground excitation. The normal velocity of the boundaries is then given by

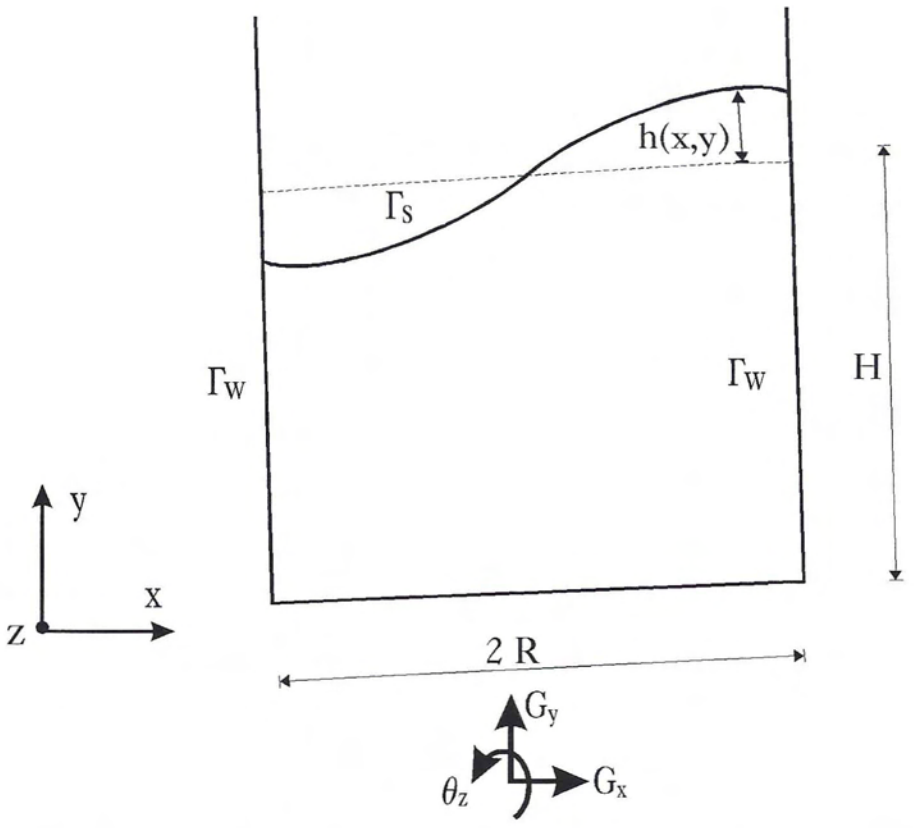

Figure 4.3: Geometry of the Nonlinear Liquid Sloshing in a Rigid Tank

$$\mathbf{V}(\mathbf{x},t) = \dot{\mathbf{G}} + \begin{bmatrix} 0 & r_z & -r_y \\ -r_z & 0 & r_x \\ r_y & -r_x & 0 \end{bmatrix} \begin{Bmatrix} \dot{\theta}_x \\ \dot{\theta}_y \\ \dot{\theta}_z \end{Bmatrix} \tag{4.27}$$

$$v_n(\mathbf{x},t) = \mathbf{V}.\mathbf{n} \tag{4.28}$$

where $\mathbf{n}$ is the normal to the liquid boundary, (r_x, r_y, r_z) is the position vector of a generic point on the liquid boundary, $\dot{\mathbf{G}}$ is the ground translation velocity vector and $(\dot{\theta}_x, \dot{\theta}_y, \dot{\theta}_z)$ is the ground rotational velocity vector. In plane problems, Equation (4.27) is reduced to

$$\mathbf{V}(\mathbf{x},t) = \dot{\mathbf{G}} + \begin{Bmatrix} -r_y \\ r_x \end{Bmatrix} \dot{\theta}_z \tag{4.29}$$

The strong form of the boundary value problem that represent the nonlinear liquid sloshing in a rigid tank is stated as follows:

Given $v_n(\mathbf{x},t) : \Gamma_w \times [0,T] \rightarrow \mathbf{R}$, the initial free surface Γ_{so}, and the initial conditions of the potential function $\phi_o(\mathbf{x}) : \Omega_f \rightarrow \mathbf{R}$, find $\phi(\mathbf{x},t) : \overline{\Omega}_f \times [0,T] \rightarrow \mathbf{R}$ and $\Gamma_s \times [0,T] \rightarrow \mathbf{R}$ such that

$$\text{Continuity Condition:} \qquad \nabla^2\phi(\mathbf{x},t) = 0, \qquad \forall\ \mathbf{x} \in \overline{\Omega}_f \tag{4.30}$$

$$\text{Initial Conditions:} \qquad \phi(\mathbf{x},0) = \phi_o(\mathbf{x}), \qquad \forall\ \mathbf{x} \in \Omega_f \tag{4.31}$$

$$\Gamma_s(0) = \Gamma_{so} \tag{4.32}$$

$$\text{Kinematic Condition:} \qquad \frac{\partial\phi}{\partial\mathbf{n}} = v_n, \qquad \forall\ \mathbf{x} \in \Gamma_w \tag{4.33}$$

$$\text{Dynamic Condition:} \qquad \frac{\partial\phi}{\partial t} = -\frac{\nabla^2\phi}{2} - gh, \qquad \forall\ \mathbf{x} \in \Gamma_s \tag{4.34}$$

$$\text{Kinematic Condition:} \qquad \frac{\partial\phi}{\partial y} = \frac{\partial h}{\partial t} + \frac{\partial\phi}{\partial x}\frac{\partial h}{\partial x} + \frac{\partial\phi}{\partial z}\frac{\partial h}{\partial z}, \qquad \forall\ \mathbf{x} \in \Gamma_s \tag{4.35}$$

where Γ_s is the free surface boundary, Γ_w is liquid boundary in contact with the tank wall or base plate and h is the free surface elevation. Equation (4.34) represents the dynamic condition that comes from prescribing the pressure value at the free surface in Bernulli's equation, while Equation (4.35) represents the kinematic condition that enforces the vertical velocity compatibility between the free surface and the liquid domain.

As a result of the simplified assumptions, lack of viscosity sometimes causes undesirable contribution from the high frequency components in the numerical solution of the problem. This contribution is undesirable because of the high frequency modes in the solution that are poorly represented in the discritized system. Any wave that has a length shorter than the element width is not represented adequately due to the limited order of the shape functions. As a result, dispersion error may develop in the solution of some problems. This occurs, sometimes, when the liquid is in the

resonance zone or when the excitation level is relatively high. Numerical dissipation may be used then to damp out the high frequency wave components propagating near the free surface. A numerical dissipation term was suggested by Chen [32] for the two-dimensional solution of the problem. He reported that this term has a little effect on the low frequency modes that govern the solution. After incorporating the numerical dissipation, Equation (4.35) may be rewritten in the two-dimensional case as

$$\frac{\partial \phi}{\partial y} + \nu_x \frac{\partial^2 h}{\partial x^2} = \frac{\partial h}{\partial t} + \frac{\partial \phi}{\partial x}\frac{\partial h}{\partial x} \tag{4.36}$$

where ν_x is the damping parameters given as function of the mesh density, l_x, and the wave convection speed relative to the mesh $\mathbf{V}_r$ as

$$\nu_x = \mu \frac{l_x}{2} |V_{rx}| \tag{4.37}$$

where l_x is taken as the width of the liquid element below the free surface in the x direction and μ is a parameter varies between 0 and 1 to tune the damping globally. In addition, the simplified assumptions, sometimes, causes physical instability of the numerical solution used when the free surface slope is very steep, 70° to 80°. This is attributed to the wave breaking phenomenon which is not incorporated into the current model. This is very likely to occur when the liquid is in the resonance zone, e.g. Figure (4.23), or when the excitation level is relatively high, e.g. Figure (4.24).

In case of large amplitude surface waves, it is desirable to update the mesh to follow the liquid boundaries and to avoid distorted elements. In such a case, the time derivatives of any spatial function should be modified to account for mesh speed according to the following relation

$$\frac{\partial F}{\partial t} = \frac{\partial f}{\partial t} - \mathbf{V}_m \cdot \nabla f \tag{4.38}$$

where $\mathbf{V}_m$ is the mesh speed and F is the function defined with respect to the fixed coordinate system while f is the function defined with respect to the moving mesh.

Discrete Finite Element Implementation

Discrete finite element implementation is achieved by enhancing the isoparametric element developed in Section 4.2.1 to model large amplitude free surface liquid sloshing in rigid tank. This is performed by enforcing the nonlinear dynamic and kinematic conditions given by Equations (4.34) and (4.35) directly on each of the free surface nodes iteratively, as follows

$$(R_d)_i = \rho_f A_i \left(\frac{\partial \phi}{\partial t} + \frac{\nabla^2 \phi}{2} + gh \right)_i \tag{4.39}$$

$$(R_k)_i = \rho_f A_i \left(\frac{\partial h}{\partial t} + \frac{\partial \phi}{\partial x}\frac{\partial h}{\partial x} + \frac{\partial \phi}{\partial z}\frac{\partial h}{\partial z} - \frac{\partial \phi}{\partial y} \right)_i \tag{4.40}$$

where A_i is the liquid free surface node tributary area projected in the horizontal plane, h is the free surface elevation, and $(R_d)_i$ and $(R_k)_i$ are the residuals corresponding to the dynamic and the kinematic equations at the node after iteration i, respectively. Physically, R_d represent the pressure force applied at the free surface node due to violation of the dynamic condition, while R_k is the discharge vector at the free surface node resulting from violating the kinematic condition. At equilibrium, the global residual vector of the entire system should be zero, which means that both the dynamic and kinematic conditions are satisfied at the free surface nodes. Taking the first variation of R_k and R_d gives, after linearization, the following modified Newton-Rapson Iterative scheme at each free surface node

$$\begin{bmatrix} 0 & \rho_f A_i \\ \rho_f A_i & 0 \end{bmatrix} \begin{Bmatrix} \delta\dot{\phi} \\ \delta\dot{h} \end{Bmatrix} + \begin{bmatrix} 0 & 0 \\ 0 & \rho_f A_i g \end{bmatrix} \begin{Bmatrix} \delta\phi \\ \delta h \end{Bmatrix} = \begin{Bmatrix} R_k \\ R_d \end{Bmatrix} \tag{4.41}$$

It should be pointed out that the variation of the liquid velocity and free surface slopes are ignored in Equation (4.41). This linearized version of the iterative scheme yields a symmetric coefficient matrix on the left hand side, however, it requires few more iterations to satisfy equilibrium. Although nonlinear schemes may be faster to converge, but they produce a nonsymmetric coefficient matrix on the left hand side, which requires almost double of the symmetric storage and computational cost.

Continuous Finite Element Implementation

Continuous finite element implementation is achieved by working directly from the variational indicator. In order to derive the virtual work statements to be discretized, the variations of Equation (4.10) with respect to ϕ and u_n are taken, thus

$$\delta\phi: \qquad \rho_f \int_{\Omega_f} \nabla(\delta\phi)\, \nabla\phi \; d\Omega_f - \rho_f \int_{\Gamma_f} \delta\phi \; \dot{u}_n \; d\Gamma_f = 0 \tag{4.42}$$

$$\delta u_n: \qquad \int_{\Gamma_s} P\delta u_n \; d\Gamma_s = 0 \tag{4.43}$$

Equation (4.42) may be rewritten as

$$\delta\phi: \quad \rho_f \int_{\Omega_f} \nabla \; (\nabla\phi) \; \delta\phi \; d\Omega_f - \rho_f \int_{\Gamma_f} \delta\phi \; \left(\dot{u}_n - \frac{\partial\phi}{\partial \mathbf{n}}\right) \; d\Gamma_f = 0 \tag{4.44}$$

Since the virtual variables are arbitrary, the Euler equations that govern the liquid behavior are

$$\text{Continuity Condition:} \qquad \nabla^2\phi = 0 \quad \text{on } \Omega_f \tag{4.45}$$

$$\text{Kinematic Condition:} \qquad \dot{u}_n = \frac{\partial\phi}{\partial \mathbf{n}} \quad \text{on } \Gamma_f \tag{4.46}$$

$$\text{Dynamic Condition:} \qquad P = 0 \quad \text{on } \Gamma_s \tag{4.47}$$

Equation (4.46) represents the kinematic condition at the liquid-structure interface Γ_w and at the free surface Γ_s. On the other hand, Equation (4.47) represents the

dynamic condition only at the free surface Γ_s because u_n is considered as unknown only at the free surface.

Linearization of Equations (4.42) and (4.43) is achieved by assuming that the free surface elevation h is equal to the normal displacement of the free surface u_n and ignoring the term $\nabla^2\phi$ in Equation (4.12), this yields to

$$\begin{bmatrix} 0 & \mathbf{M}_f^j \\ \mathbf{M}_f^j & 0 \end{bmatrix} \begin{Bmatrix} \delta\dot{\Phi} \\ \delta\dot{\mathbf{h}} \end{Bmatrix} + \begin{bmatrix} 0 & 0 \\ 0 & g\mathbf{M}_f^j \end{bmatrix} \begin{Bmatrix} \delta\Phi \\ \delta\mathbf{h} \end{Bmatrix} = \begin{Bmatrix} \mathbf{R}_k \\ \mathbf{R}_d \end{Bmatrix} \tag{4.48}$$

$$\mathbf{R}_d = \mathbf{M}_f^j \left\{ \frac{\partial\phi}{\partial t} + \frac{\nabla^2\phi}{2} + gh \right\} \tag{4.49}$$

$$\mathbf{R}_k = \mathbf{M}_f^j \mathbf{v}_n - \rho_f \int_\Omega \mathbf{B}_f^T \mathbf{V}_f \, d\Omega \tag{4.50}$$

where j is the free surface edge number, $\mathbf{V}_f$ is the liquid velocity vector and $\mathbf{v}_n$ is the normal velocity vector at free surface nodes. The normal velocity at a free surface node i is computed as

$$v_{ni} = \mathbf{n}_i^T \begin{Bmatrix} V_x \\ \dot{h} \\ V_z \end{Bmatrix}_i \tag{4.51}$$

where $\mathbf{n}_i$ is the normal vector to the free surface at the node, and V_x and V_z are the velocity of free surface node i in the x and z directions due to the mesh speed, respectively.

4.2.3 Nonlinear Liquid Sloshing in Flexible Tanks

The modified Newton-Rapson method is used to solve the nonlinear system of equations. The left hand side of the system represent the tangent coefficient matrix,

while the right hand side represent the residual vector. Most elements have contribution to both sides. In this section, the contribution of the liquid-structure interaction element to both sides is presented.

On the Right Hand Side

As shown in Figure (4.4), a tank node in contact with the liquid domain is subjected to the liquid pressure and, at the same time, delivers energy to the liquid. Since the liquid mesh is updated after each iteration to comply with the new free surface shape and deformed boundaries of the structure, the liquid nodes are moving with respect to the structure nodes. A geometric analysis, similar to what need to be performed in contact analysis, is applied on liquid and structure nodal coordinates and displacements to determine which liquid element is in contact with the current structure node. The normal velocity compatibility condition at liquid-structure interfaces gives

$$\dot{u}_n = \frac{\partial \phi}{\partial \mathbf{n}} \tag{4.52}$$

This condition causes an external discharge vector to be applied on the liquid element due to the normal velocity of the structure boundary. Hence,

$$\mathbf{F}_{ext} = \rho_f \int_{\Gamma_w^f} \mathbf{N} \; d\Gamma_w^f \;\; \mathbf{n}^T \dot{\mathbf{u}} \tag{4.53}$$

where Γ_w^f is the liquid element surface in contact with the tank wall and $\mathbf{N}$ is the shape function vector for the element nodes located on that surface. The dynamic condition at liquid-structure interfaces requires that the liquid pressure be integrated and applied on the structure node, which gives

$$\mathbf{F}^I = \int_{T_a} P \; \mathbf{n} \; dT_a = T_a \; P \; \mathbf{n} \tag{4.54}$$

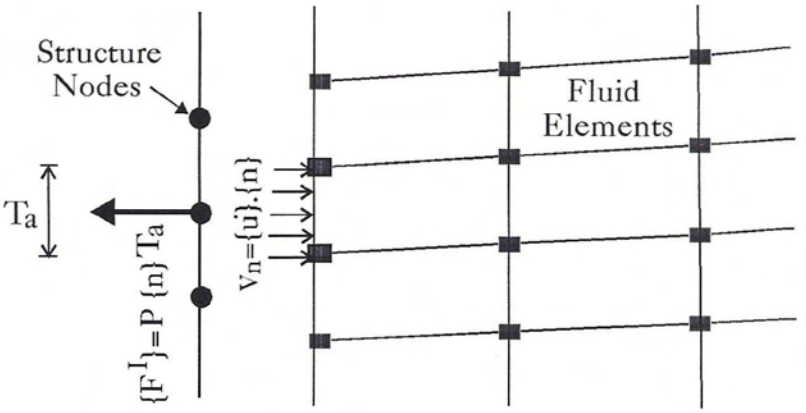

Figure 4.4: Boundary Conditions at a Structure Node in Contact with a Liquid Element

where T_a is the tributary area served by the structure node and P is the total pressure at the structure node given by Equation (4.12).

On the Left Hand Side

Invoking the variation of Equation (4.53) gives

$$\delta \mathbf{F}_{ext} = \rho_f \int_{\Gamma_w^f} \mathbf{N}\, d\Gamma_w^f\, \mathbf{n}^T\, \delta \dot{\mathbf{u}} \tag{4.55}$$

while invoking the variation of equation (4.54) provides

$$\delta \mathbf{F}^I = T_a\, \mathbf{n}\, \delta P \tag{4.56}$$

$$= T_a\, \mathbf{n}\, \delta \left(P_o - \gamma_f \left[\frac{1}{g} \frac{\partial \phi}{\partial t} + \frac{\nabla \phi . \nabla \phi}{2g} + y \right] \right) \tag{4.57}$$

which after linearization gives

$$\delta \mathbf{F}^I = T_a\, \rho_f\, \mathbf{n}\, \delta \dot{\Phi} = T_a\, \rho_f\, \mathbf{n}\, \mathbf{N}^T\, \delta \dot{\Phi} \tag{4.58}$$

Equation (4.55) simulates the effect of small change in the structure degrees of freedom on the liquid discharge vector, while Equation (4.58) simulates the effect of small

change in the liquid degrees of freedom on the pressure force vector applied on the structure. Therefore, the liquid-structure coupling matrix is given as

$$\mathbf{C}_{fs} = \rho_f \int_{\Gamma_w^f} \mathbf{N}\ d\Gamma_w^f\ \ \mathbf{n}^T \tag{4.59}$$

while the structure-liquid coupling matrix is given as

$$\mathbf{C}_{sf} = T_a\ \rho_f\ \mathbf{n}\ \mathbf{N}^T \tag{4.60}$$

In order to achieve symmetric equations, the liquid-structure coupling matrix should be equal to the transpose of the structure-liquid coupling matrix. For this to be so, to satisfy this condition, one states

$$T_a \mathbf{N} = \int_{\Gamma_w^f} \mathbf{N}\ d\Gamma_w^f \tag{4.61}$$

which could be easily maintained by choosing the finite element mesh of both the liquid and the structure domains on the interface to posses the following properties

1. The tributary area served by the structure node coincide with the liquid element edge in contact with the structure, i.e. $T_a = \Gamma_w^f$

2. The structure node location is chosen such that the shape function vector of the fluid element at the structure node equals to the vector that consists of the ratios of the surface area served by each fluid node to the total surface area in contact with the structure, i.e. the following relation is satisfied

$$T_a\ \mathbf{N}_{\text{At the structure node location}} = \frac{1}{\rho_f} \mathbf{M}_f^j\ \mathbf{I} \tag{4.62}$$

where j is the liquid element edge in contact with the structure node and $\mathbf{I}$ is a unit column. For example, in case of linear shape functions, the structure node should be in the middle of the liquid element face, as shown in Figure (4.4).

In case of large amplitude free surface waves, the mesh is updated to follow the liquid boundaries. This makes it impossible to maintain the symmetry conditions. One or more structure nodes may be located along the same liquid element edge and in positions that violate the symmetry conditions. In this case, the closest structure node to the symmetric position is chosen and $\mathbf{C}_{fs}$ is used to couple the liquid element with this structure node only. This technique is found to produce good quadratic convergence. Although using nonsymmetric matrices may be faster to converge, it requires almost double of the symmetric storage and computational cost. The developed approach is found to be convenient and efficient.

The global right hand side is then given as

$$\begin{bmatrix} \mathbf{M}_s & \mathbf{0} & \mathbf{0} \\ \mathbf{0} & \mathbf{0} & \mathbf{0} \\ \mathbf{0} & \mathbf{0} & \mathbf{0} \end{bmatrix} \begin{Bmatrix} \delta\ddot{\mathbf{u}} \\ \delta\ddot{\Phi} \\ \delta\ddot{\mathbf{h}} \end{Bmatrix} + \begin{bmatrix} \mathbf{C}_s & \mathbf{C}_{fs}^T & \mathbf{0} \\ \mathbf{C}_{fs} & \mathbf{0} & \mathbf{C}_{\phi h} \\ \mathbf{0} & \mathbf{C}_{\phi h}^T & \mathbf{0} \end{bmatrix} \begin{Bmatrix} \delta\dot{\mathbf{u}} \\ \delta\dot{\Phi} \\ \delta\dot{\mathbf{h}} \end{Bmatrix} + \begin{bmatrix} \mathbf{K}_s & \mathbf{0} & \mathbf{0} \\ \mathbf{0} & \mathbf{K}_f & \mathbf{0} \\ \mathbf{0} & \mathbf{0} & \mathbf{K}_h \end{bmatrix} \begin{Bmatrix} \delta\mathbf{u} \\ \delta\Phi \\ \delta\mathbf{h} \end{Bmatrix} \tag{4.63}$$

where $\mathbf{C}_{\phi h}$ and $\mathbf{K}_h$ are the matrices resulting from the assembly of either Equation (4.41) or Equation (4.48), and $\mathbf{h}$ is the free surface elevation degrees of freedom vector.

It should be pointed out that the developed liquid-structure interaction implementation could be also used to handle the nonlinear sloshing problem. The liquid free surface could be treated as a liquid-structure boundary on which the structure has zero stiffness. In order to fulfill the equilibrium condition, the liquid pressure has to be eliminated on this boundary.

4.3 Computer Implementation and Testing

The formulation of the nonlinear sloshing problem and the liquid-structure interaction are incorporate into DYNAZ, the nonlinear multi-system-analysis finite element code. The developed liquid element uses selective uniform integration techniques. It also allows the use of variable nodes to accommodate wide variety of problems and to allow for appropriate mesh refinements. Several cases are then tested and compared with previous investigations.

4.3.1 Two-Dimensional Examples

Example 1: Linear Response to Sinusoidal Ground Excitation

A rectangular tank of 10 m. width and 10 m. liquid height was tested for small ground excitation. The excitation has 0.16 second period and given by

$$\dot{G}_x = 0.01 \sin t \ \text{m/sec}$$

Two finite element meshes are used: one consists of 10×10 liquid elements while the other consists of 20×20 elements. Figure (4.5) shows a comparison of the liquid response to the ground excitation with the analytical solution using the linear wave theory presented in [32]. Figure (4.6) shows the effect of the mesh density on the linear liquid response.

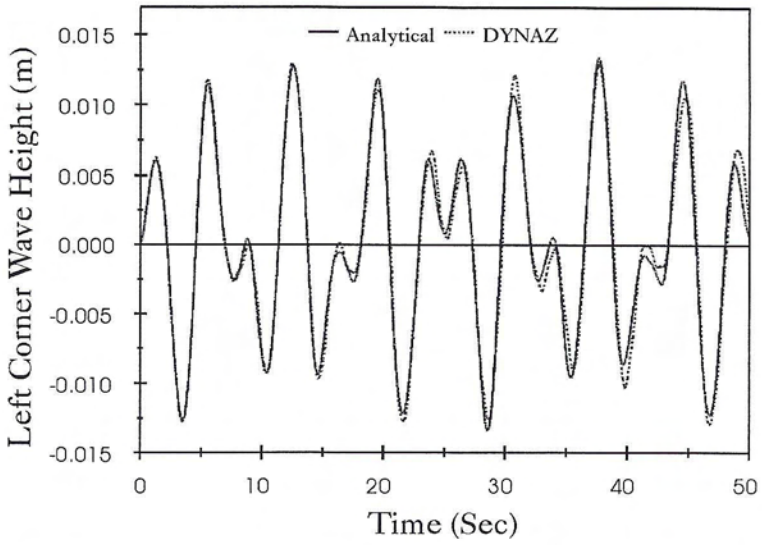

Figure 4.5: Example 1: Comparison with the Analytical Solution of the Linear Wave Theory.

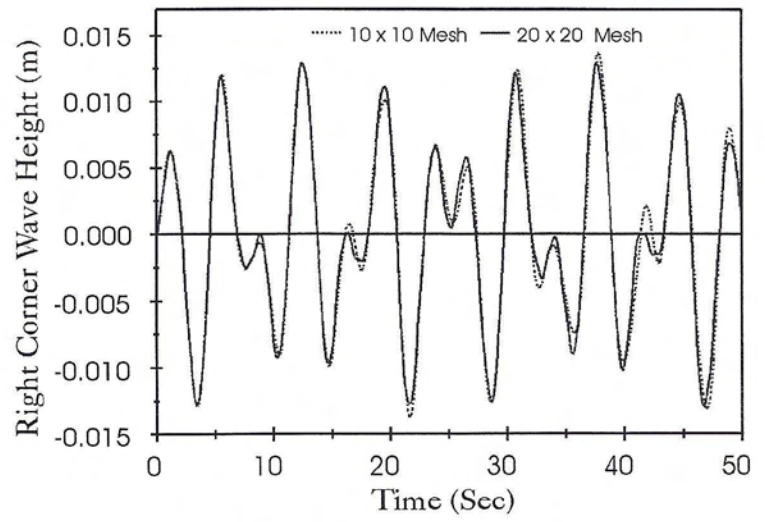

Figure 4.6: Example 1, Effect of Mesh Density on the Response.

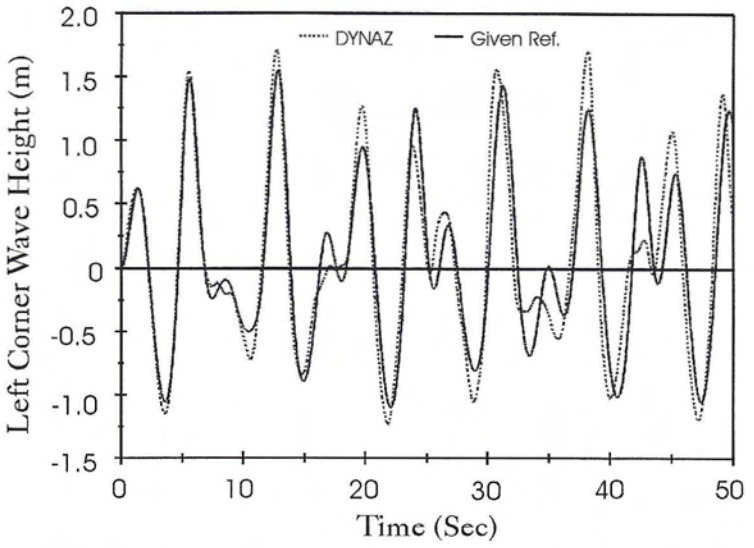

Figure 4.7: Example 2, Comparison of Wave Height Response at the Left Corner.

Example 2: Nonlinear Response to Sinusoidal Ground Excitation

The same rectangular tank used in the previous test is subjected to strong ground excitations. The excitation has 0.16 second period and given by

$$\dot{G}_x = 1.0 \sin t \ \text{m/sec}$$

A finite element mesh that consists of 10×10 liquid elements is used. Figures (4.7) and (4.8) shows a comparison of the liquid response to the strong ground motion with that obtained from Ref. [32]. Figure (4.9) shows the liquid mesh during the time history analysis.

Example 3: Effect of Tank Width on the Response to Sinusoidal Ground Excitations

In order to study the effect of tank width on the nonlinear liquid response to a sinusoidal ground excitation, a group of four tanks, as shown in Table (4.1), that

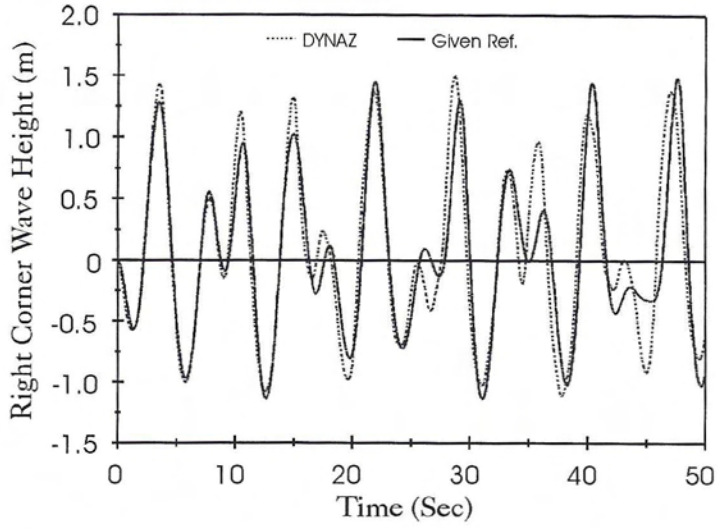

Figure 4.8: Example 2, Comparison of Wave Height Response at the Right Corner.

have the same H/R ratio, but vary in width, are subjected to two groups of sinusoidal ground excitations; the first group of excitation is given by

$$\ddot{G}_x = 0.1g\cos(1.1\omega_1 t)$$

while the second group of excitation is given by

$$\ddot{G}_x = 0.1g\cos(1.2\omega_1 t)$$

where ω_1 is the first sloshing mode frequency of the liquid free surface. It is found that the normalized time history responses of the four tanks are very close. This means

$2R = H$ ft.	ω_1 rad/sec.	T_1 sec.
5	4.49	1.40
10	3.17	1.98
15	2.59	2.42
20	2.25	2.78

Table 4.1: Example 3, Fundamental Frequencies the Four Tanks

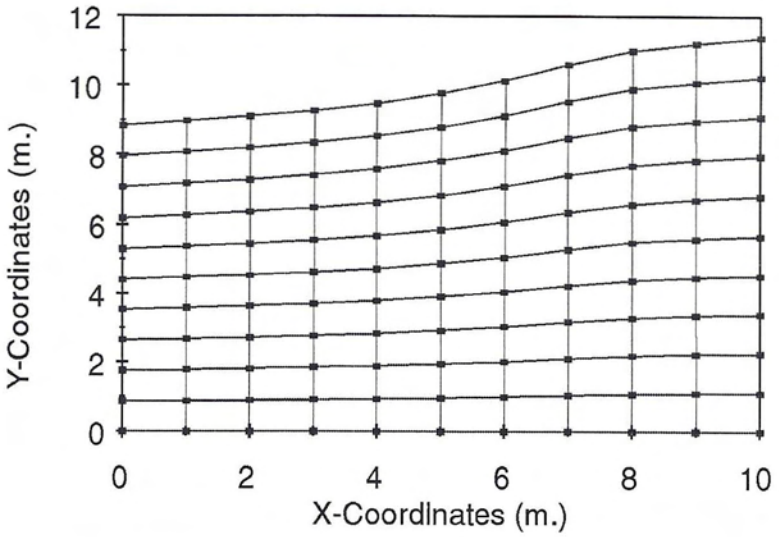

Figure 4.9: Example 2, Liquid Mesh at Time $t = 3.6$ Sec.

that the rigid tank width has no effect on the normalized response time history of the liquid. The same finite element mesh which consists of 20×20 elements is used in all cases. Figures (4.10) and (4.11) show the results for the first group of excitation while Figures (4.12) and (4.13) show the results for the second group of excitations.

Example 4: Nonlinear Response to Mexico City Earthquake

A rectangular tank of 30 ft. width and 15 ft. liquid height is subjected to the North West component of the Mexico City earthquake, shown in Fig (4.22) in the period domain. This particular liquid height to base ratio $H/2R = 0.5$ was reported as the ratio that is most affected by the nonlinear sloshing effect. The peak ground acceleration of this component of Mexico City earthquake is $0.168g$. The liquid has a specific gravity of 62.4 lb/ft^3. In order to filter high frequency surface wave components that propagate along the free surface, a dissipation factor of 0.75 is used. A

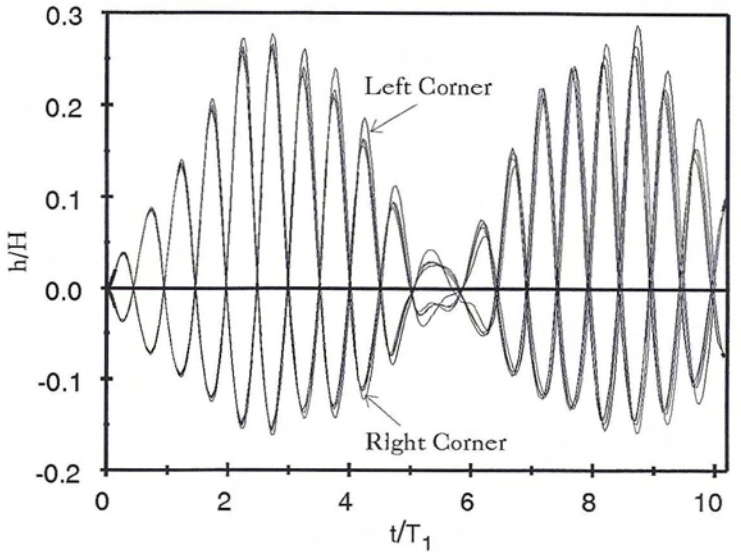

Figure 4.10: Example 3, First Excitation Group, Wave Heights at Left and Right Corners

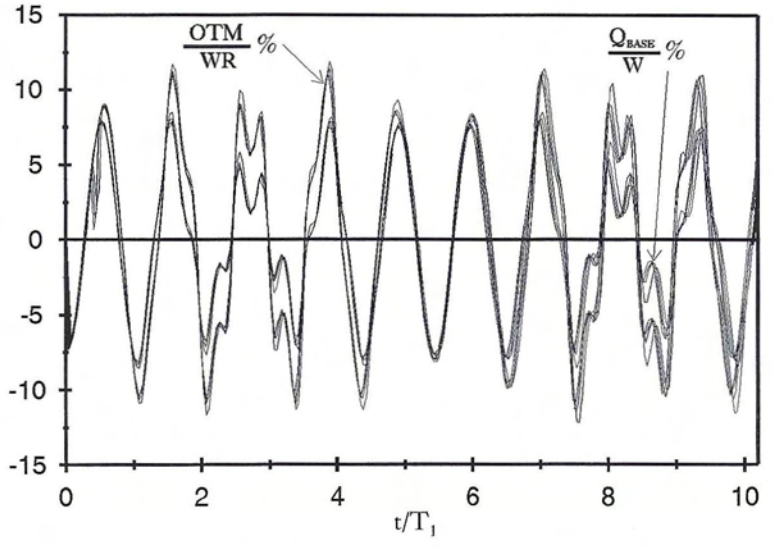

Figure 4.11: Example 3, First Excitation Group, Base Shear and Base Overturning Moment

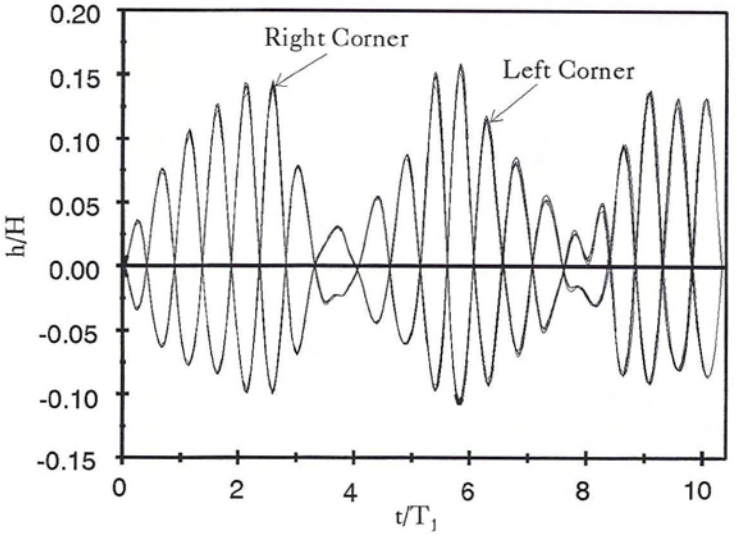

Figure 4.12: Example 3, Second Excitation Group, Wave Heights at Left and Right Corners

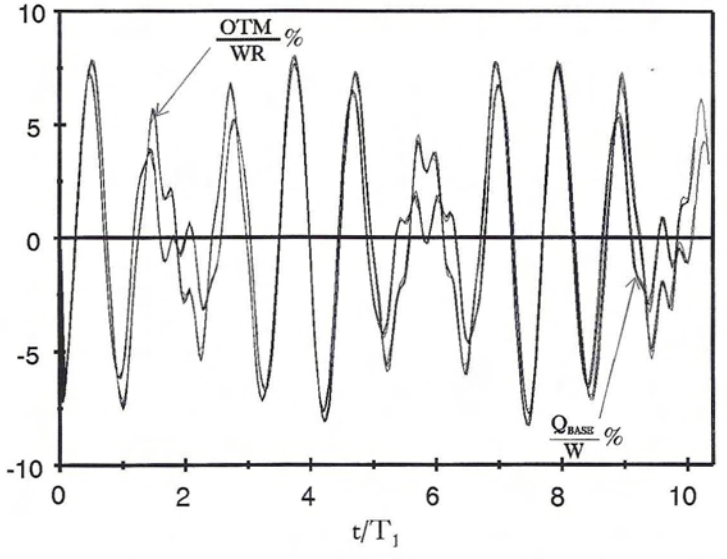

Figure 4.13: Example 3, Second Excitation Group, Base Shear and Base Overturning Moment

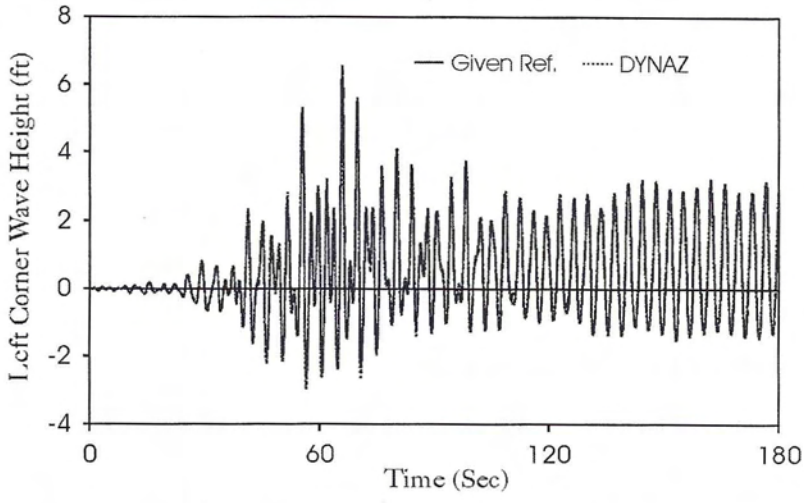

Figure 4.14: Example 4, Wave Heights at Left Corner

finite element mesh that consists of 20 × 20 4-noded isoparametric liquid elements with a total of 441 nodes is used. Results are obtained and compared to those obtained from Ref. [32]. Figures (4.14) and (4.15) show wave height time history along the tank left and right wall, respectively. Figures (4.16) (4.17) show the free surface profile at two different time instants. Figures (4.18) and (4.19) show the base shear and overturning moments applied on the tank walls and base plate due to the hydrodynamic pressure, respectively.

Example 5: Nonlinear Response to El Centro Earthquake

A rectangular tank of 30 ft. width and 15 ft. liquid height is subjected to the East West component of the El Centro earthquake record measured at the Imperial Valley site. The peak ground acceleration of this record is $0.21g$. In order to filter high frequency surface wave components that propagate along the free surface, a dissipation factor of 0.025 is used. A finite element mesh that consists of 10 × 10 9-noded isoparametric liquid elements with a total of 441 nodes is used. Results are

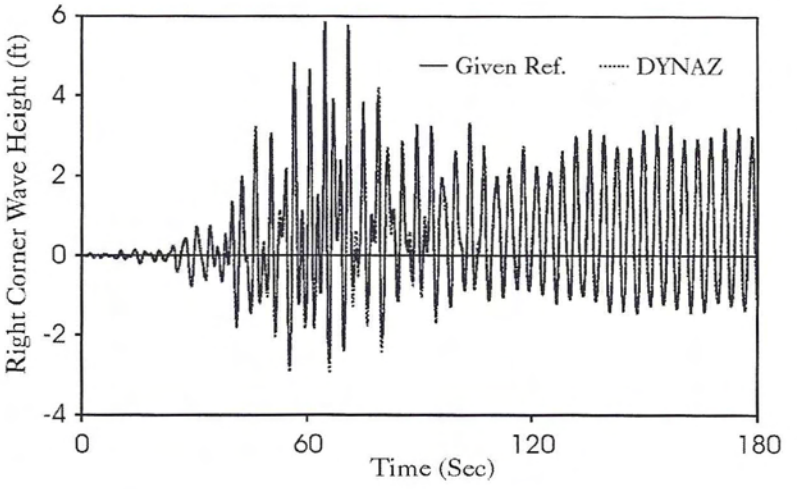

Figure 4.15: Example 4, Wave Heights at Right Corner

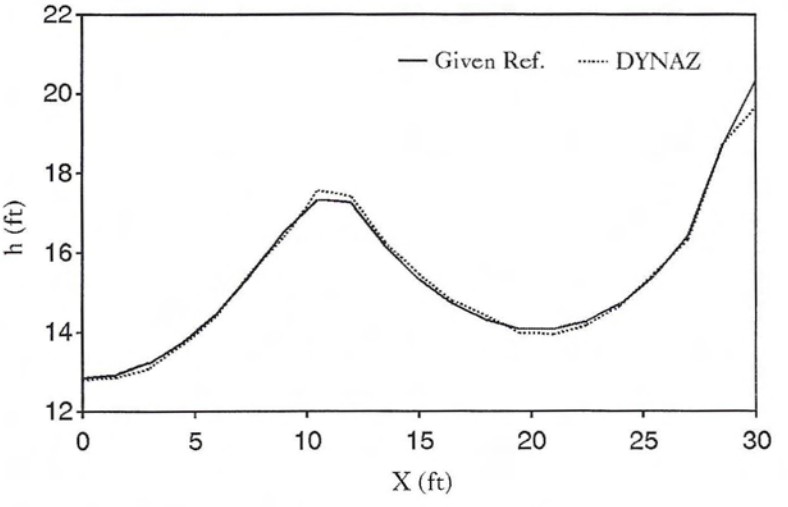

Figure 4.16: Example 4, Free Surface Profile at Time $t = 65.0$ sec

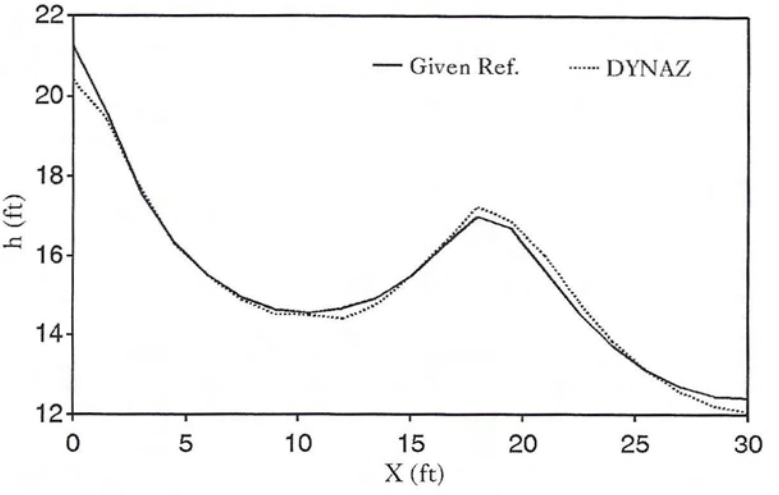

Figure 4.17: Example 4, Free Surface Profile at Time $t = 66.1$ sec

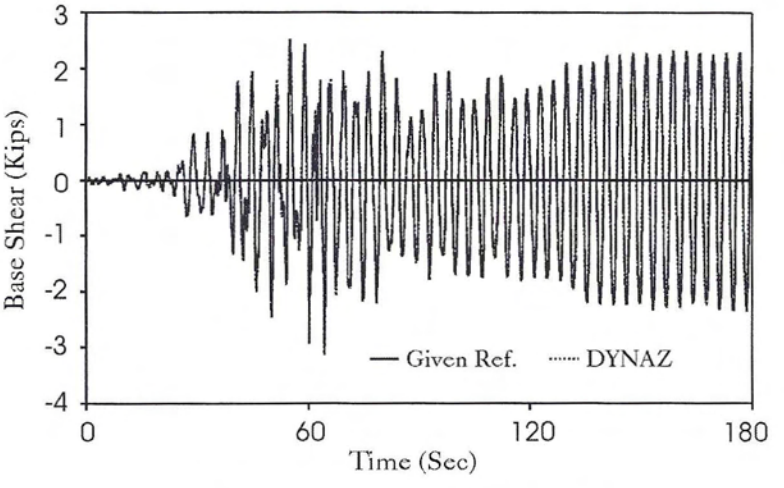

Figure 4.18: Example 4, Base Shear

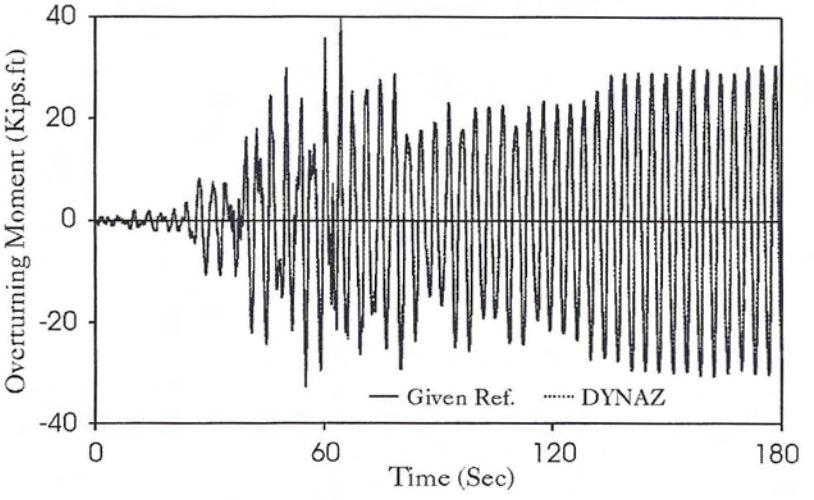

Figure 4.19: Example 4, Base Overturning Moment

obtained and compared to those obtained from Ref. [32]. In order to show the free vibration response of the free surface, the time histories were obtained till time $t = 80$ sec. although the earthquake duration was 53.48 sec. Figures (4.20) and (4.21) show wave height time history along the tank left and right wall, respectively.

Example 6: Free Surface Wave Breaking Due to Resonance

A rectangular tank of 12 ft. width and 12 ft. liquid height is subjected to the North West component of the Mexico City earthquake. The earthquake, shown in Fig (4.22) in the period domain, is found to posses strong components of period range between 1.9 and 3.0 seconds with its maximum at period 2.05 second. Using the linear analytical solution presented in [32], the liquid fundamental period is computed as follows

$$\begin{aligned} \alpha_1 &= \frac{\pi}{2R} = 0.262 \\ \omega_1 &= \sqrt{\alpha_1 g \tanh(\alpha_1 H)} = 2.898 \text{ rad/sec} \\ T_1 &= 2.168 \text{ sec.} \end{aligned}$$

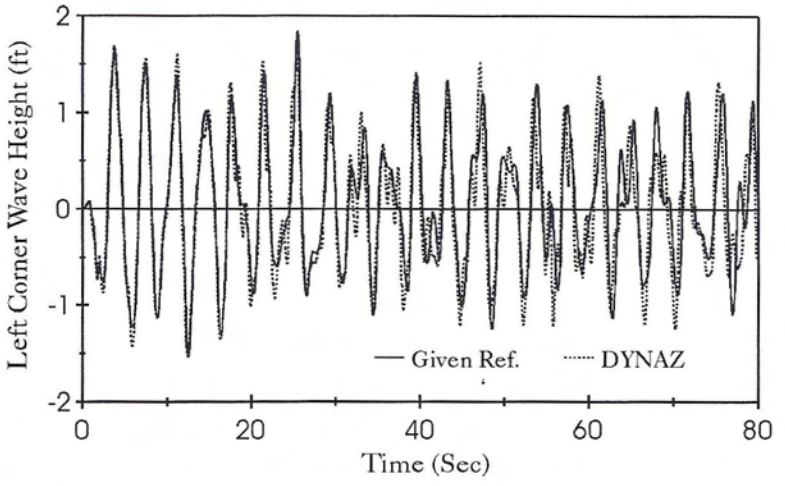

Figure 4.20: Example 5, Wave Heights at Left Corner

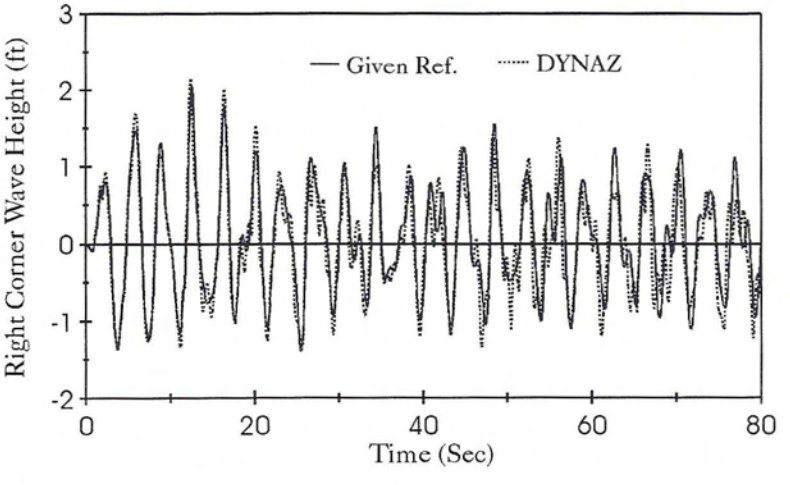

Figure 4.21: Example 5, Wave Heights at Right Corner

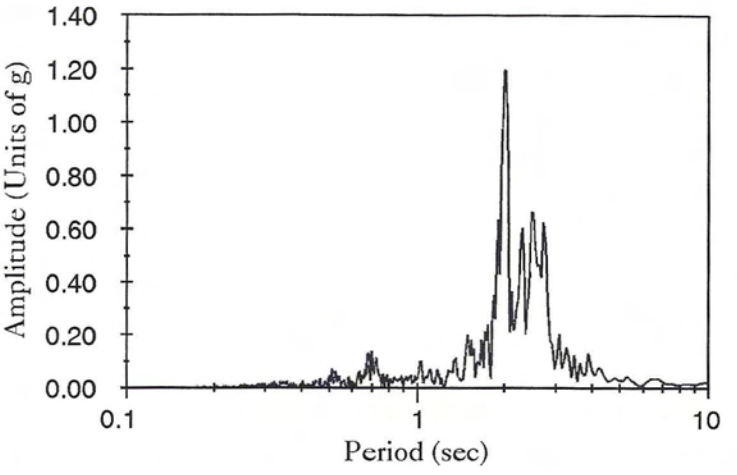

Figure 4.22: Example 6, Period Content of the Mexico City Earthquake, NW-Component

Since the free surface sloshing fundamental period is within the range of the strong components of the ground excitation, the free surface wave is expected to break. As expected, it is observed that the free surface wave breaks at time 61.8 seconds, as shown in Fig (4.23).

Example 7: Free Surface Wave Breaking Due to High Level of Excitation

A rectangular tank of 10 ft. width, 10 ft. liquid height and 2 inches wall thickness is subjected to a sinusoidal ground excitation given by

$$\ddot{G}_x = 1.0g\cos(3.81t)$$

Since the level of excitation is relatively high, the liquid is expected to respond violently to the strong high frequency vibrations delivered to the liquid throughout the tank walls. As expected, the free surface wave breaks at time 4.0 seconds, as shown in Fig (4.24).

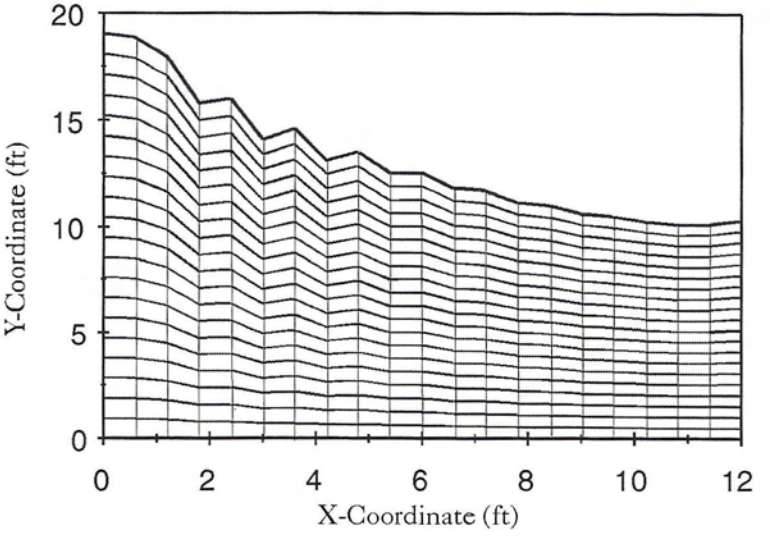

Figure 4.23: Example 6, Liquid Domain Just Before the Free Surface Wave Breaks

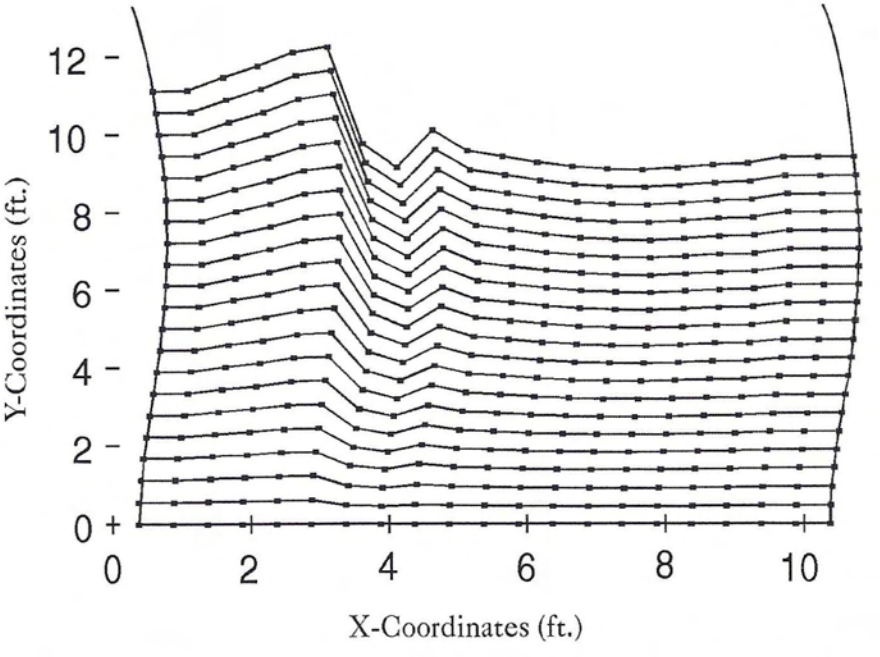

Figure 4.24: Example 7: Liquid Domain Just Before the Free Surface Wave Breaks

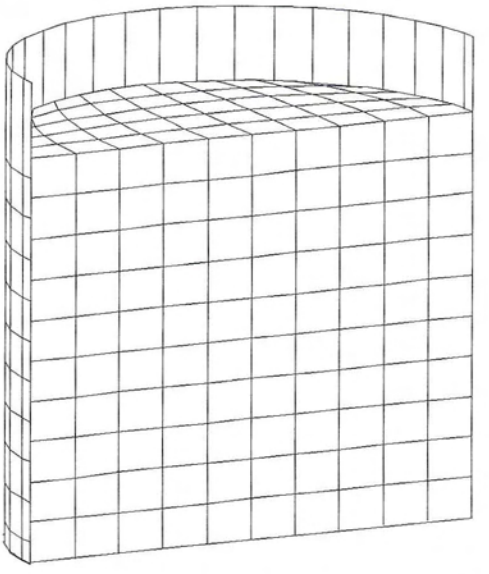

Figure 4.25: Example 8: Finite Element Mesh of the Coupled Liquid-Tank System

4.3.2 Three-Dimensional Examples

Example 8: Linear Response of an Anchored Liquid Storage Tank

The linear response of a cylindrical liquid storage tank to the Channel 3:360 corrected record of the Northridge earthquake measured at Arleta cite which has a peak ground acceleration of $0.344g$, was found. The finite element mesh is used is shown in Figure (4.25). The tank has 37 ft. diameter, 32 ft. height, 28.3 ft. liquid height, 3/8 in. wall thickness, and 1/2 in. base plate and roof thickness. Results were compared to those obtained from the analysis presented in reference [103]. Figure (4.26) shows the time history response of the horizontal acceleration of the tank shell top node. Figure (4.27) shows shell base axial stress time history. Figure (4.28) shows shell hoop stress time history at 25% of the shell height measured from the bottom of the tank. Figures (4.29) and (4.30) show the tank base shear and base overturning moment time histories due to pressure on tank wall, respectively.

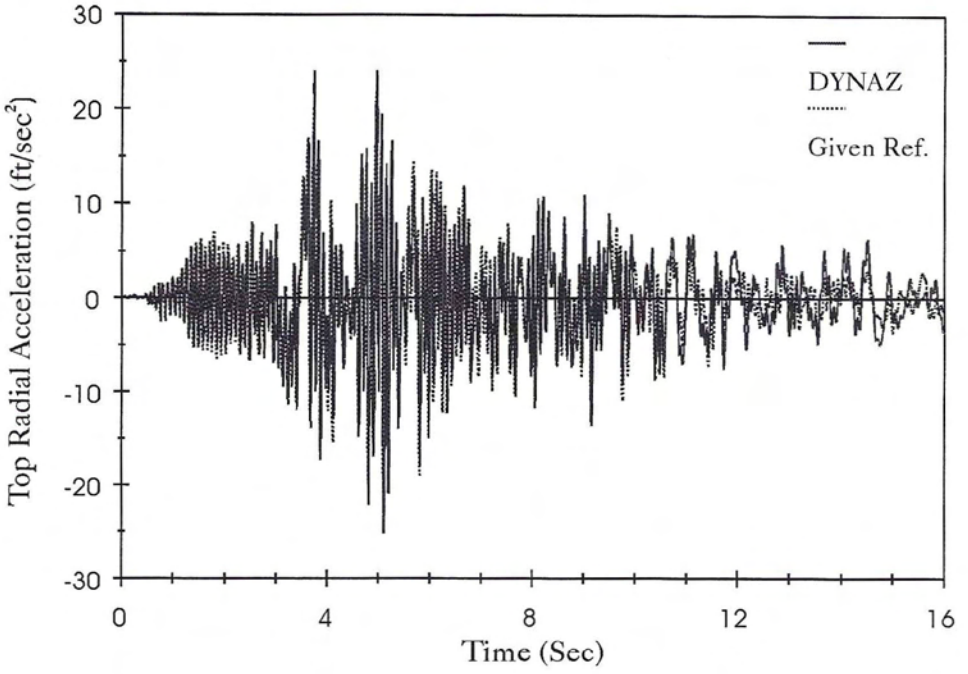

Figure 4.26: Example 8: Shell Top Horizontal Acceleration

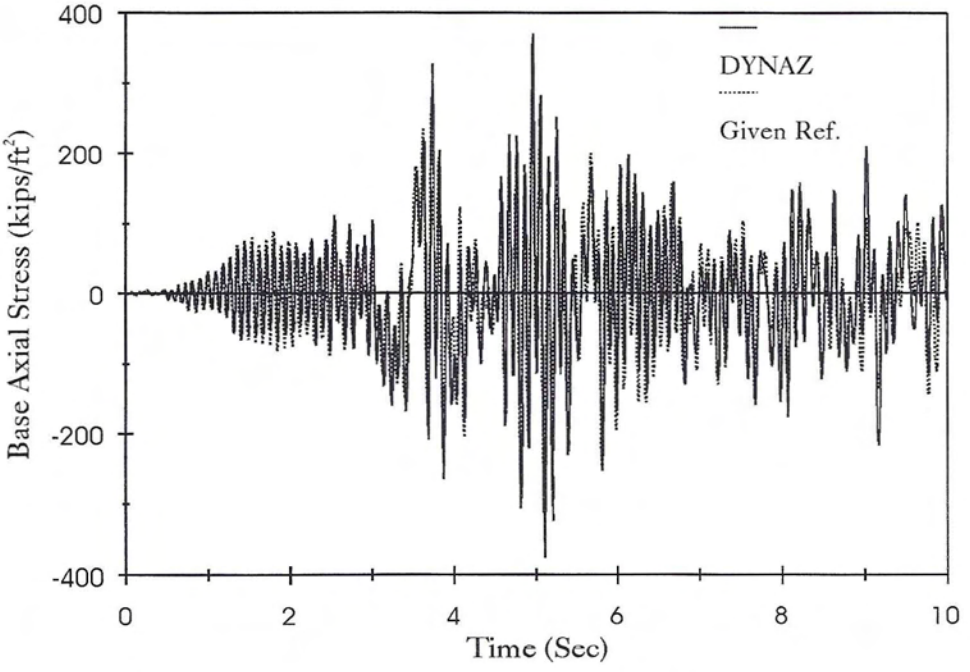

Figure 4.27: Example 8: Shell Bottom Axial Stress

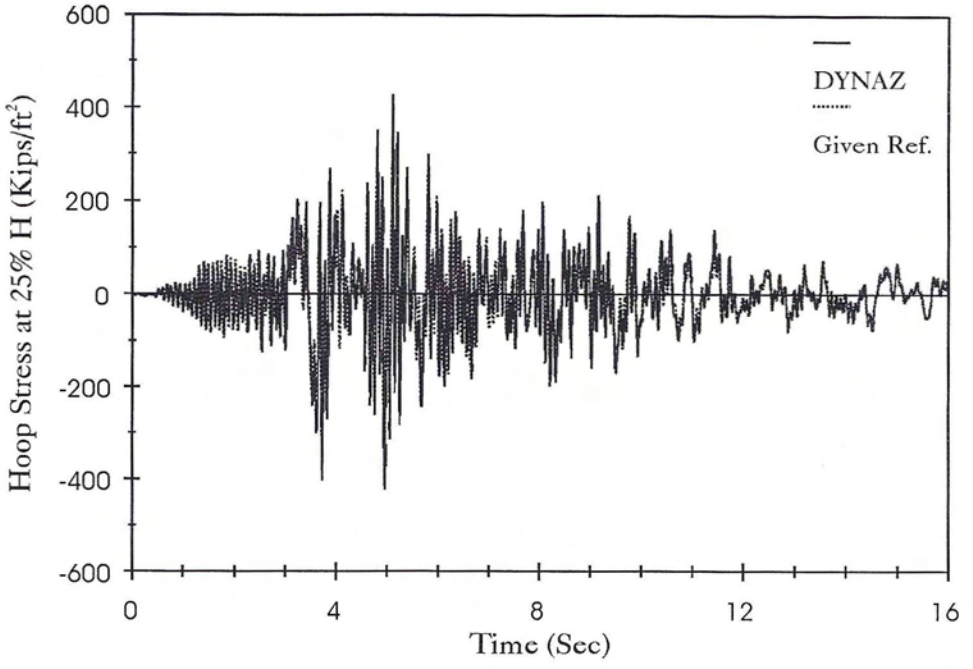

Figure 4.28: Example 8: Shell Hoop Stress at 25% of the Tank Height

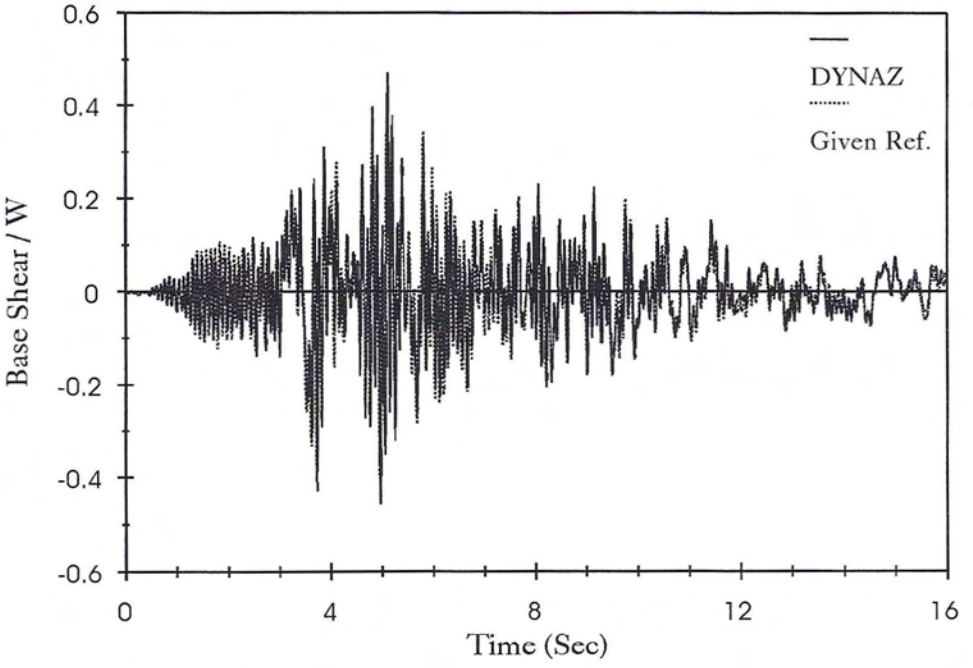

Figure 4.29: Example 8: Base Shear

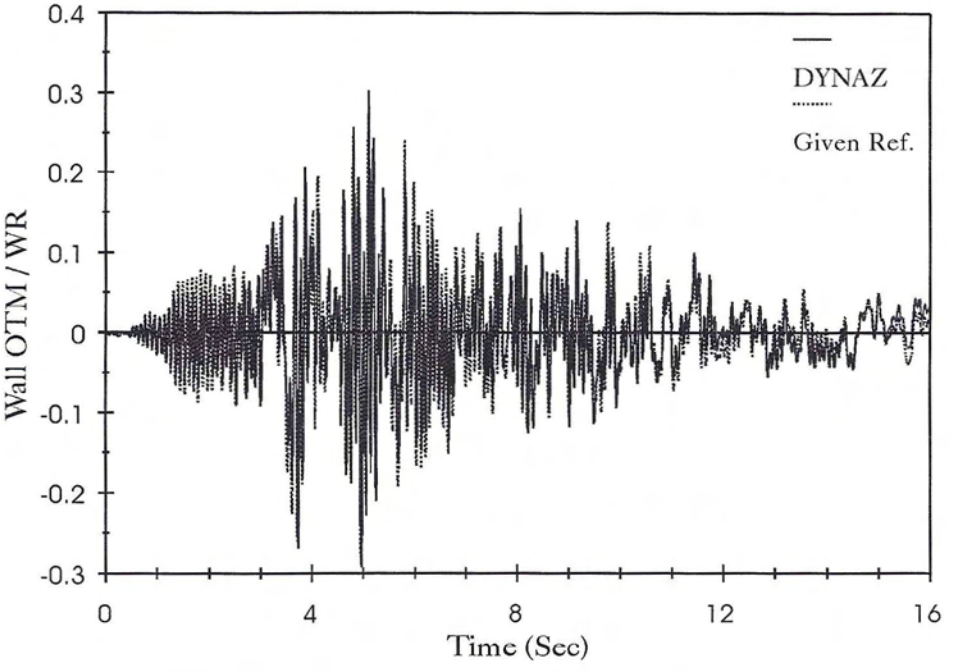

Figure 4.30: Example 8: Base Overturnig moment

Chapter 5

Nonlinear Earthquake Response of Liquid Storage Tanks

The nonlinear finite element code DYNAZ was utilized to estimate the earthquake response of two liquid storage tanks of different aspect ratios: a broad tank and a tall tank. The broad tank is 40 ft high and has a radius of 60 ft. The shell thickness is assumed constant of 1 inch and the base plate is considered having 1 inch of uniform thickness. The tall tank is 72 ft of high, 24 ft in radius, and has both shell and base thickness of 1 inch. Both tanks are assumed full of water to capacity. Each of the two tanks were subjected to two different earthquake motions: the East-West component of the 1940 El Centro earthquake which has a peak ground acceleration of $0.214g$, as shown in Figure (5.1), and the record from the Northridge earthquake measured at the Arleta site which has a peak ground acceleration of $0.344g$, as shown in Figure (5.2), and measured in a direction of 90° from the hypocenter direction. The responses of the two tanks were estimated assuming different boundary conditions: rigid tank walls, flexible tank walls completely anchored and flexible unanchored tank walls.

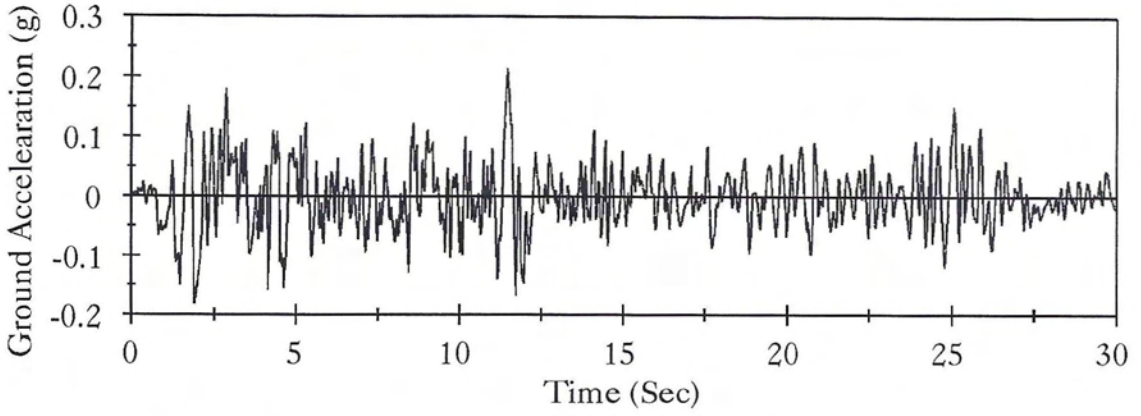

Figure 5.1: East West Component of the 1940 El Centro Earthquake

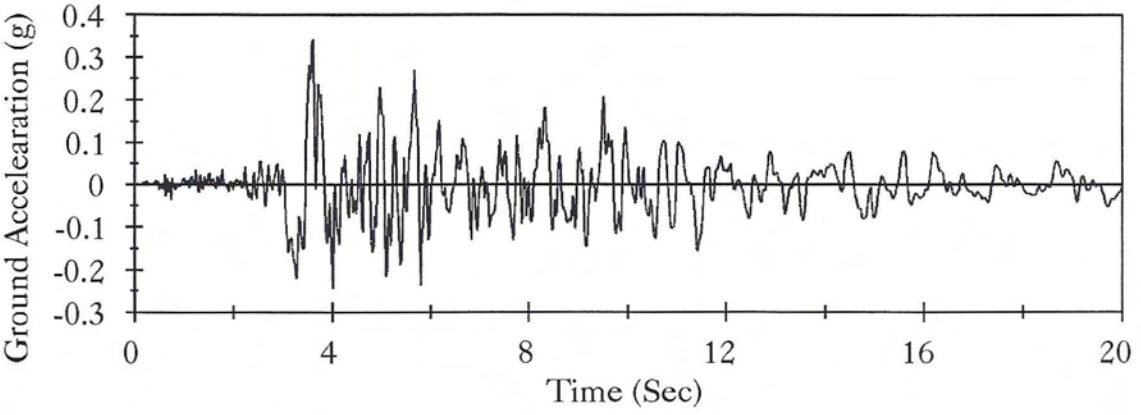

Figure 5.2: Northridge Earthquake Measured at Arleta Site in a Direction of 90° from the Hypocenter Direction

5.1 Response of Tanks with Rigid Walls

Liquid motion in rigid containers reflects primarily the effect of sloshing on the response of these tanks. As a simplification for the analysis of circular cylindrical tanks, one may consider a rectangular strip in the middle of the tank and analyze it as a two-dimensional problem. Alternatively, the full three-dimensional model may be used. The linear fundamental period of the two-dimensional model is given by

$$T_1 = \frac{2\pi}{\sqrt{\frac{\pi g}{2R}\tanh\frac{\pi H}{2R}}} \tag{5.1}$$

whereas for the three-dimensional model, it is given by

$$T_1 = \frac{2\pi}{\sqrt{\frac{1.84g}{R}\tanh\frac{1.84H}{R}}} \tag{5.2}$$

where H is the liquid depth. Although the linear fundamental periods of both the two and the three-dimensional models are close, as shown in Table (5.1), the corresponding wave heights may differ significantly. It is unconservative to use the two-dimensional model for predicting the response of cylindrical liquid storage tanks. This is attributed to the difference in the mode shapes of both models. The maximum response calculated based on two and three-dimensional models are presented and compared in Tables (5.2) and (5.3). Note that W denotes the total weight of the contained liquid and R is the tank radius. Results show that using the linear sloshing assumptions at the free surface underestimates its wave height. However, it predicts well the base shear exerted on the tank. Using the nonlinear sloshing assumptions shows that the positive sloshing amplitude is larger than the negative amplitude.

Figures (5.3) and (5.4) show the free surface wave heights of the two extreme opposite points on the principal diameter which parallels the earthquake excitation of

	Model Type	
Tank Type	2-D Model	3-D Model
Broad Tank	7.74 sec	6.89 sec
Tall Tank	4.33 sec	4.00 sec

Table 5.1: Periods of Different Models for Liquid Sloshing in Rigid Tanks

the broad and tall tanks, respectively. Figures (5.5) and (5.6) present the deformed finite element mesh for both broad and tall tanks, respectively. Several ways to discretize the liquid domain were attempted to obtain the earthquake response of the liquid. It was found that the performance of an orthogonal finite element mesh yields better results and smoother free surface profile. This is attributed to the fact that the orthogonal mesh provides orthogonal mapping between the Cartesian and curvilinear coordinates, which is compatible with the stream and equipotential lines resulting from the solution of Laplace equation. Using other forms of finite element mesh in the nonlinear sloshing problem may result in a broken free surface profile and, as a result, the analysis may fail to converge.

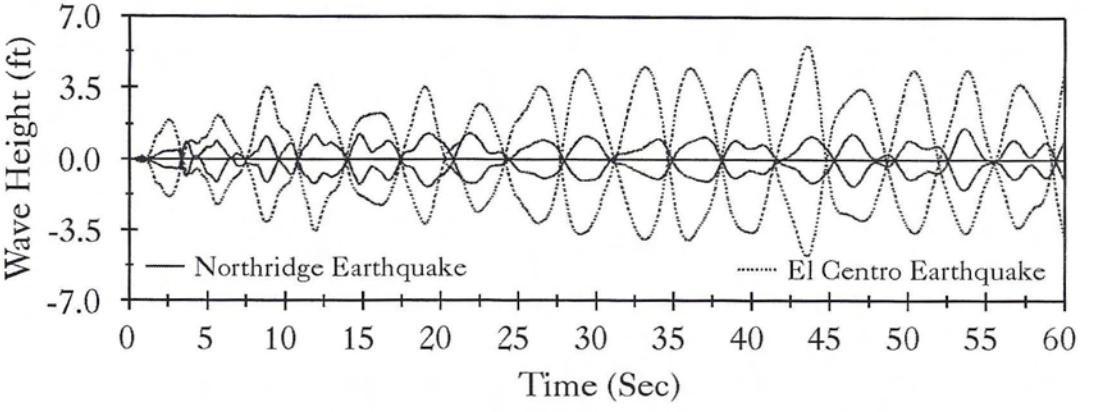

Figure 5.3: Nonlinear Time History Response of the Wave Height in the Broad Tank, 3-D Model

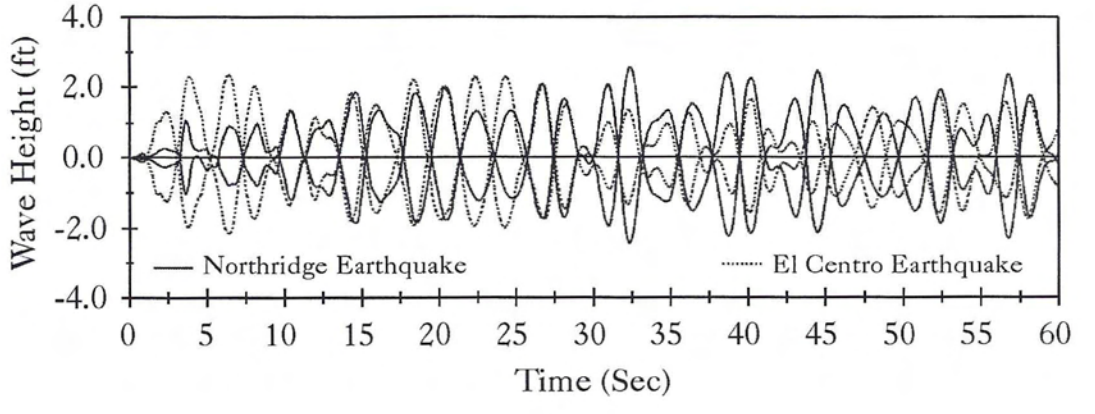

Figure 5.4: Nonlinear Time History Response of the Wave Height in the Tall Tank, 3-D Model

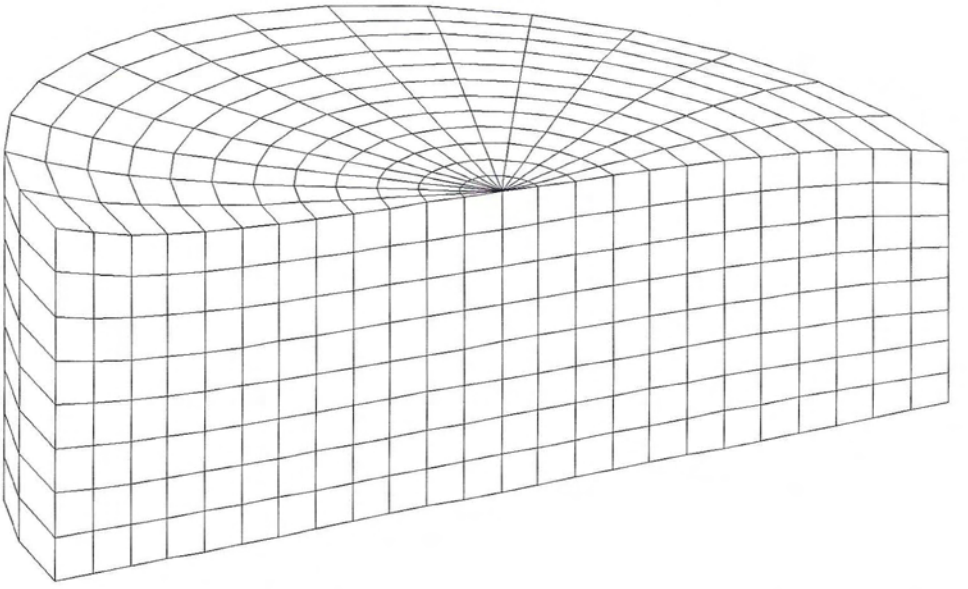

Figure 5.5: Deformed Liquid Domain of the Broad Tank at $t = 43.5$ Sec, Northridge Record

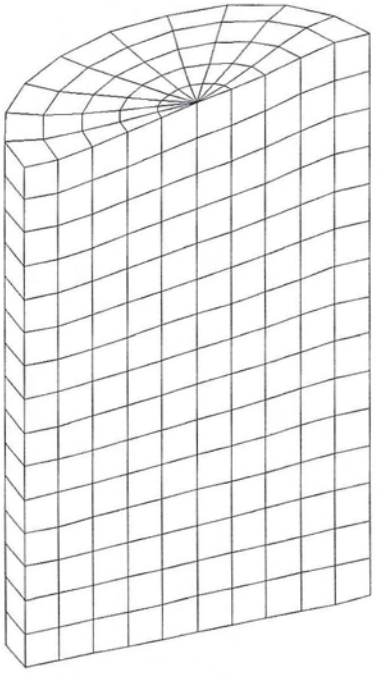

Figure 5.6: Deformed Liquid Domain of the Tall Tank at $t = 32.5$ Sec, El Centro Record

Case		Wave Height (ft)		OTM/WR	Base Shear/W
		Left End	Right End		
Broad Tank-	2-D	2.27	2.27	0.053	0.064
Linear Sloshing	3-D	5.19	5.19	0.066	0.096
Broad Tank-	2-D	2.18	2.35	0.052	0.062
Nonlinear Sloshing	3-D	4.77	3.61	0.067	0.103
Tall Tank-	2-D	3.84	3.84	0.197	0.141
Linear Sloshing	3-D	2.23	2.23	0.216	0.155
Tall Tank-	2-D	4.24	3.56	0.196	0.143
Nonlinear Sloshing	3-D	2.32	2.36	0.216	0.155

Table 5.2: Liquid Sloshing in Rigid Containers Under El Centro Record

5.2 Anchored Tank Response

In order to evaluate the effect of flexibility of the tank wall on the response of liquid storage tanks, both the tank and the liquid were modeled using the finite element method. Figures (5.7) and (5.8) show the finite element mesh used for the broad and tall tanks, respectively. The tank base was assumed to be fixed to a rigid foundation, and consequently, the nodes of the bottom of the tank were assumed to have a specified acceleration equal to the ground acceleration. A Raleigh damping coefficient which provides 3% damping to the first mode and increasing values for the higher modes was chosen for the flexible-impulsive component. Using the added mass matrix approach presented in [103], the fundamental period of this component was found to be 0.162 sec for the broad tank and 0.189 sec for the tall tank.

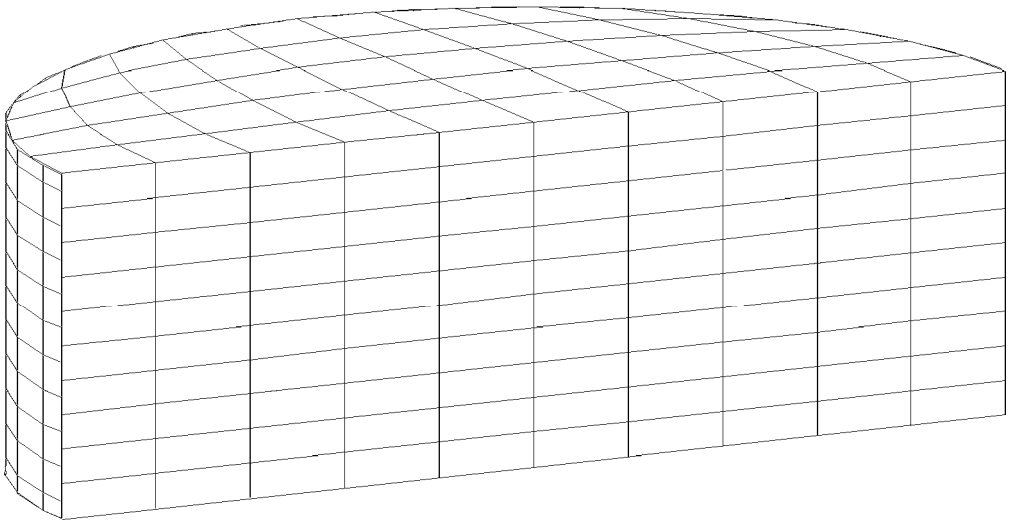

Figure 5.7: Finite Element Mesh of the Coupled Liquid-Broad Tank System

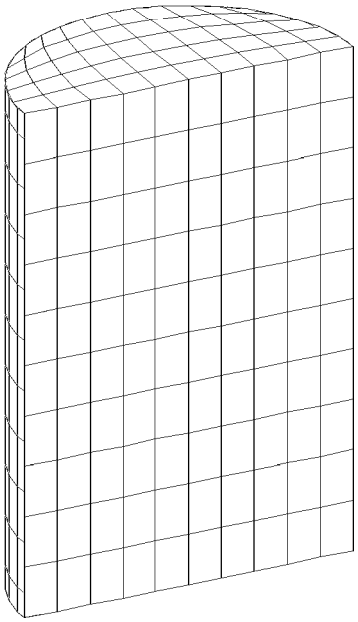

Figure 5.8: Finite Element Mesh of the Coupled Liquid-Tall Tank System

Case		Wave Height (ft)		OTM/WR	Base Shear/W
		Left End	Right End		
Broad Tank-	2-D	1.62	1.62	0.094	0.113
Linear Sloshing	3-D	1.52	1.52	0.086	0.125
Broad Tank-	2-D	1.59	1.64	0.092	0.105
Nonlinear Sloshing	3-D	1.47	1.59	0.089	0.127
Tall Tank-	2-D	1.64	1.64	0.379	0.262
Linear Sloshing	3-D	2.46	2.46	0.362	0.266
Tall Tank-	2-D	1.68	1.67	0.366	0.259
Nonlinear Sloshing	3-D	2.43	2.59	0.378	0.266

Table 5.3: Liquid Sloshing in Rigid Containers Under the Northridge Record

Several conclusions may be drawn by observing the values in Table (5.4). For both broad and tall tanks, the acceleration at the top of the tank shell is much greater than that of the ground. Thus, the total overturning moment and base shear exerted on the flexible tank are much greater than those exerted on the rigid tank. This is due to the fact that the impulsive liquid loads arise through the acceleration of the shell. If the shell is flexible, two acceleration components must be considered: the acceleration of the undeformed shell, i.e., the ground acceleration, and the relative acceleration due to shell deformations. In a rigid tank, only the acceleration of the undeformed shell is considered leading to the noticeable difference in the magnitude of the base shear and the overturning moments.

A comparison between the response of the broad and the tall tank shows that the component of the overturning moment exerted on the tank wall in the tall tank dominates that exerted on the tank base. On the contrary, the component of the

Response Parameter	El Centro Record		Northridge Record	
	Broad	Tall	Broad	Tall
Top Lateral Acceleration	0.576 g	0.800 g	0.664 g	1.210 g
Top Lateral Deflection (in)	0.385	0.421	0.193	0.533
Total OTM / WR	0.148	0.605	0.176	0.943
Wall OTM / WR	0.067	0.581	0.090	0.921
Base Shear / W	0.214	0.377	0.254	0.577
Axial Stress - Beam Theory (Ksi)	-0.97	-5.46	-1.26	-8.52
Base Axial Stress (Ksi)	-2.03	-5.77	-2.11	-9.10
Base Hoop Stress (Ksi)	0.99	3.16	0.96	3.89
Axial Stress at 0.25H (Ksi)	-0.59	-3.48	-0.47	-5.78
Hoop Stress at 0.25H (Ksi)	17.3	8.95	18.83	9.45

Table 5.4: Anchored Tank Response

overturning moment exerted on the base of the broad tank is dominant. In addition, hoop stress near the base of the broad tank is greater than that of the tall tank. This explains the difference in the observed buckling modes of the two tanks. Previous damage observations of liquid storage tanks after major earthquakes showed that Elephant Foot buckling was the most common damage in broad tanks while tall tanks suffered Diamond-shaped buckling spreading around the circumference.

Current seismic standards for liquid storage tanks suggest the use of a response spectrum to evaluate the overturning moment exerted on the tank wall. This moment is assumed to be resisted mainly by a compression in the tank shell and a tension in the anchors. To calculate the resulting compressive stress at the bottom of the tank shell, flexural beam formula is used. This assumption yields the following compressive

stress

$$\sigma_b = \frac{\text{OTM}}{\pi R^2 t} + \gamma_w H_w \tag{5.3}$$

where t is the shell thickness near the tank base and H_w is height of the tank wall. It is evident from Table (5.4) that this assumption is valid only for high values of H/R. As the tank gets broader, the plane section assumption becomes unconservative to use. The actual stress distribution around the circumference of the broad tank shows a stress concentration towards the principal diameter which parallels the earthquake excitation, leading to an amplified peak stress.

5.3 Unanchored Tank Response

In order to evaluate the effect of the base boundary conditions on the response of liquid storage tanks, the tank base plate was considered supported on a tensionless elastic foundation of a uniform stiffness of 1000 lb/in/in^2 in compression. Table (5.5) provides the unanchored tank response using the small deflection theory.

Figures (5.9), (5.10), (5.11) and (5.12) display time history comparisons between the anchored and the unanchored broad tank for the overturning moment measured at the center of the base plate and for the base axial stresses when subjected to Northridge and El Centro ground motions, respectively. Figures (5.13), (5.14), (5.15) and (5.16) show the same comparison for the tall tank. The response of the unanchored tank was governed primarily by a rocking motion. This mode was found to have a dominant "period" of 0.41 sec for the broad tank and 0.82 sec for the tall tank. Based on these periods, the foundation rocking damping is estimated to be

Response Parameter	El Centro Record		Northridge Record	
	Broad	Tall	Broad	Tall
Top Lateral Acceleration	1.999 g	0.934 g	2.001 g	0.845 g
Top Lateral Deflection (in)	7.43	5.66	6.24	13.49
Total OTM / WR	0.200	0.380	0.198	0.477
Wall OTM / WR	0.075	0.317	0.065	0.353
Base Shear / W	0.292	0.243	0.258	0.293
Base Axial Stress (Ksi)	-4.75	-6.71	-4.62	-7.90
Base Hoop Stress (Ksi)	9.56	8.46	10.84	8.07
Axial Stress at 0.25H (Ksi)	-2.47	-4.69	-2.04	-5.58
Hoop Stress at 0.25H (Ksi)	19.85	11.51	21.50	12.89
Maximum Uplift Displacement (in)	1.05	1.75	1.50	2.87
Minimum Contact Area	0.732	0.671	0.733	0.610

Table 5.5: Unanchored Tank Response – Small Deflection Assumptions

5%. On the other hand, the response of the anchored tank was governed primarily by the flexible-impulsive pressure component which has a fundamental period of 0.162 sec for the broad tank and 0.189 sec for the tall tank. Since the rocking period is relatively large as compared to the flexible-impulsive period, the overturning moment exerted on the anchored tank may be larger than that exerted on the unanchored tank. However, due to the nature of the boundary conditions associated with the base of the unanchored tank, the axial and hoop stresses at the bottom of the unanchored tank shell were larger than those of the anchored tank. The response of unanchored tanks was dominated by the uplift mechanism which varied nonlinearly with the intensity and frequency of input motions. The coupling of uplift mechanism with out-of-round distortions resulted in high compressive axial membrane stresses

developed over a narrow contact zone. This effect is reflected by the sharp peaks on the compression side of the time history diagrams of the axial stress that occurred simultaneously with large uplifting displacements. The cases on which the axial stress at the bottom of the anchored tank shell were larger than those of the unanchored tank are attributed to the large difference between the overturning moments in the two tanks. Yet, sharp peaks are still shown on the compression side of the axial stress time history diagrams of these tanks.

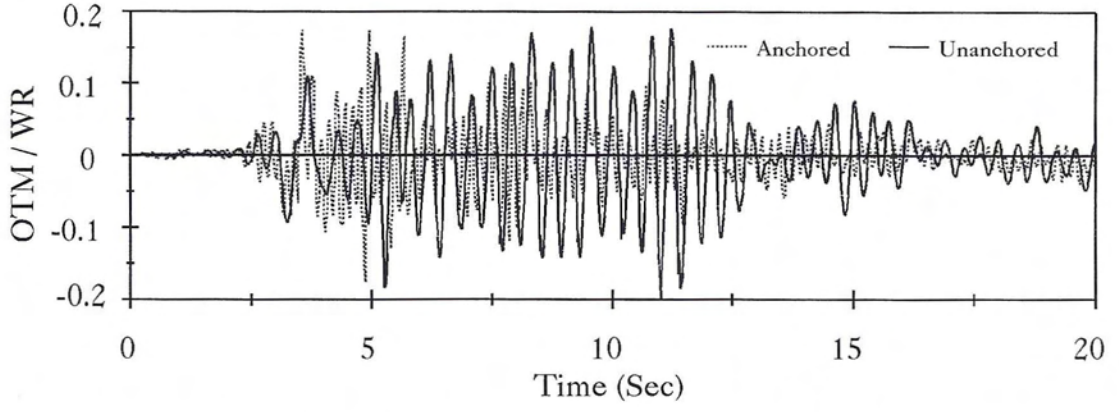

Figure 5.9: Overturning Moment at Center of Base of the Broad Tank, Northridge Record

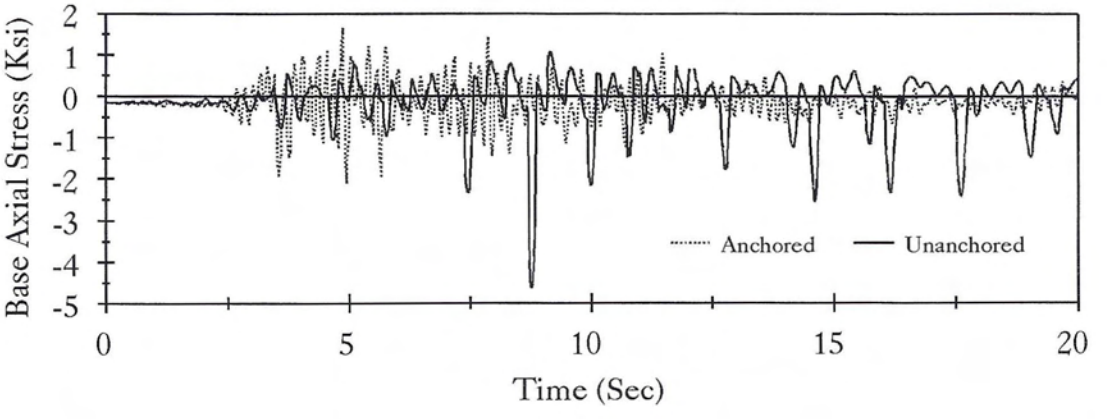

Figure 5.10: Base Axial Stress in the Broad Tank Shell, Northridge Record

The contact characteristics of the unanchored tank with its foundation are important factors in evaluating the response of such a tank. Figures (5.17), (5.19),

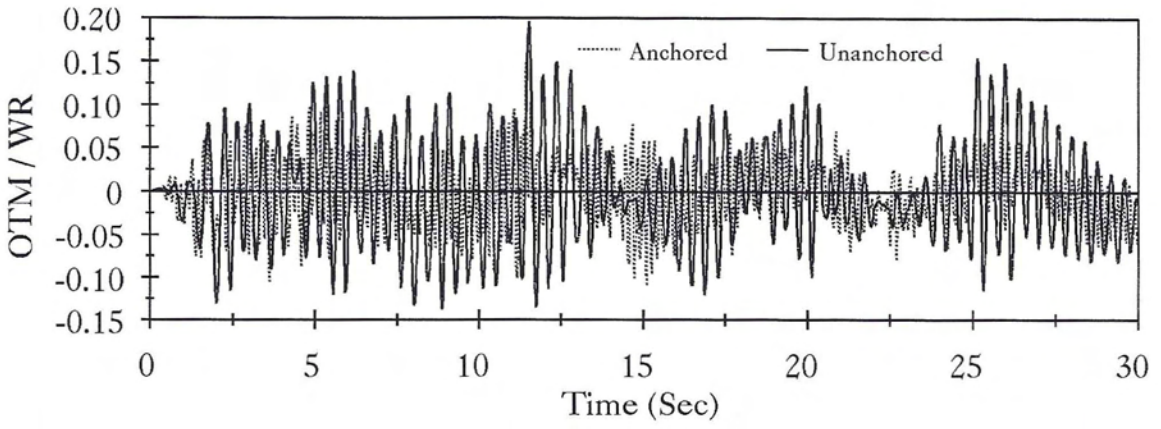

Figure 5.11: Overturning Moment at Center of Base of the Broad Tank, El Centro Record

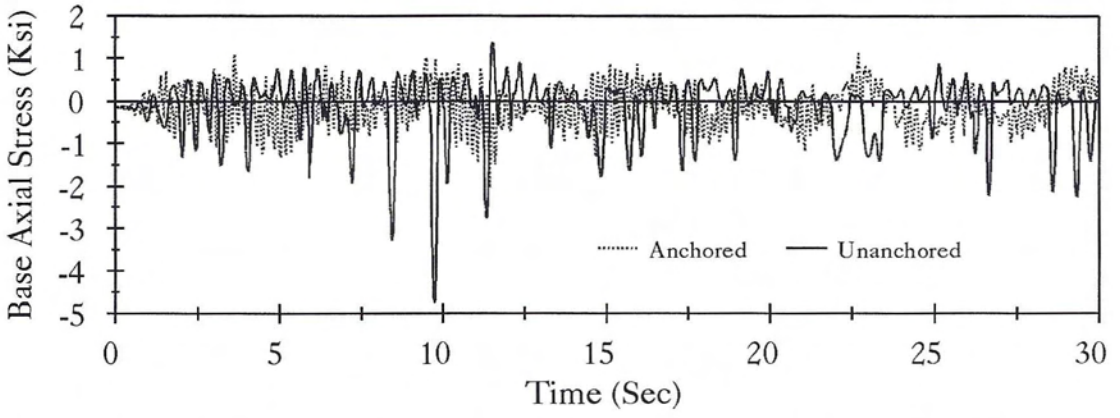

Figure 5.12: Base Axial Stress in the Broad Tank Shell, El Centro Record

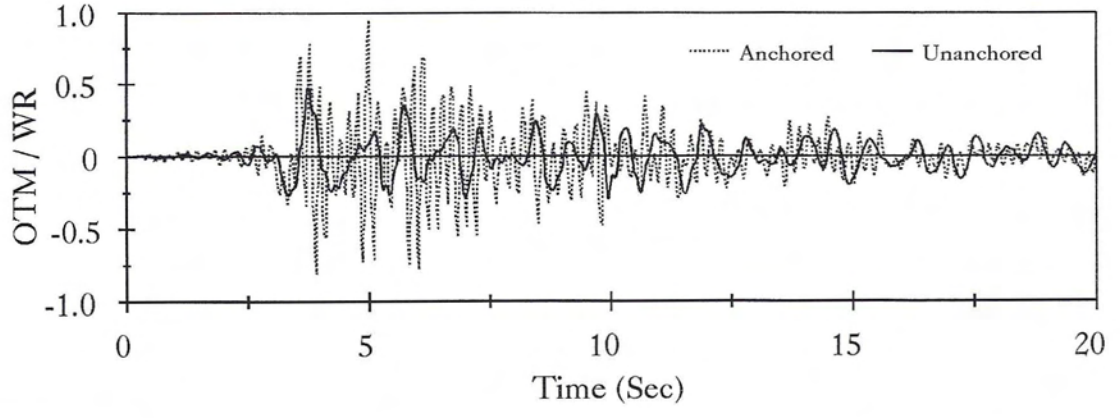

Figure 5.13: Overturning Moment at Center of Base of the Tall Tank, Northridge Record

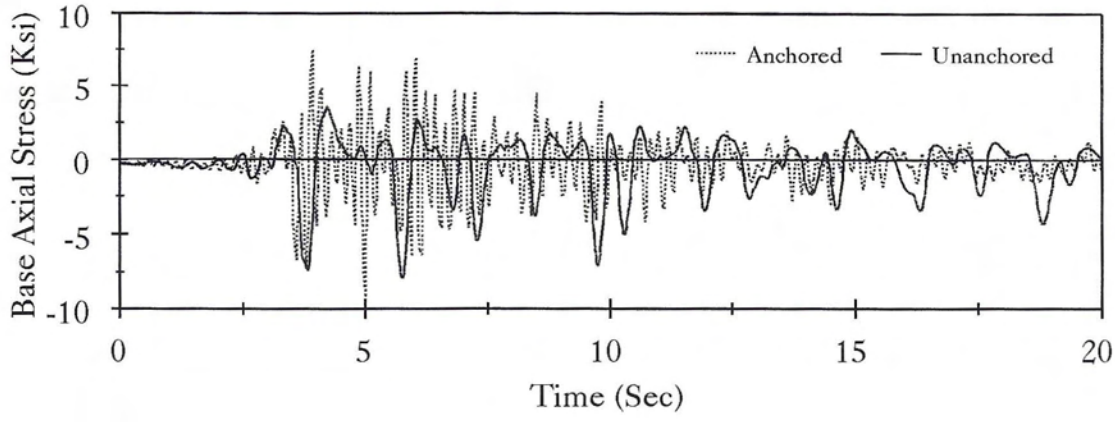

Figure 5.14: Base Axial Stress in the Tall Tank Shell, Northridge Record

(5.21) and (5.23) show the uplift displacement of the two extreme opposite points on the principal diameter which parallels the earthquake excitation of the broad and tall tanks, respectively, when subjected to the Northridge and El Centro ground motions. They show that the uplift displacement on the tension side is much higher than the penetration displacement on the compression side. Such a behavior is expected due to the tensionless nature of the foundation. In addition, Figures (5.18), (5.20), (5.22) and (5.24) show the time history of the change in the area of contact of the base plate with the foundation (A_c) as compared to the total area (A_t).

5.3.1 Effect of Foundation Stiffness

In order to evaluate the effect of the stiffness of the supporting foundation on the dynamic response of unanchored tanks, the tank base plate was considered supported on a tensionless elastic foundation of a uniform stiffness of 100 lb/in/in^2 in compression. Table (5.6) shows the unanchored tank response using the small deflection theory. The dominant period of the rocking mode of the tall tank increased to 1.16 sec while the one for the broad tank showed almost no change. This is

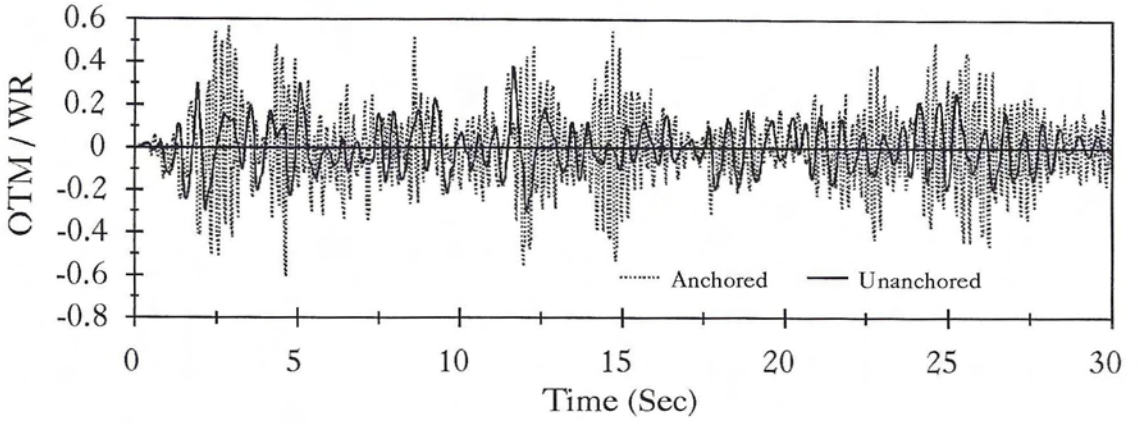

Figure 5.15: Overturning Moment at Center of Base of the Tall Tank, El Centro Record

attributed to the fact that the portion of the base plate of the broad tank located in the middle of the tank remains inactive in a horizontal position during the earthquake, as shown in Figure (5.25). The portion near the edges is frequently penetrating into the foundation and uplifting above it. Because of high foundation stiffness, the penetration displacement is small as compared to the uplift displacement. As a result, the resistance of the base plate to the uplifting force becomes the governing factor in the rocking motion of the tank. On the other hand, as shown in Figure (5.26), most of the base plate of the tall tank showed rocking motion. Thus, the period of the

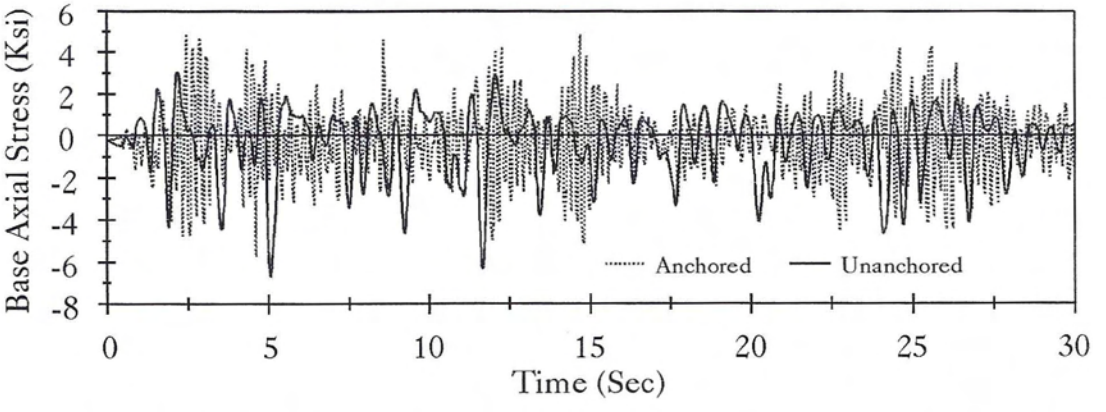

Figure 5.16: Base Axial Stress in the Tall Tank Shell, El Centro Record

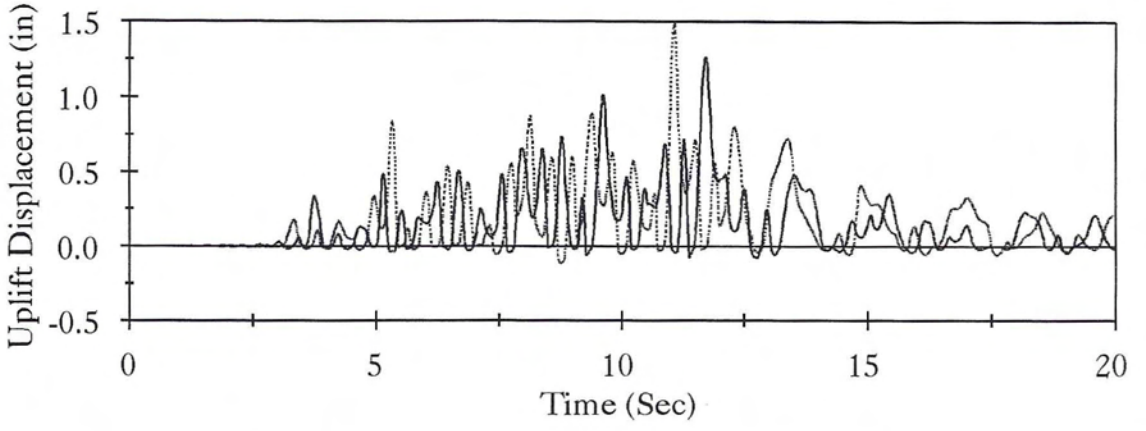

Figure 5.17: Uplift Displacement of the Two Corner Points on the Principal Diameter of the Broad Tank, Northridge Record

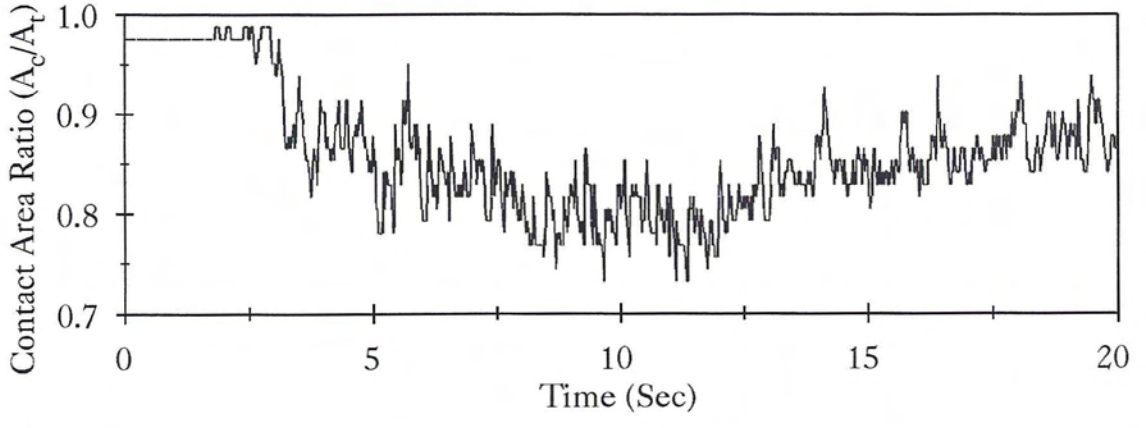

Figure 5.18: Percentage of Bottom Plate Area of Broad Tank in Contact with the Foundation, Northridge Record

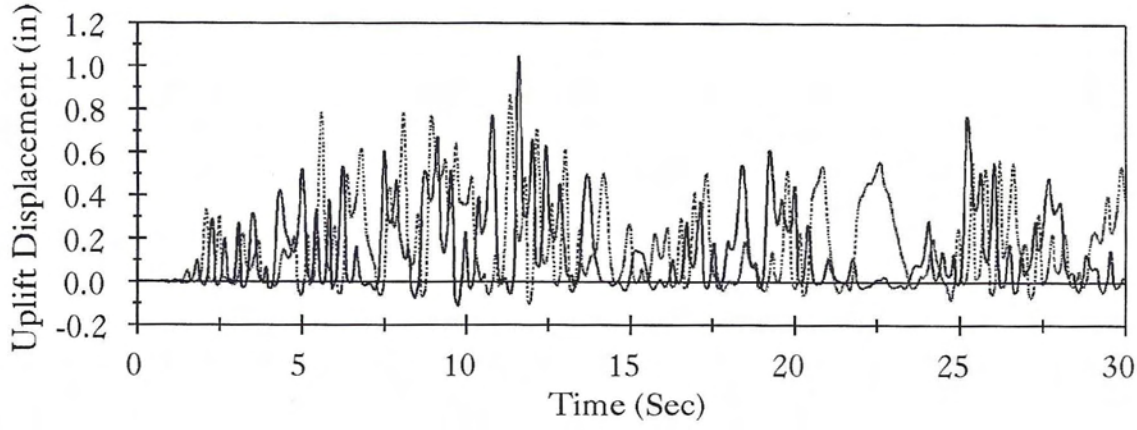

Figure 5.19: Uplift Displacement of the Two Corner Points on the Principal Diameter of the Broad Tank, El Centro Record

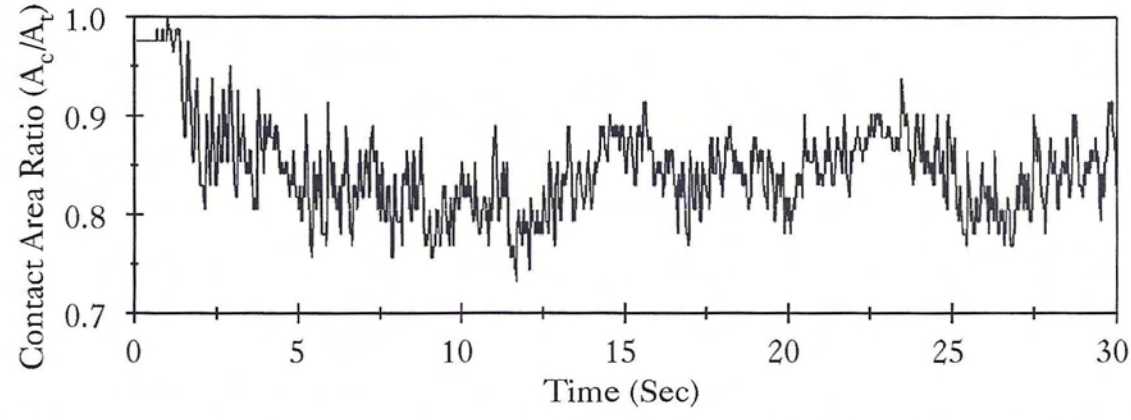

Figure 5.20: Percentage of Bottom Plate Area of Broad Tank in Contact with the Foundation, El Centro Record

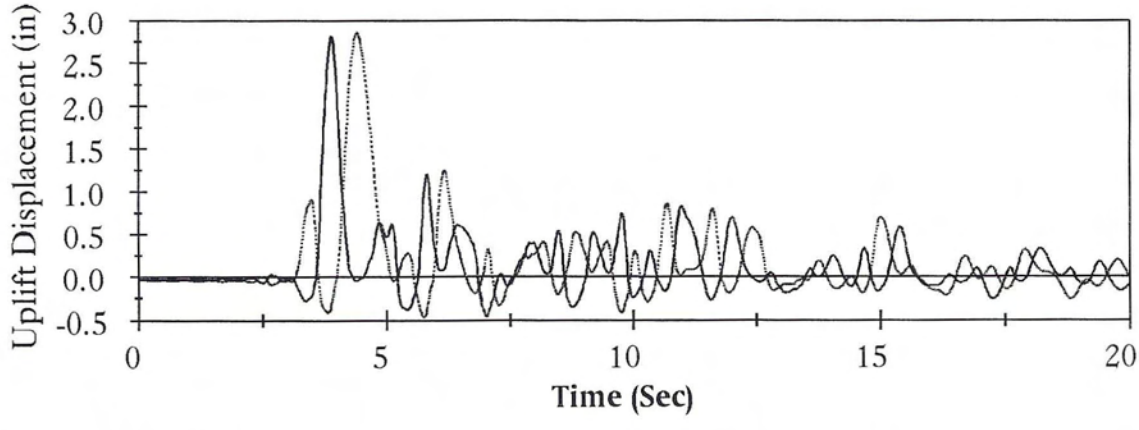

Figure 5.21: Uplift Displacement of the Two Corner Points on the Principal Diameter of the Tall Tank, Northridge Record

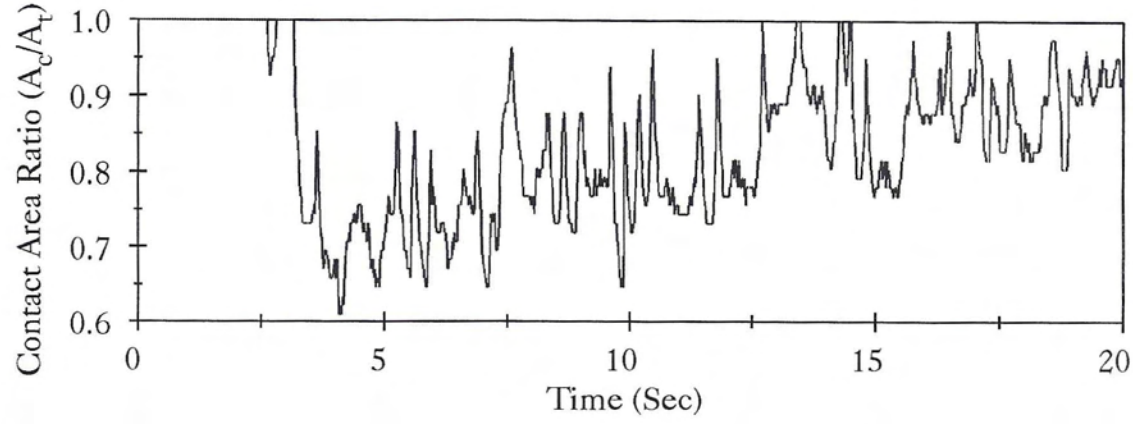

Figure 5.22: Percentage of Bottom Plate Area of Tall Tank in Contact with the Foundation, Northridge Record

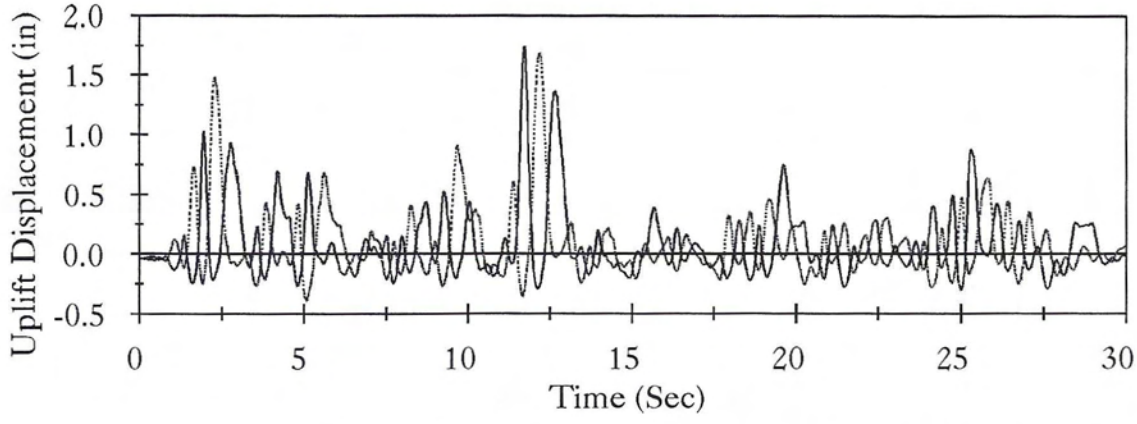

Figure 5.23: Uplift Displacement of the Two Corner Points on the Principal Diameter of the Tall Tank, El Centro Record

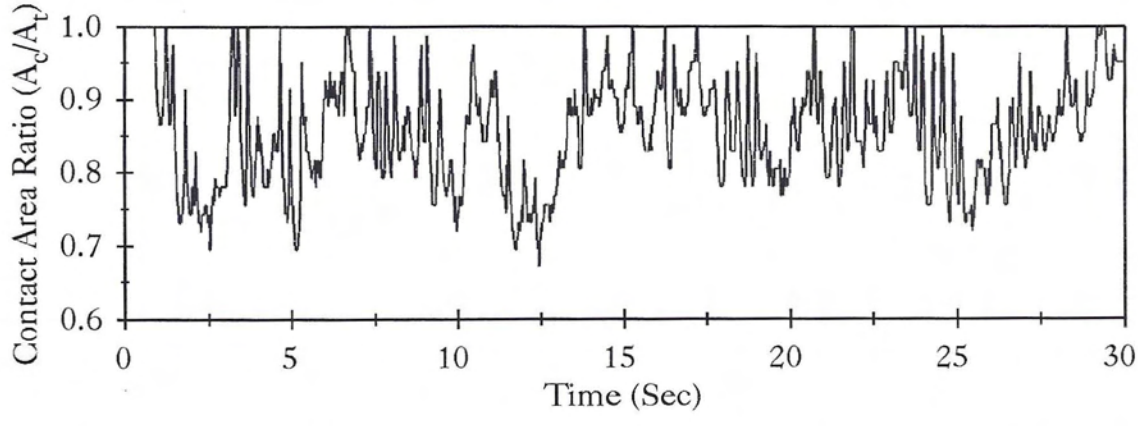

Figure 5.24: Percentage of Bottom Plate Area of Tall Tank in Contact with the Foundation, El Centro Record

Response Parameter	El Centro Record		Northridge Record	
	Broad	Tall	Broad	Tall
Top Lateral Acceleration	0.851 g	0.504 g	0.831 g	0.824 g
Top Lateral Deflection (in)	10.16	5.91	6.03	15.01
Total OTM / WR	0.161	0.228	0.200	0.277
Wall OTM / WR	0.057	0.191	0.057	0.245
Base Shear / W	0.224	0.144	0.227	0.220
Base Axial Stress (Ksi)	-2.41	-4.52	-1.92	-4.50
Base Hoop Stress (Ksi)	8.11	5.39	7.95	7.40
Axial Stress at 0.25H (Ksi)	-1.01	-3.55	-0.72	-3.63
Hoop Stress at 0.25H (Ksi)	18.72	10.53	19.76	12.22
Maximum Uplift Displacement (in)	1.58	1.74	1.90	3.60
Minimum Contact Area	0.817	0.768	0.817	0.732

Table 5.6: Response of Unanchored Tanks on Softer Foundation

tank increased due to the decrease in the rotational stiffness of the base plate. This results in hydrodynamic forces which are lower than those exerted when the tank was supported on a stiffer foundation. In addition, increasing the foundation flexibility caused the contact zone to be larger and pressure distribution on the foundation was more uniform than those of stiffer foundations. As a result, the compressive stresses in the bottom of the tank shell were lower, because they were distributed more widely along the base of tank wall, and the uplift displacements were higher than those of tanks supported over more rigid foundations.

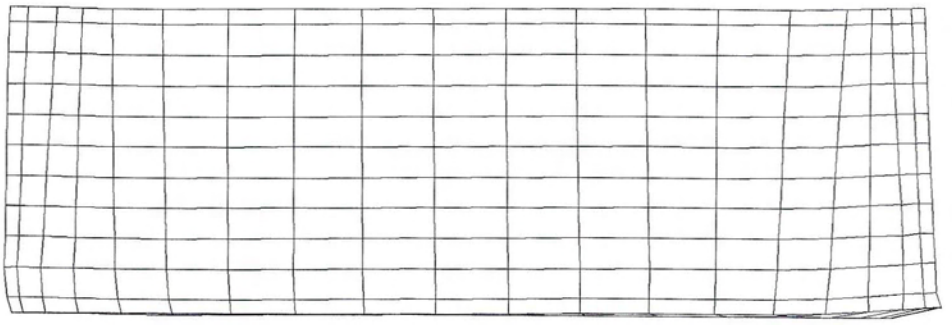

Figure 5.25: The Deformed Shape of the Broad Tank

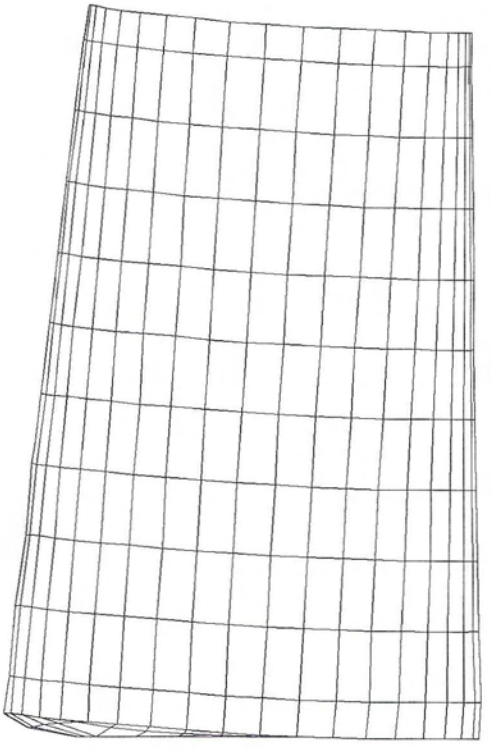

Figure 5.26: The Deformed Shape of the Tall Tank

5.3.2 Large Deflection Effect

The response of the two tanks was estimated using the large deflection assumption and the tank base plate was considered supported on a tensionless elastic foundation of a uniform stiffness of 1000 lb/in/in^2 in compression. Table (5.7) shows the response of these tanks to El Centro and Northridge earthquakes, respectively. The table shows a reduction in the uplift displacements of the base plate and an increase in the contact area of the base plate with the foundation due to the membrane effect that increased its uplifting stiffness. This also has caused the dominant period of the rocking motion to decrease to 0.21 sec for the broad tank and 0.55 sec for the tall tank. In addition, the membrane effect of the tank shell has reduced the deflection and acceleration at top of the broad tank. As a result, the impulsive acceleration was less and the resulting hydrodynamic forces were also less. For a tall tank, which acts more like a cantilever, this did not have much effect on the tank shell acceleration and the hydrodynamic forces were also were not altered much.

Axial stresses at the bottom of the tank shell were less than those using the small deflection assumption. This is attributed to the reduction in the uplift displacements as well as the increase in the contact area of the tank base plate.

5.3.3 Effect of Plasticity

The excessive uplifting displacement of the base plate of an unanchored liquid storage tank usually causes a plastic hinge to develop in the connection between the base plate and the shell. Table (5.8) shows the response of the unanchored tanks to El Centro and Northridge earthquakes, respectively, taking into consideration the

Response Parameter	El Centro Record		Northridge Record	
	Broad	Tall	Broad	Tall
Top Lateral Acceleration	1.345 g	0.812 g	1.652 g	0.853 g
Top Lateral Deflection (in)	1.65	6.65	1.30	8.90
Total OTM / WR	0.127	0.374	0.167	0.470
Wall OTM / WR	0.047	0.314	0.060	0.348
Base Shear / W	0.183	0.232	0.237	0.291
Base Axial Stress (Ksi)	-1.68	-6.55	-1.79	-6.50
Axial Stress at 0.25H (Ksi)	-0.93	-4.61	-0.81	-4.62
Hoop Stress at 0.25H (Ksi)	17.46	11.25	18.73	12.49
Maximum Uplift Displacement (in)	0.36	1.56	0.46	2.52
Minimum Contact Area	0.792	0.683	0.793	0.622

Table 5.7: Unanchored Tank Response – Large Deflection Assumption

possibility of the formation of this plastic hinge and the large deflection effect. The tank base plate was considered supported on a tensionless elastic foundation of a uniform stiffness of 1000 lb/in/in^2 in compression.

The lateral stiffness of the unanchored tank shell may be divided into two components: a vertical stiffness and a horizontal stiffness. The vertical stiffness is caused by the cantilever effect which depends mainly on the rotational stiffness provided from the connection between the base plate and the tank shell. The horizontal stiffness is caused by the hoop effect due to the horizontal curvature of the shell. The formation of the plastic hinge decreases the vertical stiffness of the tank shell leading to a longer period for its lateral vibration. As a result, the hydrodynamic forces on the tank wall are less than those exerted when the plasticity was ignored. In addition, formation of

Response Parameter	El Centro Record		Northridge Record	
	Broad	Tall	Broad	Tall
Top Lateral Acceleration	2.810 g	0.576 g	1.390 g	0.785 g
Top Lateral Deflection (in)	3.47	4.70	1.08	9.44
Total OTM / WR	0.118	0.305	0.154	0.394
Wall OTM / WR	0.039	0.260	0.055	0.312
Base Shear / W	0.148	0.185	0.218	0.254
Base Axial Stress (Ksi)	-2.75	-5.43	-1.86	-6.74
Axial Stress at 0.25H (Ksi)	-1.54	-3.66	-1.00	-4.45
Hoop Stress at 0.25H (Ksi)	17.20	8.19	18.02	8.56
Maximum Uplift Displacement (in)	1.22	1.73	0.52	3.13
Minimum Contact Area	0.732	0.720	0.768	0.659

Table 5.8: Unanchored Tank Response – Large Deflection and Plasticity Assumptions are Included

the plastic hinge increased the uplift displacements of the base plate and decreased the contact area of the base plate with the foundation.

5.3.4 Effect of Base Plate Thickness

The uplift mechanism that governs the response of unanchored tanks is influenced by the thickness of the base plate. Tanks with thinner base plate uplift more and consequently more axial stresses are developed at the bottom of the tank shell. In addition, decreasing the thickness of the base plate reduces the rocking stiffness and consequently lengthens the rocking period. This causes developed hydrodynamic forces to be slightly less than those of tanks with thicker base plate. Table (5.9) shows

Response Parameter	El Centro Record		Northridge Record	
	Broad	Tall	Broad	Tall
Top Lateral Acceleration	1.22g	0.78 g	2.09 g	0.80 g
Top Lateral Deflection (in)	1.75	6.46	1.89	9.9
Total OTM / WR	0.104	0.358	0.156	0.430
Wall OTM / WR	0.039	0.304	0.055	0.345
Base Shear / W	0.147	0.220	0.214	0.288
Base Axial Stress (Ksi)	-1.64	-7.03	-2.36	-7.40
Axial Stress at 0.25H (Ksi)	-0.76	-5.15	-1.36	-5.40
Hoop Stress at 0.25H (Ksi)	16.39	10.82	17.71	11.60
Maximum Uplift Displacement (in)	0.46	1.71	0.727	2.96
Minimum Contact Area	0.768	0.646	0.756	0.622

Table 5.9: Response of Unanchored Tanks with Reduced Base Plate Thickness – Large Deflection Assumption

the response of the unanchored tanks to El Centro and Northridge earthquakes, respectively, assuming that the base plate thickness is 0.5 inch and considering the large deflection effect.

5.3.5 Effect of Vertical Excitation

In order to assess the effect of the vertical component of an earthquake excitation on the response of unanchored liquid storage tanks, both broad and tall tanks were subjected to the vertical component of the Northridge Record that has a peak ground acceleration of $0.552g$, as shown in Figure (5.27). Table (5.10) shows the maximum response when the broad and tall tanks were subjected to the vertical component

Response Parameter	Broad	Tall
Top Lateral Acceleration	1.64g	0.82 g
Top Lateral Deflection (in)	1.31	8.70
Total OTM / WR	0.193	0.461
Wall OTM / WR	0.059	0.358
Base Shear / W	0.234	0.278
Base Axial Stress (Ksi)	-1.65	-6.64
Axial Stress at 0.25H (Ksi)	-0.84	-4.73
Hoop Stress at 0.25H (Ksi)	19.13	12.58
Maximum Uplift Displacement (in)	0.60	2.55
Minimum Contact Area	0.793	0.610

Table 5.10: Response of Unanchored Tanks Subjected to Northridge Vertical Record – Large Deflection Assumption

of the Northridge earthquake in addition to the horizontal component. Apparently vertical component altered the hydrodynamic forces exerted on unanchored tanks. If the peak response of the vertical component of an earthquake occurred simultaneously and in the same direction with the peak response of the horizontal component, it may significantly increase the exerted hydrodynamic forces excerted on the tank. Tables (5.11) and (5.12) summarize the effect of the aforementioned factors on the response of broad and tall liquid storage tanks, respectively.

			Base Axial Stress (Ksi)	Max. Uplift Displ. (in)	Total OTM/WR	Base Shear/W
Anchored		El Cen.	-2.03	-	0.148	0.214
		Northr.	-2.11	-	0.176	0.254
U	Small	El Cen.	-4.75	1.05	0.200	0.292
n	Deflection	Northr.	-4.62	1.50	0.198	0.258
a	Softer	El Cen.	-2.41	1.58	0.161	0.224
n	Foundation	Northr.	-1.92	1.90	0.200	0.227
c	Large	El Cen.	-1.68	0.36	0.127	0.183
h	Deflection	Northr.	-1.79	0.46	0.167	0.237
o	Plasticity	El Cen.	-2.75	1.22	0.118	0.148
r		Northr.	-1.86	0.52	0.154	0.218
e	Plate Thick.	El Cen.	-1.64	0.46	0.104	0.147
d	is 0.5 inch	Northr.	-2.36	0.73	0.156	0.214
	Vl. Excit.	Northr.	-1.65	0.60	0.193	0.234

Table 5.11: Maximum Response Summary of the Broad Unanchored Tank

5.4 Lateral Static Push Response of Unanchored Tanks

The lateral static push analysis is performed to investigate the behavior of unanchored liquid storage tanks when subjected to lateral earthquake loads. As the tank is pushed in the lateral direction, it uplifts from its foundation and develops a similar uplifting mechanism to that occurred under earthquake excitations. As shown in Figure (5.28), a hydrodynamic pressure distribution was assumed on the tank wall

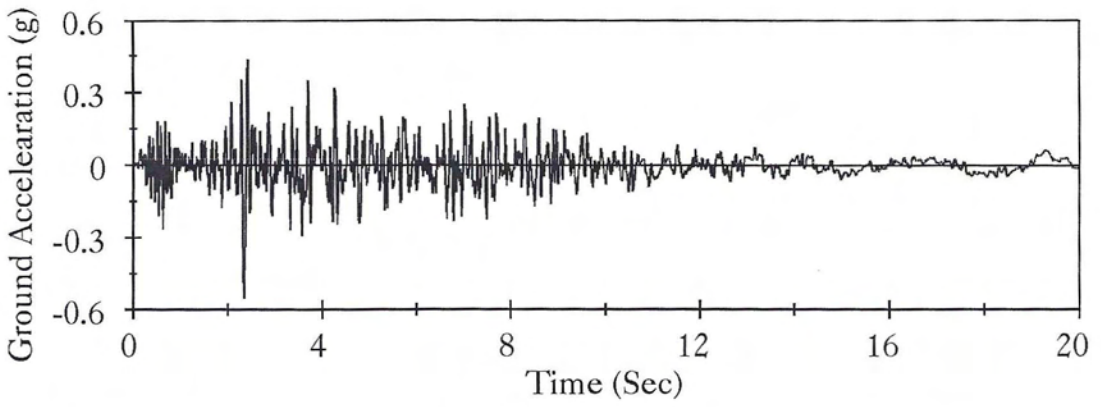

Figure 5.27: Northridge Earthquake Record Measured at Arleta Site in the Vertical Direction

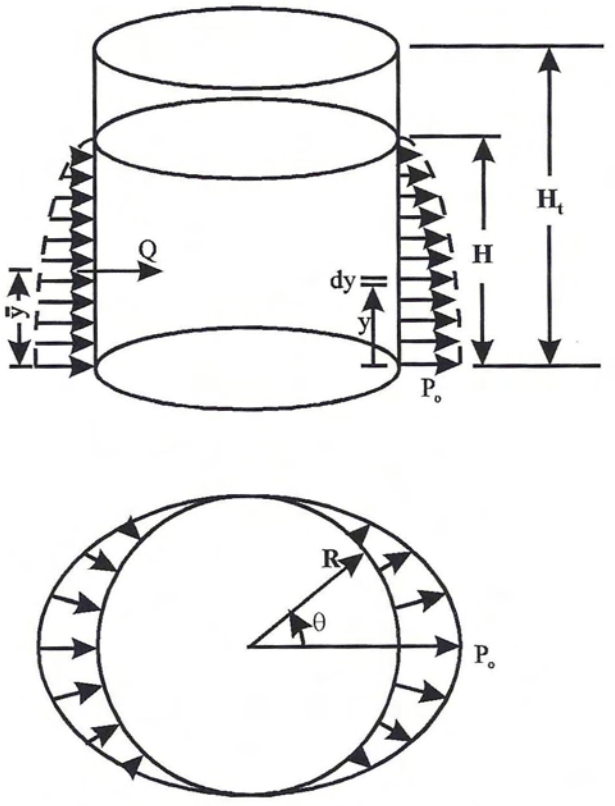

Figure 5.28: Pseudo-Dynamic Loads Applied on Tank Wall

			Base Axial Stress (Ksi)	Max. Uplift Displ. (in)	Total OTM/WR	Base Shear/W
Anchored		El Cen.	-5.77	-	0.605	0.377
		Northr.	-9.10	-	0.943	0.577
U	Small	El Cen.	-6.71	1.75	0.380	0.243
n	Deflection	Northr.	-7.90	2.87	0.477	0.293
a	Softer	El Cen.	-4.52	1.74	0.228	0.144
n	Foundation	Northr.	-4.50	3.60	0.277	0.220
c	Large	El Cen.	-6.55	1.56	0.374	0.232
h	Deflection	Northr.	-6.50	2.52	0.470	0.291
o	Plasticity	El Cen.	-5.43	1.73	0.305	0.185
r		Northr.	-6.74	3.13	0.394	0.254
e	Plate Thick.	El Cen.	-7.03	1.71	0.358	0.220
d	is 0.5 inch	Northr.	-7.40	2.96	0.430	0.288
	Vl. Excit.	Northr.	-6.64	2.55	0.461	0.278

Table 5.12: Maximum Response Summary of the Tall Unanchored Tank

as

$$p = p_o \left(1 - \frac{y^2}{H^2}\right) \cos\theta \tag{5.4}$$

where y is the elevation of a point on the shell measured from the base, H is the fluid depth, θ is the angle measured from the axis of excitation and p_o is the pressure amplitude at the tank base at $\theta = 0°$. If M denotes the overturning moment about the center of the base, then

$$\begin{aligned} M &= \int_0^H \int_0^{2\pi} pRy \cos\theta \, d\theta \, dy = \frac{\pi}{4} H^2 p_o R \\ &= 75360 \, p_o \quad \text{For broad tank} \end{aligned} \tag{5.5}$$

$$= 97667\, p_o \quad \text{For tall tank}$$

and similarly, if Q is the base shear, then

$$\begin{aligned} Q &= \int_0^H \int_0^{2\pi} pR\cos\theta\, d\theta\, dy = \frac{2\pi}{3} H p_o R \qquad (5.6) \\ &= 5024\, p_o \quad \text{For broad tank} \\ &= 3617\, p_o \quad \text{For tall tank} \end{aligned}$$

and accordingly

$$\bar{y} = \frac{M}{Q} = 0.375H \qquad (5.7)$$

Figures (5.29) and (5.30) show the finite element mesh used to model the broad and the tall tanks, respectively. The broad tank showed buckling at a value of OTM/WR=0.077 which indicates that the broad tank may have buckled during transient responses presented before. On the contrary, the tall tank did not experience buckling until it overturns. Figures (5.31) and (5.32) show that uplift displacements predicted from static analyses were larger than those predicted from dynamic analyses presented before. However, predicted axial stresses at the bottom of the tank shell were compared to those predicted from dynamic analyses.

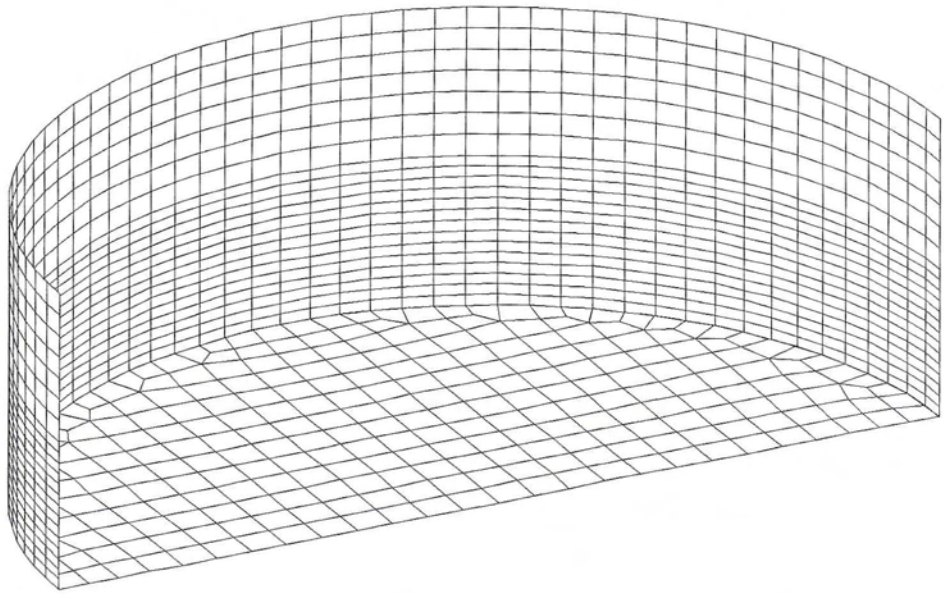

Figure 5.29: Finite Element Model of the Broad Tank

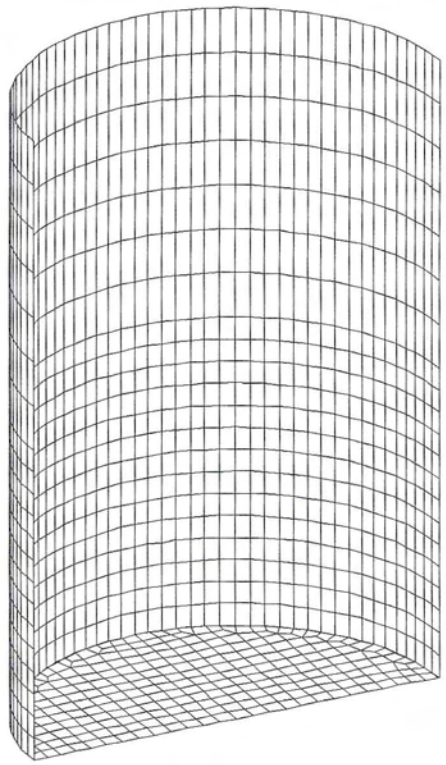

Figure 5.30: Finite Element Model of the Tall Tank

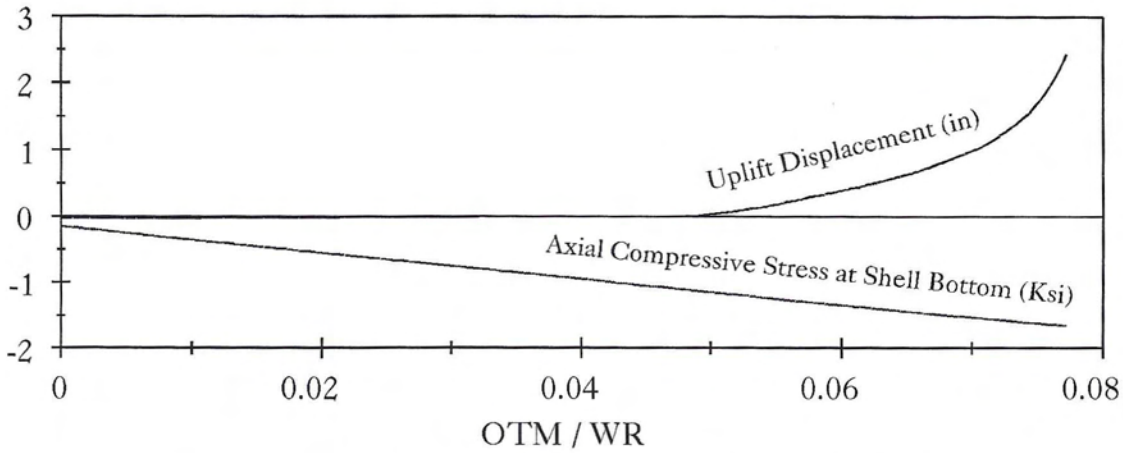

Figure 5.31: Static Response of the Broad Tank

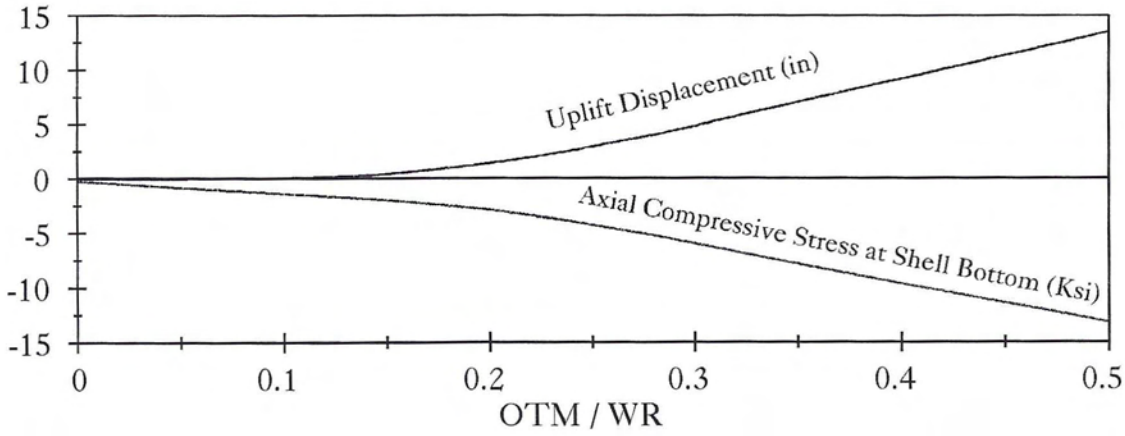

Figure 5.32: Static Response of the Tall Tank

Chapter 6

Conclusion

A finite element program was developed to analyze the complexities associated with the nonlinear dynamic response of unanchored liquid storage tanks. The program is capable of modeling curved shells with material and geometric nonlinearities, nonlinear sloshing behavior of fluids, nonlinear fluid-structure interaction and a general class of contact problems. It was observed that the overturning moment exerted on an unanchored tank may be smaller than that exerted on a similar anchored tank due to the longer-period characteristic of the rocking motion, which dominates the behavior of unanchored tanks. However, due to the nature of the boundaries associated with unanchored tanks at their base, the axial and hoop stresses at the bottom of an unanchored tank shell may be larger than those of a similar anchored tank subjected to the same ground motion. The response of unanchored tanks was dominated by the uplift mechanism that varied nonlinearly with the intensity and frequency of the input motion. The coupling of the uplift mechanism with out-of-round distortions resulted in high compressive axial membrane stresses developed over a narrow contact zone. This effect is reflected by the sharp peaks on the compression side of the time histories of axial stresses, which occurred simultaneously with large uplifting displacements. The cases on which axial stresses at the bottom of an anchored tank shell were larger than those of a similar unanchored tank are attributed to the

large difference between the overturning moments in the two tanks. Yet, sharp peaks appear on the compression side of the axial stress time history of these tanks.

Many factors that affect the seismic response of unanchored tanks were investigated. It was found that unanchored tanks supported on flexible foundations exhibit lower compressive stresses and higher uplift displacements than those supported over more rigid foundations. This was attributed to flexible foundations, where the contact zone is larger and the pressure distribution on the soil is more uniform than those of rigid foundations. In addition, foundation softness lengthens the rocking period of the tank resulting in less hydrodynamic forces. Membrane forces induced due to large deflections were found to reduce uplift displacements and consequently axial stresses. Formations of a plastic hinge in the connection between the tank shell and base plate increase uplift displacements. Reducing the thickness of the base plate causes the tank to uplift more and consequently more axial stresses are developed at the bottom of the tank shell. In addition, decreasing the base plate thickness reduces the rocking stiffness and consequently lengthens the rocking period. Thus, the developed hydrodynamic forces were less than those for tanks with thicker base plates. Vertical ground motions were found to alter the hydrodynamic forces exerted on unanchored tanks. If the peak response to the vertical component of an earthquake occurred simultaneously and in the same direction with the peak response to the horizontal component, the exerted hydrodynamic forces on the tank may significantly increase.

Bibliography

[1] Abboud, N.N., and Pinsky, P.M., *Mixed Variational Principle for the Structure-Exterior Fluid Interaction Problem*, Proceedings of the International Symposium on Flow-Induced Vibration and Noise: Acoustic Phenomena and Interaction in Shear Flows over Compliant and Vibrating Surfaces, ASME, New York, 1988, pp. 137-148.

[2] Abramson, H.M., *The Dynamic Behavior of Liquids in Moving Containers*, NASA SP-106, National Aeronautics and Space Administration, Washington D.C., 1966.

[3] Adams, N., *Seismic Design Rules for Flat Bottom Cylindrical Liquid Storage Tanks*, International Journal of Pressure Vessels and Piping, January 1992, Vol. 19, pp. 61-95.

[4] Aita, S., Combescure, A., and Gibert, R.J., *Imperfections on Thin Axisymmetric Shells - Fluid Structure Interaction Aspects*, Proceedings of the 9th International Conference on Structural Mechanics in Reactor Technology (SMIRT-9), Lausanne, Switzerland, August 1987.

[5] Allen, L.R., Hutchinson, G.L., and Stevens, L.K., *Buckling Considerations in the Design of Elevated Steel Water Tanks*, N.W. Murray Symp. on Thin-Walled Structures: Developments in Theory and Practice, Monash University, Melbourne, Australia, November 1988, pp. 389-406.

[6] American Water Works Association, *AWWA Standard for Welded Steel Tanks for Water Storage*, American Welding Society, New England Water Works Association, AWWA D100-84, Denver, Colorado, March 1985.

[7] American Petroleum Institute, *Welded Steel Tanks for Oil Storage*, API Standard 650, 7th Edition, Washington, D.C., 1980.

[8] Argyris, J.H., and Kelsey, S., *Energy Theorems and Structural Analysis*, Butterworths, London, 1960, Reprinted from a Series of articles in Aircraft Engineering, 1954-55.

[9] Asai, K., Yanabu, K., Goto, Y., and Kikuchi, T., *Studies on Earthquake Response of On-Ground LNG Storage Tank Based on Observed Record*, Proceedings of the Sloshing Vibration and Seismic Response of Fluid-Structure Systems, PVP, ASME, Vol. 145, Pennsylvania, June 1988, pp. 71-76.

[10] Aslam, M. *Finite Element Analysis of Earthquake-Induced Sloshing in Axisymmetric Tanks*, International Journal of Numerical Methods in Engineering, Vol. 17, 1981, pp. 159-170.

[11] Auli, W., Fischer, F.D., and Rammerstorfer, F.G., *Uplifting of Earthquake Loaded Liquid Filled Tanks*, Pressure Vessels and Piping Conference, ASME, PVP-Vol. 98-4, New Orleans, June 1985, pp. 71-85.

[12] Badawi, H., *Seismic Behavior of Unanchored Liquid Storage Tanks*, Ph.D. Dissertation, Dept. of Civil Engineering, University of California, Irvine, 1989.

[13] Bains, G., *Nonlinear Analysis of Plates and Shells With Application to Liquid Containers*, Ph.D. Dissertation, Dept. of Civil Engineering, University of California, Irvine, 1989.

[14] Balendra, T., and Nash, W., *Earthquake Analysis of a Cylindrical Liquid Storage Tank With a Dome by Finite Element Method*, Report, University of Massachusetts Amherst, Civil Engineering Dept., May 1987.

[15] Barron, R., and Chng, S.W., *Dynamic Analysis and Measurement of Sloshing of Fluid in Containers*, Journal of Dynamic Systems, Measurements and Control, Transactions of ASME, Vol. III, No. 1, March 1989, pp. 63-90.

[16] Barton, D.C., and Parker, J.V., *Finite Element Analysis of the Seismic Response of Anchored and Unanchored Liquid Storage Tanks*, International Journal of Earthquake Engineering and Structural Dynamics, Vol. 15, 1987, pp. 299-322.

[17] Bathe, K., and Chaudhary, A., *A Solution Method for Planar and Axisymmetric Contact Problems*, International Journal for Numerical Methods in Engineering, Vol. 21, 1985, pp. 65-88.

[18] Bathe, K., and Hahn, W., *On Transient Analysis of Fluid-Structure Systems*, Journal of Computers and Structures, Vol. 10, 1979, pp. 383-391.

[19] Bauer, H.F., and Eidel, W., *Nonlinear Hydroelastic Vibrations in Rectangular Containers*, Journal of Sound and Vibration, Vol. 125, No. 1, August 1988, pp. 93-114.

[20] Belytschko, T., *Fluid-Structure Interaction*, Journal of Computers and Structures, Vol. 12, 1980, pp. 459-469.

[21] Belytschko, T., and Kennedy, J., *Computer Models For Subassembly Simulation*, Journal of Nuclear Engineering and Design, Vol. 49, 1978, pp. 17-38.

[22] Belytschko, T., and Kennedy, J., *A Fluid-Structure Finite Element Method For the Analysis of Reactor Safety Problems*, Journal of Nuclear Engineering and Design, Vol. 38, 1976, pp. 71-81.

[23] Bigham, R.E., *Distortion of Steel Tanks Due to Settlement of their Walls - Discussion*, Journal of Geotechnical Engineering-ASCE, Vol. 117, No. 9, 1991, pp. 1440-1442.

[24] Birk, A.M., and Chidley, D., *Slosh Pressure in Cylindrical Tanks Undergoing Impact Induced Accelerations*, Joint ASCE/ASME Applied Mechanics, Biomechanics, and Fluids Engineering Conference, California, July 1989, FE16.

[25] Bleich, H.H., *Longitudinal Forced Vibrations of Cylindrical Fuel Tanks*, Jet Propulsion, Vol. 26, 1956, pp. 109-111.

[26] Butko, A.M, and Novichkov, Y.N., *Natural Frequencies and Collapse Strength of Radioactive Waste Transport Casks*, Mechanics of Solids, Vol. 23, No. 2, 1988, pp. 133-143.

[27] Cambra, F.J., *A Study of Liquid Storage Tank Seismic Uplift Behavior*, Proceedings of the Pressure Vessels and Piping Technology Conference, ASME, PVP-Vol. 77, Oregon, June 1983, pp. 37-46.

[28] Cambra, F.J., *Earthquake Response Considerations of Broad Liquid Storage Tanks*, Earthquake Engineering Research Center, Report UCB/EERC 82-25, November 1982.

[29] Chan, S.K., and Tuba, I.S., *A Finite Element Method for Contact Problems of Solid Bodies - Part I, Theory and Validation*, International Journal of Mechanical Sciences, Vol. 13, 1971, pp. 615-625.

[30] Chang, Y.W., Ma, D.C., Gvildys, J., and Liu, W.K., *Seismic Analysis of LMR Reactor Tanks*, Journal of Nuclear Engineering and Design, Vol. 106, No. 1, February 1988, pp. 19-33.

[31] Chaudhary, A., *A Solution Method for Static and Dynamic Analysis of Three-Dimensional Contact Problems with Friction*, Journal of Computers and Structures, Vol. 24, No. 6, 1986, pp. 855-873.

[32] Chen, W., *Nonlinear Liquid Sloshing Motion in Seismically-Excited Rectangular Tanks*, Ph.D. Dissertation, Dept. of Civil Engineering, University of California, Irvine, 1993.

[33] Chiba, M., Yamashida, T., Sugiyama, H., and Tani, J., *Dynamic Stability of Liquid-Filled Cylindrical Shells Under Periodic Shearing Forces*, Proceedings of International Symposium on Flow-Induced Vibration and Noise: Flow-Induced Vibrations due to Internal and Annular Flows, and Special Topics in Fluid elasticity, ASME, Illinoy, November 1988, pp. 241-253.

[34] Chopra, A., Wilson, E., and Farhoomand, I., *Earthquake Analysis of Reservoir-Dam Systems*, Proceedings of the 4th World Conference on Earthquake Engineering, Santiago, Chile, 1969.

[35] Clarke, M.J., and Rotter, J.M., *Technique for the Measurement of Imperfections in Prototype Silos and Tanks*, Research Report, University of Sydney, School of Civil and Mechanical Engineering, No. R565, March 1988.

[36] Clough, D.P., *Experimental Evaluation of Seismic Design Methods for Broad Cylindrical Tanks*, Earthquake Engineering Research Center, Report UCB/EERC 77-10, May 1977.

[37] Clough, R.W., Niwa, A., and Clough, D.P., *Experimental Seismic Study of Cylindrical Tanks*, Journal of Structural Engineering, ASCE, Vol. 105, No. 12, 1979, pp. 2565-2590.

[38] Clough, R.W., and Niwa, A., *Static Tilt Tests of a Tall Cylindrical Liquid Storage Tank*, Earthquake Engineering Research Center, Report UCB/EERC 79-06, February 1979.

[39] Clough, R.W., *The Finite Element Method in Plane Stress Analysis*, In Proceedings of the 2nd ASCE Conference on Electronic Computation, Pittsburgh, 1960.

[40] Conry, T.F., and Seireg, A., *A Mathematical Programming Method for Design of Elastic Bodies in Contact*, Journal of Applied Mechanics, Vol. 38, 1971, pp. 387-392.

[41] Costley, A.C., *Critical Buckling Load Determination of Thin-Walled Cylinders Using Experimental Modal-Analysis*, Proceedings of the 37th Annual Technical Meeting of the Inst. of Environmental Sciences: Technical Solutions through Technical Cooperation, California, May 1991, pp. 512-519.

[42] Costley, A.C., Mourad, S.A., Kazanji, R.P., and Pardoen, G.C., *Determination of Critical Buckling Load of Thin-Walled Cylinders Using Modal Analysis*, Proceedings of the 9th International Modal Analysis Conference, Florence, Italy, April 1991.

[43] Courant, R., *Calculus of Variations and supplementary Notes and Exercises*, New York University, 1962.

[44] Crisfield, M.A., Nonlinear Finite Element Analysis of Solids and Structures, Volume 1, John Wiley & Sons, New York.

[45] Dargush, G.F., and Banerjee, P.K., *Development of an Integrated BEM for Hot Fluid-Structure Interaction*, Journal of Engineering for Gas Turbines and Power-Transactions of the ASME, Vol. 112, No. 2, April 1990, pp. 243-250.

[46] D'Orazio, T.B., Duncan, J.M., and Bell, R.A., *Distortion of Steel Tanks due to Settlement of their Walls - Closure*, Journal of Geotechnical Engineering-ASCE, Vol. 117, No. 9, 1991, pp. 1446-1447.

[47] D'Orazio, T.B., *Radial Displacement of Open Tanks Under Seismic Excitation*, PVP, ASME, Vol. 197, Tennessee, June 1990, pp. 265-267.

[48] D'Orazio, T.B., and Duncan, J.M., *Differential Settlements in Steel Tanks - Closure*, Journal of Geotechnical Engineering-ASCE, Vol. 115, No. 7, 1989, pp. 1036-1036.

[49] Ecer, A., and Akay, H., *Applications of Variational Principles in Computing Rotational Flows*, in W.G. Habashi (ed.), Proceedings of the Recent Advances in Numerical Methods in Fluids: Advances in Computational Transonics, Pineridge Press, Swansea, U.K., 1983.

[50] Ecer, A., Rout, R., and Ward, P., *Investigation of Solution of Navier-Stokes Equations Using a Variational Formulation*, International Journal for Numerical Methods in Fluids, Vol. 3, 1983, pp. 23-31.

[51] Edwards, N.W., *A Procedure for Dynamic Analysis of Thin Walled Cylindrical Liquid Storage Tanks subjected to Lateral Ground Motions*, Ph.D. Thesis, University of Michigan, Ann Arbor, 1969.

[52] Ellaithy, H.M., *Dynamic Analysis and Computer Modeling of Elevated Tanks and Three-Dimensional Supporting Tower*, Ph.D. Dissertation, Dept. of Civil Engineering, University of California, Irvine, 1986.

[53] Eterovic, A.L., and Bathe, K.J., *On the Treatment of Inequality Constraints Arising from Contact Conditions in Finite Element Analysis*, Journal of Computers and Structures, Vol. 40, No. 2, 1991, pp. 203-209.

[54] Everstine, G.C., and Henderson, F.M., *Coupled Finite Element Boundary Element Approach for Fluid Structure Interaction*, Journal of the Acoustical Society of America, Vol. 87, No. 5, 1990, pp. 1938-1947.

[55] Everstine, G.C., Marcus, M.S., and Quezon, A.J., *Finite Element Analysis of Fluid-Filled Elastic Piping System*, Proceedings of the Eleventh NASTRAN Users' Colloquium, NASA Conference Publication, 1983, pp. 141-160.

[56] Everstine, G.C., *A Symmetric Potential Formulation For Fluid-Structure Interaction*, Journal of Sound and Vibration, Vol. 79, 1981, pp. 157-160.

[57] Fan, D., and Tijsseling, A., *Fluid-Structure Interaction with Cavitation in Transient Pipe Flows*, Journal of Fluids Engineering-Transactions of the ASME, Vol. 114, No. 2, June 1992, pp. 268-274.

[58] Feng, Y.Q., and Quevat, J.P., *3-Dimensional Non-Linear Fluid-Structure Interaction Problems - Formulation by the Finite and Infinite Element Method*, International Journal for Numerical Methods in Engineering, Vol. 30, No. 6, October 1990, pp. 1115-1128.

[59] Fenske, C.W., *Distortion of Steel Tanks due to Settlement of their Walls - Discussion*, Journal of Geotechnical Engineering-ASCE, Vol. 117, No. 9, 1991, pp. 1442-1443.

[60] Fenske, C.W., *Differential Settlements in Steel Tanks - Discussion*, Journal of Geotechnical Engineering-ASCE, Vol. 115, No. 7, 1989, pp. 1032-1035.

[61] Fenves, G., and Vargas-Loli, L.M., *Nonlinear Dynamic Analysis of Fluid-Structure Systems*, Journal of Engineering Mechanics, Vol. 114, No. 2, 1988, pp. 219-240.

[62] Fichera, G., *Boundary Value Problems of Elasticity with Unilateral Constraints*, In C. Truesdell, editor, Mechanics of Solids II, Springer-Verlag, 1972, pp. 391-424,.

[63] Fichera, G., *Sul Problema Elastostatico di Signorini Con Ambigue condizioni al Ritorno*, Rend. Accad. Naz. Lincei, 34, 1963.

[64] Fischer, F.D., Rammerstorier, F.G., and Schreiner, W., *The Extensible Uplifted Strip*, Acta Mechanica, Vol. 80, No. 3-4, December 1989, pp. 227-257.

[65] Fischer, F.D., and Seeber, R., *Dynamic Response of Vertically Excited Liquid Storage Tanks Considering Liquid-Soil-Interaction*, Journal of Earthquake Engineering and Structural Dynamics, Vol. 16, No. 3, April 1988, pp. 329-342.

[66] Fischer, F.D., Seeber, R., and Rammerstorfer, F. G., *Refined Algorithms for the Analysis of Earthquake Loaded Tanks*, Proceedings of the 3rd International Conference On Soil Dynamics and Earthquake Engineering, New Jersey, June 1987, pp. 59-72.

[67] Fujita, K., *Flow-Induced Vibration and Fluid Structure Interaction in Nuclear Power Plant Components*, Journal of Wind Engineering and Industrial Aerodynamics, Vol. 33, No. 1-2, March 1990, pp. 405-418.

[68] Gladwell, G.L.M., *Contact Problems in the Classical Theory of Elasticity*, Sithoff & Noordhoff, Alphen aan den Rijn, 1980.

[69] Glowinski, R., Lions, J.L., and Tremoliéres, R., *Numerical Analysis of Variational Inequalities*, North-Holland, Amsterdam, 1981.

[70] Goncalves, P.B., and Batista, R.C., *Nonlinear Vibration Analysis of Fluid-Filled Cylindrical Shells*, Journal of Sound and Vibration, Vol. 127, No. 1, November 1988, pp. 133-143.

[71] Graham, E.W., and Rodriguez, A.M., *The Characteristics of Fuel Motion Which Affect Airplane Dynamics*, Journal of Applied Mechanics, Vol. 19, No. 3, 1952, pp. 381-388.

[72] Grilli, S.T., Skourup, J., and Svendsen, I.A., *The Modeling of Highly Nonlinear Water-Waves - A Step Toward a Numerical Wave Tank*, Proceedings of the 10th International Conference on Boundary Element Methods, Southampton, England, 1988, pp. 549-566.

[73] Guiggiani, M., *Fluid Structure Interaction and Buckling of Hemispherical Shells*, Res Mechanica, Vol. 27, No. 3, 1989, pp. 189-231.

[74] Gupta, R.K., and Hutchinson, G.L., *Effect of Wall Flexibility on the Dynamic Response of Liquid Storage Tanks*, Engineering Structures, Vol. 13, No. 3, July 1991, pp. 253-267.

[75] Gupta, R.K., and Hutchinson, G.L., *Free Vibration Analysis of Liquid Storage Tanks*, Journal of Sound and Vibrations, Vol. 122, No. 3, May 1988, pp. 491-506.

[76] Gupta, R.K., and Hutchinson, G.L., *Effects of Wall Flexibility on the Dynamic Response of Liquid Storage Tanks*, Journal of Engineering Structures, Vol. 13, No. 3, July 1991, pp. 253-267.

[77] Hamdi, M., Ousset, Y., and Verchery, G., *A Displacement Method For the Analysis of Vibrations of Coupled Fluid-Structure Systems*, International Journal for Numerical Methods in Engineering, Vol. 13, 1978, pp. 139-150.

[78] Hangai, Y., and Ohmori, H., *Vibration of Beams on Distributed Springs Considering Uplift*, Proceedings of 7th European Conference on Earthquake Engineering, Athens, Greece, 1982, pp. 635-645.

[79] Hanson, R.D., *Behavior of Liquid Storage Tanks*, Report, National Academy of Sciences, Washington D.C., 1973, pp. 331-339.

[80] Hashimoto, P.S., and Basak, A.K., *Seismic Capacity and Failure Modes of Flat-Bottom Vertical Tanks*, Journal of Energy Engineering-ASCE, Vol. 119, No. 2, August 1993, pp. 82-100.

[81] Haroun, M.A., and El-Zeiny, A., and Bhatia, H., *Seismic Qualification of Tanks for Storage of Liquefied Natural Gas*, Egyquake Proceedings, Egyptian Society for Earthquake Engineering, December 1993, pp. 665-674.

[82] Haroun, M.A., and El-Zeiny, A., *Seismic Design Considerations for Uplifted Tanks*, Proceeding of the Structures Congress, Structural Engineering in Natural Hazards Mitigation, Vol. 1, April 1993.

[83] Haroun, M.A., and Abou-Izzeddine, W., *Parametric Study of Seismic Soil-Tank Interaction .1. Horizontal Excitation*, Journal of Structural Engineering-ASCE, Vol. 118, No. 3, March 1992, pp. 783-797.

[84] Haroun, M.A., and Abou-Izzeddine, W., *Parametric Study of Seismic Soil-Tank Interaction .2. Vertical Excitation*, Journal of Structural Engineering-ASCE, Vol. 118, No. 3, March 1992, pp. 798-812.

[85] Haroun, M.A., *Implications of Observed Earthquake Induced Damage on Seismic Codes and Standards of Tanks*, Proceedings of the Fluid-Structure Vibration and Sloshing, PVP, ASME, California, Vol. 223, 1991, pp. 1-7.

[86] Haroun, M.A., Mourad, S.A., and Izzeddine, W.A., *Performance of Liquid Storage Tanks During the 1989 Loma Prieta Earthquake*, Proceedings of the Third U.S. Conference on Lifeline Earthquake Engineering, California, August 1991, pp. 1152-1161.

[87] Haroun, M.A., Mourad, S.A., and Pence, P.W., *Vibration Suppression through Liquid Oscillations*, Proceedings of the Engineering Mechanics Specialty Conference, ASCE, Ohio, April 1991, pp. 656-660.

[88] Haroun, M.A., and Mourad, S.A., *Buckling Behavior of Liquid-Filled Shells Under Lateral Seismic Shear*, proceedings of the Pressure Vessels and Piping conference, ASME, Tennessee, Vol. 109, June 1990, pp. 11-17.

[89] Haroun, M.A., Lee, L.R., and Ellaithy, H.M., *Dynamic Behavior of Shell Tower Supporting Liquid Filled Tanks*, Proceedings of the Sloshing and Fluid Structure Vibration, PVP, ASME, Hawaii, Vol. 157, July 1989, pp. 1-7.

[90] Haroun, M.A., Chen, W., *Seismic Large Amplitude Liquid Sloshing Theory*, Proceedings of the sessions related to seismic engineering at Structures Congress, California, May 1989, pp. 418-427.

[91] Haroun, M.A., and Badawi, H.S., *Seismic Behavior of Unanchored Ground Based Cylindrical Tanks*, Proceedings of the 9th World Conference of Earthquake Engineering, Tokyo-Kyoto, Japan, Vol. VI, 1988, pp. 643-648.

[92] Haroun, M.A., and Abdel-Hafiz, E.A., *A Simplified Seismic Analysis of Rigid Base Liquid Storage Tanks Under Vertical Excitations with Soil-Structure Interaction*, International Journal of Soil Dynamics and Earthquake Engineering, Vol. 5, No. 4, October 1986, pp. 217-225.

[93] Haroun, M.A., and Ellaithy, H.M., *Seismic Analysis of X-Braced Elevated Tanks*, Proceedings of the Third U.S. National Conference on Earthquake Engineering, Charleston, Vol. 4, August 1986, pp. 2811-2822.

[94] Haroun, M.A., and Ellaithy, H.M., *Seismically Induced Fluid Forces on Elevated Tanks*, Journal of Technical Topics in Civil Engineering, ASCE, Vol. 111, No. 1, December 1985, pp. 1-15.

[95] Haroun, M.A., and Tayel, M.A., *Response of Tanks to Vertical Seismic Excitations*, Journal of Earthquake Engineering and Structural Dynamics, Vol. 13, No. 5, September 1985, pp. 583-595.

[96] Haroun, M.A., and Ellaithy, H.M., *Model for Flexible Tanks Undergoing Rocking*, Journal of Engineering Mechanics, Vol. 111, No. 2, 1985, pp. 143-157.

[97] Haroun, M.A., *Stress Analysis of Rectangular Walls Under Seismically Induced Hydrodynamic Loads*, Bulletin of the Seismological Society of America, Vol. 74, No. 3, June 1984, pp. 1031-1041.

[98] Haroun, M.A., and Warren, W.L., *TANK - A Computer Program for Seismic Analysis of Tanks*, Proceedings of the Third Conference on Computing in Civil Engineering, ASCE, California, April 1984, pp. 665-674.

[99] Haroun, M.A., *Behavior of Unanchored Oil Storage Tanks: Imperial Valley Earthquake*, Journal of Technical Topics in Civil Engineering, Vol. 109, April 1983, pp. 23-40.

[100] Haroun, M. A., *Vibration Studies and Tests of Liquid Storage Tanks*, Journal of Earthquake Engineering and Structural Dynamics, Vol. 11, 1983, pp. 179-206.

[101] Haroun, M.A., and Housner, G.W., *Complications in Free Vibration Analysis of Tanks*, Journal of Engineering mechanics, ASCE, Vol. 108, 1982, pp. 801-818.

[102] Haroun, M.A., and Housner, G.W., *Dynamic Characteristics of Liquid Storage Tanks*, Journal of Engineering mechanics, ASCE, Vol. 108, 1982, pp. 783-800.

[103] Haroun, M.A., *Earthquake Response of Deformable Liquid Storage Tanks*, Journal of Applied Mechanics, ASME, Vol. 48, No. 2, June 1981, pp. 411-418.

[104] Haroun, M.A., and Housner, G.W., *Seismic Design of Liquid Storage Tanks*, Journal of Technical Councils, ASCE, Vol. 107, April 1981, pp. 191-207.

[105] Haroun, M.A., and Housner, G.W., *Dynamic Interaction of Liquid Storage Tanks and Foundation Soil*, Proceedings of the Specialty Conference on Dynamic Response of Structures, ASCE, Georgia, January 1981, pp. 346-360.

[106] Haroun, M.A., *Dynamic Analyses of Liquid Storage Tanks*, Earthquake Engineering Research Laboratory, Report No. EERL 80-4, California Institute of Technology, February 1980.

[107] Hertz, H., *Über die berührung fester elastische körper*, Journal fuer die Reine und angewandte Mathematik, Vol. 92, 1882, pp. 156-171.

[108] Hestenes, M.R., *Multiplier and Gradient Methods*, Journal of Optimization Theory and Applications, Vol. 4, 1969, pp. 303-320.

[109] Hori, N., *Effects of Soil on the Dynamic Response of Liquid-Tank Systems*, Journal of Pressure Vessel Technology-Transactions of The ASME, Vol. 112, No. 2, May 1990, pp. 118-123.

[110] Horvath, J.S., *Differential Settlements in Steel Tanks - Discussion*, Journal of Geotechnical Engineering-ASCE, Vol. 115, No. 7, July 1989, pp. 1035-1036.

[111] Housner, G., *The Dynamic Behavior of Water Tanks*, Bulletin of the Seismological Society of America, Vol. 53, 1963, pp. 381-387.

[112] Housner, G., *Dynamic Pressure on Accelerated Fluid Containers*, Bulletin of the Seismological Society of America, Vol. 47, 1957, pp. 15-35.

[113] Huang, C.Y., and Ansourian, P., *Nonlinear Analysis of Tanks*, Research Report No. R535, University of Sydney, School of Civil and Mechanical Engineering, November 1968.

[114] Huang, Y.Y., Wang, S.K., and Cheng, W.M., *Fluid-Structure Coupling Boundary Element Method for Analyzing Free-Vibration of Axisymmetric Thick-Walled Tanks*, Proceedings of the 10th International Conference on Boundary Element Methods, Southampton, England, 1988, pp. 521-534.

[115] Hughes, T.J.R., and Liu, W.K. *Nonlinear Finite Element Analysis of Shells: Part II. Two-Dimensional Shells*, Journal of Computer Methods in Applied Mechanics and Engineering, Vol. 27, 1981, pp. 167-181.

[116] Hughes, T.J.R., and Liu, W.K. *Nonlinear Finite Element Analysis of Shells: Part I. Three-Dimensional Shells*, Journal of Computer Methods in Applied Mechanics and Engineering, Vol. 26, 1981, pp. 331-362.

[117] Hughes, T.J.R., Taylor, R.L., Sackman, J.L., Curnier, A., and Kanoknukulchai, W., *A Finite Element Method for a Class of Contact-Impact Problems*, Journal of Computer Methods in Applied Mechanics and Engineering, Vol. 8, 1976, pp. 249-276.

[118] Hutton, R.E., *An Investigation of Resonant, Nonlinear Nonplanar Free Surface Oscillations of a Fluid*, NASA TN D-1979, 1963.

[119] Hwang, I.T., and Ting, K., *Boundary Element Method for Fluid-Structure Interaction Problems in Liquid Storage Tanks*, Journal of Pressure Vessels Technology, Vol. III, No. 4, November 1989, pp. 435-440.

[120] Hwang, I.T., and Ting, K., *Dynamic Analysis of Liquid Storage Tanks Including Hydrodynamic Interaction Boundary Element Method*, Proceedings of the 9th International Conference on Structural Mechanics in Reactor Technology (SMIRT-9), Lausanne, Switzerland, August 1987, pp. 429-434.

[121] Hwang, J.H., Kim., I.S., Seol, Y.S., Lee, S.C., and others, *Numerical Simulation of Liquid Sloshing in 3-Dimensional Tanks*, Journal of Computers and Structures, Vol. 44, No. 1-2, July 1992, pp. 339-342.

[122] Ibrahim, R.A., and Heinrich, R.T., *Experimental Investigation of Liquid Sloshing under Parametric Random-Excitation*, Proceedings of the Structural Dynamics and Materials Conference, California, April 1987, pp. 45-54.

[123] Ikegawa, M., and Washizu, K., *Finite Element Method Applied to Analysis of Flow Over a Spillway Crest*, International Journal for Numerical Methods in Engineering, Vol. 6, 1973, pp. 179-189.

[124] Isaacson, M., and Subbiah, K., *Earthquake-Induced Sloshing in a Rigid Circular Tank*, Canaoian Journal of Civil Engineering, Vol. 18, No. 6, December 1991, pp. 904-915.

[125] Ishida, K., and Mieda, T., *Calculation Method of Shear Stress in Bottom Plate of Anchored Cylindrical Tank Under Seismic Loading*, Proceedings of the Pressure Vessels Piping Conference, Sloshing and Fluid Structure Vibration, ASME, PVP, Vol. 157, Hawaii, July 1989, pp. 23-27.

[126] Ishida, K., and Kobayashi, N., *Effective Method of Analyzing Rocking Motion for Unanchored Cylindrical Tanks Including Uplift*, Journal of Pressure Vessels Technology, Transaction of ASME, Vol. 110, No. 1, February 1988, pp. 76-87.

[127] Ishida, K., Kobayashi, N., and Harima, I., *An Effective Method of Analyzing Rocking Motion for Unanchored Cylindrical Tanks Including Uplift*, Proceedings of the Pressure Vessels and Piping Conference, ASME, PVP, Vol. 98-7, New Orleans, June 1985, pp. 87-96.

[128] Ishida, K., *Rocking Behavior of Cylindrical Liquid Storage Tanks*, Proceedings of the 7th World Conference on Earthquake Engineering, Vol. 8, Istanbul, Turkey, September 1980, pp. 475-478.

[129] Jacobsen, L.S., *Impulsive Hydrodynamics of Fluid Inside a Cylindrical Tank and of a Fluid Surrounding a Cylindrical Pier*, Bulletin of the Seismological Society of America, Vol. 39, 1949, pp. 189-204.

[130] James, R., and Raba, G., *Behavior of Welded Steel Water-Storage Tank*, Journal of Structural Engineering-ASCE, Vol. 117, No. 1, January 1991, pp. 61-79.

[131] Jeans, R.A., and Mathews, I.C., *Solution of Fluid-Structure Interaction Problems using a Coupled Finite Element and Variational Boundary Element Technique*, Journal of the Acoustical Society of America, Vol. 88, No. 5, November 1990, pp. 2459-2466.

[132] Jennings, P.C., editor, *Engineering Features of the San Fernando Earthquake, February 9, 1971* Earthquake Engineering Research Laboratory Report, EERL 71-02, California Institute of Technology, Pasadena, California, June 1971.

[133] Jia, Z.H., and Ketter, R.L., *Shaking Table Study of Elephant Foot Bulge Instability of Cylindrical Liquid Storage Tanks*, Proceedings of the 4th International Colloquim on Stability of Metal Structures: Code Differences Around the World, New York, April 1989, pp. 457-468.

[134] Joos, F.M., and Huber, P.W., *Coupled Gas-Liquid-Structure Systems: Part 2 - Applications*, Journal of Applied Mechanics, Transaction of ASME, Vol. 54, No. 4, December 1987, PP. 942-950.

[135] Kalker, J.J., and Randen, Y., *A Minimum Principle for Frictionless Elastic Contact with Application to non-Hertzian Half-Space Contact Problems*, Journal of engineering mathematics, Vol. 6, 1972, pp. 193-206.

[136] Kamatsu, K., *Nonlinear Sloshing Analysis of Liquid in Tanks with Arbitrary Geometries*, National Aerospace Laboratory, Japan.

[137] Kareem, A., and Sun, W., *Stochastic Response of Structures With Fluid-Containing Appendages*, Journal of Sound and Vibration, Vol. 119, No. 3, December 1987, pp. 389-408.

[138] Kelly, T.E., and Mayes, R.L., *Seismic Isolation of Storage Tanks*, Proceedings of the sessions related to Seismic Engineering at Structures Congress, ASCE, California, May 1989, pp. 408-417.

[139] Kikuchi, N., and Oden, J.T., *Contact Problems in Elasticity: A Study of Variational Inequalities and Finite element Methods*, Vol. 8, SIAM, Philadelphia.

[140] Kobayashi, N., Mieda, T., Shbat, H., and Shinozaki, Y., *Study of the Liquid Slosh Response in Horizontal Cylindrical Tanks*, Journal of Pressure Vessel Technology, Transaction of the ASME, Vol. 111, No. 1, February 1989, pp. 32-38.

[141] Kock, E., and Olson, L., *Fluid Structure Interaction Analysis by the Finite Element Method - a Variational Approach*, International Journal for Numerical Methods in Engineering, Vol. 31, No. 3, March 1991, pp. 463-491.

[142] Kondo, H., Yamamoto, S., and Sasaki, Y., *Fluid-Structure Interaction Analysis Program for Axisymmetric Structures*, JSME International Journal, Series III - Vibration Control Engineering for Industry, Vol. 33, No. 3, September 1990, pp. 315-322.

[143] Krasnopol'skaya, T., and Shvets, A., *Regular and Chaotic Surface Waves in a Liquid in a Cylindrical Tank* , Journal of Soviet Applied Mechanics, Vol. 26, No. 8, February 1991, pp. 787-794.

[144] Kurihara, C., Masuko, Y., and Sakurai, A., *Sloshing Impact Pressures of Roofed Liquid Storage Tanks*, Proceedings of the Pressure Vessels Piping Conference, ASME, PVP, Vol. 232, Fluid-Structure Vibration and Sloshing, 1992, pp. 19-24.

[145] Kumar, A., *Studies of Dynamic and Static Response of Cylindrical Liquid Storage Tanks*, Ph.D. Thesis, Rice University, Houston, Texas, 1981.

[146] Lamb, H., *Hydrodynamics*, 6th Edition, Dover Publications, New York, 1945.

[147] Lau, D.T., and Zeng, X., *Hydrodynamic Forces in Uplifting Cylindrical Tanks*, Proceedings of the Fluid-Structure Vibration and Sloshing, ASME, PVP, Vol. 237, California, 1991, pp. 39-44.

[148] Lau, D.T., and Zeng, X., *Simplified Uplift Analysis of Unanchored Cylindrical Tanks*, Proceedings of the Conference on Lifeline Earthquake Engineering, 1992, pp. 975-985.

[149] Lau, D.T., and Clough, R.W., *Static Tilt Analyses of Uplifting Cylindrical Tank*, Proceedings of the Sessions Related to Seismic Engineering at Structures Congress, California, May 1989, pp. 448-457.

[150] Lau, S.M., and Hearn, G.E., *Suppression of Irregular Frequency Effects in Fluid Structure Interaction Problems using a Combined Boundary Integral Equation Method*, International Journal for Numerical Methods in Fluids, Vol. 9, No. 7, July 1989, pp. 763-782.

[151] Leon, G.S., and Kausel, E.A., *Seismic Analysis of Fluid Storage Tanks*, Journal of Structural Engineering, ASCE, Vol. 112, No. 1, January 1986.

[152] Lepelletier, T.G., and Raichlen, F., *Nonlinear Oscillations in Rectangular Tanks*, Journal of Engineering Mechanics, Vol. 114, No. 1, 1988, pp. 1-23.

[153] Li, X., and Brekke, H., *Large Amplitude Water Level Oscillations in Throttled Surge Tanks*, Journal of Hydraulic Research, Vol. 27, No. 4, 1989, pp. 537-551.

[154] Liu, W.K., *Finite Element Procedures for Fluid-Structure Interactions and Applications to Liquid Storage Tanks*, Journal of Nuclear Engineering and Design, Vol. 65, 1981, pp. 221-238.

[155] Liu, W.K., and Lam, D., *Nonlinear Analysis of Liquid-Filled Tank*, Presented in the ASCE EMD Specialty Conference at Purdue University, May 1983.

[156] Liu, W.K., *A Method of Computation for Fluid Structure Interaction*, Journal of Computers and Structures, Vol. 20, 1985, pp. 311-320.

[157] Liu, W.K., and Uras, R.A., *Variational Approach to Fluid-Structure Interaction with Sloshing*, Journal of Nuclear Engineering and Design, Vol. 106, No. 1, February 1988, pp. 69-85.

[158] Liu, W.K., and Uras, R.A., *Transient Buckling Analysis of Liquid-Storage Tanks Part-I*, Proceedings of the Pressure Vessels Piping Conference, Sloshing and Fluid Structure Vibration, ASME, PVP, Vol. 157, Hawaii, July 1989, pp. 35-40.

[159] Liu, W.K., and Uras, R.A., *Transient Buckling Analysis of Liquid-Storage Tanks Part-II*, Proceedings of the Pressure Vessels Piping Conference, Sloshing and Fluid Structure Vibration, ASME, PVP, Vol. 157, Hawaii, July 1989, pp. 41-46.

[160] Luenberger, D.G., *Linear and Nonlinear Programming*, Addison-Wesley, Reading, 2nd edition, 1984.

[161] Lui, A., and Lou, J., *Dynamic Coupling of A Liquid-Tank System Under Transient Excitations*, Journal of Ocean Engineering, Vol. 17, No. 3, 1990, pp. 263-277.

[162] Luke, I., *A Variational Principle For a Fluid With a Free Surface*, Journal of Fluid Mechanics, Vol. 27, 1967, pp. 395-397.

[163] Luzzato, E., *[Analysis of Linear Dynamic-System Interaction - Application to Fluid-Structure Coupling]*, Journal De Physique, Vol. 51 NC3, September 1990, pp. 177-186.

[164] Ma, L., and Chang, C.S., *Pressures Exerted on Soil Due to Rocking of Liquid Storage Tanks*, Journal of Geotechnical Engineering-ASCE, Vol. 119 No. 11, November 1993, pp. 1679-1695.

[165] Malhotra, P.K., and Veletsos, A.S., *Beam Model for Base-Uplifting Analysis of Cylindrical Tanks*, Journal of Structural Division, ASCE, Vol. 120, No. 12, 1994, pp. 3471-3488.

[166] Malhotra, P.K., and Veletsos, A.S., *Uplifting Analysis of Base Plates in Cylindrical Tanks*, Journal of Structural Division, ASCE, Vol. 120, No. 12, 1994, pp. 3489-3505.

[167] Manos, G.C., *Evaluation of the Earthquake Performance of Anchored Wine Tanks During the San-Juan, Argentina, 1977 Earthquake*, Journal of Earthquake Engineering and Structural Dynamics, Vol. 20, No. 12, December 1991, pp. 1099-1114.

[168] Manos, G.C., *Testing of Cylindrical Liquid Storage Tank*, Proceedigns of the Pressure Vessels and Piping Conference, Sloshing Vibration and Seismic Response of Fluid Structure Systems, ASME, PVP, Vol. 191, Tennessee, June 1990, pp. 19-24.

[169] Manos, G.C., *Study of the Behavior of Cylindrical Storage Tanks When Subjected to Lateral Loads*, Proceedings of the Pressure Vessels Piping Conference, Sloshing and Fluid Structure Vibration, ASME, PVP, Vol. 157, Hawaii, July 1989, pp. 75-81.

[170] Manos, G.C., Shibata, H., and Shigita, T., *Correlation of Cylindrical Tank Wall Bucking with an Earthquake Motion Recorded at a Small Distant from the Tank*, Journal of Earthquake Engineering and Structural Dynamics, Vol. 18, No. 2, February 1989, pp. 169-184.

[171] Manos, G.C., and Talaslidis, D., *Experimental and Numerical Study of Tanks Subjected to Lateral Loads*, Proceedings of the 3rd International Conference on Computational Methods and Experimental Measurements, Porto Carras, Greece, September 1986, pp. 487-496.

[172] Manos, G.C., *Earthquake Tank-Wall Stability of Unanchored Tanks*, Journal of Structural Engineers, ASCE, Vol. 112, August 1986, pp. 1863-1879.

[173] Manos, G.C., and Clough, R.W., *Tank Damage During the Coalinga Earthquake*, International Journal of Earthquake Engineering and Structural Dynamics, Vol. 13, July 1985, pp. 449-466.

[174] Manos, G.C., and Clough, R.W., *The Measured and Predicted Shaking Table Response of a Broad Tank Model*, Proceedings of the Pressure Vessels and Piping Conference, ASME, PVP, Vol. 77, New York, June 1983, pp. 14-20.

[175] Manos, G.C., and Clough, R.W., *Further Study of the Earthquake Response of a Broad Cylindrical Liquid Storage Tank*, Earthquake Engineering Research Center, Report UCB/EERC 82-07, July 1982.

[176] Marchaj, T.J., *Importance of Vertical Acceleration in the Design of Liquid Containing Tanks*, Proceedings of the 2nd U.S. National Conference on Earthquake Engineering, Stanford, California, August 1979, pp. 146-155.

[177] Mclver, P., *Sloshing Frequencies for Cylindrical and Spherical Containers Tilled to an Arbitrary Depth*, Journal of Fluid Mechanics, Vol. 201, April 1989, pp. 243-257.

[178] Melerski, E.S., *An Efficient Computer Analysis of Cylindrical Liquid Storage Tanks Under Conditions of Axial Symmetry*, Journal of Computers and Structures, Vol. 45, No. 2, October 1992, pp. 281-295.

[179] Melerski, E.S., *Simple Elastic Analysis of Axisymmetric Cylindrical Storage Tanks*, Journal of Structural Engineering-ASCE, Vol. 117, No. 11, November 1991, pp. 3239-3260.

[180] Miles, J., *Hamilton's Principle For Surface Waves*, Journal of Fluid Mechanics, Vol. 83, 1977, pp. 153-158.

[181] Min, Z., Zheng, S.L., and Wei, Z., *Study on Elephant-Foot Buckling of Broad Liquid Storage Tanks by Nonlinear Theory of Shells*, Journal of Computers and Structures, Vol. 44, No. 4, August 1992, pp. 783-788.

[182] Minowa, C., *Surface Sloshing Behavior of Fluid Storage Tanks*, Proceedings of the Pressure Vessels Piping Conference, Sloshing and Fluid Structure Vibration, ASME, PVP, Vol. 157, Hawaii, July 1989, pp. 83-88.

[183] Minowa, C., Ogawa, N., and Chiba, T., *Shaking Table Test of Cylindrical Tank with a Spring-Mass System*, Proceedings of the Sloshing Vibration and Seismic Response of Fluid-Structure Systems, PVP, ASME, Vol. 145, Pennsylvania, June 1988, pp. 77-82.

[184] Moore, T.A., and Wong, E.K., *The Response of Cylindrical Liquid Storage Tanks to Earthquakes*, Proceedings of 8th World Conference on Earthquake Engineering, Vol. V, California, July 1984, pp. 239-246.

[185] Morand, H., and Ohayon, R., *Substructure Variational Analysis of the Vibrations of Coupled Fluid-Structure Systems. Finite Element Results*, International Journal of Numerical methods in Engineering, Vol. 14, 1979, pp. 741-755.

[186] Mourad, S.A., *Modal Analysis and Buckling Effects on Steel Structures Under Dynamic Loading*, Ph.D. Dissertation, Civil Engineering Department, University of California, Irvine, 1991.

[187] Mourad, S.A., *Modal Response of Liquid-Storage Cylindrical Shells*, Proceedings of the 37th annual technical meeting and equipment exposition, Institute of Environmental Sciences, California, May 1991, pp. 506-511.

[188] Mourad, S.A., and Haroun, M.A., *Dynamic Characteristics of Liquid-Filled Tanks by Modal Analysis Techniques*, Proceedings of the 9th International Modal Analysis Conference, Part 1, Florence, Italy, April 1991, pp. 810-815.

[189] Mourad S.A., and Haroun, M.A. *Experimental Modal Analysis of Cylindrical Liquid-Filled Tanks*, Proceedings of the Fourth U.S. National Conference on Earthquake Engineering, Vol. 3, California, May 1990, pp. 177-187.

[190] Nagashima, H., Kokubo, K., Takayanagi, M., and Saitoh, K., *Experimental Study on Dynamic Buckling of Cylindrical Tanks*, Nippon Kikai Gakkai Ronbunshu A Hen, Vol. 55, No. 517, September 1989, pp. 1992-1997.

[191] Nakayama, T., and Washizu, K., *The Boundary Element Method Applied to The Analysis of Two-Dimensional Nonlinear Sloshing Problems*, International Journal For Numerical Methods in Engineering, Vol. 17, 1981, pp. 1631-1646.

[192] Nakayama, T., and Washizu, K., *Nonlinear Analysis of Liquid Motion in a Container Subjected to Forced Pitching Oscillation*, International Journal for Numerical Methods in Engineering, Vol. 15, 1980, pp. 1207-1220,

[193] Nash, W.A., Yu, B.Q., and Kirchhoff, R.H., *Structural Behavior of Liquid-Elastic Solid Systems*, Proceedings of the Pressure Vessels Piping Conference, Sloshing and Fluid Structure Vibration, ASME, PVP, Vol. 157, Hawaii, July 1989, pp. 89-93.

[194] National Research Council, *Earthquake Engineering Research - 1982* National Academy Press, Washington D.C., 1982.

[195] National Society for Earthquake Engineering, *Seismic Design of Storage Tanks*, Recommendations of a Study Group of the New Zealand National Society for Earthquake Engineering, December 1986.

[196] Natsiavas, S., *Simplified Models for the Dynamic Response of Tall Unanchored Liquid Containers*, Proceedings of the Pressure Vessels Piping Conference, Sloshing and Fluid Structure Vibration, ASME, PVP, Vol. 157, Hawaii, July 1989, pp. 15-21.

[197] Natsiavas, S., *Analysis for the Seismic Response of Liquid Containers*, Proceedings of the sessions related to seismic engineering at Structures Congress, California, May 1989, pp. 458-467.

[198] Natsiavas, S., *An Analytical Model for Unanchored Fluid-Filled Tanks under Base Excitation*, Journal of Applied Mechanics, Vol. 55, September 1988, pp. 648-653.

[199] Natsiavas, S., and Babcock, C.D., *Behavior of Unanchored Fluid-Filled Tanks subjected to Ground Excitation*, Journal of Applied Mechanics, Transactions of ASME, Vol. 55, No. 3, September 1988, pp. 654-659.

[200] Natsiavs, S., and Babcock, C.D., *Buckling at the Top of Fluid-Filled Tank During Base Excitation*, Journal of Pressure Vessel Technology, Transactions of the ASME, Vol. 109, No. 4, November 1987, pp. 374-380.

[201] Nidowicz, B., Bruggers, D., and Manikian, V., *Storage Tank Foundation Design*, Proceedings of the 5th International Conference on Permafrost, Trondheim, Norway, August 1988, pp. 1301-1306.

[202] Nitikitpaiboon, C., and Bathe K.J., *An Arbitrary Lagrangian-Eulerian Velocity Potential Formulation for Fluid Structure Interaction*, Journal of Computers and Structures, Vol. 47, No. 4-5, June 1993, pp. 871-891.

[203] Niwa, A., and Clough, R.W., *Buckling of Cylindrical Liquid Storage Tanks Under Earthquake Loading*, Journal of Earthquake Engineering and Structural Dynamics, Vol. 10, January 1982, pp. 107-122.

[204] Niwa, A., *Seismic Behavior of Tall Liquid Storage Tanks*, Earthquake Engineering Research Center, Report UCB/EERC 78-04, University of California, Berkeley, February 1978.

[205] Ohayon, R., *Fluid-Structure Modal Analysis. New Symmetric Continuum-Based Formulations. Finite Element Applications*, Proceedings of the International Conference on Advances in Numerical Methods in Engineering: Theory and Applications, Swansea, U.K., 1987.

[206] Ohayon, R., and Valid, R., *True Symmetric Formulation of Free Vibration of Fluid-Structure Interaction - Applications and Extensions*, Proceedings of the International Conference of Numerical Methods for Coupled Problems, University College, Swansea, September 1981.

[207] Okamoto, T., and Kawahara, M., *Two-Dimensional Sloshing Analysis by the Arbitrary Lagrangian-Eulerian Finite Element Method*, Proceedings of JSCE, Structural engineering/ earthquake engineering, Vol. 8, No. 4, January 1992, pp. 207-216.

[208] Okamoto, K., Madarame, H., and Hagiwara, T., *Self Induced Oscillation of Free-Surface in a Tank with Circulating Flow*, International Conference on Flow Induced Vibrations, Brighton, England, May 1991, pp. 539-546.

[209] Okamoto, T., *Two-Dimensional Sloshing Analysis by Lagrangian Finite Element Method*, International Journal for Numerical Methods in Fluids, Vol. 11, 1990, pp. 453-477.

[210] Olson, L., and Vandini, T., *Eigenproblem from Finite Element Analysis of Fluid-Structure-Interactions*, Computer and Structure, Vol. 33, No. 3, 1989, pp. 679-687.

[211] Olson, L., and Bathe, K.J., *An Infinite Element for Analysis of Transient Fluid-Structure Interaction*, Journal of Engineering with Computers, Vol. 2, December 1985, pp. 319-329.

[212] Olson, L., and Bathe, K.J., *Analysis of Fluid-Structure Interactions. A Direct Symmetric Coupled Formulation Based on the Fluid Velocity Potential*, Journal of Computers and Structures, Vol. 21, No. 12, December 1985, pp. 21-32.

[213] Olson, L.G., and Bathe, K.G., *A Study of Displacement-Based Fluid Finite Elements For Calculating Frequencies of Fluid and Fluid-Structure Systems*, Journal of Nuclear Engineering and Design, 1983, Vol. 76, pp. 137-151.

[214] Panagiotopoulos, P.D., *A Nonlinear Programming Approach to the Unilateral Contact and Friction-Boundary Value Problem in the Theory of Elasticity*, Ingenieur-Archiv, Vol. 44, 1975, pp. 421-432.

[215] Papadopoulos, P., *On the Finite Element Solution of General Contact Problems*, Ph.D. Dissertation, Civil Engineering Department, University of California at Berkeley, 1991.

[216] Pavlovic, M.N., and Papamakarios, A., *Structural Behavior of Liquid-Filled Spherical Vessels, Part 1, Background and Theoretical Preliminaries*, Journal of Thin-Walled Structures, Vol. 10, No. 3, 1990, pp. 195-214.

[217] Peek, R., and Bkaily, M., *Postbuckling Behavior of Liquid Storage Tanks Under Lateral Loads*, Proceedigns of the Pressure Vessels and Piping Conference, Flow-Structure Vibration and Sloshing, ASME, PVP, Vol. 191, Tennessee, June 1990, pp. 37-45.

[218] Peek, R., *Buckling Criteria for Earthquake-Induced Overturning Stresses in Cylindrical Liquid Storage Tanks*, Proceedings of the Sessions Related to Seismic Engineering at Structures Congress, ASCE, California, May 1989, pp. 428-437.

[219] Peek, R., *Analysis of Unanchored Liquid Storage Tanks Under Lateral Loads*, Journal of Earthquake Engineering and Structural Dynamics, Vol. 16, No. 7, October 1988, pp. 1087-1100.

[220] Peek, R., and Jennings, P.C., *Simplified Analysis of Unanchored Tanks*, Journal of Earthquake Engineering and Structural Dynamics, Vol. 16, No. 7, October 1988, pp. 1073-1085.

[221] Peek, R., Jennings, P.C., and Babcock, C.D., *Preuplift Method to Anchor Liquid Storage Tanks*, Journal of Structural Engineering, Vol. 114, No. 2, February 1988, pp. 475-486.

[222] Peek, R., *Analysis of Unanchored Liquid Storage Tanks Under Seismic Loads*, Earthquake Engineering Research Laboratory Report, EERL 86-01, California Institute of Technology, California, May 1986.

[223] Pian, T., and Kubomura, K., *Formulation of Contact Problem by Assumed Stress Hybrid Elements*, In Nonlinear Finite Element Analysis in Structural Mechanics, W. Wunderlich et al, Editors, Springer-Verlag 1981, pp. 49-59.

[224] Pinsky, P.M., and Abboud, N.N., *Two Mixed Variational Principles for Exterior Fluid Structure Interaction Problems*, Journal of Computers and Structures, 1989, Vol. 33, No. 3, pp. 621-635.

[225] Popov, G., Vatistas, G., Sankar, S., and Sankar, T.S., *Liquid Sloshing in a Horizontal Cylindrical Container*, Proceedings of the ASME Computers in Engineering Conference, 1989, pp. 145-149.

[226] Powell, M.J.D., *A Method for Nonlinear Constraints in Minimization Problems*, In R. Fletcher, Editor, *Optimization*, Academic Press, London, 1969.

[227] Rajasankar, J., Iyer, N.R., and Rao, T., *A New 3-D Finite Element Model to Evaluate Added Mass for Analysis of Fluid-Structure Interaction Problems*, International Journal for Numerical Methods in Engineering, Vol. 36, No. 6, March 1993, pp. 997-1012.

[228] Ramaswamy, B., and Kawahara, M., *Arbitrary Lagrangian-Eulerian Finite Element Method for Unsteady, Convective, Incompressible Viscous Free Surface Fluid Flow*, International Journal For Numerical Methods in Fluids, Vol. 7, 1987.

[229] Ramaswamy, B., Kawahara, M., and Nakayama, T., *Lagrangian Finite Element Method for the Analysis of Two-Dimensional Sloshing Problem*, International Journal For Numerical Methods in Fluids, Vol. 6, 1986.

[230] Rammerstorfer, F.G., Holl, H.J., Fischer, F.D., and Seeber, R., *Influence of the Vertical Motion Component on the Plastic Collapse of Earthquake Excited Tanks*, Proceedings of the 9th International Conference on Structural Mechanics in Reactor Technology (SMIRT-9), Lausanne, Switzerland, August 1987, pp. 793-798.

[231] Rinne, J.E., *The Prince William Sound, Alaska, Earthquake of 1964, and Aftershocks*, Vol. II, Part A, U.S. Coast and Geodetic Survey, 1967, pp. 245-252.

[232] Romano, A.J., Williams, E.G., Russo, K.L., and Schuette, L.C., *On the Visualization and Analysis of Fluid-Structure Interaction from the Perspective of Instantaneous Intensity*, Journal De Physique III, Vol. 2, No. 4, April 1992, pp. 597-600.

[233] Ruiz, C., Salvatorelli-D'Angelo, F., and Thompson, V.K., *Elastic Response of Thin-Wall Cylindrical Vessels to Blast Loading*, Computer and Structures, Vol. 32, No. 5, 1989, pp. 1061-1072.

[234] Sakai, F., and Isoe, A., *Partial Sliding During Earthquakes in an Anchor-Strapped Cylindrical Tank*, Proceedigns of the Pressure Vessels and Piping Conference, Flow-Structure Vibration and Sloshing, ASME, PVP, Vol. 191, Tennessee, June 1990, pp. 69-74.

[235] Sakai, F., and Isoe, A., *Influence of Partial Sliding of Bottom Plate in an Anchored Cylindrical Tank During Earthquakes*, Gakkai Rombun Hokokushu, No. 410, pt. 1-12, October 1989, pp. 385-393.

[236] Sakai, F., and Isoe, A., *Big-Scaled Tilt Test On Uplifting Behavior of Oil Storage Tank*, Seismic Engineering: Research and Practice, ASCE, New York, 1989, pp. 438-447.

[237] Sakai, F., Isoe, A., Hirakawa, H., and Mentani, Y., *Large Scale Tilt Test of Seismic Behavior of Flat-Bottomed Cylindrical Liquid Storage Tank*, Proceedings of the Pressure Vessels Piping Conference, Sloshing and Fluid Structure Vibration, ASME, PVP, Vol. 157, Hawaii, July 1989, pp. 69-74.

[238] Sakai, F., and Isoe, A., *Computation and Experiment on Base-Uplift Behavior of Cylindrical Oil Storage Tanks During Earthquakes*, Proceedings of the Pressure

Vessels Piping Conference, Sloshing and Fluid Structure Vibration, ASME, PVP, Vol. 157, Hawaii, July 1989, pp. 9-14.

[239] Sakai, F., Isoe, A., Hirakawa, H., and Montani, Y., *Experimental Study on Uplift Behavior of Large-sized Cylindrical Liquid Storage Tanks*, Pressure Vessels and Piping Conference, ASME, PVP-Vol. 127, San Diego, June 1987, pp. 349-355.

[240] Sakai, F., Ogawa, H., and Isoe, A., *Horizontal, Vertical and Rocking Fluid-Elastic Response and Design of Cylindrical Liquid Storage Tanks*, Proceedings of the 8th World Conference on Earthquake Engineering, Vol. 5, California, July 1984, pp. 263-270.

[241] Sauve, R.G., Morandin, G.D., and Nadeau, E., *Impact Simulation of Liquid-Filled Containers Including Fluid-Structure Interaction .2. Experimental Verification*, Journal of Pressure Vessel Technology, Transactions of the ASME, Vol. 115, No. 1, February 1993, pp. 73-79.

[242] Sauve, R.G., Morandin, G.D., and Nadeau, E., *Impact Simulation of Liquid-Filled Containers Including Fluid-Structure Interaction .1. Theory*, Journal of Pressure Vessel Technology, Transactions of the ASME, Vol. 115, No. 1, February 1993, pp. 68-72.

[243] Scharf, K., Rammerstorfer, F.G., and Fischer, F.D., *Earthquake Resistant Design of Unanchored Liquid Storage Tanks*, Proceedings of the International Conference on Earthquake Resistant Construction and Design, Berlin, Fed. Rep. Ger., June 1989, pp. 283-292.

[244] Seeber, R., Fisher, F., and Rammerstorfer, F., *Analysis of A 3-Dimensional Tank-Liquid-Soil Interaction Problem*, Journal of Pressure Vessel Technology, Transactions of The ASME, Vol. 112, No. 1, Febreuary 1990, pp. 28-33.

[245] Seliger, R., and Whitham, G., *Variational Principles in Continuum Mechanics*, Proceedings of the Royal Society, Series A, Vol. 305, 1968, pp. 1-25.

[246] Serrin, J., *Mathematical Principles of Classical Fluid Mechanics*, Encyclopedia of Physics, Vol. 8, Spnnger-Verlag, Berlin, 1959, pp. 125-263.

[247] Seybert, A.F., WU, T.W., and Li, W.L., *A Coupled FEM BEM for Fluid-Structure Interaction using Ritz Vectors and Eigenvectors*, Journal of Vibration and Acoustics, Transactions of the ASME, Vol. 115, No. 2, April 1993, pp. 152-158.

[248] Shaaban, S.H., and Nash, W.A., *Finite Element Analysis of a Seismically Excited Cylindrical Storage Tank, Ground Supported and Partially Filled With Liquid*, Report, University of Massachusetts, Amherst, August 1975.

[249] Shih, C.F., and Babcock, C.D., *Buckling of Oil Storage Tanks in SPPL Tank Farm during the 1979 Imperial Valley Earthquake*, Proceedigs of the Pressure Vessels and Piping Conference, ASME, Preprint 84-PVP-74, San Antonio, June 1984.

[250] Shih, C.F., and Babcock, C.D., *Scale Model Buckling Tests of a Fluid Filled Tank under Harmonic Excitation*, Proceedigns of the Pressure Vessels and Piping Conference, ASME, Preprint 80-C2/66, San Francisco, August 1980.

[251] Shimizu, N., *Advances and Trends in Seismic Design of Cylindrical liquid Storage Tank*, JSME International Journal Series III, Vibration Control Engineering, Engineering for Industry, Vol. 33, No. 2, June 1990, pp. 111-124.

[252] Shimizu, N., *Seismic Design of Cylindrical Tank on Elastic Soil*, Proceedings of the Pressure Vessels Piping Conference, Sloshing and Fluid Structure Vibration, ASME, PVP, Vol. 157, Hawaii, July 1989, pp. 83-88.

[253] Shimizu, N., *Seismic Design of Cylindrical Tanks (Fifth Report, Seismic Response Analysis of Tank on Elastic Foundation)*, Nippon Kikai Gakkai Ronbunshu C Hen, Vol. 53, No. 495, November 1987, pp. 2277-2282.

[254] Shimizu, N., *Seismic Design of Cylindrical Tanks*, Nippon Kikai Gakkai Ronbunshu C Hen, Vol. 53, No. 492, August 1987, pp. 1676-1682.

[255] Shimura, M., and Sekine, A., *Interaction Analysis between Structure and Fluid Flow for Wind Engineering*, Journal of Wind Engineering and Industrial Aerodynamics, 1993 August V46-7, pp. 595-604.

[256] Shtaerman, I.Y., *Contact Problems in the Theory of Elasticity*, Gostekhizdat, Moscow, 1949, in Russian.

[257] Signorini, A., *Sopra akune questioni di elastostatica*, Societa Italiana per Il Progresso delle Scienze. Atti. 1933.

[258] Singhal, R.K., and Williams, K.J., *Theoretical and Experimental Study of Vibrations of Thick Circular Cylindrical Shells and Rings*, Journal of Vibration, Acoustics, Stress, Reliability in Design, Vol. 110, No. 4, 1988, pp. 533-537.

[259] Sone, A., and Suzuki, K., *Conventional Calculation Method for the Aseismic Design of a Liquid Storage Tank and Nonlinear Piping System (evaluation of correlation among loads and reduction effect due to nonlinearity)*, Nippon Kikai Gakkai Ronbunshu C Hen, Vol. 54, No. 503, July 1988, pp. 1439-1444.

[260] Sovinc, I., and Vogninic, G., *Settlement Observations of Tanks on Soft Soil*, Proceedings of the 10th European Conference of Soil Mechanics and Foundation Engineering, Florence, Italy, May 1991.

[261] Su, T., and Wang, Y., *Numerical Simulation of Three-Dimensional Large Amplitude Liquid Sloshing in Cylindrical Tanks Subjected to Arbitrary Excitation*, Proceedigns of the Pressure Vessels and Piping Conference, Flow-Structure Vibration and Sloshing, ASME, PVP, Vol. 191, Tennessee, June 1990, pp. 127-148.

[262] Su, T., *Numerical Simulation of Three-Dimensional Large Amplitude Liquid Sloshing in Rectangular Containers Subjected to Vertical Excitation*, Proceedings of the Pressure Vessels Piping Conference, Sloshing and Fluid Structure Vibration, ASME, PVP, Vol. 157, Hawaii, July 1989, pp. 115-126.

[263] Sweeney, M., Craig, H.A., and Lambson, M.D., *Distortion of Steel Tanks due to Settlement of their Walls - Discussion*, Journal of Geotechnical Engineering, ASCE, Vol. 117, No. 9, September 1991, pp. 1443-1446.

[264] Sweeney, M., and Lambson, M.D., *Long Term Settlements of Storage Tanks on Sand*, Proceedings of the 10th European Conference of Soil Mechanics and Foundation Engineering, Florence, Italy, May 1991.

[265] Tani, J., and Teraki, J., *Free Vibration Analysis of Partially Liquid-Filled Shells of Revolution*, Nihon Kikaigakkai Rombunshu, Transactions of the Japan Society of Mechanical Engineers, Vol. 54, No. 497, January 1988, pp. 73-79.

[266] Tani, S., Hori, N., and Yamaguchi, K., *Nonlinear Dynamic Analysis of Cylindrical Tanks with Imperfect Circular Section Containing Liquid*,

Proceedings of the 8th World Conference on Earthquake Engineering, Vol. 5, California, July 1984, pp. 247-254.

[267] Tedesco, J., Landis, D., and Kostem, C., *Seismic Analysis of Cylindrical Liquid Storage Tanks*, Journal of Computers and Structures, Vol. 32, No. 5, 1989, pp. 1165-1174.

[268] Tedesco, J., Kostem, C., and Kalnins, A., *Free Vibration Analysis of Cylindrical Liquid Storage Tanks*, Journal of Computers and Structures, Vol. 26, No. 6, 1987, pp. 957-964.

[269] Thompson, V., and Ruiz, C., *Dynamic Elastic and Plastic Deformation of Double-Walled Cylindrical Storage Tanks*, International Journal of Impact Engineering, Vol. 8, No. 4, 1989, pp. 341-354.

[270] Timoshenko, S., *Theory of Plates and Shells*, McGraw-Hill Book Company Inc., 1940.

[271] Turner, M.J., Clough, R.W., Martin, H.C., and Topp, L.J., *Stiffness and Deflection Analysis of Complex Structures*, Journal of the Aero/Space Sciences, Vol. 23, 1956, pp. 805-823.

[272] United States Atomic Energy Commission, *Nuclear Reactors and Earthquakes*, TID-7024, Washington, D.C., 1963, pp. 367-390.

[273] Uras, R., Liu, W., and Chen, Y., *Study of the Influence of Imperfections on the Dynamic Stability of Tanks*, Proceedigns of the Pressure Vessels and Piping Conference, Flow-Structure Vibration and Sloshing, ASME, PVP, Vol. 191, Tennessee, June 1990, pp. 47-54.

[274] URS Consultants/John A Blume & Associates Engineers, *Seismic Verification of Nuclear Plant Equipment Anchorage*, Report to Electrical Power Research Institute, June 1991.

[275] Vallabhan, C., and Das, Y., *Analysis of Circular Tank Foundations*, Journal of Engineering Mechanics, ASCE, Vol. 117, No. 4, April 1991, pp. 789-797.

[276] Veletsos, A.S., and Shivakumar, P., *Sloshing Response of Layered Liquids in Rigid Tanks*, Journal of Earthquake Engineering and Structural Dynamics, Vol. 22, No. 9, September 1993, pp. 801-821.

[277] Veletsos, A.S., Tang, Y., and Tang, H., *Dynamic Response of Flexibly Supported Liquid-Storage Tanks*, Journal of Structural Engineering, ASCE, Vol. 118, No. 1, January 1992, pp. 264-283.

[278] Veletsos, A.S., and Tang, Y., *Soil-Structure Interaction Effects for Laterally Excited Liquid Storage Tanks*, Journal of Earthquake Engineering and Structural Dynamics, Vol. 19, No. 1, May 1990, pp. 473-496.

[279] Veletsos, A.S., and Tang, Y., *Rocking Response of Liquid Storage Tanks*, Journal of Engineering Mechanics, Vol. 113, No. 11, November 1987, pp. 1774-1792.

[280] Veletsos, A.S., *Seismic Response and Design of Liquid Storage Tanks*, Proceedings of the Technical Council on Life Line Earthquake Engineering, Guidelines for the Seismic Design of Oil and Gas Pipeline Systems, ASCE, Newyork, 1984, pp. 255-370 and 443-461.

[281] Veletsos, A.S., and Kumar, A., *Dynamic Response of Vertically Excited Liquid Storage Tanks*, Proceedings of the 8th World Conference on Earthquake Engineering, California, Vol. VII, July 1984, pp. 453-459.

[282] Veletsos, A.S., and Yang, J.Y., *Earthquake Response of Liquid Storage Tanks*, Proceedings of the EMD Specialty Conference, ASCE, Raleigh, N.C., 1977, pp. 1-24.

[283] Veletsos, A.S., and Yang, J.Y., *Dynamics of Fixed Base Liquid Storage Tanks*, Proceedings of U.S.-Japan Seminar on Earthquake Engineering Research with Emphasis on Lifeline Systems, Japan Society for Promotion of Earthquake Engineering, Tokyo, Japan, November 1976, pp. 317-341.

[284] Veletsos, A.S., *Seismic Effects in Flexible Liquid Storage Tanks*, Proceedings of the 5th World Conference on Earthquake Engineering, Rome, Italy, Vol. 1, 1974, pp. 630-639.

[285] Vonestorff, O., and Antes, H., *On FEM BEM Coupling for Fluid Structure Interaction Analyses in the Time Domain*, International Journal for Numerical Methods in Engineering, Vol. 31, No. 6, May 1991, pp. 1151-1168.

[286] Ward, P., Desai, R., Kebede, W., and Ecer, A., *A New Clebsch Formulation For Incompressible Viscous Flow*, First National Fluid Dynamics Conference, Cincinnati, July 1988.

[287] Wiesner, T.J., and Walker, A.B., *Tank Foundations in Townsville*, Proceedings of the 7th International Conference on Computer Methods and Advances in Geomechanics, Cairns, Autralia, May 1991, pp. 1041-1046.

[288] Williams, A.N., and Moubayed, W.I., *Greens Function Solution for Axisymmetric Vibration of Flexible Liquid-Filled Tanks*, Journal of Engineering Structures, Vol. 12, No. 1, January 1990, pp. 49-59.

[289] Williams, A.N., and Moubayed W.I., *Earthquake-Induced Hydrodynamic Pressures on Submerged Cylindrical Storage Tanks*, Journal of Ocean Engineering, Vol. 17, No. 3, 1990, pp. 181-199.

[290] Williams, K.J., *Boundary Integral Equation Method for the Solution of Wave-Obstacle Interaction*, International Journal of Numerical Methods in Fluids, Vol. 8. No. 2, February 1988, pp. 227-242.

[291] Wilson, E., and Khalvati, M., *Finite Elements For the Dynamic Analysis of Fluid-Solid Systems*, International Journal of Numerical Methods in Engineering, Vol. 19, 1983, pp. 1657-1668.

[292] Wozniak, R.S., and Mitchell, W.W., *Basis of Seismic Design Provisions for Welded Steel Oil Storage Tanks*, Proceedings of the Session on Advances in Storage Tank Design, API, Toronto, Canada, May 1978.

[293] Yamada, Y., Iemura, H., Noda, S., and Shimada, S., *Long-Period Response Spectra from Nonlinear Sloshing Analysis Under Horizontal and Vertical Excitations*, Journal of Natural Disaster Science, Vol. 9, No. 2, 1987, pp. 39-54.

[294] Yi, W., and Natsiavas, S., *Seismic Response of Unanchored Fluid-Filled Tanks Using Finite Elements*, Journal of Pressure Vessel Technology, Transactions of The ASME, Vol. 144, No. 1, February 1992, pp. 74-79.

[295] Yoshida, S., and Miyoshi, T., *Seismic Response Analysis of a Multi-Walled Coaxial Cylindrical Tank*, Nippon Kikai Gakkai Ronbunshu C Hen, Vol. 53, No. 492, August 1987, pp. 1670-1675.

[296] Zaman, M.M., and Koragappa, N., *Analysis of Tank-Foundation-Half-Space Interaction Using an Energy Approach*, Applied Mathematical Modeling, Vol. 13, No. 2, February 1989, pp. 66-78.

[297] Zaman, M.M., and Mahmood, I.U., *Analysis of Cylindrical Storage Tank-Foundation Interaction Using Finite Element Method*, Indian Geotechnical Journal, Vol. 18, No. 4, October 1988, pp. 356-384.

[298] Zeng, X.G., Bielak J., and MacCamy, R.C., *Stable Variational Coupling Method for Fluid-Structure Interaction in Semiinfinite Media*, Journal of Vibration and Acoustics, Transactions of the ASME, Vol. 114, No. 3, July 1992, pp. 387-396.

[299] Zhou, M., Zheng, S., and Zhang, W., *Study on Elephant-Foot Buckling of Broad Liquid Storage Tanks by Nonlinear theory of Shells*, Journal of Computers and Structures, Vol. 44, No. 4, August 1992, pp. 783-788.

[300] Zienkiewicz, O., and Bettess, P., *Fluid-Structure Dynamic Interaction and Wave Forces. An introduction of Numerical Treatment*, International Journal of Numerical Methods in Engineering, Vol. 13, 1978, pp. 1-16.

[301] Zienkiewicz, O., and Newton, R., *Coupled Vibrations of a Structure Submerged in a Compressible Fluid*, Symposium on Finite Element Techniques, Stuttgart, 1969.